Investigating the humoral and B cell response during HIV infection to identify phenotypes associated with the development of HIV broadly neutralising antibodies

Sarah A Griffith

A thesis submitted for the degree of
Doctor of Philosophy

Division of Infection and Immunity
University College London

April 2023

Declaration

I, Sarah Griffith, confirm that the work presented in this thesis is my own. Where information has been derived from other sources, I confirm that this has been indicated in the thesis.

Abstract

Only 1-10% of HIV-1 infected individuals produce antibodies with broad neutralisation against heterologous viruses. These broadly neutralising antibodies (bnAbs) and their development are of interest due to *in vivo* studies showing that bnAbs can provide passive protection in animal models and delay viral rebound in humans. However, attempts to elicit bnAb responses during immunisation studies and vaccine trials have been largely unsuccessful. Therefore, there is a need to investigate host immune responses associated with HIV bnAb development. To address this, a cohort of treatment naïve HIV-infected individuals were assessed for neutralisation breadth and identified the top neutraliser, T125. Fluorescence-activated cell sorting (FACS) using HIV envelope probes was performed to clone single B cells and isolate antibodies from T125. This produced monoclonal antibodies with different HIV neutralisation profiles, including a bnAb. The phenotype of B cells from two timepoints of this viraemic bnAb donor was also assessed during FACS and revealed that the tissue-like CD21-/CD27- B cell population was not enlarged, as canonically seen in HIV viraemia. A Smart-Seq2 single-cell RNA-sequencing pipeline was also established to investigate rare antigen-specific cell phenotypes. This yielded single-cell transcriptomes for HIV-specific IgG+ B cells from the bnAb donor which were compared to larger scRNA-seq datasets from HIV-infected donors and uninfected controls. This validated flow cytometry observations that the viraemic bnAb donor had a normalised B cell population, similar to uninfected controls. In addition, limited inflammatory stimulation was found in the memory B cells of uninfected controls, unlike viraemic donors. It was therefore proposed that preservation of memory B cell homeostasis and bnAb development, in the face of viraemia, was linked to IFN suppression. In support of this, plasma from top neutralisers in the cohort were capable of blocking type II IFN, which has previously been associated with the disruption of memory B cell subsets.

Impact statement

HIV broadly neutralising antibodies (bnAbs) have been studied extensively, however, the B cells that produce them have not. Although HIV does not infect B cells, the indirect effects of ongoing immune activation and inflammation leads to the disruption of B cell subsets in chronic HIV infection. This thesis revealed that despite having uncontrolled viraemia, the memory B cell population of a bnAb donor was not perturbed. Specifically, a predominantly resting phenotype was observed at the cell surface and transcriptomic level that was similar to uninfected controls, regardless of the antibody functionality. This novel finding suggests that there is not a difference between bnAb and non-bnAb B cells as originally hypothesised, instead, maintenance of B cell homeostasis during HIV infection may be required to enable ongoing maturation to antigenic stimulation for the development of bnAbs. Furthermore, preliminary data indicates that this phenotype may be achieved by suppressing the type II IFN-γ response. While these findings stem from the investigation of only one bnAb donor, this offers promise that an HIV vaccine to elicit bnAbs could be achieved in uninfected individuals who have a non-perturbed B cell population, if sufficient antigenic stimulation can be provided. Additionally, this provides insight into how alterations of the memory subsets could be avoided or potentially reversed by limiting the level of inflammation, for example as part of a therapeutic vaccine in people living with HIV, although this remains to be explored.

Acknowledgements

Completing this PhD would not have been possible without all of the amazing people in my life, who have been incredibly supportive and encouraging. In particular, I want to thank my husband Callum who has always believed in me and been my rock throughout this journey. Brownie points for all of the meals you've cooked, all the cups of tea to get me through writing and all of the conversations where you've pretended to understand my research, even though I lost you at the word bnAb! I also want to thank my family who have always been there for me and without their support, I wouldn't be where I am today.

I would next like to give a huge thank you to my fantastic supervisor Dr Laura McCoy for giving me this opportunity and for having confidence in my ability from day one, even when I doubted myself. You have provided me with invaluable training and guidance that enabled me to develop into an independent scientist and I felt inspired to discover more with every discussion that we had. I feel very lucky to have been a part of the McCoy group, and that extends to the rest of the team who have been amazing to work alongside. Luke, Chloe, Emma, Peter, Chris, Audrey and everyone else who has come and gone – your support both in and out of the lab means so much and I couldn't have gotten this far without you! I'd also like to thank the past and present members of the Jolly group who were like my second lab during our time together at the Cruciform Building. Finally, I want to thank Prof. Clare Jolly and Prof. Mahdad Noursadeghi for their continued advice and guidance whilst completing this research, as well as everyone else in the division who has helped me along the way!

Statement of contributions

Chapter 1

Parts of this introduction chapter (section 1.4) were included in a modified form in a review paper which I co-authored with my supervisor Dr Laura McCoy:

Griffith, Sarah A., and Laura E. McCoy. 2021. 'To bnAb or Not to bnAb: Defining Broadly Neutralising Antibodies Against HIV-1', *Frontiers in Immunology*.

Chapter 2

Operation of the FACS machines for the isolation of single B cells was performed by Jamie Evans at UCL (section 2.3.2) or by Dr Katherine Doores at Kings College London in the containment 3 lab (section 2.7.8).

The Smart-Seq2 method for generating scRNA-seq libraries was optimised by Dr Luke Muir, who also assisted in the generation of scRNA-seq libraries from the HIV-negative single IgG+ B cells (section 2.3.3). Pooled libraries were sequenced by the Pathogens Genomic Unit at UCL, and initial processing of the scRNA-seq data as well as quality control checks (section 2.3.4) was performed by Dr José Afonso Guerra-Assunção. All of the scRNA-seq analyses (section 2.11) were performed by Dr Ondrej Suchanek and Dr Kelvin Tuong in Professor Menna Clatworthy's lab group at the University of Cambridge.

The cloning and production of mAbs from the second T125 timepoint single B cells and epitope mapping of mAbs (sections 2.8.3 and 2.9) was completed with assistance from Audrey Fung, as part of her MSc project under my supervision.

Flow cytometry analysis of beads in the LEGENDplex assay (section 2.12.1) was conducted with assistance from Dr Christopher Pinder.

Chapters 3-7

These chapters are solely my work, with input from my supervisor Dr Laura McCoy.

Table of Contents

List of Figures

List of Tables

Abbreviations

AA	Amino acid
AID	Activation-induced cytidine deaminase
AIDS	Acquired immune deficiency syndrome
AM	Activated memory
AMP	Antibody mediated prevention
ART	Antiretroviral therapy
BCR	B cell receptor
bnAb	Broadly neutralising antibody
bp	Base pair
C	Constant
cART	Combination antiretroviral therapy
cDNA	Complementary DNA
CDR	Complementarity determining region
CDRH	Heavy chain complementarity determining region
CDRL	Light chain complementarity determining region
CD4bs	CD4 binding site
CLP	Common lymphoid progenitor
CRF	Circulating recombinant form
CSR	Class switch recombination
CTL	Cytotoxic T lymphocyte
CTLA-4	Cytotoxic T-lymphocyte associated protein 4
c/mL	Copies per millilitre
D	Diversity
DC	Dendritic cell
DEG	Differentially expressed genes
DNA	Deoxyribonucleic acid
ds	Double-stranded
DZ	Dark zone
E. coli	Escherichia coli

EM	Electron microscopy
env	HIV envelope gene
Env	HIV envelope protein
ER	Endoplasmic reticulum
Fab	Fragment antigen binding domain
FACS	Fluorescence-activated cell sorting
Fc	Fragment crystallisable region
FSC	Forward scatter
FWR	Framework region
g	Gram
GC	Germinal centre
GEM	Gel beads in emulsion
GNL	Galanthus nivalis lectin
GSEA	Gene set enrichment analysis
HC	Heavy chain
HIV	Human immunodeficiency virus
HLA	Human leucocyte antigen
HMP	High mannose patch
hr	Hour
HSC	Hematopoietic stem cell
HUSH	Human silencing hub
IC_{50}	Concentration for 50% inhibition
ID_{50}	Dilution for 50% inhibition
IFN	Interferon
Ig	Immunoglobulin
IgH	Immunoglobulin heavy chain
IgK	Immunoglobulin kappa chain
IgL	Immunoglobulin lambda chain
ISG	Interferon stimulated genes
J	Joining
J_H	Joining heavy
J_K	Joining kappa

J_L	Joining lambda
kDa	Kilodalton
L	Litre
LANL	Los Alamos National Laboratory
LC	Light chain
LTR	Long terminal repeat
Luc	Luciferase
LZ	Light zone
M	Molar
mAb	Monoclonal antibody
MBC	Memory B cell
MHC	Major histocompatibility complex
min	Minute
µg	Microgram
µL	Microlitre
mL	Millilitre
mm	Millimetre
MLV	Murine leukaemia virus
MPN	Maximum percentage neutralisation
MPER	Membrane proximal region
nAb	Neutralising antibody
NES	Normalised enrichment score
ng	Nanogram
NK	Natural killer
Non-nAb	Non-neutralising antibody
PBMC	Peripheral blood mononuclear cells
PBS	Phosphate buffered saline
PCA	Principal component analysis
PCR	Polymerase chain reaction
PD-1	Programmed death protein 1
pg	picogram
PID	Patient ID

PLWH	People living with HIV
PNGS	Potential N-linked glycosylation site
Poly-A	Polyadenylated
PV	Pseudo-typed virus
QC	Quality control
RAG	Recombination activating gene
RCF	Relative centrifugal force
RLU	Relative light units
RM	Resting memory
rpm	Rotations per minute
RNA	Ribonucleic acid
scRNA-seq	Single cell RNA sequencing
SDM	Site-directed mutagenesis
SDS-PAGE	Sodium dodecyl-sulfate polyacrylamide gel electrophoresis
sec	Second
SGA	Single-genome amplification
SHM	Somatic hypermutation
SIV	Simian immunodeficiency virus
SLE	Systemic lupus erythematosus
SOSIP	Mutation to introduce a stabilising disulphide bond and isoleucine to proline into recombinant, trimeric HIV Env
SSC	Side scatter
TAR	Transactivation response
tat	Trans-activator of transcription
$TCID_{50}$	Tissue culture infectious dose for 50% infection
T/F	Transmitter founder
Tfh	T follicular helper
Th17	T helper 17
TLM	Tissue-like memory
TLR	Toll-like receptor
Treg	T regulatory

TSO	Template switch oligo
U	Units
UMI	Unique molecular identifier
URF	Unique recombinant form
V	Variable
V_H	Variable heavy
V_K	Variable kappa
V_L	Variable lambda
VL	Viral load
WHO	World Health Organisation
WT	Wild type

Chapter 1: Introduction

1.1 HIV pathogenesis

1.1.1 The HIV pandemic

The first documented cases of acquired immune deficiency syndrome (AIDS) arose in 1981 after otherwise healthy individuals contracted *Pneumocystis* pneumonia which typically arises as an opportunistic infection during immune suppression (CDC 1981). However, it wasn't until 1983 that the human immunodeficiency virus (HIV) was isolated and discovered as the causative agent of AIDS (Barré-Sinoussi et al. 1983; Gallo et al. 1984; Popovic et al. 1984).

Since the start of the HIV/AIDS epidemic, it has been estimated that 84.2 million people have been infected with HIV and 40.1 million have succumbed to an AIDS-related illness (UNAIDS 2022). In 2021, the World Health Organisation (WHO) reported that there were approximately 38.4 million people living with HIV (PLWH) around the world and that 75% received life-saving antiretroviral therapy (ART). Africa continues to be the most affected region in the world and accounted for 60% of the 1.5 million new HIV infections documented in 2021. Despite this, there has been a substantial decline in the number of HIV-related deaths in Africa, of almost 55% from 2010, suggested to be a result of increased awareness, expanded access to antiviral drugs and fewer incidences of infection.

1.1.2 HIV classification and viral clades

HIV is a lentivirus that belongs to the retrovirus family (*Retroviridae*) which has a positive-sense single-stranded RNA genome that can be reverse transcribed for integration into the host genome (Weinberg et al. 1991). Lentiviruses, such as HIV, are complex retroviruses that contain additional genes that encode regulatory and accessory proteins for efficient viral replication and are also able to infect and integrate into the genome of both dividing and non-dividing cells. Although there are two types of HIV, type-1 (HIV-1) is more transmissible

and has higher infectivity compared to type-2 (HIV-2) (Nyamweya et al. 2013). This difference accounts for the worldwide spread of HIV-1 compared to HIV-2 with the latter predominantly limited to West Africa and has a slower progression to AIDS (Nyamweya et al. 2013). Both types of HIV are the result of interspecies transmission of simian immunodeficiency virus (SIV), from either infected chimpanzees or western gorillas which gave rise to HIV-1 or sooty mangabeys which gave rise to HIV-2 (Sharp and Hahn 2011).

For HIV-1 there are four distinct lineages, group M and N that originated from chimpanzees as well as group O and P that originated from western gorillas, with group M (the “major” group) being responsible for greater than 98% of global HIV-1 infections (Sharp and Hahn 2011; D'arc et al. 2015). Within group M, viruses can be classified into a further nine subtypes/clades: A, B, C, D, F, G, H, J and K based on differences in the genome (Geretti 2006). In particular, clade C is the most prevalent, representing almost half of the circulating viruses, while clades F, H, J and K make up less than 1% of the global HIV-1 infections (Figure 1.1). Phylogenetic analysis has also exposed recombination events of genetically distinct strains (Robertson, Hahn, and Sharp 1995), resulting in circulating recombinant forms (CRFs) that add to the diversity of HIV-1, as well as unique recombinant forms (URFs) that appear to have no onward transmission (Robertson et al. 2000; Tongo, Dorfman, and Martin 2015). Virus clades and CRFs are typically found in specific geographical locations (Buonaguro, Tornesello, and Buonaguro 2007), with clade B predominantly found in the Americas and Europe, clade C in India and CRF01_AE in Southeast Asia (Hemelaar et al. 2019). However, there are often multiple HIV-1 clades and CRFs found within each region and the distribution can be dynamic (Bbosa, Kaleebu, and Ssemwanga 2019). A key example is the distribution across Africa, which is primarily clade C in the south, a mix of clade A, B, C or D in the east but in the west and central Africa all clades and many CRFs are present (Hemelaar et al. 2011; Hemelaar et al. 2019).

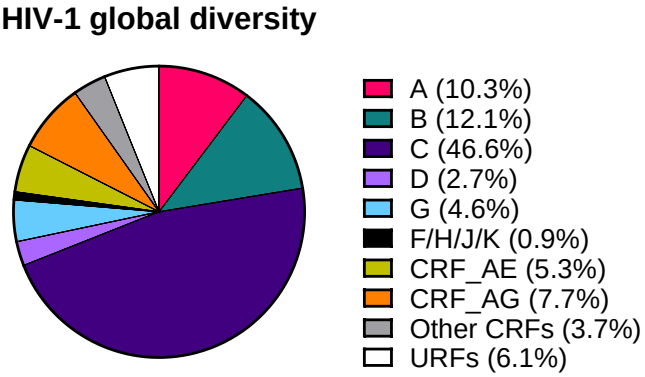

Figure 1.1 Global diversity of HIV-1 clades and recombinant forms.

Proportion of different clades, circulating recombinant forms (CRF) or unique recombinant forms (URF) from individuals infected around the world with HIV-1 between 2010 and 2015. Adapted from (Hemelaar et al. 2019).

1.1.3 HIV-1 genome and structure

The HIV-1 RNA genome is ~9.2kb and consists of nine viral genes that are flanked by long terminal repeats (LTRs) required for recognising integration sites in the host genome as well as initiating and regulating transcription (Burnett et al. 2009). As shown in Figure 1.2, the genes encoding for structural and enzymatic proteins are *gag*, *pol* and *env*. The *gag* gene encodes a 55 kDa polyprotein (p55) that is processed by the protease enzyme into proteins including the matrix (p17), capsid (p24), nucleocapsid and p6 which are essential for the internal structure of the virion (Freed 2015). The *pol* gene encodes the enzymatic proteins: protease, reverse transcriptase and integrase which are vital for HIV replication. The *env* gene encodes the gp160 envelope glycoprotein (Env), required for entry into host cells, that is cleaved into a gp120 subunit, exposed on the surface, and a transmembrane subunit, gp41 (Merk and Subramaniam 2013). Additional genes in the viral genome include *vif*, *vpr*, *vpu* and *nef* which encode accessory proteins for efficient replication. The final two genes are *tat* and *rev* which encode regulatory proteins for transcription and translation of the viral genome. The overall structure of the HIV-1 virion is also depicted in Figure 1.2, which is spherical in shape and approximately 120nm (Gentile et al. 1994), encapsulating all of

the viral proteins within a host-derived membrane, including the capsid core which contains the ssRNA genome.

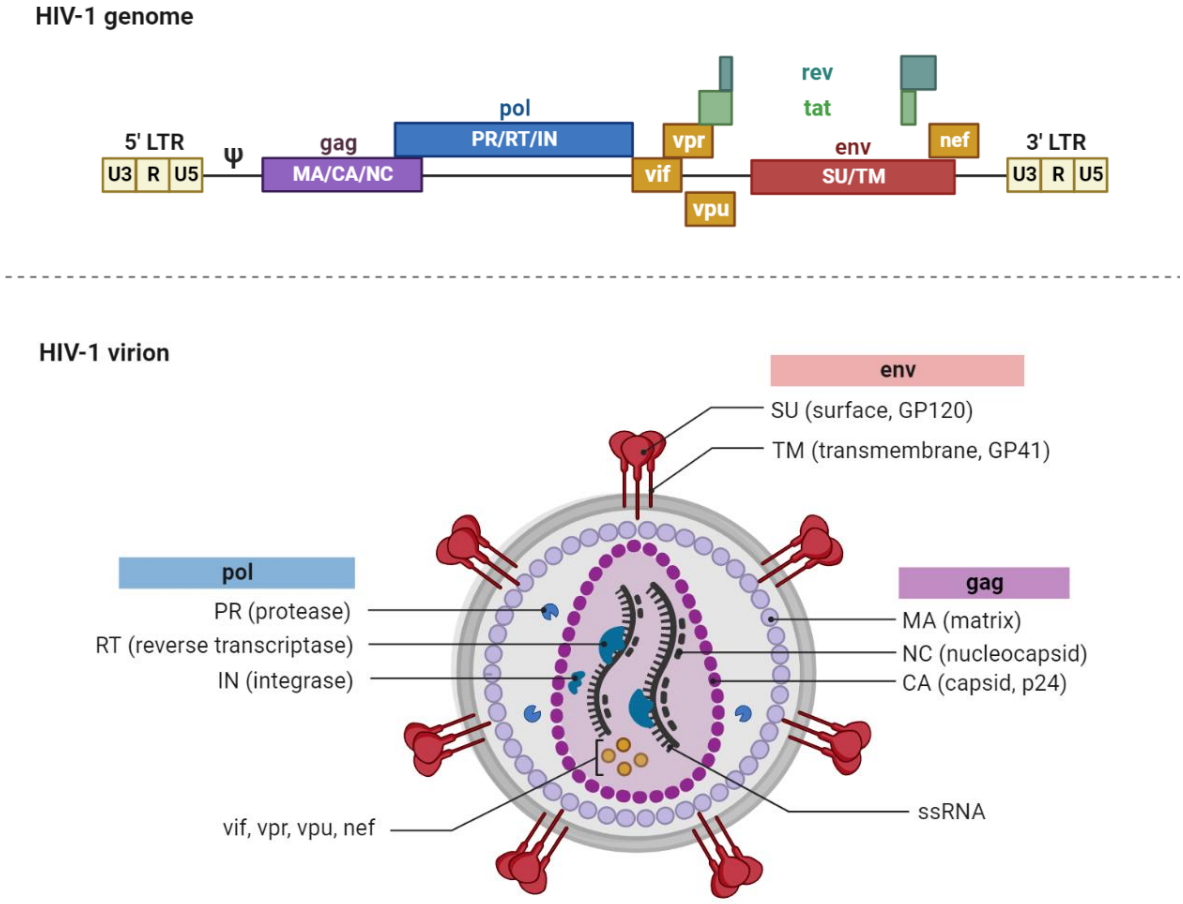

Figure.1.2 HIV-1 genome and virion structure.

Two identical single-stranded (ss), positive-sense, RNA molecules form the HIV-1 genome which consists of nine genes: *gag, pol, vif, vpr, vpu, tat, rev, env* and *nef* flanked by long terminal repeats (LTRs). This genome is packaged with nucleocapsid inside the capsid core of the HIV-1 virion, along with reverse transcriptase, integrase and accessory proteins (vif, vpr, vpu and nef). The capsid core is enclosed within a lipid biolayer derived from the host cell membrane containing Env proteins, with matrix proteins forming an inner membrane layer. Diagram created using Biorender.

1.1.4 HIV clinical course

Transmission of HIV occurs upon breaching physical barriers, predominantly through sexual contact but also by needle sharing and from mother to child during pregnancy, childbirth or breastfeeding (Shaw and Hunter 2012). In the absence of treatment, HIV infection can progress at different rates (Rutherford et al. 1990) but in adults has been predicted to occur over an average of 9.5 years before resulting in AIDS (Ross et al. 2018), which is defined by the development of a serious, life-threatening disease or by a CD4+ T cell count that persists below 200 cells/µL (Gazzard 2008). The course of acute and chronic HIV infection prior to AIDS can be determined by measuring a variety of viral markers (Fiebig et al. 2003).

After transmission, HIV initially becomes established in host cells at the point of entry before entering the systemic system and spreading to lymphoid organs, with HIV RNA detectable in the blood on average 5 days post-infection (Fiebig et al. 2003). The extent of viraemia is indicated by the level of HIV RNA (Mellors et al. 1996), often referred to as the viral load (VL), which peaks during acute infection due to the rapid dissemination of HIV. At this stage, other viral markers become detectable, beginning with the HIV p24 (capsid) antigen (Fiebig et al. 2003). In addition, the early innate immune response to HIV results in a cascade of cytokines that can also be detected in plasma (Stacey et al. 2009). Then, after a few weeks of infection, the onset of the humoral response and thus seroconversion can be identified, which in some individuals coincide with flu-like symptoms (Schacker et al. 1996). Another immunological marker of the acute phase of infection is the reduction in CD4+ T cells, with considerable depletion of cells in the gastrointestinal tract that are targeted for infection and result in cell death (Brenchley et al. 2004; Guadalupe et al. 2003). Additionally, it has been suggested that this cell depletion leads to disruption of the intestinal wall and consequently increased permeability (Kapembwa et al. 1991), allowing microbial translocation and release of LPS that contributes to immune activation during HIV infection (reviewed by (Sandler and Douek 2012)). Finally, detection of HIV envelope (gp120, gp41 or gp160) and p31 (polymerase) antigens occurs as the viral load declines to a steady state,

known as the viral set point, marking the end of the acute phase of infection (Fiebig et al. 2003). This reduction in viraemia is largely due to the depletion of CD4+ T cells but can also be mediated by the CD8+ T cell response (Ndhlovu et al. 2015; Goonetilleke et al. 2009). It has also been found that the viral set point can be an indicator of the length of the latency phase on infection, with a lower set point leading to prolonged latency (Lyles et al. 2000).

The initial immune response to HIV is mediated by innate cells in an attempt to restrict infection through cytotoxic activity and antigen presentation as well as the secretion of cytokines to orchestrate cellular responses, such as the activation and recruitment of additional immune cells (Carrington and Alter 2012). Notably, plasmacytoid dendritic cells are essential to this response, secreting more type I interferon (IFN)-α than any other immune cell to induce IFN-stimulated genes (ISGs) for antiviral activity, as well as presenting antigen to stimulate the adaptive immune response (Beignon et al. 2005). In contrast, natural killer (NK) cells mediate the direct killing of infected cells and secrete IFN-γ for proinflammatory responses (Roff, Noon-Song, and Yamamoto 2014). A limited level of control to maintain the viral set point is also achieved by cytotoxic T lymphocytes (CTLs) along with the humoral response produced by B cells during the chronic yet asymptomatic stage of infection, although ultimately HIV can escape recognition by introducing mutations into the epitopes targeted (Wei et al. 2003; Barton et al. 2016). Even the extremely small population of HIV-infected individuals (<1%) who can spontaneously suppress the viral load to undetectable levels (<50 c/mL), known as elite controllers, eventually lose control over time and progress to disease (Borrell et al. 2021).

The development of ART to suppress viral replication and thus achieve sustained control of HIV below the level of detection was vital for PLWH and was first introduced in 1986 as a monotherapy (Furman et al. 1986). However, with the emergence of drug resistance, this approach was changed to combination ART (cART) which is more effective due to the administration of multiple drugs with different inhibitory mechanisms (Arts and Hazuda 2012). While ART enables PLWH to live a near-normal lifespan, this treatment needs to be taken daily to be effective and is not capable of eliminating the latent

reservoir of HIV, thus interruption of ART leads to viral rebound (Chun et al. 1999; Zhang et al. 1999).

1.1.5 Target cells of HIV and dissemination

While CD4+ T cells are the main target of HIV infection, dendritic cells, macrophages and monocytes that also express CD4 can be infected by HIV, which is mediated by the Env glycoprotein located on the surface of the virion (Dalgleish et al. 1984; McDougal et al. 1986). HIV Env initially engages with host cells via the CD4 receptor, causing the Env to undergo a conformational change required for binding to the co-receptor CCR5 or CXCR4 (Sattentau and Moore 1991; Trkola et al. 1996; Feng et al. 1996). Following co-receptor binding, the HIV Env undergoes another conformational change to initiate membrane fusion with the host cell (Jones, Korte, and Blumenthal 1998). Typically HIV-1 uses only one type of co-receptor and thus determines the viral tropism. HIV that enters cells via the CCR5 co-receptor is described as R5-tropic, while HIV that enters cells via the CXCR4 co-receptor is described as X4-tropic and those that are capable of using either co-receptor are R5X4 dual tropic (Berger et al. 1998). Transmitter founder (T/F) viruses are predominantly R5 tropic, with resistance to HIV infection observed in individuals with cells lacking CCR5 expression (CCR5-Δ32 mutation) (Samson et al. 1996) and more recently have been successfully used in haemopoietic stem-cell transplantation for long-term remission of HIV-1 (Gupta et al. 2020; Allers et al. 2011). The emergence of X4-tropic viruses, known as co-receptor or tropism switching, instead appears to arise more frequently in the later stages of infection (Huang et al. 2007; Esbjörnsson et al. 2010).

Most new HIV infections in adults occur from mucosal transmission following sexual contact. Mounting evidence suggests that CD4+ T cells with high CCR5 expression, in particular T helper 17 (Th17) cells, are critical to the establishment of infection in the mucosa and thus are likely to be the first cell type infected, leading to their rapid depletion (as reviewed by (Xu, Wang, and Veazey 2013)). In addition, a subset of monocyte-derived macrophages in the vaginal mucosa are CCR5+ and thus susceptible to HIV infection and support

replication (Shen et al. 2009). Circulating monocytes are also targets of HIV infection, yet replication is limited by restricted factors and thus enables these cells to have a longer lifespan than infected CD4+ T cells (Nicholson et al. 1986). Although HIV virions can bud from an infected cell and disseminate until coming into contact with another target cell, HIV can also be transmitted directly from an infected cell to a target cell, with viral transfer occurring by cell-to-cell spread (Jolly and Sattentau 2004). For instance, a virological synapse between cells can be formed following the interaction between CD4 on the uninfected target cell and Env presented on the infected cell, leading to the polarisation of proteins for efficient viral assembly and budding (Jolly et al. 2004). The spread of HIV from cell to cell has also been found to be more efficient than cell-free infection and is thought to be the main mode of viral dissemination (Chen et al. 2007).

1.1.6 HIV replication

The replication lifecycle of HIV is represented in Figure 1.3 and indicates the stages that can be inhibited by ART. HIV replication begins with attachment and entry into the target cell by fusion with the plasma membrane. First, the trimeric form of the Env glycoprotein binds to CD4 on the surface of the cell via the gp120 subunit, which results in conformational rearrangement of the gp120 variable loops to expose the co-receptor binding site (discussed further in section 1.2.1). As mentioned earlier, CCR5 or CXCR4 can act as the co-receptor depending on the HIV tropism. Although binding to the co-receptor does not appear to induce additional conformational changes (Shaik et al. 2019), this interaction is thought to stabilise the open (CD4-bound) conformation of Env and anchor the virion near the target cell membrane to enable fusion. Structural analysis has indicated that the initial CD4 binding induces refolding of the gp41 subunit for insertion of the fusion peptide into the cell membrane and formation of a pore to allow the viral capsid to enter the cell (Melikyan et al. 2000; Ozorowski et al. 2017). Once the capsid core containing the viral RNA enters the cell it is converted into viral DNA by the viral reverse transcriptase. While it has previously been proposed that disassembly of the capsid core occurs directly after entering the cytoplasm for

the release of the viral RNA prior to reverse transcription (Mamede et al. 2017) (as shown in Figure 1.3), more recent evidence has challenged this dogma. Studies now suggest that reverse transcription occurs within the capsid core, but the timing of capsid disassembly is still under debate as to whether this is triggered once viral DNA has been synthesised in the cytoplasm (Rankovic et al. 2017), upon docking at the nuclear pore (Francis and Melikyan 2018) or once imported into the nucleus (Dharan et al. 2020).

Integration of newly synthesised viral DNA into the genome of the target cell is then mediated by the viral integrase enzyme and transcription is initiated from the 5' LTR after the viral protein tat (trans-activator of transcription) recruits CDK9, cyclin and other host factors to the transactivation response (TAR) element (Ne, Palstra and Mahmoudi 2018). The viral protein encoded by the *rev* gene then provides stabilisation to the transcribed, singly spliced or unspliced viral mRNA by binding to the Rev response element for export from the nucleus (Blissenbach et al. 2010). Once in the cytoplasm, viral mRNA is translated by cellular (ribosomal) machinery to produce each of the viral proteins (described in section 1.1.3) that are assembled at the plasma membrane. The newly formed virions then bud from the plasma membrane and are released from the cell. Finally, maturation of the HIV-1 virion is mediated by the viral protease enzyme that cleaves the Gag polyprotein into the structural proteins required to produce infectious virus.

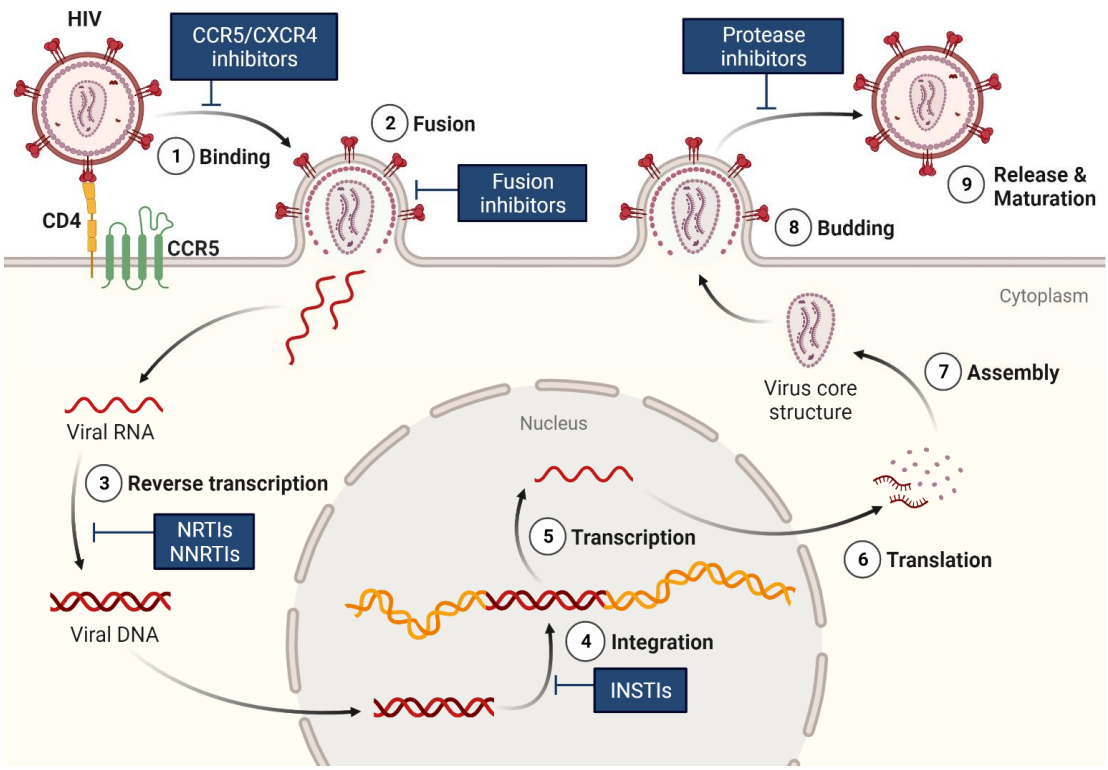

Figure 1.3 HIV-1 replication cycle.

Entry of HIV-1 into the host cell begins with (1) binding of the Env glycoprotein to receptors (CD4 and CCR5/CXCR4) on the cell surface, followed by (2) fusion of HIV-1 with the cell membrane for release of the capsid core into the cytoplasm. The viral single-stranded RNA undergoes (3) reverse transcription into viral double-stranded DNA that is imported into the nucleus and is (4) integrated into the host genome for (5) transcription and (6) translation of viral proteins that are (7) assembled at the cell membrane. The immature virus is encapsulated in the cell membrane, incorporating Env on the surface, in a process called (8) budding. Finally, the (9) release and maturation of the virion occurs as the viral protease cleaves Gag for the formation of infectious HIV-1. Stages during the replication cycle of HIV-1 that are inhibited by antiretroviral drugs are highlighted in blue boxes, such as reverse transcriptase inhibitors (NNRTIs and NRTIs) and integrase inhibitors (INSTIs). Diagram created using Biorender.

1.1.7 The latent HIV reservoir

During HIV replication, viral DNA is predominantly integrated into chromatin with high gene density and transcriptional activity (Schröder et al. 2002), yet can also integrate into transcriptionally silent areas in more quiescent cells such as resting CD4+ T cells forming a latent reservoir (Siliciano et al. 2003). In addition, it has been shown that the human silencing hub (HUSH) complex can remodel chromatin to silence gene expression, not only of cellular genes but also of HIV proviral genes (Tchasovnikarova et al. 2015). The involvement of the HUSH complex in establishing HIV latency has also been supported by the finding that antagonism of this complex by the HIV-2 accessory protein vpx resulted in reactivation (Yurkovetskiy et al. 2018).

Although effective ART is now initiated as soon as HIV infection is clinically evident, this is too late to prevent the establishment of latently infected cells which arise during acute infection (Henrich et al. 2017) and persist as long-lived memory cells that continue to proliferate (Reeves et al. 2018). In agreement with this, monkeys infected with SIV that had ART initiated by day 3 showed that this was not early enough to prevent the seeding of a viral reservoir, which was reactivated upon interruption of ART (Whitney et al. 2014). The capacity of HIV to form a latent reservoir also poses a problem for the development of an antibody HIV vaccine, which would need to induce sterilising immunity to prevent integration events.

1.2 HIV Env

1.2.1 Structure and function

The *env* gene that encodes the gp160 polyprotein is integrated into the host genome and thus is transcribed and translated by host cell machinery. Specifically, translation of gp160 occurs in the rough endoplasmic reticulum (ER), yet remains attached to the membrane with the cytoplasmic tail facing out into the cytoplasm (Haffar, Dowbenko, and Berman 1988). This results in an orientation where the cytoplasmic tail remains inside the virion during Env

incorporation at the plasma membrane. In addition, during processing, N-linked glycans are added by the host according to glycosylation sites (N-X-S/T, where X can be any amino acid except proline) encoded in the viral sequence and monomeric gp160 oligomerises into trimers, although can also lead to the assembly of dimers (Earl, Doms, and Moss 1990). Finally, the glycosylated Env is trafficked to the Golgi network for further processing as well as cleavage by the host protease furin into gp120 and gp41, which remain non-covalently associated (Dubay et al. 1995). In particular, the formation of trimers and the cleavage step are crucial to producing functional, fusion competent Env required for entry into host cells (Checkley, Luttge, and Freed 2011).

On the surface of HIV virions, the functional Env glycoprotein is formed of a trimer of gp120-gp41 heterodimers (Zhu et al. 2003). Each heterodimer consists of the gp120 subunit presented on the surface of the virion which is anchored into the membrane by the gp41 subunit and thus only partially protrudes from the surface. Within the gp120 subunit there are five relatively conserved regions (C1-C5) that form the core inner and outer domains as well as five variable loops that stem from the core (V1-V5) (Kwong et al. 1998; Huang et al. 2005). As mentioned earlier, the initial attachment to target cells is mediated via Env binding of CD4 and CCR5/CXCR4. The CD4 binding site on gp120 is located within a recessed hydrophobic pocket at the inner and outer domain interface (Kwong et al. 1998). Upon binding, this induces outward rotation of gp120 and rearrangement of the V1 and V2 loops from their apical position to expose the V3 loop concealed beneath, resulting in a more open conformation of the trimeric Env (Mbah et al. 2001; Julien et al. 2013). The relevance of the V3 loop is due to its involvement in co-receptor binding, specifically the base and the tip (also known as the crown) which are more conserved than the variable stem (Huang et al. 2005). In comparison to the gp120 subunit, the gp41 subunit is more conserved and is likely due to its role in mediating the fusion of the virion with the cell membrane. The gp41 subunit consists of a fusion peptide and two heptad repeats that facilitate fusion, as well as a transmembrane domain and a cytoplasmic tail for anchoring into the virion membrane. While the fusion peptide initially breaches

the cell membrane, the heptad-repeat domains in each gp41 fold together to form a six-helix bundle that acts as a pore for the transfer of the viral capsid across the cell membrane (Melikyan et al. 2000).

Interestingly, even in the absence of a ligand, it has been observed that gp120 in the trimeric Env is capable of fluctuating between different conformations reversibly, with changes in the positioning of the V1/2 loops (Munro et al. 2014). The spontaneous repositioning of variable loops, consistent with a shift from the closed, pre-fusion conformation to a CD4-bound state, suggests a dynamic nature of the Env glycoprotein. Furthermore, while the presence of ligand was shown to stabilise the trimeric Env in a single conformation that was more open, this was not true for Env from HIV isolates less susceptible to antibody neutralisation (Munro et al. 2014). The link between Env conformation and neutralisation can be classified by a tiering system that will be discussed further in section 1.4.1.

1.2.2 Env evasion of neutralising antibodies

During the humoral immune response neutralising antibodies (nAbs) directed towards the Env trimer can block viral entry and prevent infection by interfering with the engagement of host cell receptors (CD4) or co-receptors (CCR5 or CXCR4), by stabilising pre-fusion Env to prevent membrane fusion or by inducing Env decay (Ugolini et al. 1997; Julien et al. 2013; Platt, Gomes, and Kabat 2012; Ruprecht et al. 2011; Kim, Leaman, and Zwick 2014; Blattner et al. 2014; Wang et al. 2017). However, the number of properly folded, functional Env trimers on the surface of each virion is estimated to be as few as 7-10 per virion (Zhu et al. 2003). The instability of the Env trimer likely contributes to the limited number of functional Env that can be targeted by nAbs. For instance, non-functional Env in the form of uncleaved trimers, non-oligomerised gp120-gp41 monomers and gp41 stumps (after the shedding of gp120 from trimers) are also present on the surface of the virion, which expose non-neutralising epitopes that are usually occluded in the functional trimer (Haim, Salas, and Sodroski 2013; Moore et al. 2006). Furthermore, the dissociation of gp120 from gp41 during the fusion of HIV virions with target cells contributes to the

presence of circulating gp120 monomers that expose immunodominant epitopes. These aberrant versions of Env are thought to assist HIV in evading nAbs by acting as decoys. Consequently, many antibodies are elicited by the humoral response that can bind Env but not neutralise HIV.

The HIV-1 Env is also a glycoprotein and as such is covered by a high density of N-linked glycans that consist of ~50% of the gp120 mass (Doores et al. 2010). These large heterogeneous glycans are generally less immunogenic than the protein itself due to being host-derived and shield sites on Env from nAb access (Berndsen et al. 2020). In fact, the structure of gp120 has revealed that the majority of the Env surface is concealed by N-linked glycans and the more conserved regions, such as those involved in receptor binding, are recessed or obscured by the surrounding highly variable loops (Wyatt et al. 1998). The length of gp120 variable loops such as V1/2 can additionally impact the ability of nAbs to reach Env epitopes, and the observation of longer variable loops arising over the course of infection is another mechanism that aids evasion of the humoral response (Sagar et al. 2006). As such, these factors contribute to the elicitation of nAbs that are often only strain-specific. Finally, as mentioned earlier, HIV is capable not only of cell-free dissemination but also of cell-to-cell spread which is more efficient and reduces the length of time and opportunity for nAbs to target functional Env on the virion surface before infecting another cell (Chen et al. 2007; McCoy et al. 2014).

1.2.3 Env diversity and the antibody arms race

HIV virions that avoid the immune response enter target cells and integrate their genome into the host genome using the viral reverse transcriptase that is highly error-prone, with a mutation rate of 3.4×10^{-5} per base during a single round of replication due to a lack of proofreading (Mansky and Temin 1995). Consequently, this introduces random mutations into the genome that contribute to the diversity of HIV-1. In particular, mutations introduced into the *env* gene can result in the removal of residues in nAb epitopes, or introduce new potential N-linked glycosylation sites (PNGS) that if glycosylated hinder access to epitopes, leading to Env variants that are neutralisation resistant

(Bar et al. 2012). These variants of HIV are therefore able to persist and continue to infect new cells. Over time this selects affinity-matured nAbs that can target the new variants and thus exert selection pressure on the virus, resulting in an ongoing cycle regarded as an evolutionary, immunological arms race (Bonsignori, Liao, et al. 2017). The high mutational rate of HIV-1 in addition to a short replication cycle and the capacity to recombine results in an increasing quasi-species within an individual, and thus viral diversity, over the course of infection (Hemelaar 2012).

For context, the extent of HIV-1 variation that can occur within a single individual after six years of infection has been found comparable to that of global influenza A in a single year (Weiss 2003). This highlights the extreme antigenic diversity that the humoral response has to contend with. Although most individuals can produce effective nAbs against the infecting (autologous) virus, demonstrated by the selection pressure applied on HIV-1 (Wei et al. 2003; Richman et al. 2003), ultimately the humoral response is always one step behind due to the requirement for additional antibody maturation to respond to the resulting viral variant. Therefore, this dynamic between the maturation of the humoral response and the evolving HIV Env leads to reoccurring viral escape, with antibodies failing to effectively control HIV-1 infection.

1.3 Antibodies

B cells each produce a unique immunoglobulin (Ig) that is initially displayed as a surface-bound B cell receptor (BCR) and, after terminal differentiation into a plasma blast or plasma cell can be secreted as an antibody. The vital role of antibodies is to mediate the humoral response in the defence against pathogens, by recognising and binding to diverse antigens.

Structurally, antibodies are Y-shaped glycoproteins comprised of two identical heavy chains (HCs) and two identical light chains (LCs) with a molecular weight of approximately 150 kDa. The two arms of an antibody are held together by disulphide bonds between the two HCs, and each arm is formed of one HC paired with one LC which are also linked by disulphide bonds

(Figure 1.4). Within each HC and LC there is a variable region and a constant region. While the variable regions determine the antigen specificity, the constant region is primarily responsible for the effector function and determines the isotype of the antibody. These functions are attributable to the fragment antigen binding (Fab) domain and the fragment crystallisable (Fc) region respectively, which are held together by a hinge region (Schroeder and Cavacini 2010). This hinge provides a degree of flexibility in the movement of the two Fab domains which each have an antigen binding site formed of three complementary determining regions (CDRs) from each chain, as depicted in Figure 1.4, that consist of highly variable loops connected by framework regions (FWRs). Given that an antigen often has many epitopes, different antibodies can bind to the same antigen in distinct ways. In addition, similarity in epitopes on different antigens can enable antibodies to have cross-reactivity.

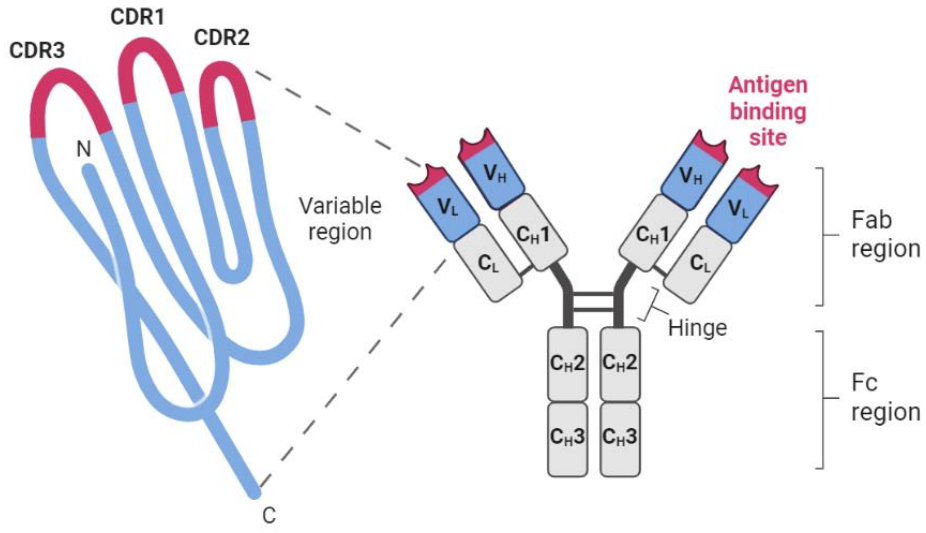

Figure 1.4 The antibody structure of IgG.

Two heavy chains and two light chains form the antibody structure which is held together by disulphide bonds. The Fab domain required for antigen binding consists of variable (V) regions from both the heavy and light chain, as well as constant (C) regions from the heavy and light chain. The antigen binding site is formed of three complementary determining regions (CDRs) from the variable regions of both the heavy and light chain. The hinge region links the Fab domains to the Fc region, which is comprised of constant regions from only the heavy chain. Diagram created using Biorender.

1.3.1 Role of different isotypes

The specific isotype of an antibody is defined by the heavy chain Fc and is determined based on the chain used for the constant region: IgM (μ chain), IgD (δ chain), IgG (γ chain), IgA (α chain) and IgE (ε chain). In addition, the IgG isotype can be further divided into four subclasses: IgG1, IgG2, IgG3 and IgG4 and the IgA isotype can be divided into two subclasses: IgA1 and IgA2 (Schroeder and Cavacini 2010). These different isotypes each have a distinct protein structure, glycosylation, effector function and tissue distribution.

For instance, the size of antibodies based on their isotype differs, with IgM and IgE having an additional constant region domain that extends the Fc region and overall makes these molecules larger than IgD, IgG or IgA. Moreover, while IgG and IgE are monomeric, IgA has the potential to form dimers and IgM forms pentamers. As IgM antibodies are the first to be secreted in the primary response to pathogen exposure these tend to be low-affinity, however, the formation of a pentametric structure gives rise to 10 antigen binding sites which can provide high avidity and are effective at activating the complement system (Czajkowsky and Shao 2009). Conversely, IgG and IgA antibodies that arise following maturation to a specific antigen are higher-affinity and predominantly function by blocking toxins or preventing viruses from entering cells, known as neutralisation. The dimeric form of IgA enables transport across epithelial barriers to protect mucosal surfaces (Fagarasan and Honjo 2003), yet monomeric IgG typically remains in circulation within the blood and extrafollicular fluid which constitutes almost 75% of the total antibodies in plasma (Dietzen 2018). As well as differences in isotype tissue distribution, the high proportion of IgG in plasma is also likely to be a result of the longer half-life of IgG compared to other isotypes (Schroeder and Cavacini 2010).

In addition to neutralisation, IgG can mediate effector functions indirectly via the Fc, such as activating the complement system. Binding antigen by IgG can also result in the formation of immune complexes which cross-link Fc receptors expressed by innate immune cells for activation, to induce phagocytosis or cytotoxic effects (Hogarth 2015; Bournazos and Ravetch 2017). The multiple

different effector functions mediated by IgG, therefore, make these antibodies crucial to the humoral response.

1.3.2 B cell development

In the bone marrow, hematopoietic stem cells (HSC) undergo differentiation via several stages to form immature B cells in an antigen-independent manner. The initial stage of B cell development begins with the differentiation of HSCs into common lymphoid progenitor (CLP) cells that are the precursor for both B and T cells, yet are fated to become B cells upon interaction with IL-7 (Kikuchi et al. 2005). Formation of the pro-B cell occurs following rearrangement and recombination of the Ig heavy chain gene until an intact heavy chain is produced (Melchers 2015). The heavy chain, in conjunction with a surrogate light chain, is then presented on the surface of pre-B cells that upon productive signalling halts further recombination events and initiates proliferation to generate multiple clones with the same heavy chain (Hess et al. 2001). Termination of this proliferation stage enables VJ recombination of light chain genes which begins at the kappa (κ) locus but if unsuccessful switches to the lambda (λ) locus (Collins and Watson 2018). Expression of the complete IgM BCR on the cell surface marks the transition into an immature B cell (Figure 1.5), which is screened for autoreactivity based on the BCR binding of self-antigen before exiting the bone marrow. This central tolerance checkpoint of B cells is necessary due to the finding that as high as 75% of immature B cells have autoreactive BCRs (Wardemann et al. 2003), although only strong autoreactivity is selected for clonal deletion. Immature B cells with BCRs that exhibit weak autoreactivity instead undergo receptor editing that can rescue many cells (Halverson, Torres, and Pelanda 2004) or are silenced by anergy and so can persist but are unresponsive to self-antigen (Goodnow et al. 1988).

Once B cells enter the periphery they are deemed as transitional B cells which co-express IgM and IgD (Figure 1.5). These transitional B cells are subjected to a second checkpoint, known as peripheral tolerance, which is poorly defined but thought to ensure the deletion of autoreactive B cells that may have bypassed the first, central tolerance, checkpoint (Carsetti, Köhler, and Lamers

1995; Wardemann et al. 2003). However, this can lead to the removal of B cells that also recognise foreign antigens, which often have overlapping epitopes with self-antigens (Watanabe et al. 2019). B cells that pass this second checkpoint mature into naïve B cells (Figure 1.5), which also co-express IgM and IgD but are characterised by the downregulation of cell surface markers such as CD38, CD24 and CD10 (Sims et al. 2005). Mature B cells in the periphery can then enter the final stage of development which leads to the activation and differentiation of B cells into memory or antibody-secreting cells, discussed in more detail in section 1.3.6.

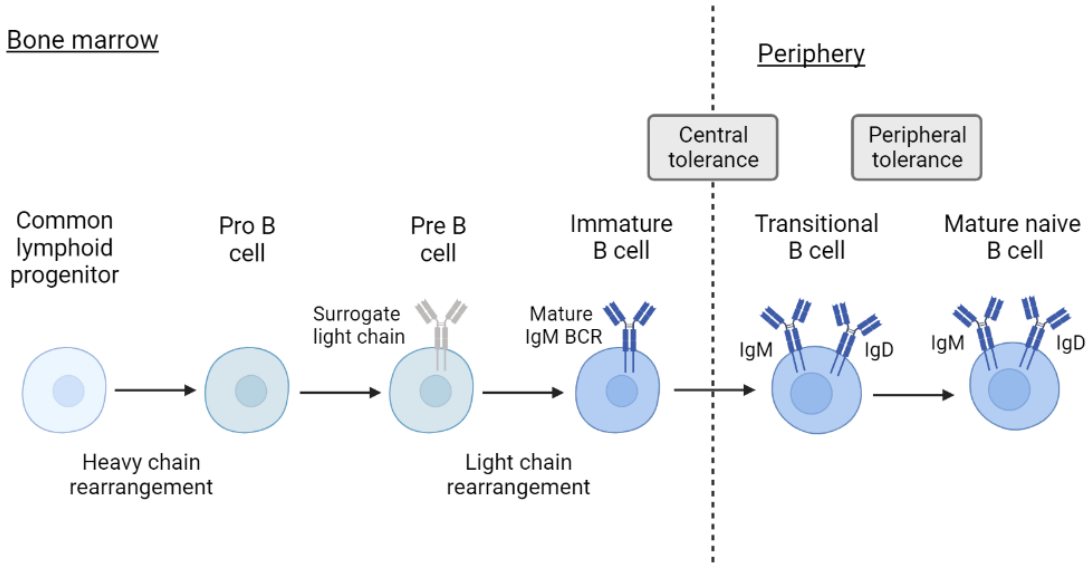

Figure 1.5 B cell development.

The early stages of human B cell development occur within the bone marrow, differentiating from common lymphoid progenitor cells into immature B cells, with the assembly of a mature BCR. Entry of immature B cells into the periphery as transitional B cells is permitted after passing central tolerance checks and following peripheral tolerance checks can mature into naïve B cells that can respond to antigen. Diagram created using Biorender.

1.3.3 VDJ recombination

The diversity of the antibody repertoire is essential to be able to respond to a vast array of different antigens. Rearrangement of Ig germline sequences in the heavy chain locus and kappa (κ) or lambda (λ) light chain locus during the early stages of B cell development generates each a unique BCR. As mentioned earlier, the variable regions of Ig heavy and light chains contain antigen binding sites, comprised of the three hypervariable CDRs on each chain, and therefore it is the combination of both the heavy and light chains that determine the specificity. The heavy chain variable region is encoded by a variable (V), diversity (D) and joining (J) gene segment, yet the light chain variable region is encoded by only a V and J gene segment. In the heavy chain locus, there are 39 functional V gene segments (categorised into seven different families), 25 functional D gene segments (also categorised into seven different families) and six J gene segments (Matsuda et al. 1998). In the kappa chain locus, there are 40 V gene segments (categorised into seven different families) and five J gene segments (Zachau 2000; Hieter, Maizel, and Leder 1982). Finally, in the lambda chain locus, there are 30 functional V gene segments (categorised into 11 different families) and seven J gene segments (Pallarès et al. 1998). Assembly of individual gene segments into variable regions is known as V(D)J recombination, which is directed by recombination signal sequences and mediated by recombination activating gene 1 (RAG1) and 2 (RAG2) to create combinatorial diversity (Oettinger et al. 1990; Tonegawa 1983).

Specifically, double-stranded DNA breaks are introduced by RAG1/2 to rearrange the gene segments and bring them into close proximity for recombination by non-homologous end joining. For the heavy chain, a single D and J gene segment are first brought together, before being joined with a V gene segment to form the complete VDJ sequence. For the (kappa or lambda) light chain, only one recombination event occurs to assemble a single V and J gene segment into the complete VJ sequence. Imprecise joining of Ig gene segments following recombination further contributes to the diversity, known as junctional diversity, especially within the CDR3 which is the product of gene

recombination in each chain. However imprecise joining can also lead to frameshifts that result in non-productive sequences (Tonegawa 1983). Nevertheless, this process is capable of generating a large repertoire from a limited number of Ig gene segments and, when also taking into consideration the diversity introduced upon pairing of the heavy and light chain, it was estimated that at least 10^{12} different antibodies can be produced (Alberts B 2002). Investigation of the actual antibody sequences in circulation instead proposed that within a single individual, there was an upper limit of around 3 million to 9 million different antibodies, based on the number of unique heavy chain CDR3 (CDRH3) sequences (Arnaout et al. 2011).

1.3.4 Importance of the CDRH3 in antibodies

The antigen binding site is predominantly comprised of the CDR1, CDR2 and CDR3 loops from both the Ig heavy and light variable chains, although the FWRs that link the CDRs can also influence antigen binding (Sela-Culang, Kunik, and Ofran 2013). In particular, the CDR3 is the most diverse due to being encoded by the junction of V, D and J genes in the heavy chain and the junction of the V and J gene in the light chain, whereas the CDR1 and CDR2 are encoded solely by germline V genes. As the CDRH3 has the greatest variation (from combinatorial and junctional diversity) this region is a key determinant of the antigen specificity and affinity of an antibody and is also used to identify clonal relationships between antibodies (Xu and Davis 2000).

The length of the CDRH3 is also known to play a significant role in antigen binding, with long CDRH3 loops (>20 AAs) being a unique feature of many HIV-1 broadly neutralising antibodies (bnAbs) (Yu and Guan 2014). For instance, a long CDRH3 alters the structure of the antigen binding site and can provide antibodies with the ability to access recessed epitopes, such as the HIV Env protein surface beneath the glycan shield (Yu and Guan 2014). In agreement with this, it has been observed that the length of the CDRH3 can relate to the nature of the antigen targeted, with antibodies specific for large antigens such as viruses and proteins possessing longer CDRH3 loops than antibodies against smaller antigens such as peptides (Johnson and Wu 1998;

Collis, Brouwer, and Martin 2003). However, long CDRH3s are often associated with autoreactivity and thus are infrequent features in the antibody repertoire, due to negative selection during B cell development (Wardemann et al. 2003).

1.3.5 Class switch recombination

Rearrangement of the constant genes within the Ig heavy chain locus enables mature B cells to alter the isotype of their BCR for different effector functions, without affecting the antigen specificity. This process is known as class switch recombination (CSR) and is achieved by intrachromosomal deletion and recombination between switch regions located upstream of each constant region gene (except Cδ) (Stavnezer, Guikema, and Schrader 2008). Class-switching is initiated by activation-induced deaminase (AID) and other enzymes to introduce double-stranded DNA breaks to allow for recombination of the VDJ with a different constant chain gene (Xu et al. 2012). In the heavy chain locus, the constant region genes are organised in the following order: Cμ, Cδ, Cγ3, Cγ1, Cα1, Cγ2, Cγ4, Cε, Cα2. Mature, naïve B cells already express both IgM (μ) and IgD (δ), therefore activation upon pathogen exposure induces CSR to downstream isotypes IgG (γ), IgA (α) or IgE (ε). As class-switching follows the order of the locus, genes between switch regions are deleted and thus prevent subsequent switching back to isotypes upstream.

The induction of CSR in B cells following antigen stimulation can be T cell dependent, activated by the engagement of CD40 on B cells, or T cell independent, activated by dual engagement of receptors including the Toll-like receptor (TLR) and the BCR (Park et al. 2009; Pone et al. 2010). A recent *in vivo* study has shown that, even in response to T-cell dependant antigens, CSR can occur within the first few days of primary infection (Roco et al. 2019). And although T-cell dependant CSR was originally thought to occur within the germinal centre (GC), there is now mounting evidence to suggest that this occurs predominantly in B cells before entering the GC (Roco et al. 2019; King et al. 2021).

The specific isotype induced has also been associated with the type of antigen that the B cell is exposed to, with T-cell dependent antigens such as protein antigens resulting in IgG1 and IgG3, while stimulation in a T-cell independent manner such as by polysaccharide antigens may instead induce IgG2 (Vidarsson, Dekkers, and Rispens 2014). Furthermore, the isotype selected can also be influenced by cytokine stimuli that activate transcription factors to direct class-switching to specific switch regions for recombination (Chen and Wang 2019). B cells can also undergo subsequent CSR such as during a secondary immune response but are limited by the constant genes remaining and thus the terminal position of IgG4 may explain why this is associated with repeated antigen exposure (Aalberse et al. 2009).

1.3.6 The germinal centre response and affinity maturation

Following antigenic stimulation, B cells can further diversify their BCR and undergo somatic hypermutation (SHM) and affinity maturation in the GC, which is a specialised microenvironment (depicted in Figure 1.6). The establishment of a GC occurs upon the entry of antigen into secondary or tertiary lymphoid organs, via draining lymph nodes. Antigen that is displayed on the surface of dendritic cells can migrate to a site concentrated with T cells (T cell zone) where the antigen is presented in major histocompatibility (MHC) class II complexes (Randolph 2001). Naïve, cognate CD4+ T cells capable of binding to the peptide MHC-II complex are activated and differentiate into T follicular helper (Tfh) cells, which upregulate the chemokine receptor CXCR5 (Ansel et al. 1999). This enables Tfh cells to migrate along a chemokine gradient towards B cell follicles that express the CXCR5 ligand (CXCL13). Concurrently, binding of the cognate antigen by B cells via their BCR results in activation that leads to the upregulation of CCR7, as well as antigen internalisation and processing (Reif et al. 2002). The former enables stimulated B cells to migrate along a chemokine gradient towards the T cell zone in lymphoid tissue, which express CCR7 ligands (CCL19 and CCL21). Once at the border of the B cell follicle and T cell zone, B cells present antigen peptides in MHC-II complexes to Tfh cells and receive help in the form of stimulatory signals by cytokines and through the CD40L engagement of CD40

on the B cell for survival and proliferation to initiate the GC (Schwickert et al. 2011; Yang Shih et al. 2002). Conversely, these B cells may instead differentiate into early, extrafollicular memory B cells (Taylor, Pape, and Jenkins 2012) or short-lived plasma cells that provide an early antibody response to infection and this fate is thought to be driven by high affinity for the antigen (Chan et al. 2009).

About a week after the initial antigen encounter, the rapid clonal expansion of GC precursor B cells forms two distinct compartments, the light zone (LZ) and the dark zone (DZ) (Allen, Okada, and Cyster 2007). B cells within the DZ continue to proliferate and express the chemokine receptor CXCR4 which maintains their localisation in the DZ (Allen et al. 2004). During this time, SHM is introduced into Ig V(D)J genes by AID at specific sequence motifs, known as hotspots, that are more frequent within the CDRs required for antigen binding than the FWRs required for structural integrity (Rogozin and Diaz 2004; Tang et al. 2020). Migration of B cells into the LZ occurs as B cells downregulate CXCR4 and upregulate CXCR5 (Allen et al. 2004). In the LZ, B cells express their newly mutated BCR to acquire antigen presented on follicular DCs. BCRs with the highest affinity for the antigen can obtain more antigen and thus can present more peptide MHC-II complexes to Tfh cells which provide signalling for positive selection (Victora et al. 2010). This results in the selected cells returning to the DZ for additional rounds of division and selection in the GC, cycling between the DZ and LZ for further SHM and affinity maturation. Alternatively, at this stage B cells can differentiate and exit the GC as a long-lived plasma cell that migrates to the bone marrow for antibody secretion or exit as a memory B cell (MBC) that persists in circulation to provide a more rapid secondary response (Kräutler et al. 2017; Laidlaw et al. 2017). In addition, B cells in the LZ that do not receive Tfh help are subjected to the default fate of apoptosis and those with deleterious mutations introduced into the Ig V(D)J also undergo apoptosis (Mayer et al. 2017). Finally, while terminally differentiated cells, such as plasma cells, cannot re-enter the GC, it is possible for unswitched and switched activated MBCs to re-enter the GC for increased maturation (King et al. 2021). Evidence also suggests that class-

switched B cells, such as IgG B cells which have longer cytoplasmic tails and thus stronger BCR signalling than IgM B cells, are retained in the GC for longer (King et al. 2021).

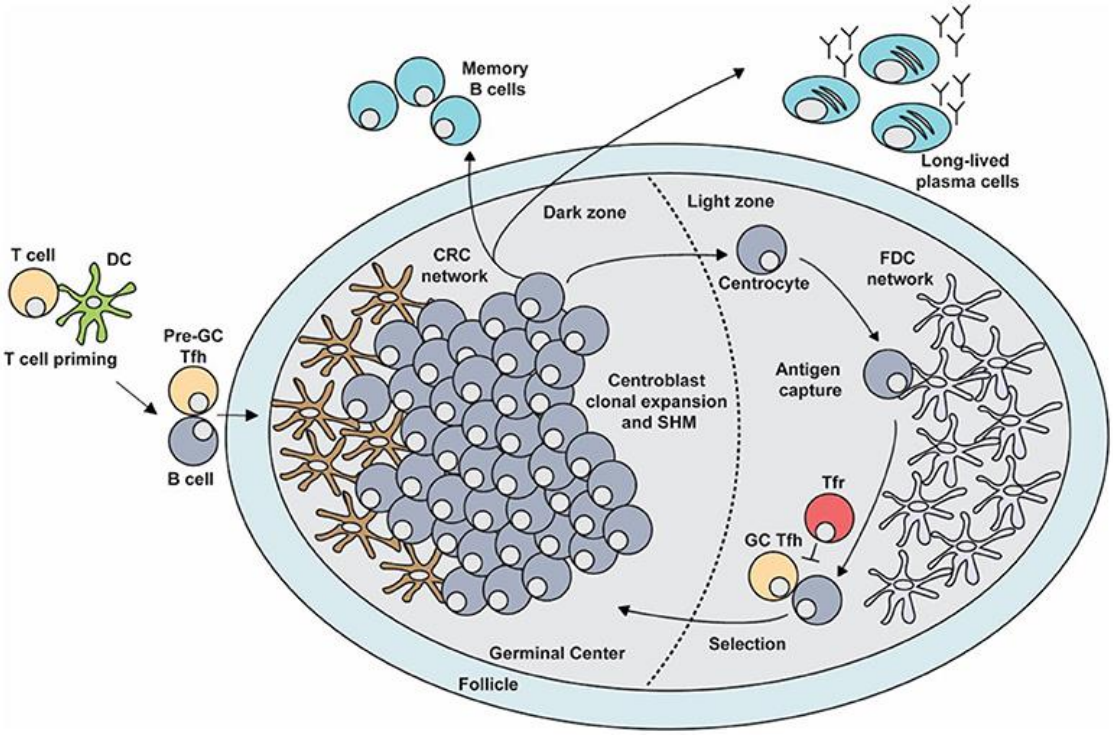

Figure 1.6 The germinal centre reaction.

The formation of a germinal centre (GC) is initiated within secondary lymphoid organs in an antigen-dependent manner. Specifically, dendritic cells (DC) display antigen that activates cognate CD4+ T cells to differentiate into T follicular helper (Tfh) cells which migrate towards B cell follicles. Presentation of antigen by B cells to Tfh cells provides stimulatory signals that result in the clonal expansion of B cells and the formation of two distinct compartments, the dark zone (DZ) and the light zone (LZ), that form a GC reaction. Rapidly dividing B cells, referred to as centroblasts, undergo somatic hypermutation (SHM) within the DZ. Downregulation of CXCR4 and upregulation of CXCR5 enables these cells to migrate into the LZ as cells referred to as centrocytes. Within the LZ, centrocytes that acquire antigen from follicular DCs can display this to Tfh cells to receive survival signals. Interference of Tfh and B cell interactions by T follicular regulatory (Tfr) cells that have a suppressive function also play a role in regulating the GC reaction. Positively selected centrocytes then downregulate CXCR5 to re-enter the DZ for additional rounds of clonal expansion and SHM or can differentiate into effector cells that exit the GC as an affinity-matured memory B cell or plasma cell. Image from (Stebegg et al. 2018).

1.4 HIV bnAbs

Most HIV-infected individuals can produce initial strain-specific nAbs that apply selection pressure on the virus and constrict HIV-1 infection (Wei et al. 2003; Richman et al. 2003). However, as mentioned earlier in section 1.2.3, this leads to viral escape and thus an immunological arms race as the humoral response adapts to respond to viral variants. Remarkably, after a few years of infection, a small subset of individuals (10-30%) can develop nAbs that exhibit cross-neutralisation of different HIV strains, and an even smaller proportion (1-10%) produce bnAbs that can neutralise numerous HIV-1 strains from different clades and thus are referred to as elite neutralisers (McCoy and McKnight 2017).

The first generation of antibodies classed as bnAbs against HIV-1 were discovered in the early 1990s and isolated using phage display (Burton et al. 1991) and hybridoma technology (Buchacher et al. 1994). Since then advances in methods to generate and assess monoclonal antibodies (mAbs) led to a second generation of more potent bnAbs being isolated via single B cell cloning, following either single B cell culture or antigen-specific sorting (McCoy and Burton 2017). More recently, a novel technique utilising a matched genomic and proteomic approach has also been used to deconvolute polyclonal plasma and successfully isolate bnAb lineages (Sajadi et al. 2018). In total, over 300 antibodies consisting of bnAbs and their lineage members have been isolated from HIV-infected individuals (Yoon et al. 2015) and have been studied to investigate their development, structural and genetic features, as well as the epitopes that they target.

1.4.1 The pseudo-typed virus system and tiering for determining neutralisation capacity

A fundamental step in the isolation of bnAbs against HIV-1 was to first identify individuals with broad and potent plasma/serum neutralisation. An efficient *in vitro* system to measure the neutralisation activity of plasma against HIV Env pseudo-typed virus (PV) was first described in 2003 using TZM-bl luciferase reporter cells to quantify the level of infection (Wei et al. 2003). This TZM-bl

assay was later optimised and validated to enable a standardised assessment of antibody-mediated neutralisation (Sarzotti-Kelsoe et al. 2014). However, the high diversity of HIV-1 (described earlier in sections 1.1.2 and 1.2.3) meant that a vast array of Env variants have been pseudo-typed for use in these assays, making comparisons between neutralisation capacities difficult. The screening of a diverse virus panel from all major circulating clades and different stages of infection using a plasma pool enabled viruses to be ranked based on their sensitivity to antibody neutralisation, leading to the development of a tiering system to facilitate systematic characterisation of neutralising responses (Seaman et al. 2010). The tier of the virus has also been found to relate to the Env conformation, with circulating, harder-to-neutralise strains typically classed as tier 2/3 viruses having a predominantly closed trimeric conformation, unlike tier 1A/B viruses that have more of an open/intermediate Env conformation that is easier to neutralise (Montefiori et al. 2018; Munro et al. 2014).

The establishment of reference viruses and standard panels of Env PVs such as the 6 PV panel, 12 PV global panel and 118 multi-clade PV panel has also been essential for the assessment of the neutralisation breadth by mAbs and polyclonal plasma (Griffith and McCoy 2021). In particular, the standard 6 PV panel was identified following the evaluation of neutralisation exhibited by large numbers of plasma samples from epidemiologically diverse HIV-infected individuals against multiple panels of PVs from globally circulating strains (Simek et al. 2009). This minimal set of six (tier 2) PVs from four different clades was capable of reflecting the neutralisation breadth of plasma against the larger panels of viruses and thus provides a rapid screening tool for neutralisation capacity. In addition, this analysis revealed individuals with elite activity against HIV-1, which was defined as the ability to neutralise a minimum of one PV with an ID_{50} titre of 300 or more, across four different clades (Simek et al. 2009). A neutralisation scoring system was later devised, based on the average log-transformed titres achieved against PVs, to rank and characterise the neutralisation capacity of plasma (Landais et al. 2016). Furthermore, the identification of individuals with elite neutralisation (score >2) has proven

valuable, with follow-up studies confirming that bnAbs can be isolated from the B cells of these donors (Walker et al. 2009; Walker et al. 2011).

1.4.1.1 Elite neutralisers vs elite controllers

Elite neutralisers are HIV-infected individuals that have extremely broad plasma neutralisation and thus have the capacity to produce bnAbs (Walker et al. 2009; Walker et al. 2011). However, only 1-10% of individuals exhibit elite neutralisation (McCoy and McKnight 2017), and despite demonstrating plasma breadth against heterologous viruses are unable to control their autologous virus. The factors associated with the development of a broadly neutralising response are still in contention and will be addressed in detail in section 1.5.

In contrast, elite controllers (who in some contexts have also been referred to as long-term non-progressors depending on the level of control) are an even rarer subset of individuals that are infected with replication-competent HIV-1, yet are capable of maintaining the viral load below the level of detection (< 50 c/mL) in the absence of ART (Woldemeskel, Kwaa, and Blankson 2020; Okulicz and Lambotte 2011). The spontaneous suppression of viraemia by elite controllers results in stabilised CD4+ T cell counts, limits the development of disease and reduces the chance of HIV transmission, although transient blips in viraemia and gradual loss of control occur over time (Borrell et al. 2021). The mechanism of viral control in these individuals is heterogenous but is not thought to be mediated by antibodies (Pereyra et al. 2008; Deeks and Walker 2007). Instead, control has been largely associated with the expression of specific human leucocyte antigen (HLA) alleles, that encode MHC proteins for antigen presentation, and the prevalence of strong Gag-specific cytolytic CD8+ T cell responses (Migueles et al. 2000; Bailey et al. 2006; Kiepiela et al. 2007; Lambotte et al. 2005). However, it is thought that control by cytolytic CD8+ T cells is lost due to exhaustion and/or viral escape (Rosás-Umbert et al. 2019).

1.4.2 Defining bnAbs and their epitopes

Currently, a specific criterion of what constitutes an HIV bnAb has not yet been established (as reviewed by (Griffith and McCoy 2021)). However, evaluation of the neutralisation breadth and potency achieved against the standard 118 multi-clade PV panel revealed that second-generation bnAbs could neutralise 30-100% of the PVs with a geometric mean of 3.6 µg/mL or less (Griffith and McCoy 2021). The capacity of bnAbs to neutralise such a diverse range of heterologous strains from multiple clades is ultimately achieved by targeting the most conserved regions on the functional, trimeric Env. Characterisation of bnAb binding to HIV-Env has revealed five main epitopes: the CD4 binding site (CD4bs), trimer apex, high mannose patch (HMP), gp120-gp41 interface (including the fusion peptide) and the membrane-proximal region (MPER), illustrated in Figure 1.7.

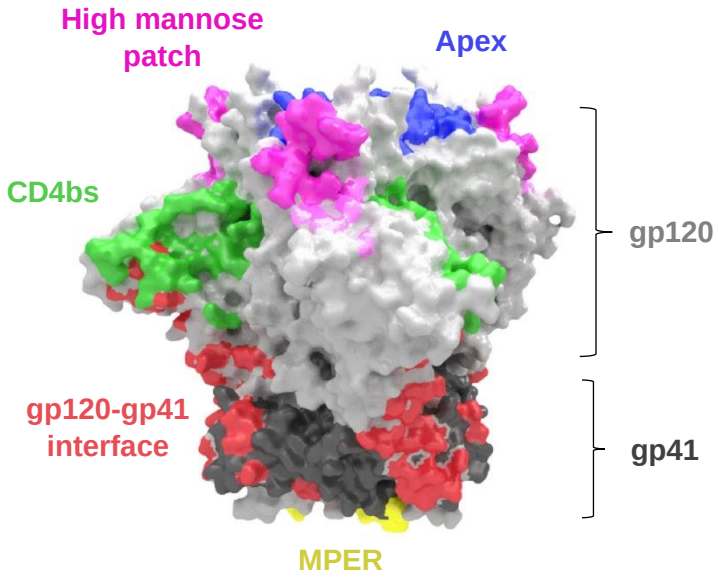

Figure 1.7 HIV-1 Env epitopes targeted by bnAbs.

The gp120 and gp41 subunits, coloured in light grey and dark grey, that form the trimeric Env structure are modelled based on glycosylated BG505 SOSIP.664. Epitopes targeted by bnAbs are shown by the coloured regions, with the CD4bs in green, the apex in blue, the high mannose patch in pink, the gp120-gp41 interface in red and the MPER in yellow. Adapted with permission from (McCoy and Burton 2017).

1.4.2.1 CD4bs

The initial interaction of HIV with CD4 on the host cell is mediated by the CD4bs on the HIV Env trimer. This conserved region on Env is therefore a site of vulnerability that can be targeted by the humoral response to block HIV entry. However, the CD4bs is located in a recessed hydrophobic pocket at the interface of the outer and inner domains of the gp120 subunit (Kwong et al. 1998) and is more accessible on monomeric gp120 than the functional Env trimer (Lyumkis et al. 2013). Nevertheless, neutralising antibodies against the CD4bs can be elicited, and the ability of bnAbs to access this epitope on harder-to-neutralise tier 2/3 viruses is dependent on their angle of approach, predominantly using their CDRH2 (for antibodies with VH1-2 or VH1-46 gene usage) or their CDRH3 for binding (Zhou et al. 2015).

Most CD4bs bnAbs, and even nAbs with limited breadth, contact the residue D368 on the CD4 binding loop which is highly conserved (Zhou et al. 2015), although there are a few exceptions which are glycan dependent instead (Wibmer et al. 2016; Balla-Jhagjhoorsingh et al. 2013; Freund et al. 2015). While glycans such as N276 and N462 surrounding the CD4bs do not substantially mask this epitope they can limit antibody access. Yet these glycans can be accommodated or in some cases be bound by bnAbs that possess short and compact light chain CDR (CDRL) loops which avoid steric clashing (West et al. 2014; Balla-Jhagjhoorsingh et al. 2013; Pancera et al. 2014). It has additionally been shown through structural analysis that the VH1-2 gene restricted, VRC01-class of bnAbs require a short 5 AA CDRL3 for packing in between the Loop D and V5 loop to allow the CDRH2 to contact the CD4 binding loop (Zhou et al. 2013). However, progression towards greater neutralisation breadth has ultimately been achieved by bnAbs that acquire extensive mutations that enable them to mimic CD4 binding by burying into gp120 to engage conserved residues in the CD4 binding loop and have reduced contact with more variable regions nearby, such as the V5 loop (Bonsignori et al. 2016; Sajadi et al. 2018; Huang et al. 2016; Scheid et al. 2011).

1.4.2.2 Trimer apex

While the trimer apex is not directly involved in viral entry the V1/V2 loops in this region are necessary to shield the V3 loop that is involved in co-receptor binding (Wang et al. 2018; Ozorowski et al. 2017). As a consequence, nAbs targeting the apex can prevent the opening of the trimer and co-receptor binding. In the closed pre-fusion conformation of the Env trimer, the V1/V2 loops are comprised of a five-stranded β-barrel, with the strands consisting of conserved residues while more variable residues are located in the loops connecting each strand (Pan et al. 2015). However, analysis of the predominantly open Env conformation, found on tier 1A viruses or after CD4-binding, has revealed that residues in the V2 domain can instead adopt a coil or helical conformation that exposes a short linear peptide that can be bound by nAbs (Wibmer et al. 2018; Liao, Bonsignori, et al. 2013). Although analysis has revealed that the residues in this peptide contacted by nAbs with limited breadth are similar to those targeted by bnAbs, for instance residues at position 168-171 in the positively-charged V2 site (Andrabi et al. 2015; Liao, Bonsignori, et al. 2013; van Eeden et al. 2018; Pinter et al. 2005), the different secondary structures that the V2 can adopt results in distinct epitopes. Indeed, trimer apex bnAbs have instead been found to have a preference for the quaternary Env structure which exhibits a β-conformation of the V2 (McLellan et al. 2011), and are therefore capable of targeting tier 1B and tier 2/3 viruses that exhibit an intermediate and/or closed conformations of the Env trimer (Montefiori et al. 2018; Ivan et al. 2019).

Although glycans that protrude from the V2 strand B mask the cavity at the trimer apex and the positively-charged lysine-rich site on the V2 strand C, this region is accessible to bnAbs with a long, negatively charged CDRH3 (Gorman et al. 2020). In addition, glycans at the trimer apex have been shown to form part of the epitope targeted by bnAbs, with the glycan at position 160, in particular, being necessary for binding, demonstrated by the partial or complete loss of neutralisation against mutant viruses lacking N160 (Andrabi et al. 2015). In contrast to most apex bnAbs, V2-specific nAbs with limited neutralisation breadth have shorter CDRH3s and as a result, are unable to neutralise viruses with long V2 loops (Gorny et al. 2012). Nevertheless, as

demonstrated by the CAP256 antibody lineages, nAbs with a long CDRH3 do not always have neutralisation breadth as this must protrude out from the antibody with a certain orientation (Doria-Rose et al. 2016). However, another binding approach by bnAb BG1 has revealed that a protruding CDRH2 can also contact the protein residues in the V2 beneath the glycan shield, yet exhibit lower neutralisation breadth than other apex bnAbs (Wang et al. 2017).

1.4.2.3 High mannose patch

Another vulnerable region of Env is the V3 loop, which is required for co-receptor binding and makes contact via the base and the tip (known as a crown) but also consists of a variable stem (Huang et al. 2005). Most V3 targeting antibodies are only capable of neutralising tier 1 viruses with a predominantly open conformation that is similar to the CD4-bound state where the V3 loop is exposed, and due to the high sequence variability of the V3 stem often elicits strain-specific antibodies (Moody et al. 2015). However, V3-specific nAbs capable of binding to the V3 tip/crown, for instance 447-52D, have demonstrated the capacity to target tier 2 viruses, although only weak/incomplete neutralisation has been observed and thus implies access to the epitope is poor or transient (Han et al. 2019; Hioe et al. 2010). Analysis of strain-specific neutralisation following the immunisation of rabbits revealed that nAbs had an overlapping footprint at the base of the V3 with high mannose patch bnAbs, however, the specific epitope targeted and the binding mechanism differed by making contact with peptide residues in the V1 loop rather than V3 glycans (Nogal et al. 2020).

The conserved $_{324}$GDIR$_{327}$ linear sequence at the base of the V3 loop is masked not only by the V1/V2 domain but also by the N-linked glycan supersite (N295, N301, N332, N339, N385 and N392) in the closed Env trimer, typical of circulating tier 2 viruses (Krachmarov et al. 2006; Behrens et al. 2016). BnAbs to this site can incorporate glycans into their epitope and often bind to the N332 glycan, however, the use of long CDR loops also enables bnAbs to extend beyond this glycan supersite to make contact with the conserved peptide residues below (Mouquet et al. 2012; Sok et al. 2016). An exception to this is the bnAb 2G12 which binds solely to glycans (Sanders et al. 2002). In fact, high mannose patch bnAbs can often bind to multiple V3

glycans or glycans in close proximity, which gives a degree of flexibility in their epitope (Sok, Doores, et al. 2014; Barnes et al. 2018), and can enable these bnAbs to accommodate changes to N-linked glycosylation sites that arise from selection pressure.

1.4.2.4 Gp120-gp41 interface

The trimeric Env is comprised of three heterodimers of gp120 and gp41 subunits that require cleavage to be functional and mediate viral fusion. The gp120-gp41 interface can therefore be bound by nAbs to inhibit fusion, either by stabilising Env to prevent gp41 conformational changes (Blattner et al. 2014) or by destabilising Env to induce decay (Lee et al. 2015). As the interface of each heterodimer is also next to the interface of the other two heterodimers, this forms one large contiguous area on the Env trimer. Consequently, nAbs that target the gp120-gp41 interface have distinct modes of binding, with dependence on different glycans and peptide residues across the subunits, as well as different angles of approach (McCoy 2018; Parker Miller et al. 2021). Despite this, most gp120-gp41 interface bnAbs target the pre-fusion, trimeric conformation of Env, with only 35O22 found to have improved binding following CD4 engagement due to greater access to the epitope as the Env initiates fusion (Huang et al. 2014).

In addition, the ability to bind highly conserved glycans at the interface is common to bnAbs, except for clonally related bnAbs 3BC176 and 3BC315 which can accommodate glycans but do not bind them (Lee et al. 2015). In particular, the glycan at position 88 in the gp120 subunit is targeted by several interface-specific bnAbs, with the removal of this glycan reducing their neutralisation capacity (Huang et al. 2014; van Gils et al. 2016; Kong et al. 2016). Conversely, the epitope of 3BC176 and 3BC315, located at the base of the trimer between two gp41 subunits, is partially occluded by the glycan at position 88 and upon removal leads to enhanced neutralisation (Lee et al. 2015). Additional glycans at positions 230, 241, 234 or 276 in the gp120 subunit are also bound by some interface bnAbs (Huang et al. 2014; Scharf et al. 2014), while other bnAbs have a dependency on glycans in the gp41 subunit, at positions 611, 625 or 637 (Falkowska et al. 2014; Huang et al. 2014).

A subset of interface bnAbs is also capable of binding to the conserved fusion peptide in the gp41 subunit, namely ACS202 and VRC34.01 as well as PGT151 which can partially bind to this region (van Gils et al. 2016; Kong et al. 2016). Although ACS202 and PGT151 both contact the fusion peptide predominantly using a long CDRH3 with a hydrophobic YYYY motif, these bnAbs have different angles of approach (Yuan et al. 2019). On the other hand, VRC34.01 has a much shorter CDRH3 and instead forms a hydrophobic groove to bind the exposed N-terminal residues in the fusion peptide using all CDRs, except CDRL2 (Kong et al. 2016). Lastly, many of the gp120-gp41 interface-specific nAbs with limited breadth (elicited in non-human primate immunisation studies) appear to have overlapping footprints with bnAbs and can even target the fusion peptide, yet differ by contacting more variable residues and/or are less accommodating of the glycan at position 611 (Cottrell et al. 2020).

1.4.2.5 MPER

The MPER of the gp41 subunit consists of two identical, highly conserved α-helices that are partly embedded in the lipid membrane of the virion (Sun et al. 2008). For that reason, nAbs capable of binding to this region on Env have the potential for breadth in neutralisation by blocking structural rearrangement of the gp41 necessary for fusion, or in the case of the bnAb 10E8 can even destabilise the Env trimer before fusion (Kim, Leaman, and Zwick 2014). However, the mechanism of binding to the MPER epitope by bnAbs has revealed an initial requirement for lipid binding to bring the antibody into close proximity to the base of the gp41 (Alam et al. 2007; Alam et al. 2009; Williams et al. 2017), and hence have a degree of polyreactivity. In addition, the MPER epitope in gp41 is hydrophobic and only accessible in the pre-fusion intermediate Env conformation triggered by receptor binding, giving a very brief opportunity for nAbs to bind (Frey et al. 2008).

The majority of bnAbs that are specific for the MPER epitope have a long CDRH3 (≥ 20 AAs) with a hydrophobic tip to mediate binding and have been found to approach MPER from a similar direction (Williams et al. 2017). Another common trait of MPER bnAbs is the usage of an IgG3 isotype, which could suggest a requirement for a long, flexible hinge region for binding to this

epitope, yet MPER bnAbs with an IgG1 isotype and thus shorter hinge have also been identified more recently (Krebs et al. 2019; Zhang et al. 2019). These IgG1 MPER bnAbs were found to share the same V-genes as bnAb 4E10, yet had a shorter CDRH3 of an average length (15 AAs). Nevertheless, the IgG1 bnAbs with an average length CDRH3 had reduced neutralisation potency compared to 4E10, which is thought to be attributed to fewer interactions by the CDRH3 with the MPER epitope (Zhang et al. 2019). Finally, analysis of the inferred germline and intermediate antibodies in MPER bnAb lineages has revealed that increasing SHM was required for neutralisation breadth (Williams et al. 2017; Pinto et al. 2019).

1.4.3 Unusual features of bnAbs

In the germinal centre B cells that undergo multiple rounds of maturation result in the generation of antibodies with higher affinity for the antigen and increasing levels of SHM. Antigen-experienced (IgG) antibodies display an average SHM in the variable heavy gene (V_H) of between 5.6% and 9.4% (IJspeert et al. 2016). However, within HIV-infected individuals, Env-specific antibodies (gp140 reactive) were found to have a significantly higher number of V_H mutations than non-specific antibodies (Scheid et al. 2009). Moreover, the level of mutation in HIV bnAbs is higher than in nAbs with limited breadth (Scheid et al. 2009; Klein et al. 2013). Longitudinal studies have provided evidence that the accumulation of mutations in bnAbs occurs over time, in response to emerging variants of HIV, and that increasing SHM can result in increasing neutralisation breadth (Liao, Lynch, et al. 2013; MacLeod et al. 2016; Bonsignori, Kreider, et al. 2017; Bonsignori et al. 2016). This demonstrates the role of the evolutionary arms race between the humoral response and HIV in the development of bnAbs, which often requires 2-3 years and in some cases up to 5 years of ongoing infection (Gray et al. 2011; Liao, Lynch, et al. 2013; Sajadi et al. 2018; Doria-Rose et al. 2014; MacLeod et al. 2016; Bonsignori, Kreider, et al. 2017). While all bnAbs exhibit at least 9% SHM in the V_H, there are also bnAbs within each epitope specificity that have extreme levels of SHM, attaining up to 43% V_H mutation (Griffith and McCoy 2021). This high level of SHM is unusual even in antigen-experienced

antibodies and suggests excessive rounds in the GC or the ability to re-enter the GC for further rounds of maturation. It has also been found that bnAbs can acquire increased insertions and/or deletions, predominantly in their CDRs (Kepler et al. 2014), again reflecting a complex affinity maturation pathway.

Another unusual feature of HIV bnAbs is that many have a CDRH3 length that exceeds 20 AAs and can be as long as 37 AAs (Doria-Rose et al. 2014), yet the average CDRH3 length of antibodies in the human repertoire is 15-16 AAs (Shi et al. 2014; DeKosky et al. 2016). As discussed above in section 1.4.2, long CDRH3s appear to be favourable for nAbs targeting conserved regions on the HIV Env that are recessed or harder to access, yet are often autoreactive and thus removed during B cell development (Wardemann et al. 2003). Indeed, many bnAbs have been reported to be autoreactive or polyreactive (Liu et al. 2015; Prigent et al. 2018), which may imply the tolerance for self is altered to enable these B cells to pass checkpoints during development (as discussed in section 1.3.2). Antibodies with long CDRH3 sequences are primarily generated during VDJ recombination and arise from the selection of specific D and J gene segments, rather than due to an accumulation of insertions in the CDRH3 during SHM (Briney, Willis, and Crowe 2012), which was an earlier theory. In particular, the use of the longest J_H gene (JH6) was more frequently identified in antibodies with a long CDRH3 and the introduction of nucleotides by N-addition or P-addition during recombination also correlated with a longer CDRH3 (Briney, Willis, and Crowe 2012). In agreement with this, HIV bnAbs with a long CDRH3 have skewed use of the JH6 gene (Burton and Hangartner 2016). Furthermore, while mAbs with CDRH3s as long as 30 AAs, which is comparable to the CDRH3 length of the apex bnAb PG9, have also been found in the B cell repertoire of HIV naïve individuals, these were rare due to being predisposed to negative selection (Willis et al. 2016). This shows that while long CDRH3s are not unique to HIV bnAbs they are also not frequently found in antibody repertoires. Therefore the high prevalence of bnAbs with a long CDRH3 is unusual and suggests that this feature is selected. Additionally, an unusually short CDRL3 of 5 AAs has been observed in many bnAbs from different donors that target the same epitope, specifically, CD4bs bnAbs with a VH1-2 gene usage, which

has structural similarity necessary to avoid steric clashes upon binding (Zhou et al. 2013).

1.4.4 Epitope mapping of broadly neutralising plasma

BnAbs can be isolated from HIV-infected individuals with elite plasma neutralisation, but to do so it is beneficial to first identify the specificity of the neutralising response. However, evaluation of antibodies in plasma that mediate neutralisation breadth is challenging due to the complex, polyclonal nature of the humoral response with diverse antibody lineages that can target a variety of epitopes on the HIV Env. The extensive characterisation of previously isolated bnAbs has identified the key regions and residues on Env that are targeted (as reviewed in section 1.4.2), and this knowledge can be employed to epitope map the plasma response.

The neutralising response of bnAbs is predominantly targeted towards epitopes on the gp120 subunit, therefore broad plasma is typically tested first for gp120-specific neutralisation using protein absorption assays with recombinant monomeric gp120 (Landais et al. 2016; Walker et al. 2010; Doria-Rose et al. 2017). Epitope mapping studies have also made use of mutant PVs with alterations to peptide residues or glycans found in each of the bnAb epitopes to map the neutralisation specificity of plasma (Landais et al. 2016; Walker et al. 2010; Doria-Rose et al. 2017). In addition, HIV-2 chimeric PVs containing the HIV-1 MPER can also be used to identify plasma neutralisation directed to the MPER epitope (Gray et al. 2009). Although these studies are often capable of mapping broad plasma responses to only one or two bnAb epitopes, the presence of multiple epitope specificities in plasma can make this difficult to decipher. To try and overcome this problem, computational analysis using an algorithm to delineate the antibody specificities of polyclonal plasma was developed to predict bnAb specificities based on the neutralisation of reference bnAbs against the same, pre-defined PV panel, termed neutralisation fingerprinting (Georgiev et al. 2013). This fingerprinting algorithm has been used to investigate super-infection and responses following immunisation as well as to epitope map individual nAbs and thus has

been optimised further to expand its use, such as with large-scale cohorts (Doria-Rose et al. 2017).

The recent advancement of proteomic and genomic approaches has also enabled the polyclonal response to be deconvoluted, by purifying out antigen-specific mAbs from plasma, digesting them for mass spectroscopy analysis and comparing resolved sequences to genetic databases (Wine et al. 2015). Although this has only been achieved by one research group so far (Sajadi et al. 2018), this approach has successfully identified one of the broadest CD4bs-specific bnAbs, using affinity chromatography to isolate the IgG1, gp120-specific mAbs from plasma. However, classical techniques such as the use of binding ELISAs with mutations in recombinant gp120 protein were still required to epitope map nAbs to the CD4bs (Sajadi et al. 2018). Finally, another more recent approach has been established to map the epitope clusters of polyclonal antibody response using cryo-EM, to generate high-resolution imaging of mAb binding (Bianchi et al. 2018; Antanasijevic et al. 2021), yet it is not possible to determine which of these mAb specificities are responsible for neutralisation breadth. Therefore, the use of mutant PVs continues to be the most informative approach to epitope mapping plasma neutralising responses.

1.4.5 HIV vaccine attempts to date

The induction of a neutralising antibody response upon vaccination provides the correlate of protection in most existing vaccines (Plotkin 2010). However, attempts so far to elicit protective antibodies against HIV-1 have been unsuccessful (Flynn et al. 2005; Pitisuttithum et al. 2006; Rerks-Ngarm et al. 2009; Hammer et al. 2013; Gray et al. 2021; Barouch et al. 2018). While the RV144 vaccine trial with recombinant canarypox vector and gp120 protein is the only study reported to have a level of efficacy in preventing HIV infection, this was very low (31%) and only just above the significance threshold (Rerks-Ngarm et al. 2009). Additionally, this elicited a poor neutralising antibody response that was unable to target tier 2 viruses typical of those in circulation (Rerks-Ngarm et al. 2009; Montefiori et al. 2012) and was not identified as a correlate of protection (Haynes et al. 2012). Moreover, follow-up studies

designed to improve upon the RV144 trial also failed to induce effective neutralising antibodies (Rerks-Ngarm et al. 2017), and the minimal efficacy was unable to be replicated (Gray et al. 2021), bringing the reliability and reproducibility of the original study results into question. The use of monomeric gp120 in these trials likely hinders the induction of nAbs, due to the presentation of non-neutralising epitopes that are usually occluded in the functional trimeric Env. An effective HIV-1 vaccine instead needs to elicit nAbs that can target the functional Env trimer of many different viral variants and thus have broad neutralisation before infection to cope with a level of diversity and prevent viral escape. It should also be noted that vaccines designed to induce protective CD8+ T cell responses have also proved challenging and, as a consequence, none have been successful so far in human trials (Buchbinder et al. 2008; Hammer et al. 2013), although the use of CMV as a vaccine vector offers more promise (Picker et al. 2023).

1.4.6 Clinical impact of bnAbs

Even though the ability to produce bnAbs against HIV-1 does not provide clinical benefit to the infected individual, these antibodies are still of high interest due to their potential to provide protection prior to infection. In particular, the passive transfer of bnAbs in non-human primate models has demonstrated the ability to provide *in vivo* protection even after repeated low-dose mucosal challenge, as an approximation of HIV-1 exposure by sexual transmission in humans (Gautam et al. 2016). This study also revealed that the level of protection, and thus time to infection, was related to the potency of the bnAb, yet could be extended by introducing two mutations into the Fc domain (LS mutation) to increase the bnAb half-life (Gautam et al. 2016). Although the administration of individual bnAbs was not enough to confer protection against challenge with more than one virus, the combination of two bnAbs was capable of providing 100% efficacy for the duration of the study (120 days) (Julg et al. 2017). Finally, in addition to the intrarectal challenge that was used in the above studies, it has also been demonstrated that the passive transfer of bnAbs can protect against both penile and vaginal infections (Garber et al. 2020). In humans, the use of bnAbs as prophylaxis

has only been assessed in a recent Phase 2b trial from the Antibody-Mediated Prevention (AMP) studies. While it was reported that the CD4bs bnAb VRC01 was 75% effective at preventing acquisition of susceptible strains, it was also acknowledged that only 30% of the circulating HIV strains where this trial was conducted were VRC01-sensitive (NIH News Release, 2021). Taken together, this demonstrates the potential that bnAbs have in providing protection against HIV-1, but also highlights the prevalence of circulating strains with bnAb resistance.

There is also interest in the clinical use of bnAbs to suppress HIV-1 during the interruption of ART. This was initially trialled in humans with the administration of individual bnAbs, which found that three doses of VRC01 were capable of suppressing viral rebound of HIV-1 for a median of 4 weeks, while two doses of 3BNC117 suppressed viral rebound for approximately 6.7 weeks on average (Bar et al. 2016; Scheid et al. 2016). Moreover, the administration of a single dose of 3BNC117 was found to boost the autologous nAb response as well as increase tier 2 heterologous neutralisation (Schoofs et al. 2016). However, the most successful human clinical trial reported to date used two bnAbs in combination (3BNC117 and 10-1074) to target different regions on the HIV-1 Env, which sustained viral suppression for a median of 21 weeks (Mendoza et al. 2018). In the context of bnAb therapeutics, this combination approach or the use of bi-specific antibodies may therefore be more effective in preventing the emergence of HIV-1 variants capable of neutralisation escape (Kong et al. 2015; Wagh, Seaman, et al. 2018). Ongoing trials with modified bnAbs, bi-specific bnAbs or novel bnAb combinations (reviewed in (Caskey, Klein, and Nussenzweig 2019; Liu et al. 2020; Julg and Barouch 2019)) should provide more clarity on the requirements to achieve durable rather than transient HIV-1 suppression. The first results from a triple bnAb combination phase 1 clinical trial for the treatment of individuals with viraemia showed the ability to suppress the viral load but were unsuccessful in maintaining suppression (Julg et al. 2022). Instead, the use of triple bnAbs as a treatment during ART interruption, as done with previous bnAbs, may have more success and is another ongoing study. However, the frequent administration of mAbs owing to their short half-life is expensive and is not a

viable solution for low/middle income countries where the majority of HIV transmission occurs, thus the development of a vaccine is still required.

1.4.7 HIV immunisation studies

The goal of many HIV vaccine candidates is to elicit a bnAb response to confer the protection that bnAbs provide when passively transferred in animal models, as discussed above in section 1.4.6. However, the development of bnAbs in HIV-infected individuals is rare and often requires years of ongoing HIV infection which is hard to replicate in a vaccine setting. As a result, most attempts to elicit a bnAb response in immunisation studies so far have been largely unsuccessful, and often result in the production of autologous nAbs (van Schooten and van Gils 2018; Pollara, Easterhoff, and Fouda 2017), similar to the limited breadth in neutralisation exhibited by the humoral response in the majority of HIV-1 infected individuals. The unusual characteristics of bnAbs required for breadth, such as long CDRH3s, short CDRL3s and extensive SHM, previously discussed in section 1.4.3, have also indicated why it is a challenge to elicit bnAbs through vaccination (Stephenson et al. 2020).

Advancements in the production of recombinant Env protein have been achieved by the introduction of an artificial disulphide bond (SOS) and mutation I559P (IP), known as ‘SOSIP’ modifications to stabilise gp145 trimers and mimic the cleaved, pre-fusion native conformation for the display of bnAb epitopes (Ringe et al. 2013; Sanders et al. 2013). Consequently, these stabilised Env trimers have enhanced the quality of the antibody response in eliciting tier 2 autologous neutralisation following immunisation (Sanders et al. 2015; Havenar-Daughton, Carnathan, et al. 2016; Pauthner et al. 2017). However, these strain-specific responses have been shown to target holes in the glycan shield that are not found in many HIV isolates, and thus limit their breadth (McCoy et al. 2016). Even the masking of non-neutralising antibody (non-nAb) epitopes on SOSIP immunogens has failed to induce broadly neutralising responses (Ringe Rajesh et al. 2017).

The discovery that inferred germlines of bnAbs with certain specificities were not able to bind to the same recombinant Env as mature bnAbs indicated that a different approach may be required to elicit neutralisation breadth (Zhou et al. 2010; Scheid et al. 2011; Hoot et al. 2013; Mouquet et al. 2012). Efforts to design immunogens to target germline sequences have primarily focused on CD4bs specific bnAbs (Jardine et al. 2013; Jardine et al. 2016; McGuire et al. 2013), in particular those with structural similarity and modes of binding resulting from specific gene usage of VH1-2 and use of an unusually short CDRL3 of 5 AAs, known as VRC01-like bnAbs (Zhou et al. 2015). However, animals used in immunisation studies do not express VH1-2 and thus transgenic mice have been engineered to express germline heavy chain genes, yet, immunogens targeting these had limited success in eliciting B cells that also have a short CDRL3 of 5 AAs (Dosenovic et al. 2015; Jardine et al. 2015). Similarly, naïve human B cells with a VH1-2 can be targeted, yet none paired with a light chain that had a 5 AA CDRL3 (Jardine et al. 2016) which highlights the rarity of these VRC01-like bnAb precursors. Nevertheless, the ability to elicit B cells with the desired gene usage and features using transgenic mice with germline genes for both the heavy and light chain has been achieved with germline targeting immunogens (Lin et al. 2020), but the challenge remains on how to mature these into bnAbs.

Investigation of the antibody response in transmission pairs also led to the idea that only specific Env may be capable of inducing a bnAb response (Kouyos et al. 2018). The CH505 Env from a T/F virus that resulted in bnAb production in human infection was produced in SOSIP form and used to immunise animals. The induction of heterologous tier 2 neutralisation was observed in two of eight (25%) rabbits, yet was less potent than autologous neutralisation (Saunders et al. 2017). Sequential immunisation with CH505 Env from different stages of infection, with the intention of guiding the immune response, only led to heterologous tier 2 neutralisation in one of the eight non-human primates (Saunders et al. 2017). Therefore, this suggests that other factors such as the antibody maturation pathway and cooperating lineages likely contribute to the development of breadth. In other studies, epitope-targeted immunogens have also been used to try and focus the immune response

towards conserved neutralising epitopes, but with varying degrees of success (Cai et al. 2017; Escolano et al. 2019; Kong et al. 2016; Xu et al. 2018; Duan et al. 2018). The most effective immunisation used trimeric Env for priming the immune response, followed by fusion peptide boosts and a final boost with trimeric Env, which elicited modest neutralisation in all five mice (Xu et al. 2018). In particular, one of these mice had breadth that met the criteria of elite neutralisation and produced a bnAb capable of 31% neutralisation of a 208 PV panel (Xu et al. 2018).

Finally, a more recent immunisation study that used slow delivery of trimeric Env in conjunction with a new particulate vaccine adjuvant (over the course of 12 days) has shown that GC reactions can persist for at least 6 months for the accumulation of SHM (Lee et al. 2022). Encouragingly this also led to the generation of broad heterologous tier 2 neutralisation, however, this was not induced in all of the animals. Consequently, the robust and reproducible elicitation of bnAbs remains to be achieved and therefore indicates a need for further investigation of cellular responses associated with their development.

1.5 The development of bnAbs

The shift from strain-specific to broad neutralisation only occurs in a small subset of HIV-1 infected individuals, and although certain traits have been associated with the gain of neutralisation breadth, none appear to be solely responsible or able to predict bnAb development (McCoy and McKnight 2017). These factors include; the length of untreated infection, viral load and diversity, CD4+ T cell frequency and autoreactivity, which will be discussed in more detail below.

1.5.1 Time since infection

Multiple serum studies have shown an association between the duration of HIV-1 infection and the acquisition of neutralisation breadth (Sather et al. 2009; Rusert et al. 2016; Landais et al. 2016; Gray et al. 2011). In an acute infection cohort, autologous neutralisation developed months (3-12 months)

after initial infection, and even after a year only limited heterologous neutralisation was detected (Gray et al. 2007). Yet a steady increase in neutralisation breadth can occur in some individuals after 2 years of infection and peaks at 4 years (Gray et al. 2011). Another longitudinal study of a primary infection cohort enabled serum neutralisation to be monitored for over 200 participants over the course of two years, starting from 24 months after the presumed date of infection (Landais et al. 2016). The extent of neutralisation breadth was determined using the standard 6 PV panel to calculate a neutralisation score and revealed a gradual increase in the breadth over time, which peaked at 48 months and then appeared to plateau, with a mean time of 3.5 years to achieve broad neutralisation (score ≥1) (Landais et al. 2016). In line with these findings, the largest study to date categorised individuals based on the length of infection and showed that while there was an association with the development of cross, broad and elite neutralisation, this was not seen after more than 3-5 years of infection (Rusert et al. 2016). In addition, the identification of individual bnAbs and longitudinal analysis has shown that the development of lineages with breadth occurs over time, often taking up to 2-3 years but in some cases up to 5 years after original HIV-1 exposure (Liao, Lynch, et al. 2013; Doria-Rose et al. 2014; MacLeod et al. 2016; Bonsignori, Kreider, et al. 2017). Although plasma breadth has been observed as early as one year post-infection (Goo et al. 2014; Makhdoomi et al. 2017), and bnAb development as early as 15 months (Simonich et al. 2016), these cases were in infants which have a distinct immune response.

1.5.2 Viral load and diversity

The high mutational rate and short replication cycle of HIV-1 results in the viral diversity increasing over the course of infection if left unchecked (Hemelaar 2012). As there is an association between neutralisation breadth and the duration of untreated HIV-1 infection, it is logical that an association with high viral load and diversity has also been identified (Doria-Rose et al. 2010; Landais et al. 2016; Rusert et al. 2016). In particular, the viral load set-point was significantly associated with the neutralisation score achieved by serum in a longitudinal study, and although there was also an association with the

clade of infection, this was only different between clade C and clade A infections (Landais et al. 2016). Similarly, a higher viral load was associated with increasing neutralisation breadth in another study using a larger cohort, which also revealed an association with viral diversity based on the *pol* gene, showing that this was independent of *env* diversity which can be driven by antibody selection pressures (Rusert et al. 2016). Enhanced viral diversity is also observed in cases of superinfection, where individuals already infected with HIV-1 become infected with another strain of HIV-1, and was associated with significantly broader neutralisation compared to matched controls with single HIV infection (Cortez et al. 2015). However, the concept of greater antigenic stimulation being necessary for the development of neutralisation breadth is contradicted by the finding that some viraemic controllers, with low or no viral load, display broad neutralisation and can produce bnAbs (Sajadi et al. 2018; Scheid et al. 2011; Freund et al. 2017), including the VRC01 donor who was a slow progressor (Wu, Yang, et al. 2010).

1.5.3 Co-evolution of HIV-Env and antibodies

The selection pressure exhibited by the humoral response can shape the viral variants that arise during escape from neutralisation (Wei et al. 2003), and in some instances can influence the epitope specificity for the development of breadth against heterologous viruses (Bhiman et al. 2015; Wibmer et al. 2013). This co-evolution between the HIV-1 Env and nAbs from acute infection has been investigated in a number of individuals to investigate the development of bnAbs (Bonsignori, Liao, et al. 2017).

Pyrosequencing and phylogenetic analysis revealed that the unmutated common ancestor of the CH103 CD4bs bnAb lineage branched and matured in different ways to the T/F virus, one which led to the development of neutralisation breadth and one which neutralised only the autologous virus (Liao, Lynch, et al. 2013). Single-genome amplification (SGA) also enabled the evolution of the Env to be studied and revealed extensive mutation near the CD4bs epitope within 3 months of infection, which was the target of neutralisation (Liao, Lynch, et al. 2013). In addition, a second CD4bs bnAb

lineage (CH235) that had a different angle of approach was identified in the same individual, and early nAbs in this lineage were shown to select Env variants that helped to drive the development of the first bnAb lineage (Gao et al. 2014; Bonsignori et al. 2016). Similar studies of antibody and Env co-evolution have also been reported for bnAbs targeting two additional epitopes, the V2 apex (Doria-Rose et al. 2014) and high mannose patch (Bonsignori, Kreider, et al. 2017; MacLeod et al. 2016), which again showed the acquisition of SHM in nAb lineages over the course of infection that contributed to their neutralisation breadth. Co-operating lineages that selected the quasispecies were also thought to contribute to the development of bnAbs against the high mannose patch (Bonsignori, Kreider, et al. 2017; MacLeod et al. 2016). Yet in the V2 apex bnAb donor, increasing Env diversity arose from superinfection shortly after the primary infection and was compounded by recombination events of these viruses (Doria-Rose et al. 2014; Bhiman et al. 2015).

1.5.4 Autoreactivity

The HIV Env is shielded by glycans which are added upon translation. Despite being host-derived, glycans can still be recognised by B cells without being fully autoreactive due to the manner of presentation and proximity to protein, which is different from self. Additionally, a low level of autoreactivity is allowed to pass tolerance checkpoints during B cell development to enable B cells to target foreign antigens that mimic self (Watanabe et al. 2019). Nevertheless, a high proportion of self-reactive mAbs have long CDRH3s with frequent use of JH6 (Watanabe et al. 2019) and are therefore negatively selected during development, yet is a feature often found in HIV bnAbs. In particular, bnAbs targeting the MPER epitope have a CDRH3 length of at least 20 AAs and demonstrate a degree of autoreactivity and/or polyreactivity (Liu et al. 2015; Prigent et al. 2018). One such antigen that MPER bnAbs 2F5 and 4E10 can bind is cardiolipin, which is a phospholipid (Haynes et al. 2005), and this reactivity is necessary for binding near the viral membrane to access the MPER epitope (Alam et al. 2007; Alam et al. 2009). However, knock-in mice generated to express the MPER bnAbs 2F5 & 4E10 revealed that these B cells were not tolerated by immune checkpoints, and were deleted or had reduced

BCR expression and signalling capacity (Verkoczy et al. 2010; Chen et al. 2013), indicating silencing by anergy. Furthermore, a large-scale protein screen has revealed that autoreactivity and polyreactivity were significantly more frequent in HIV bnAbs than non-bnAbs and that certain bnAbs were capable of being polyreactive regardless of their epitope specificity (Liu et al. 2015). The development of such bnAbs, therefore, implies a level of B cell dysregulation in tolerance checks. In line with this, autoimmune diseases such as SLE have impaired tolerance and in a rare case of co-existence with HIV led to the development of a CD4bs-specific bnAb (CH98), which was polyreactive (Bonsignori et al. 2014). A recent immunisation study has additionally shown that administration of an immune checkpoint inhibitor was able to improve the nAb response to autologous Env and resulted in alterations in the B cell transcriptome for enhanced survival (Bradley et al. 2020).

1.5.5 Genetic influence

Another influence on the development of neutralisation breadth that has been considered is patient-related parameters, including ethnicity and gender. In the large cohort study mentioned above, there was a strong association between neutralisation breadth and black ethnicity, but not white ethnicity, even after accounting for potential confounding factors (Rusert et al. 2016). Conversely, a study focusing on differences between injecting drug users with HIV and sexually acquired HIV in men found no significant difference in neutralisation breadth based on ethnicity (Euler et al. 2019). Instead, this study observed a difference in gender, with a higher percentage of males developing elite neutralisation in the injecting drug user cohort, although this difference was not found to be significant (Euler et al. 2019). Indeed, a larger study that also considered gender did not find any correlation between gender and neutralisation breadth (Landais et al. 2016).

1.5.6 Immunological phenotypes

CD4+ T cells are the main target of HIV-1 and consequently, these cells are progressively depleted over the course of infection. It has been found that the

CD4+ T cell count at the viral setpoint in a large cohort of HIV-infected individuals was inversely associated with the neutralisation score of the plasma response, suggesting that the development of neutralisation breadth was linked with a lower CD4+ T cell count (Landais et al. 2016). This has also been observed in other studies, where the development of neutralisation breadth was associated with a low CD4+ T cell count at setpoint or early on in infection (van Gils et al. 2009; Euler et al. 2010; Gray et al. 2011). However, CD4+ T cells can either be regulatory cells (Treg) that have an immunosuppressive function, or helper cells (Tfh) required for B cell survival, affinity maturation and differentiation. In particular, the frequency of a subset of Tfh cells circulating in the periphery (characterised by moderate levels of PD-1, expression of CXCR5 but not CXCR3) has been found to correlate with the development of neutralisation breadth (Locci et al. 2013; Moody et al. 2016) and was proposed to be a biomarker for the ability to drive high SHM. In agreement with this, the proportion of circulating Env-specific Tfh cells in infected non-human primates correlated with the acquisition of SHM in HIV Env+ IgG+ B cells, and the neutralisation score achieved by plasma (Yamamoto et al. 2015). Furthermore, high levels of chemokine CXCL13, the ligand for CXCR5, in plasma have also been associated with neutralisation breadth and early cross-neutralising responses (Havenar-Daughton, Lindqvist, et al. 2016; Mabuka et al. 2017; Cohen et al. 2014). As CXCL13 is primarily expressed for the recruitment of CXCR5+ cells to the GC, this suggests that the GC reactions are enhanced in HIV-infected individuals that develop neutralisation breadth.

An association with broadly neutralising responses in HIV-infected individuals has also been identified using bulk transcriptomic analysis of peripheral blood mononuclear cells (PBMCs), with upregulation of *RAB11FIP5* that encodes a protein associated with endosomal recycling in cells, that was particularly high in NK cells (Bradley et al. 2018). These NK cells appeared to have a dysfunctional phenotype and impaired effector functions, including reduced expression of IFN-γ and TNF-α, which was associated with the overexpression of *RAB11FIP5.* As activated NK cells were capable of reducing the number of CD4 Tfh and class-switched MBCs *in vitro*, it was proposed that impairment of

NK cell functionality was beneficial to the development of broad neutralisation (Bradley et al. 2018).

Investigation into the phenotype of B cells associated with neutralisation breadth is limited and instead studies have mainly focused on the difference in antibody repertoires between HIV-infected individuals based on their neutralisation capacity. One such study sequenced antibody heavy chains of B cells from HIV-infected individuals with and without broadly neutralising plasma, as well as uninfected controls. The most striking finding was that IgG antibodies from HIV-infected individuals had on average a lower level of SHM than controls, yet those with neutralisation breadth had repertoires that were not perturbed and instead capable of exhibiting similar SHM to controls (Roskin et al. 2020). In addition, the average CDRH3 length in individuals with neutralisation breadth had a significant negative correlation with the frequency of CTLA-4 Treg cells (Roskin et al. 2020). More recently, analysis of the HIV Env-specific repertoire using paired antibody sequences from HIV controller B cells has been conducted. This also revealed that higher SHM correlated with cross-reactive serum neutralisation, even in the context of low plasma viraemia, however, this neutralisation capacity was determined using a panel of only clade B viruses that reflects clade-specific breadth, rather than breadth across clades that is typically used to define broad neutralisation (Cizmeci et al. 2021).

1.6 HIV and immune dysfunction

Immune dysfunction occurs even during acute HIV infection, as demonstrated by the benefit of early initiation of ART which can boost CD4+ T cell counts and reduce the amount of serious AIDS-related events (Lundgren J 2015), as well as partially restore the B cell population (Moir et al. 2010; Tanko et al. 2017). Nevertheless, HIV-infected individuals receiving ART show that restoration is not complete by exhibiting reduced and shorter-lived neutralisation responses compared to uninfected individuals in response to vaccination (Rees-Spear and McCoy 2021; Touizer et al. 2022). This is

thought to stem from sustained inflammation and immune dysfunction that arises due to disruption of the intestinal wall, enabling microbial translocation and the presence of circulating microbial products such as LPS, which is lowered upon initiating ART but continues to persist (Brenchley et al. 2006).

1.6.1 T cell responses in HIV infection

The T cell compartment can be broadly categorised based on CD4 or CD8 expression and these cells recognise antigens presented in MHC-II and MHC-I complexes respectively. CD4+ T cells are primarily associated with providing help to regulate other immune cells in response to pathogens, including CD8+ T cells which mediate cytotoxic functions (Laidlaw, Craft, and Kaech 2016). Following T cell receptor (TCR) recognition of antigen presented in MHC complexes on antigen-presenting cells a second co-stimulatory signal is required to initiate activation, typically induced by the binding of CD28 to CD80 or CD86 on the antigen-presenting cell (Chen and Flies 2013). Once the immune system has cleared the infection, further signalling is necessary for T cells to return to a resting state, which is mediated by immune checkpoint inhibitors such as PD-1 and CTLA-4 (Chen and Flies 2013).

In the context of HIV-1, activated CD8+ T cells play a vital role in the initial restriction of infection and contribute to establishing the viral setpoint, with a strong and rapid response that lowers the viral load (Ndhlovu et al. 2015), and those targeting epitopes in the Gag protein have been linked to a sustained low viral load (Kiepiela et al. 2007). However, during HIV-1 replication mutation of epitopes targeted by the CD8+ T response ultimately leads to escape from this level of control (Goonetilleke et al. 2009). Concurrently CD4+ T cells are activated to provide help to CD8+ T cells as well as other types of immune cells such as B cells. However, CD4+ T cells are targeted for infection by HIV-1, causing cell death and the decline of this population. Furthermore, the inability to resolve HIV infection leads to persisting antigenic stimulation and a state of chronic activation and T cell exhaustion. Specifically, the increase in PD-1 to reduce activation leads to CD4+ and CD8+ T cell dysfunction, with the loss of cytokine production, reduced proliferation and ultimately disease

progression (Day et al. 2006; Fuller and Zajac 2003). Additionally, dysfunction of the CD4+ T cell population reduces the ability to provide help to immune cells and thus impaired or reduced frequencies of Tfh cells can impact the B cell response (Yamamoto et al. 2015).

1.6.2 B cell responses in HIV infection

Despite not being directly infected, there are profound effects on the B cell compartment as a result of HIV-1 infection, with a significantly lower number of total CD19+ B cells as well as significant alterations to B cell subsets compared to HIV-negative individuals (Moir et al. 2010). Fundamentally this stems from the hyperactivation of B cells, resulting in a decreased proportion of naïve cells and an increased proportion of both immature/transitional cells and plasmablasts in circulation (Moir et al. 2010). HIV-infected individuals also have an increased frequency of plasma cells in the bone marrow (Montezuma-Rusca et al. 2015), but this population is terminally differentiated and therefore unable to adapt to antigenic changes required to contend with HIV. Additionally, this gives rise to polyclonal hypergammaglobulinemia, which is characterised by high levels of spontaneous IgG secretion that are not HIV-specific (De Milito et al. 2004; Lane et al. 1983).

Alterations to the distribution of memory subsets in the periphery have also been observed following HIV infection, particularly those characterised by the differential expression of CD27 and CD21 on the B cell surface (as shown in Figure 1.8). Briefly, subsets can be divided into resting memory (RM; CD27+ CD21+), activated memory (AM; CD27+ CD21-) and tissue-like memory (TLM; CD27- CD21-). In particular, the TLM subset in HIV-infected individuals was only identified in 2008, based on similarities to a memory population isolated from human tonsils, such as expressing FCRL4, an immunoregulatory receptor for IgA (Moir et al. 2008; Ehrhardt et al. 2005). Even during early viraemia an increase in AM and TLM B cells and a decrease in RM B cells have been found compared to HIV-negative individuals (Moir et al. 2010). It has also been demonstrated that a TLM subset is enhanced in other chronic infections such as malaria, which identified the immunoregulatory receptor for

IgG (FCRL5) as a more accurate marker for this subset in the periphery (Portugal et al. 2015). However, TLM B cells have also been characterised by their enhanced expression of inhibitory receptors that overlap with those on exhausted T cells, as well as homing receptors to inflammatory sites for effector functions, rather than the GC for continued maturation (Wherry et al. 2007). Investigation of HIV Env-specific antibodies from TLM B cells revealed a lower level of SHM than antibodies from RM B cells (Meffre et al. 2016), suggesting restricted affinity maturation. Moreover, B cells with low CD21 expression, typical of AM and TLM B cells that are increased in HIV infection, exhibited high expression of IFN-induced and/or terminal differentiation genes, which predisposed cells to apoptosis (Moir et al. 2004). This suggests that the humoral response may be limited in HIV-infected individuals with high proportions of TLM B cells.

Overall, the indirect impact of persistent HIV-1 infection and inflammation leads to perturbations of the B cell population, phenotype and functionality that impairs the humoral response and restricts the pool of B cells that can respond to viral variants that arise during infection. Although ART can improve B cell homeostasis, with increased frequencies of HIV Env-specific RM B cells and decreased frequencies of HIV Env-specific AM B cells (Kardava et al. 2014), the level of B cell activation is only partly normalised (Tanko et al. 2017).

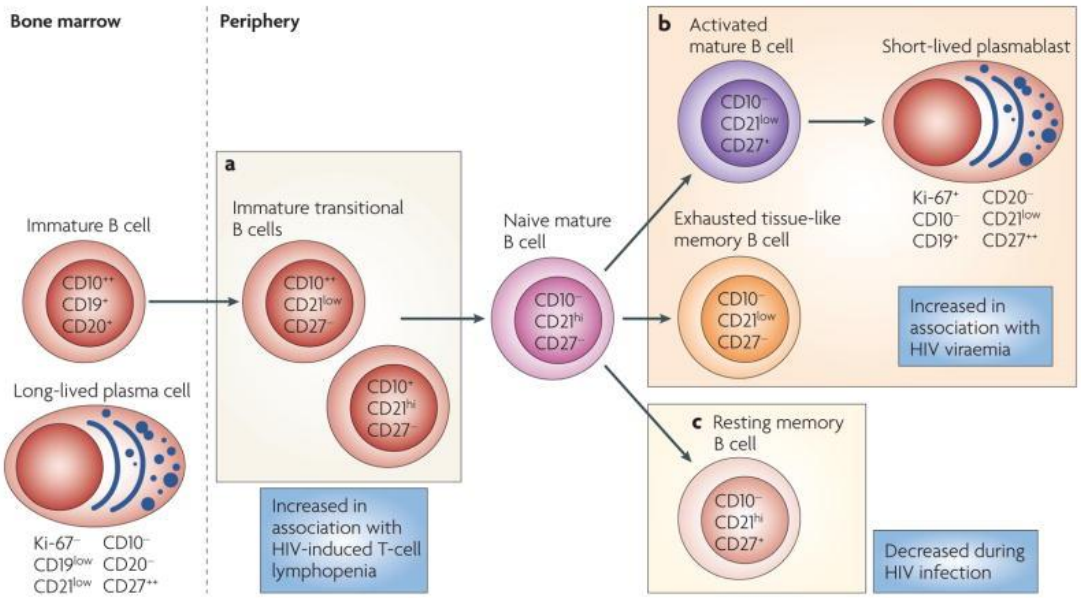

Figure 1.8 Perturbation of B cell subsets induced by HIV-1 infection.

After B cell development (a) CD20+ CD19+ CD10++ immature B cells enter the periphery from the bone marrow as immature transitional B cells that are CD27- and CD21- or CD21+, both of which are increased in HIV infection. The $CD21^{high}$ population downregulate CD10 to form naïve mature B cells that are (b) stimulated in response to HIV infection, giving rise to an increased population of activated B cells that express CD27 but downregulate CD21 and can terminally differentiate into short-lived plasmablasts that express Ki-67+ and downregulate CD20. HIV infection also results in an increased tissue-like memory population which remains CD27- and downregulates CD21, but also (c) a loss of CD27+ CD21+ resting memory B cells. Image from (Moir and Fauci 2009).

1.7 Single B cell technologies

1.7.1 mAb generation

The first mAbs were produced using hybridoma technology in 1975, by fusing mouse antibody-secreting B cells with immortal myeloma cells to create hybrid cells (hybridomas) capable of sustained proliferation and antibody production (KÖhler and Milstein 1975). However, the process of generating hybridomas is highly inefficient, with the loss of many B cells that are not immortalised and is only viable with mouse B cells. In addition, the process of identifying antigen-specific B cells is labour-intensive, with the requirement for separating single clones by limited dilution and screening individual cultures for antigen binding. Nevertheless, three of the first HIV bnAbs were isolated in this manner by instead immortalising human B cells from HIV-infected PBMCs using electrofusion with a modified version of the myeloma cell line and/or EBV transformation (Buchacher et al. 1994).

The development of combinatorial display technologies, such as phage display in 1985, offered an alternative method to generate antigen-specific mAbs and can be used to mimic the selection process *in vitro* (Smith 1985; Winter et al. 1994). This approach involves isolating Ig variable (V) regions from B cells and assembling these at random for display on the surface of bacteriophage, generating recombinant antibody libraries for antigen binding and selection. Antigen-specific mAbs on phage can be subjected to affinity maturation within bacteria and are screened for improved binding (Hoogenboom 2005). While phage display can be used to screen large antibody repertoires and generate mAbs with improved affinity, this process is time-consuming and the antigen used during selection may introduce bias. Moreover, the use of random heavy and light chain combinations results in the generation of mAbs that likely have artificial pairings. However, one HIV bnAb 2G12 has been isolated using this approach (Burton et al. 1991).

The natural pairing of antibody heavy and light chain variable regions in B cells is important due to CDRs from each variable region forming the antigen

binding site and having already undergone affinity maturation towards antigen *in vivo* (Tiller 2011). Given this, and the limitations of the immortalisation process and phage display stated above, a more favourable technology for mAb generation is the direct amplification of Ig variable regions from single B cells by PCR, followed by cloning into antibody expression vectors to produce BCRs as soluble, recombinant mAbs. This process is referred to as single B cell cloning and was first established for use with human B cells in 2008 (Tiller et al. 2008) and has subsequently been used to isolate the majority of HIV bnAbs to date.

The isolation of single B cells for antibody cloning has typically been carried out using fluorescent-activated cell sorting (FACS), due to the ability to easily identify populations of interest based on cell surface markers. While any B cell subset with a mature BCR can be sorted into single cell suspensions and processed for single B cell cloning, the antigen-experienced subsets such as class-switched memory B cells are usually of most interest. Antigen-specific single B cells can be identified following B cell culture and screening of antibody containing supernatants for antigen binding, or during FACS with the inclusion of fluorescently labelled antigen probes (McCoy and Burton 2017). However, the antigen-specific population in HIV-infected individuals is rare and thus the identification of single HIV-specific B cells before isolation eliminates the need to screen hundreds or even thousands of B cell cultures for antigen binding prior to single B cell cloning (Walker et al. 2009). On the other hand, the use of antigen probes in FACS requires the presence of BCR on the surface of the B cell, making this approach incompatible with plasma cells. Additionally, prior knowledge of the BCR specificity is necessary to use appropriate antigen probes in FACS.

1.7.2 Single B cell transcriptomics

Although cell surface proteins are a good indication of the cellular state and can be used to identify different immune populations, the complexity of the cell phenotype can only be explored fully using more in-depth analyses. Many studies have employed bulk transcriptomics to characterise subsets based on

their gene expression, however, the heterogeneity of cells within populations can only be uncovered using single-cell transcriptomics and is increasingly being used in the field of immunology (Jaitin et al. 2015).

Analysis of the transcriptome initially requires the isolation of RNA from cells, followed by reverse transcription to convert messenger RNA (mRNA) into complementary DNA (cDNA) before amplification and the generation of sequencing libraries to obtain the gene expression profile. A challenge of sequencing the transcriptome of single cells is the limited amount of RNA as starting material, however, this has been overcome by advances in the amplification strategy (Kurimoto et al. 2006). In addition, adaptation of single-cell microarray techniques for next-generation sequencing led to a more sensitive and accurate single-cell RNA-sequencing (scRNA-seq) approach (Tang et al. 2009). Since then multiple different methods for conducting scRNA-seq have been developed to offer high throughput sequencing. These often make use of Illumina (short-read) sequencing, with template DNA primed to an adaptor to form dsDNA to initiate sequencing by synthesis, with the addition of fluorescently labelled dNTPs that are detected upon incorporation. The generation of libraries for next-generation sequencing can be divided into methods that provide full-length coverage, such as Smart-Seq2 (Picelli et al. 2013), or those that can be multiplexed and enable the use of unique molecular identifiers (UMI), such as STRT (Islam et al. 2014), MARS-Seq (Jaitin et al. 2014), Drop-Seq (Macosko et al. 2015) and 10x Genomics (Zheng et al. 2017).

The Smart-Seq method was established as a plate-based method to process single cells in individual wells and was developed to amplify polyadenylated (poly-A) RNA and use a template-switching mechanism during reverse transcription to generate full-length cDNA (Ramsköld et al. 2012). This method was later optimised (Smart-Seq2) to improve the cDNA yield and increase the sensitivity for the detection of genes with low expression (Picelli et al. 2014). Out of the scRNA-seq methods that can be multiplexed, the 10x Genomics Chromium approach is favoured due to the high throughput of cells and it also amplifies poly-A RNA in combination with template switching. However, 10x differs from Smart-Seq2 in that single cells are captured in droplets containing

gel beads in emulsion (GEM) with barcoded oligonucleotides (Zheng et al. 2017), enabling all cells to be pooled for processing together. A direct comparison of these two scRNA-seq methods revealed that Smart-Seq2 was capable of detecting more genes than 10x, and thus has a greater sequencing read depth (Wang et al. 2021). In particular, these two scRNA-seq methods have been used to study B cells and have provided insight into the different stages of differentiation and related gene signatures, as well as characterising dysregulation such as in disease settings (Morgan and Tergaonkar 2022). Yet in the context of HIV infection, the primary focus has been on the T cell population and although RNA-seq of total PBMCs has been conducted from PLWH (Bradley et al. 2018), scRNA-seq analysis of the B cell population is lacking (Pollara et al. 2022).

1.8 Conclusion and Research Question

The development of a broadly neutralising response against HIV-1 occurs in only a minority of chronically infected individuals, after an average of 2-3 years of untreated viral replication. Moreover, the isolation of bnAbs from these individuals has revealed that bnAbs have unusual features that are thought to have arisen as a result of ongoing antigenic stimulation. Despite extensive characterisation of bnAbs and the epitopes targeted on the HIV-1 Env trimer, a broadly neutralising response has yet to be robustly elicited in immunisation studies or vaccination trials. In addition, studies that have investigated factors associated with the development of neutralisation breadth have been limited by making distinctions between bnAb and non-bnAb responses based on serum or plasma neutralisation, which is polyclonal. There has also been no conclusive cause or combination of factors that are predictive or causative of the ability of only certain individuals to acquire breadth. Importantly, there has been very limited consideration of the phenotypes of B cells that produce bnAbs in response to HIV infection. Considering that bnAbs have high SHM and/or long CDRH3s that are infrequent in the antibody repertoire, this may indicate a difference in the phenotype of the B cells that produce bnAbs.

The aim of the research in this thesis is to investigate the B cell response during HIV infection to address whether there are phenotypes associated with the development of broadly neutralising antibodies, both at the cell surface and transcriptional level. It is hypothesised that there is a difference in the B cells capable of producing bnAbs compared to B cells that produce mAbs with limited breadth.

Chapter 2: Materials and methods

2.1 PBMC isolation

Whole blood was collected in heparin-coated tubes and peripheral blood mononuclear cells (PBMCs) were isolated via density-gradient sedimentation. Blood was first diluted 1:2 with 1xPBS and layered over Ficoll-Paque Plus (Sigma), then spun via centrifugation for 20 mins at 800 RCF without brake. Plasma was collected, aliquoted and stored at −80°C. The PBMC layer was then collected and washed with 1xPBS before being spun via centrifugation for 10 mins at 800 RCF. PBMCs were resuspended in 1xPBS, stained with trypan blue and counted using a haemocytometer. PBMCs were then cryopreserved at $1x10^7$ cells/mL in a cryovial (Greiner) in cell recovery freezing medium containing 10% dimethyl sulfoxide (DMSO) (Sigma) and 90% heat-inactivated fetal bovine serum (FBS) and stored at −80 °C in a Mr Frosty freezing container overnight before being transferred into liquid nitrogen for further storage.

2.2 Plasma and PBMC samples

PBMCs from HIV-negative donors were collected from UCL staff with participant approval and processed as outlined in section 2.1. Plasma and PBMCs from HIV-infected participants in the East London cohort were previously collected and cryopreserved with ethical approval (06/Q0603/59) (Dreja et al. 2010). Plasma and PBMCs from HIV-infected participants from an elite controller cohort were previously collected as approved by the local Research Ethics Committee (REC) London – City & East (REC 12/LO/1572) and processed as outlined in section 2.1. Plasma samples from HIV-infected participants on ART and HIV-negative participants in the VCI cohort were previously collected and processed with ethical approval by South Central – Hampshire B (REC 19/SC/0423) (Touizer et al. 2022).

All plasma samples were heat inactivated at 56°C for 30 mins followed by 10 mins centrifugation at 10000 rpm (Fisher Scientific AccuSpin Micro Benchtop Centrifuge) before use in cell-based assays.

2.3 Single B cell analysis

2.3.1 Cell staining and phenotypic analysis

PBMCs were thawed briefly at 37°C, added to complete DMEM and pelleted by centrifugation at 800 RCF for 5 mins. The cell pellet was washed with PBS, pelleted again (800 RCF for 5 mins) and then cells were counted under a microscope using a haemocytometer. Zombie Aqua dead cell stain (1 µL in 400 µL PBS) was added per $1x10^7$ cells and left to incubate for 20 mins, protected from light. The panel of antibodies for cell staining was then prepared, in the dark, according to the table below to identify CD19+ IgG+ B cell subsets.

Panel for staining $5x10^6$ cells		
Antibody / antigen probe	**Fluorophore**	**1x**
CD4	BV510	2 µL
CD19	FITC	1 µL
CD21	PE-Cy7	1 µL
CD27	BV421	2 µL
IgM	APC-Cy7	1 µL
IgG	APC	10 µL
PBS		Up to 100 µL

Complete DMEM was added to quench the stain, then cells were pelleted (800 RCF for 5 mins) and washed with PBS before adding 100 µL of antibody stain per $5x10^6$ cells and incubating for 30 mins at room temperature, in the dark. Finally, cells were washed with 1x PBS and then resuspended in PBS. Unstained PBMCs were kept aside as a control and compensation controls were prepared for individual antibodies by adding the same volume as in the panel to BD anti-Ig compensation beads (one antibody per FACS tube containing one drop of beads) and incubating for 30 mins in the dark. Stained

PBMCs were analysed by flow cytometry using a BD FACS**-**Aria and data were visualised and gated using FlowJo v10.7.1.

Complete DMEM

Dulbecco's Modified Eagle's Medium (DMEM; Gibco) supplemented with 10% heat-inactivated foetal bovine serum (FBS; Gibco) and 100 U/mL penicillin plus 100 µg/mL streptomycin (Pen/Strep; Gibco).

2.3.2 Isolation of single memory B cells

Single IgG+ CD19+ memory B cells identified after being stained in section 2.3.1 were isolated from HIV-negative donor PBMCs using the BD FACS**-**Aria, sorting one cell per well into a 96-well plate containing lysis buffer (0.2% Triton X-100 and RNase inhibitor), oligo-DT primers and dNTPs as outlined in the Smart-Seq2 protocol (Picelli et al. 2014). Column 12 of the plate was left blank for negative controls and a positive control of high quality RNA (20 pg).

2.3.3 Library generation for scRNA-seq

The Smart-Seq2 protocol (Picelli et al. 2014) was followed to carry out full-length scRNA-seq on single memory B cells, with modification of the pre-amplification step that was optimised to reduce primer-dimer by excluding the IS PCR primers from the PCR mix. Briefly, the total mRNA in each well was reverse transcribed and then pre-amplified using 18 PCR cycles to generate cDNA that was purified using Ampure XP beads. The purified cDNA was assessed by Agilent Tapestation to confirm a peak at 1-2 kb and was quantified by Qubit for normalisation to 1.5 ng for optimal tagmentation (adjusted from 1 ng to account for the presence of primer-dimer). Libraries for sequencing were then generated by performing an enrichment PCR of 12 cycles using an Illumina Nextera XT DNA Library Preparation kit with 96 indices, then assessed by Agilent Tapestation to confirm a peak at 300-800 bp and quantified by Qubit for normalisation to 5 nM. The pooled libraries were submitted to the UCL Pathogen Genomics Unit for sequencing on Illumina NextSeq 500 with 75 bp paired-end reads.

2.3.4 scRNA-seq data processing and quality control

The Smart-Seq2 sequencing data were mapped to the GRCh38 reference human genome in Ensembl version 84, using the STAR algorithm. The transcript and gene abundance were estimated using RSEM (Li and Dewey 2011) to generate a count matrix. Data were then analysed by isOutlier to assess the quality of libraries based on the count depth, the number of genes detected and the percentage of mitochondrial genes. BCR sequences were assembled from V(D)J transcripts using BraCeR (Lindeman et al. 2018).

The dataset of 87 single B cells from the HIV-negative donor that passed quality control (QC) measures was normalised and highly variable ribosomal and VDJ genes were removed prior to conducting principal component analysis (PCA). Normalisation scores were assigned to each cell based on their similarity in gene expression to the upregulated atypical B cell gene signature (Holla et al. 2021).

2.3.5 Single cell V-gene amplification

The pre-amplified and purified cDNA generated in section 2.3.3 was also used as the starting material for nested PCRs (PCR1 and PCR2) to amplify the antibody variable regions from heavy, kappa or lambda sequences from each IgG+ B cell, according to the conditions shown below and using primer pools based on those from (Tiller et al. 2008).

PCR1	**1x**
10x Hotstar PCR Buffer	0.86 µL
10 mM dNTP mix	0.17 µL
10 µM Forward PCR1 primers	0.17 µL
10 µM Reverse PCR1 primers	0.17 µL
Hotstar Taq (Qiagen)	0.04 µL
ddH_20	6.45 µL
cDNA	0.75 µL

PCR1 cycles	**Temp (°C)**	**Time**
x1	95	5 mins
x50	94	30 secs
	50	30 secs
	72	1 min
x1	72	1 min
x1	4	∞

PCR2	1x
10x Hotstar PCR Buffer	0.86 µL
10 mM dNTP mix	0.17 µL
10 µM Forward PCR2 primers	0.17 µL
10 µM Reverse PCR2 primers	0.17 µL
Hotstar Taq (Qiagen)	0.04 µL
ddH_20	6.45 µL
Diluted (1:2) PCR1 product	1 µL

PCR2 cycles	Temp (°C)	Time
x1	95	5 mins
x50	94	30 secs
	55	30 secs
	72	1 min
x1	72	1 min
x1	4	∞

The V-regions amplified from HIV-negative donor IgG+ B cells were visualised on a 2% agarose E-Gel (Thermo), then purified using a QIAquick PCR purification Kit (Qiagen) and sent for Sanger sequencing. The sequencing reads obtained were analysed using the IMGT V-Quest tool (Brochet, Lefranc, and Giudicelli 2008).

2.4 Cell lines and cell culture

Adherent HEK-293T cells, HEK-293 ISRE reporter cells and HeLa TZM-bl cells were cultured in complete DMEM in a humidified incubator at 37°C with 5% CO_2. Once confluent (every 2-3 days), the medium was aspirated off and the adherent cell monolayer was gently washed with PBS before being disrupted by trypsin/EDTA (Gibco) and diluted with complete DMEM.

HEK-293F suspension cells were cultured in Freestyle™ 293 Expression Medium (Gibco) in a humidified Eppendorf New Brunswick S41i shaking incubator at 180 rpm at 37°C with 8% CO_2.

2.5 Bacterial culture and plasmid preparation

2.5.1 Transformation, DNA extraction and glycerol stocks

Plasmids were transformed into NEB 10-beta (C3019H) competent *E. coli* cells according to the manufacturer's protocol (with the incubator changed to 30°C following transformation of unstable plasmids). Single colonies were picked

from LB agar plates with antibiotic selection into 5 mL LB broth containing 100 µg/mL ampicillin or 50 µg/mL kanamycin (depending on the plasmid's antibiotic resistance) and grown overnight at 37°C (or at 30°C for unstable plasmids) in a shaking incubator at 200 rpm (Kuhner ISF-1-W Incubator Shaker Pred ISF1-X/Z). DNA was extracted from cultures using a QIAprep Spin Miniprep Kit (QIAGEN) and the concentration was measured by Nanodrop. Glycerol stocks were made by mixing equal volumes of bacterial culture and 80% glycerol for long-term storage at -80°C.

LB Agar

20 g of LB Agar granules (Sigma) dissolved in 1 L of dH_2O, then sterilised in an autoclave for 15 mins at 121°C and allowed to cool before use.

LB Broth

20 g of Luria-Bertani (LB) Broth powder (Sigma) dissolved in 1 L of dH_2O, then sterilised in an autoclave for 15 mins at 121°C and allowed to cool before use.

2.5.2 Large-scale preparation of DNA plasmids

Glycerol stocks were used to inoculate 5 mL LB broth containing the appropriate antibiotic (100 µg/mL ampicillin or 50 µg/mL kanamycin) and were grown at 37°C in a shaking incubator at 200 rpm overnight (Kuhner ISF-1-W Incubator Shaker Pred ISF1-X/Z). Starter cultures were scaled up into an Erlenmeyer flask containing 200 mL of LB with antibiotics and grown overnight at 37°C in a shaking incubator at 200 rpm (Kuhner ISF-1-W Incubator Shaker Pred ISF1-X/Z). DNA was extracted from cultures using a Qiagen HiSpeed Plasmid Maxi Kit (QIAGEN) and the concentration was measured by Nanodrop.

2.6 Virus production and neutralisation assays

2.6.1 PV production

Pseudo-typed virus (PV) capable of single-round infection was produced by incubating 8 µg HIV-1 backbone plasmid lacking envelope (pSG3ΔEnv), 4 µg of envelope plasmid (variable) and 600 µL Opti-MeM (Gibco) with 36 µL PEI-

MAX for 20-30 mins at room temperature before transfecting into HEK-293T cells (seeded at $3x10^6$ cells/T75 flask the day before). Supernatants containing PV were collected 48 hrs post-transfection, filtered (0.45 µM) and stored at 4°C short-term or in liquid nitrogen long-term.

Plasmid constructs for Env pseudo-typed virus	
pSG3delEnv	A full-length proviral clone containing a four nucleotide insertion mutation (CTAG) in the *env* sequence and a translation stop codon after amino acid residue 142 (NIBSC; #2064), for use as the backbone for generating Env pseudo-typed infectious virions.
Standard 6 HIV PV Panel	Consists of 6 constructs containing gp160 Env clones 92TH021, 94UG103 JRCSF, 92BR020, 93IN905 and IAVI C22 from clade AE, A, B and C (Simek et al. 2009).
Subtype C HIV-1 Reference Panel	Consists of gp160 Env constructs from 12 different acute/early clade C infections (NIBSC; ARP2069), for standardised assessment of Tier2/3 neutralisation.
Global HIV-1 Reference Panel	Consists of 12 different gp160 Env constructs from clade AC, AE, A, B, BC, C and G (NIBSC; 100007), representative of 219 viruses from all major genetic subtypes and CRFs of HIV-1 (deCamp et al. 2014) for standardised assessment of Tier2/3 neutralisation.
118 Multi-Clade Panel	Consists of 118 constructs each containing a different gp160 Env Clone, covering all major HIV-1 clades from different regions around the world (Seaman et al. 2010). Constructs from this panel were obtained from James Voss (Scripps, US).
CRF250 Env	A gp160 Env construct from a clade AG infection. This construct was obtained from James Voss (Scripps, US).
CRF250 N160A Env	A gp160 Env construct from a clade AG infection with mutation of the glycan site at position 160. This construct was obtained from James Voss (Scripps, US).
BG505 Env	A gp160 Env construct from a clade A infection. This construct was obtained from Marit van Gils (Amsterdam UMC).
BG505 N276D/N462D Env	A gp160 Env construct from a clade A infection, with mutation of the glycan site at position 276 and 462. This construct was obtained from Marit van Gils (Amsterdam UMC).
JRCSF N295A/N332A Env	A gp160 Env construct from a clade B infection, with mutation of the glycan site at positions 295 and 332. This construct was obtained from Elise Landais (IAVI, US).

T125_2139_e7	A gp160 Env construct containing the *env* sequence from the clade C T125 isolate 2139_e7 in the psvIII expression vector. Produced in section 2.10.4.
T125_2139_e9	A gp160 Env construct containing the *env* sequence from the clade C T125 isolate 2139_e9 in the psvIII expression vector. Produced in section 2.10.4.
T125_2139_e21	A gp160 Env construct containing the *env* sequence from the clade C T125 isolate 2139_e21 in the psvIII expression vector. Produced in section 2.10.4.

2.6.2 TZM-bl assay

PV infectivity was quantified using the HeLa TZM-bl (tat-regulated luciferase reporter) assay (Sarzotti-Kelsoe et al. 2014) by titrating 3-fold across a 96-well flat-bottom white plate (Thermo) containing complete DMEM, in duplicate, leaving the last column as a cell only control. HeLa TZM-bl cells ($1x10^4$ cells/well) containing 25 µg/mL DEAE dextran were added and incubated in a 37°C incubator with 5% CO_2. After 72 hrs the media was removed from each well and 100 µL of Bright-Glo™ luciferase substrate (Promega) diluted 1:20 in 1x lysis buffer was added. Luciferase activity in relative light units (RLU) was measured using a PheraStar Plus microplate reader (BMG Labtech). The tissue culture infectious dose for 50% infection ($TCID_{50}$) of PV stocks was determined using a macro based on the equation formulated by (REED and MUENCH 1938). The 200 $TCID_{50}$ dilution was calculated for use in assays by dividing the $TCID_{50}$ value by 4000, to also take into account the dilution factor and final volume of 200 µL per well.

10x Lysis buffer

33 g of Gly-Gly (Glycylglycine), 18.5 g of $MgSO_4$ $7H_2O$ and 18.8 g of EGTA tetrasodium were dissolved in 800 mL of dH_2O and adjusted to pH 7.8 using 5M NaOH before adding 100 mL of Triton X-100 and topping up to 1 L with dH_2O.

2.6.3 Neutralisation assays

Serum and plasma samples or monoclonal antibodies (sterile filtered, 0.22 µM) were titrated 2-fold or 3-fold down a 96-well flat-bottom white plate (Thermo) containing complete DMEM (leaving wells without sample for virus and cell only controls) and then incubated with a 200 $TCID_{50}$ dilution of PV for 1 hr at 37°C. Serum and plasma samples were diluted prior to titration to have a starting dilution of 1:100 (or 1:75 or 1:50) after the addition of PV. Monoclonal antibodies were used at different starting concentrations (0.5 µg/mL - 10 µg/mL) depending on their potency. HeLa TZM-bl reporter cells ($1x10^4$ cells/well) containing 25 µg/mL DEAE dextran were added and incubated for 48 hrs in a 37°C incubator with 5% CO_2. Media was removed from each well prior to the addition of 100 µL Bright-Glo™ luciferase substrate (Promega) diluted 1:20 in 1x lysis buffer. The luciferase activity in RLU was measured using a PheraStar Plus microplate reader (BMG Labtech). Serum and plasma 50% inhibitory dilution (ID_{50}) values were calculated from sigmoidal dose-response curves using GraphPad Prism software. Neutralisation scores were calculated from log-transformed titres as in (Simek et al. 2009), using the equation Y = log3 (dilution/100) + 1.

2.6.4 Adsorption assays

Adsorption assays were performed as in section 2.6.3 but included a pre-incubation step of the serially-diluted serum, plasma or antibody samples in the presence or absence of HIV-1 Env protein for 1 hr at 37°C before adding PV. HIV-1 BG505 D368R gp120 (made by the McCoy lab) was added at 200 µg/mL for a final concentration of 50 µg/mL and HIV-1 MPER peptide (ELLELDKWASLWNWFGITKWLWYIKIFIM, synthesised by Smart BioScience) was added at 50 µg/mL for a final concentration of 12.5 µg/mL.

2.6.5 SDM to create Env mutants

Single point mutations were introduced into plasmids encoding *env* for pseudo-type using the QuikChange Lightning Site-Directed Mutagenesis (SDM) kit (Agilent) according to the manufacturer's protocol with the following

primers. Plasmids were then transformed and processed as in section 2.5.1. Mutations were verified by Sanger sequencing.

Env plasmid	Mutation	SDM Primers
CRF250 N160A	K169T	Forward: 5’ gctgtaaccacagaactaagagataagacaaagaaagagtattcatttttttataaa 3’ Reverse: 5’ tttataaaaaaatgaatactctttctttgtcttatctcttagttctgtggttacagc 3’
JRCSF	D279A	Forward: 5’ gtaattagatctgacaattttacggccaatgctaaaaccataatagtacag 3’ Reverse: 5’ ctgtactattatggttttagcattggccgtaaaattgtcagatctaattac 3’
JRCSF	T90A	Forward: 5’ cccacaagaagtagtattggaaaatgtagcagaagattttaacatg 3’ Reverse: 5’ catgttaaaatcttctgctacattttccaatactacttcttgtggg 3’

2.7 Production and validation of Env protein probes

2.7.1 Env protein production

HEK-293F cells ($1x10^6$ cells/mL in an Erlenmeyer flask) were transfected with reagents as shown in the table below. PEI-MAX was added to sterile filtered (0.22 µM) plasmids and OptiMeM, then left to incubate for 20 mins at room temperature before transfection. For *in vivo* biotinylation of SOSIP with an avi-tag, 8 mL of the transfection mix was added to HEK-293F cells (200 mL) along with 3 mL of 10 mM biotin.

Transfection mix for Env protein production	Amount per 200 mL of HEK-293F cells
Avi-tagged *env* expression plasmid	50 µg
Furin expression plasmid	12.5 µg
BirA expression plasmid	15.6 µg
PEI-MAX (Polysciences)	2 mL
Opti-MeM (Gibco)	11 mL

Constructs for expression of soluble, recombinant trimeric Env	
CRF250 SOSIP	Expression construct with an avi-tag containing the SOSIP gp145 *env* sequence from clade 02_AG isolate CRF-T250-4.
Furin	Expression construct for the furin cleaving enzyme. This construct was obtained from Marit van Gils (Amsterdam UMC).
BirA	Expression construct for BirA biotin ligase. This construct was obtained from Marit van Gils (Amsterdam UMC).

Supernatants were harvested from HEK-293F cells 5-7 days post-transfection, then filtered (0.45 µM) and stored at 4°C.

2.7.2 Streptavidin capture ELISA

For streptavidin capture of biotinylated avi-tagged protein, wells were coated overnight at 4°C with 50 µL of 2 µg/mL streptavidin in PBS, then removed and blocked with 3% Bovine Serum Albumin (Sigma) for 1hr at room temperature. Env protein containing supernatants or purified Env protein (2 µg/mL) was applied for 2 hr, then removed and monoclonal antibodies titrated 5-fold from 25 µg/mL were applied for 1 hr. Goat anti-human IgG Fc alkaline phosphatase conjugate (Stratech) was then applied for 1 hr. Finally, alkaline phosphatase substrate (Sigma) prepared in Alkaline Phosphatase (AP) buffer was added and the optical density was measured at 405 nm on a Synergy H1 Multi-Mode Plate Reader (BioTek). Wells were washed with PBS-T (0.1% Tween-20) between each step.

0.05% PBS/Tween (PBS-T) wash buffer

500 µL Tween-20 added to 1 L of 1x PBS.

3% BSA

3 g of BSA dissolved in 100 mL of 0.05% PBS-T.

1x Alkaline Phosphatase (AP) stain buffer

2.03 g of $MgCl_2$ $6H_2O$ and 8.4 g of Na_2CO_3 were dissolved in 900 mL of dH_2O and adjusted to pH 9.8 before topping up to 1 L with dH_2O. Then 1.0 g of NaN_3 (decanted inside a fume hood whilst wearing a face mask) was added and filtered (0.22 µM).

2.7.3 Env protein purification by affinity chromatography

Working at 4°C, GNL agarose (Vector Laboratories) was added to a 1.5 x 10 cm chromatography column (Bio-Rad) and washed by letting 1x PBS drip through the column. Supernatant harvested from transfected HEK-293F cells (described in section 2.7.1) was added to the column using gravity flow and allowed to pass over the GNL agarose at a slow flow rate. Lectin-bound Env protein in the column was washed with 0.5M NaCl and then with PBS before being eluted with 1M mannose. Centrifugal 100 kDa filter units (Merck) were used to concentrate the SOSIP protein and buffer exchange into 1x PBS. The purified protein concentration was then measured by Nanodrop.

2.7.4 Size Exclusion Chromatography

A gel filtration standard (Bio-Rad) with proteins of known size and molecular weight was used to calibrate a Superdex 200 Increase 10/300 GL column (Sigma). Purified SOSIP proteins were then analysed and purified by size exclusion chromatography (SEC) using an AKTA pure with the Superdex 200 Increase 10/300 GL column (Sigma) to select fractions containing trimeric protein.

2.7.5 Biotinylation of avi-tagged protein

Avi-tagged BG505 SOSIP protein had already been produced and purified at The Scripps Research Institute using affinity chromatography and SEC. To biotinylate the avi-tag, proteins were first exchanged into 10 mM Tris-HCl (pH 8) buffer and concentrated to 10 mg/mL using a 100 kDa concentrator (Merck) to a volume of <100 µL. Biotinylation was conducted according to the Biotin Protein Ligase (genecopoeia) instructions, adding 10 µL of BiomixA, 10 µL of BiomixB, 10 µL of 10x Biotin and 2 µL BirA enzyme to the avi-tagged protein and incubated for 1 hr at 30°C. Centrifugal 100 kDa concentrators were used again to re-dialysis the biotinylated avi-tagged protein back into 1x PBS.

10 mM Tris-HCl

1.2 g of Tris dissolved in 900 mL dH_2O, adjusted to pH 8 with HCl, before topping up to 1 L with dH_2O.

2.7.6 SDS-PAGE

Protein samples for SDS-PAGE were prepared according to the table below, then heated at 95°C for 6 mins before being run alongside Precision Plus protein standards (Bio-Rad) on a Mini-PROTEAN TGX 4-20% pre-cast gel (Bio-Rad) at 200 V for 30 mins.

Protein sample	Reduced	Non-reduced
2x Laemmli Sample	7.5 µL	7.5 µL
1M DTT	1.5 µL	-
Purified Protein	2 µg	2 µg
Water	Up to 15 µL	Up to 15 µL

The gel was stained with Coomassie blue for 1 hr, then washed briefly in water before adding Coomassie de-stain solution for 1.5 hrs. The gel was rinsed again with water and then imaged on a GelDoc imaging system.

Coomassie blue stain

10 mL of Coomassie Brilliant Blue, 500 mL of methanol and 100 mL of acetic acid were added in a fume hood to 390 mL dH_2O.

Coomassie de-stain

500 mL of methanol and 100 mL of acetic acid were added in a fume hood to 400 mL dH_2O.

2.7.7 Env validation by flow cytometry

Protein G FITC beads (Spherotech) were incubated with mAbs at 25 µg/mL and 2 µg of biotinylated SOSIP proteins were incubated with fluorophores (PE or BV786) conjugated to streptavidin for 30 mins at room temperature (protected from light) before being combined and incubated for a further 30 mins at room temperature (protected from light). Unstained Protein G FITC beads (Spherotech) were used as a compensation control alongside stained beads which were analysed by flow cytometry using a BD LSR-Fortessa. Data were visualised using FlowJo v10.7.1.

2.7.8 Isolation of Env-specific B cells by flow cytometry

For antigen-specific staining of PBMCs, 3 µg of biotinylated CRF250 SOSIP and BG505 SOSIP Env probes were incubated with streptavidin-conjugated PE or BV786 fluorophores respectively, at room temperature (protected from light) for 30 mins, before adding to the panel of antibodies in section 2.3.1. The HIV Env+ IgG+ B cell subset was identified by flow cytometry using a BD FACS-Melody and single cells from this population were isolated (with the purity threshold set to yield) into individual wells of a 96-well plate containing lysis buffer (0.2% Triton X-100 and RNase inhibitor), oligo-DT primers and dNTPs as outlined in the Smart-Seq2 protocol (Picelli et al. 2014). Column 12 of the plate was left blank for negative controls. Data were visualised using FlowJo v10.7.1.

2.8 Antibody plasmid production

2.8.1 V-region amplification for antibody cloning

V-regions from HIV Env+ IgG+ B cells were amplified by nested PCR as in section 2.3.5 before conducting a final PCR as outlined below using primers with overhangs required for cloning into expression vectors.

PCR3	1x
10x High Fidelity PCR Buffer	1.25 µL
$MgSO_4$	0.5 µL
10 mM dNTP mix	0.25 µL
10 µM Forward PCR3 primer(s)	0.25 µL
10 µM Reverse PCR3 primer(s)	0.25 µL
Platinum Taq (Invitrogen)	0.1 µL
ddH_20	7.9 µL
Diluted (1:3) PCR2 product	2 µL

PCR3 cycles	Temp (°C)	Time
x1	94	2 mins
x30	94	30 secs
	55	30 secs
	68	1 min
x1	68	1 min
x1	4	∞

V-regions amplified by PCR3 were visualised on a 2% agarose E-Gel (Thermo) before cloning as outlined in 2.8.3.

2.8.2 Digestion of expression vectors

Expression vectors containing an antibody variable and constant region were double digested to remove the original antibody variable region using restriction enzymes according to the manufacturer's (NEB) protocol.

Constructs for antibody expression	
IgK	An expression vector under the control of a CMV promoter with ampicillin resistance, containing Age1 and BsiWI cut sites for insertion of the variable region sequence upstream of the human kappa chain constant region.
IgL	An expression vector under the control of a CMV promoter with ampicillin resistance, containing Age1 and Xho1 cut sites for insertion of the variable region sequence upstream of the human lambda chain constant region.

IgG1	An expression vector with ampicillin resistance, containing Age1 and Sal1 cut sites for insertion of the variable region sequence upstream of the human heavy chain IgG1 constant region.
IgG3	An expression vector with ampicillin resistance, containing XBa1 and Nhe1 cut sites for insertion of the variable region sequence upstream of the human heavy chain IgG3*01 constant region. This construct was gifted by Steven Detaeye (Amsterdam UMC).

Digestion products were separated by a 1% agarose gel and the digested vector was extracted using a QIAquick Gel Extraction kit (QIAGEN).

Agarose gel

1g or 2g of agarose dissolved in 100 mL of dH_2O, with the addition of 5 µL RedSafe, for 1% or 2% agarose gels respectively.

2.8.3 Recombinant-based antibody cloning

Recombinant-based cloning was conducted using NEBuilder HiFi Assembly Master mix, according to the manufacturer's (NEB) protocol to insert an unpurified antibody V-region (amplified in section 2.8.1) into an expression vector (digested in section 2.8.2). Each amplified heavy chain variable region was cloned into a digested IgG1 vector. Each amplified kappa chain variable region was cloned into a digested IgK vector. Each amplified lambda variable region was cloned into a digested IgL vector. For the T125 bnAb 7E7, the overhangs of the heavy chain variable region (originally amplified with primers to add overhangs to clone into the IgG1 vector) were adjusted by PCR with primers to enable cloning into a digested IgG3 vector.

Cloned plasmids were transformed into E. *coli* as in section 2.5.1, although plasmids were not extracted until confirmation of successful cloning using a screening PCR as in section 2.8.4.

2.8.4 Screening PCR

Cloning of a gene(s) into expression vectors was confirmed by PCR using the conditions listed below with primers specific for sites within the expression vector, either side of the cloning site. Template was produced by adding 2 µL of bacterial culture (grown from a single picked colony as in section 2.5.1) to

48 µL ddH_20 and frozen at -80°C for at least 1hr before denaturing at 95°C for 15 mins.

Screening PCR	1x
2x AppTaq RedMix	5 µL
10 µM Forward primer	1 µL
10 µM Reverse primer	1 µL
App Taq (Appleton Woods)	0.125 µL
ddH_20	14.9 µL
Template (denatured culture)	3 µL

Cycle	Temp (°C)	Time
x1	95	2 mins
x35	95	15 secs
	55	15 secs
	72	1 min
x1	72	1 min
x1	4	∞

The PCR products amplified were separated by a 2% agarose gel (for V-regions) or a 1% agarose gel (for gp160 sequences) alongside a 1 kb DNA ladder, and visualised using a GelDoc Imaging System.

2.9 Production and characterisation of mAbs

2.9.1 Antibody production

HEK-293T cells (1x10^6 cells/well of a 6-well plate) and HEK-293F cells (1x10^6 cells/mL in an Erlenmeyer flask) were co-transfected with antibody heavy and light chain expression plasmids, Opti-MeM and PEI-MAX as shown in the table below.

Transfection mix for antibody production	Amount per 2.5 mL well of HEK-293T cells	Amount per 200 mL flask of HEK-293F cells
IgH expression plasmid	2 µg	31.2 µg
IgK / IgL expression plasmid	2 µg	31.2 µg
Opti-MeM (Gibco)	100 µL	5 mL
PEI-MAX (Polysciences)	12 µL	187.5 µL

Antibodies were harvested from supernatants of HEK-293T cells after 72 hrs or HEK-293F cells after 5-7 days, filtered (0.45 µM) and stored at 4°C.

2.9.2 Fab-capture ELISA

Wells of a 96-well half-area ELISA microplate (Greiner Bio-One) were coated overnight at 4°C with 50 µL of 1:1000 goat anti-Human IgG F(ab')2 (Stratech) in PBS. The next day wells were blocked with 5% milk for 1hr at room temperature. Antibody supernatants and control monoclonal antibodies (starting at 25 µg/mL) titrated 5-fold in 1% milk were then applied for 1hr. Finally, 1:1000 Goat anti-human IgG Fc alkaline phosphatase conjugate (Stratech) was applied for 1 hr before adding alkaline phosphatase substrate (Sigma) prepared in AP buffer and measuring the optical density at 405 nm on a Synergy H1 Multi-Mode Plate Reader (BioTek). Wells were washed with PBS-T (0.1% Tween-20) between each step.

5% Milk

5 g of semi-skimmed milk powder dissolved in 100 mL of dH_2O.

2.9.3 Env binding ELISAs

Wells of a 96-well half-area ELISA microplate (Greiner Bio-One) were coated overnight at 4°C with 50 µL of 20 µg/mL Galanthus nivalis lectin (Vector Laboratories) in 0.1M $NaHCO_3$, then blocked with 1% casein hydrolysate (Sigma) for 1 hr at room temperature. Trimeric Env SOSIP protein (2 µg/mL) was captured via its glycans for 2 hr, then antibody-containing supernatants or monoclonal antibodies (starting from 25 µg/mL) were titrated 5-fold and applied for 1 hr. Goat anti-human IgG Fc alkaline phosphatase conjugate (Stratech) was then applied for 1 hr. Finally, alkaline phosphatase substrate (Sigma) prepared in AP buffer was added and the optical density was measured at 405 nm on a Synergy H1 Multi-Mode Plate Reader (BioTek). Wells were washed with PBS-T (0.1% Tween-20) between each step.

0.1M $NaHCO_3$

2.1 g of NaHCO3 dissolved in 200 mL dH_2O and adjusted to pH 8 before topping up to 250 mL with dH_2O, then sterilised in an autoclave for 15 mins at 121°C.

2.9.4 Antibody purification

Protein G Fastflow beads (GE Healthcare) were added to a 1.5 x 10 cm chromatography column (Bio-Rad) and then washed by letting PBS to drip through the column. Supernatant harvested from transfected HEK-293F cells (produced in section 2.9.1) was added to the column using gravity flow and allowed to pass over the Protein G beads at a slow flow rate. Antibody bound to the beads in the column was washed with PBS before being eluted with 0.1M glycine and collected in a 15 mL falcon containing 2M Tris. Centrifugal 50 kDa filter units (Merck) were used for concentration and buffer exchange into PBS. The concentration of the purified antibody was measured by Nanodrop.

2M Tris

242.2 g of Tris dissolved in 1 L dH_2O, adjusted to pH 9 and filtered (0.22 µM).

0.1M Glycine

7.5 g of glycine dissolved in 900 mL dH_2O and adjusted to pH 2.2 before topping up to 1 L with dH_2O

2.9.5 V3 peptide binding ELISA

Wells of a 96-well half-area ELISA microplate (Greiner Bio-One) were coated with 25 µL of mAbs at 25 µg/mL in 1xPBS overnight at 4°C, then blocked with 3% BSA (Sigma) for 1 hr at room temperature. V3 peptide with a biotinylated avi-tag diluted to 1 µg/mL in 1% BSA was then applied for 1 hr. Finally, 25 µL per well of Alkaline Phosphatase-conjugated Streptavidin (Jackson ImmunoResearch) diluted 1:1000 in 1% BSA was added and incubated for 1hr before adding alkaline phosphatase substrate prepared in AP buffer. The optical density was measured at 405 nm on a Synergy H1 Multi-Mode Plate Reader (BioTek). Wells were washed with PBS-T (0.1% Tween-20) between each step.

2.9.6 CD4bs binding ELISA

Wells of a 96-well half-area ELISA microplate (Greiner Bio-One) were coated directly with 25 µL of 2 µg/mL of BG505 gp120 or BG505 gp120 D368R in 1xPBS overnight at 4°C, then blocked with 3% BSA for 1 hr at room temperature. Next 25 µL per well of mAbs at 25 µg/mL in 1% BSA were applied for 1 hr. Goat anti-human IgG Fc alkaline phosphatase conjugate (Stratech) was then added for 1 hr. Finally, alkaline phosphatase substrate (Sigma) prepared in AP buffer was added and the optical density was measured at 405nm on a Synergy H1 Multi-Mode Plate Reader (BioTek). Wells were washed with PBS-T (0.1% Tween-20) between each step.

2.9.7 Competition ELISAs

Monoclonal antibodies used in competition ELISAs were biotinylated using the EZ-Link™ Micro Sulfo-NHS-LC-Biotinylation Kit (Thermo Scientific), according to the manufacturer's protocol.

For BG505 SOSIP binding competition ELISAs, wells of a 96-well half-area ELISA microplate (Greiner Bio-One) were coated with 25 µL of 20 µg/mL Galanthus nivalis lectin (Vector Laboratories) in 0.1M $NaHCO_3$ overnight at 4°C, then blocked 3% BSA (Sigma-Aldrich) for 1 hr at room temperature. BG505 SOSIP was then captured at 2 µg/mL in 1% BSA and incubated for 2 hrs at room temperature. For BG505 gp120 binding competition ELISAs, wells of a 96-well half-area ELISA microplate (Greiner Bio-One) were coated directly with 25 µL of 2 µg/mL of BG505 gp120 in 1xPBS overnight at 4°C and then blocked with 3% BSA for 1 hr at room temperature.

At this stage, ELISAs were treated the same, with the addition of 25 µL per well of mAbs at 25 µg/mL in 1% BSA for 1 hr, before adding 25 µL per well of biotinylated competitor antibody (at 0.1 - 5 µg/mL depending on the mAb) in 1% BSA for 1 hr. Finally, 25 µL per well of Alkaline Phosphatase-conjugated Streptavidin (Jackson ImmunoResearch) diluted 1:1000 in 1% BSA was added and incubated for 1hr before adding alkaline phosphatase substrate prepared in AP buffer. The optical density was measured at 405 nm on a

Synergy H1 Multi-Mode Plate Reader (BioTek). Wells were washed with PBS-T (0.1% Tween-20) between each step.

2.10 Autologous *Env* sequence analysis and PV plasmid production

2.10.1 Phylogenetic tree

Env sequences from the first timepoint T125 plasma were previously recovered from plasma using SGA and accessible on Genbank (accession numbers: KC156146-164, KC156166-178). These sequences, along with reference *env* sequences were trimmed to the beginning and end of gp160 by alignment to the HXB2 sequence. A maximum likelihood tree was constructed in IQ-TREE using the GTR+G model and 1000 non-parametric bootstrapping. The tree was rooted according to the reference clade B (BaL and NL43) and clade C (93IN905 and Du156_12) *env* sequences and annotated in FigTree to show ≥70% bootstrap significance.

2.10.2 Glycan hole analysis

T125 *env* nucleotide sequences identified in section 2.10.1 were translated into amino acid sequences using the Expasy tool and aligned to the HXB2 sequence using the Clustal Omega tool before entering into the LANL tool for glycan shield mapping and identification of conserved glycans that are missing (Wagh, Kreider, et al. 2018).

2.10.3 Generation of *env* genestrings

Env sequences from T125 isolates 2139_e7, 2139_e9 and 2139_e21 identified from different branches of the maximum likelihood tree in section 2.10.1 were aligned to the HXB2 *env* sequence to identify the location of the KpnI and BamHI cut sites. The sequence upstream of the 5' KpnI site and downstream of the 3' BamHI site was deleted from the T125 *env* sequences and replaced with a 20 bp homology sequence to the psvIII expression vector, to generate sequences compatible with cloning into this vector. These gp160 *env* sequences were synthesised as genestrings by Azenta Life Sciences.

2.10.4 Recombinant-based Env cloning

The psvIII expression vector was double digested to remove the original gp160 *env* sequence using KpnI and BamHI restriction enzymes according to the manufacturer's (NEB) protocol. Digestion products were separated by a 1% agarose gel and the digested vector was extracted using a QIAquick Gel Extraction kit (QIAGEN).

Construct for Env pseudo-typed virus	
psvIII expression vector	An expression vector containing Kpn1 and BamHI cut sites for insertion of gp160 *env* sequences, with ampicillin resistance.

Recombinant-based cloning was conducted using NEBuilder HiFi Assembly Master mix, according to the manufacturer's protocol but with assembly extended to 2.5 hrs to insert 100 ng of each gp160 *env* genestring (designed in section 2.10.3) into 100 ng of the digested psvIII expression vector. Cloned plasmids were transformed into E. *coli* as in section 2.5.1, using 30°C for incubation steps. The success of cloning was initially validated with a screening PCR as in section 2.8.4 and then confirmed by Sanger sequencing.

2.11 Transcriptomics analysis

2.11.1 Smart-Seq2 single-cell data analysis

The first Smart-Seq2 scRNA-seq dataset was produced according to section 2.3.3 from single HIV Env+ IgG+ B cells isolated according to section 2.7.8 from the bnAb donor T125. The second Smart-Seq2 scRNA-seq dataset was also produced according to section 2.3.3 contemporaneously by Dr Luke Muir from single IgG+ B cells isolated from different MBC subsets of an elite controller donor. These data were then processed using scanpy (v.1.9.1) workflow with standard quality control steps; cells were filtered if the number of genes >6000 or <600. Mitochondrial content was determined using scanpy.pp.calculate_qc_metrics function; cells with mitochondrial genes percentage <50% were retained for further analyses. Genes were retained if

they were expressed by at least 2 cells. Gene counts for each cell were normalised to contain a total count equal to 10^6 counts per cell. This led to a working dataset of 98 cells from the bnAb donor and 223 cells from the elite controller donor. The top 2000 highly variable genes were selected based on Seurat v.3 algorithm (flavor = seurat_v3) with batch key “Sequencing_batch”. Highly variable genes were further refined by removing potentially confounding genes using the following search formula: '^HLA|^IG[HKL][VDJC]|^MT|^A[A-Z][0-9]|^B[A-Z][0-0]'. The number of principal components used for neighbourhood graph construction and dimensional reduction was set at 20. Data integration from both donors was performed using the bbknn algorithm (Polański et al. 2020). Uniform Manifold Approximation and Projection (UMAP; v3.10.0) (McInnes 2018) was used for dimensional reduction and visualization with all parameters as per default settings in scanpy.

For the assessment of transcriptional similarity between cells from bnAb donor and reference cell subsets, Glmnet (Tay, Narasimhan, and Hastie 2023) and Celltypist (Domínguez Conde et al. 2022) packages were used. For Glmnet-based probability scores, trainScSimilarity / predScSimilarity functions from kelvinny tools (https://github.com/zktuong/kelvinny) were used with alpha set at 0.9 and nfolds 10. Celltypist models and probability scores were generated as per default settings. Differentially expressed genes between bnAb donor B cells and elite controller B cell subsets were assessed using scanpy.tl.rank_genes_groups function based on the Wilcoxon rank sum test.

2.11.2 Public single-cell datasets processing and analysis

(Wang et al. 2020): data from donors HD1, PID471, PID529, PID630, PID717 and PID876 were concatenated using anndata (Virshup et al. 2021) and processed with scanpy as described above with the following changes: cells were filtered if number of genes >3000 or <200, mitochondrial genes percentage >30%. Genes were retained if they are expressed by at least 3 cells. Gene counts for each cell were normalised to contain a total count equal to 10^4 counts per cell. Celltypist (model: Immune_All_Low.pkl) with majority voting was used to identify B cells. Raw B cell data were then exported as a separate h5ad object.

(Stephenson et al. 2021): all healthy controls data from Cambridge were concatenated and processed as described for Wang et al. data above.

Raw B cell data objects exported from Wang et al. and Stephenson et al. datasets were subsequently concatenated and processed by scanpy QC workflow leading to a working dataset of 4941 B cells. Top 2000 highly variable genes were selected based on Seurat v.3 algorithm (flavor = seurat_v3) with batch key “dataset” and refined by removing the following genes '^HLA|^IG[HKL][VDJC]|^MT|^A[A-Z][0-9]|^B[A-Z][0-0]'. Bbknn was used for datasets integration with batch_key = ‘dataset’. Celltypist (model: Immune_All_Low.pkl) with majority voting was used to identify memory B cells. These memory B cells data were then used for training a new Celltypist model (with feature_selection set as TRUE and check_expression as FALSE) allowing label transfer to query B cell data (bnAb HIV donor) as control, viraemic or suppressed, respectively.

The interferon α and γ response score was created by using scanpy.tl.score_genes with the reference gene sets being GSEA Hallmark ‘interferon alpha response’ and ‘interferon gamma response’. Gene set enrichment analysis (GSEA) was performed using the fgsea package available on Bioconductor and visualized with the GOChord function in the GOplot package. Briefly, genes were ranked in the descending order by the Wilcoxon statistic value from the pairwise Wilcoxon rank sum tests (suppressed vs. resting, viraemic vs. resting). All unique leading-edge genes from the ‘interferon alpha response’ and ‘interferon gamma response’ pathways were then subject to a heatmap visualisation.

2.12 Cytokine analysis

2.12.1 LEGEND plex assay

The concentration of cytokines in plasma samples was assessed using a LEGENDplex Human Anti-Virus Response Panel (13-plex) with a V-bottom plate (BioLegend), according to the manufacturer’s protocol. Beads were analysed using a BD-FACS Aria and 5,000 events per sample were acquired

for semi-quantitative analysis using the LEGENDplex Data Analysis Software Suite available online.

2.12.2 IFN titration in HEK293 ISRE cells

HEK293 ISRE reporter cells were seeded in a 96-well flat-bottom white plate at $2x10^4$ cells/well in 100 µL of complete DMEM and incubated in a 37°C incubator with 5% CO_2. After 4 hrs, 50 µL of media was removed per well and replaced with 50 µL of IFN-α2 (Miltenyi Biotec) starting at 10 ng/mL or IFN-γ (Bio-techne) starting at 150 ng/mL, titrated 3-fold and tested in duplicate. Cell only controls were included by replacing 50 µL of the complete DMEM with fresh complete DMEM. Cells were then incubated overnight for 16 hrs in a 37°C incubator with 5% CO_2. Media was removed from each well before the addition of 100 µL Bright-Glo™ luciferase substrate (Promega) diluted 1:20 in 1x lysis buffer and the luciferase activity in RLU was measured using a Synergy H1 Multi-Mode Plate Reader (BioTek).

2.12.3 HEK293 ISRE assay

HEK293 ISRE reporter cells were seeded in a 96-well flat-bottom white plate at $2x10^4$ cells/well in 100 µL of complete DMEM and incubated in a 37°C incubator with 5% CO_2. After 4 hrs, 50 µL of media was removed per well and replaced with 50 µL of IFN-α2 (Miltenyi Biotec) at 0.1 ng/mL or IFN-γ (Bio-techne) at 5 ng/mL in the presence or absence of sterile filtered (0.22 µM) serum/plasma samples with a 1:10 final dilution, tested in duplicate. Cell only controls were included by replacing 50 µL of the complete DMEM with fresh complete DMEM and mAb controls were included by replacing the 50 µL media with mAbs titrated from 0.5 µg/mL or 5 µg/mL (depending on their potency) diluted in complete DMEM in the presence of IFN-α2 (Miltenyi Biotec) at 0.1 ng/mL or IFN-γ (Bio-techne) at 5 ng/mL. Cells were then incubated overnight for 16 hrs in a 37°C incubator with 5% CO_2. Media was removed from each well before the addition of 100 µL Bright-Glo™ luciferase substrate (Promega) diluted 1:20 in 1x lysis buffer. The luciferase activity in RLU was measured using a Synergy H1 Multi-Mode Plate Reader (BioTek) and the percentage ISRE stimulation was calculated based on the median induction

from non-neutralising samples according to (Bastard et al. 2021), following background subtraction of the RLU by cell only controls.

2.13 Statistical analyses

All statistical analyses were performed using GraphPad Prism 9.0.1. For non-parametric data, the Kruskal-Wallis test with Dunn's multiple comparison post-test was used. Mann-Whitney U-test (MWU) was used to compare unpaired, non-parametric data. A non-parametric Spearman's test was used for correlation analysis between two sets of data. Statistical significance in the figures is shown as a p-value (* $p \leq 0.05$, ** $p \leq 0.005$ and *** $p \leq 0.0005$).

Chapter 3: Validating an approach to combine methods for single B cell cloning and single-cell transcriptomics from cryopreserved PBMCs

Background

Investigating B cells at the transcriptomic level has been achieved by two main single-cell RNA sequencing (scRNA-seq) methods (as discussed in section 1.7.2): 10x Genomics Chromium (10x) and Smart-Seq2. Single-cell libraries generated using these methods employ either a droplet-based approach, most commonly 10x, or a plate-based approach, for example with Smart-Seq2.

Although 10x has the advantage of being high throughput with the capacity to sequence thousands of cells at a time, this is confounded by the low recovery of cells due to a sub-optimal capture of approximately 60% (Yamawaki et al. 2021). In addition, a separate V(D)J library is required to sequence the BCR, and antibody variable regions have to be synthesised based on these sequences to test their functionality. Contrary to this, the Smart-Seq2 method has been shown to have higher coverage with more genes detected than 10x, indicating higher sensitivity (Wang et al. 2021). The plate-based approach of the Smart-Seq2 method also provides the ability to integrate single B cell cloning methods, as demonstrated by (Croote et al. 2018). This is possible due to single cells being processed in individual wells, resulting in each well containing the cDNA of a single B cell that can be used to amplify antibody genes for cloning. However, this plate-based approach is more labour-intensive than the droplet-based approach, due to cells being processed individually rather than together as a pool, and therefore limits the number of cells that can be handled at a time.

The purpose of this research was to investigate the phenotype of antigen-specific B cells in HIV-1 infection, which is a very small proportion (<1.5% HIV Env+) of IgG+ B cells found in the periphery and amounts to ~50-300 cells per 10 million PBMCs (van Gils et al. 2016; Freund et al. 2017; Schommers et al. 2020; Sok, van Gils, et al. 2014). The 10x genomics method was therefore

inappropriate for such a rare population due to the minimum requirement of 500 cells per sample, although this is typically run with 1000-10000 cells, as well as the low cell recovery meaning that not all cells would actually be sequenced. Conversely, the Smart-Seq2 method has no lower limit for the number of cells required and has the advantage of being more efficient with a greater read depth per cell (for the detection of more genes). Moreover, the main research aim was to compare the phenotype of bnAb B cells to non-bnAb B cells. To address this aim it was necessary to evaluate the neutralisation capacity of antibodies from B cells, which in turn required the ability to amplify and clone antibody variable regions into expression vectors. Considering that the Smart-Seq2 process produces cDNA for each cell in an individual well, as per standard antibody cloning from single B cells (McCoy and Burton 2017; Huang et al. 2013), it was, therefore, more plausible to use this method to link antibody functionality to the B cell transcriptome analysis.

This chapter sought to establish a method to obtain good-quality, single-cell transcriptome data from cryopreserved memory B cells isolated by FACS. In addition, the feasibility of simultaneous amplification of heavy and light chain variable regions from the cDNA generated by Smart-Seq2 was assessed for compatibility with subsequent cloning and antibody expression.

Results

3.1 Outline of a scRNA-seq and single B cell cloning pipeline

The Smart-Seq2 method has recently been used to study single memory B cells from peripheral blood acquired by FACS (Croote et al. 2018; Andrews et al. 2019; Sutton et al. 2021). The use of FACS offers an automated system to dispense single cells of interest, into individual wells of a plate, based on phenotypic information provided by fluorescence staining of cell surface markers. In addition, fluorescently-tagged antigen probes can be included to identify antigen-specific populations. The pipeline developed here was designed to also use FACS to isolate single memory B cells of interest from PBMCs. As illustrated in Figure 3.1a, single B cells are sorted into individual wells of a plate containing lysis buffer and processed using the Smart-Seq2 method to generate cDNA libraries for sequencing (Picelli et al. 2014). This involves lysing the cells in the presence of an RNase inhibitor to prevent the degradation of polyadenylated RNA (RNA with a poly-A tail). Reverse transcription with oligos specific for the poly-A tail is carried out using an enzyme that adds untemplated nucleotides to the end of the transcribed strand. This addition enables a template-switching oligo (TSO) to anneal for the synthesis of complementary DNA (cDNA), known as template switching. Finally, the full-length cDNA is amplified further (referred to as pre-amplification) and purified to remove excess PCR components.

Libraries for scRNA-seq are generated by subjecting the pre-amplified and purified cDNA to tagmentation (Figure 3.1b). In this process, a Tn5 transposase fragments the DNA into smaller sections (200-600bp) and simultaneously adds in an adaptor required for an enrichment PCR. The enrichment PCR is necessary to both amplify the DNA and introduce Illumina indexes unique to each library. Finally, libraries are quantified, diluted to the same molar concentration and pooled together for Illumina sequencing (described in section 1.7.2).

Single B cell cloning of antibodies is a well-established method that also requires cDNA as the starting material, to amplify Ig V(D)J genes of antibody

variable regions using nested PCR (Tiller et al. 2008). As mentioned earlier, this plate-based approach of processing single B cells offers the potential for Ig variable regions to be amplified from the cDNA generated by the Smart-Seq2 method. Immunoglobulin heavy chain (IgH) and immunoglobulin kappa light chain (IgK) or immunoglobulin lambda light chain (IgL) variable regions from single B cells can then be cloned into vectors containing the corresponding constant region and promoter for expression (illustrated in Figure 3.1c). By maintaining the same layout in each step the cognate IgH and IgK / L pairs from each B cell can then be brought back together for expression of the soluble version of the BCR, also referred to as an antibody. Thus, this pipeline should enable the antibody functionality to be screened and linked back to the B cell transcriptome.

At the time of setting up this pipeline, (Croote et al. 2018) had already demonstrated that it was possible to combine methods for single B cell cloning and scRNA-seq using Smart-Seq2 with freshly purified B cells from peripheral blood. The Smart-Seq2 method was also used shortly after by another group to generate libraries for scRNA-seq from cryopreserved PBMCs, to investigate memory B cells in the context of influenza (Andrews et al. 2019), but did not make reference to the particular memory subsets of interest in this project. The samples available in this project to study the memory B cell response during untreated HIV infection are both cryopreserved (for more than 10 years) and extremely limited. Therefore, it was important to first validate whether the Smart-Seq2 and single B cell cloning methods could be efficiently applied to cryopreserved memory B cells before proceeding with the PBMC samples from HIV-infected individuals.

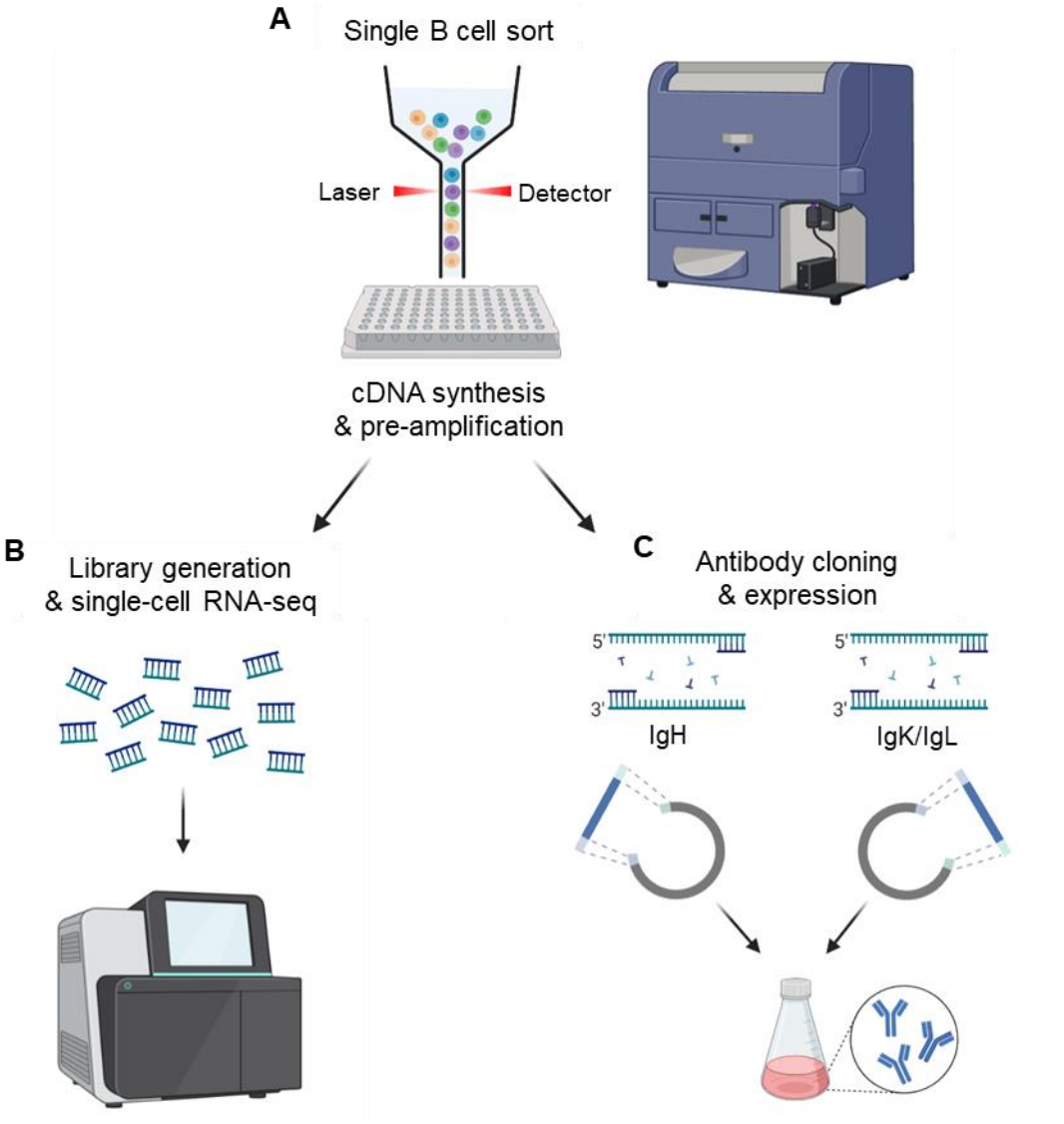

Figure 3.1 An integrated antibody cloning and Smart-Seq2 transcriptomics pipeline.

(A) Single B cells isolated from PBMCs by FACS are sorted into individual wells of a 96-well plate containing lysis buffer. Reverse transcription is used to synthesise cDNA from each B cell and is pre-amplified prior to (B) library generation for single-cell RNA-sequencing (RNA-seq) according to the Smart-Seq2 protocol (Picelli et al. 2014). (C) Antibody V(D)J genes for the heavy (IgH), kappa (IgK) and lambda (IgL) chains are also amplified from the cDNA of each B cell by nested PCR and subsequently cloned into expression vectors containing the constant region. The cloned heavy and light chain from each B cell is transiently transfected into mammalian cells for antibody expression and subsequent characterisation. Image created with BioRender.

3.2 Cryopreserved memory B cells were successfully processed using the Smart-Seq2 method to generate cDNA compatible with antibody cloning

The compatibility of methods for single B cell cloning and Smart-Seq2 was initially validated using PBMCs from an HIV-negative donor that was readily available. PBMCs were isolated from peripheral blood using a ficoll gradient before cryopreservation (as described in section 2.1), as per the processing of HIV cohort PBMCs. However, it should be noted that differences include the disease status, the people who processed the samples, the laboratory that the samples were processed, as well as the length of storage in cryopreservation. For instance, the PBMCs available from untreated HIV infection pre-date 2010 and therefore have been stored for a minimum of 10 years, yet the HIV-negative donor PBMCs used to validate the pipeline here had been stored for less than 2 years.

After thawing, the HIV-negative donor PBMCs were stained (as described in section 2.3.1) to enable single memory B cells to be sorted into individual wells of a plate by FACS. The gating strategy used to identify single memory B cells is shown in Figure 3.2a. In the first panel, FSC and SSC were used to identify the lymphocyte population, then single cells were further gated based on size using FSC-H to remove doublets. A live-dead aqua stain was used in combination with a CD4 antibody conjugated to BV510 to use the same laser for the exclusion of dead cells and CD4+ T cells. The total B cell population was selected based on the expression of CD19 and then gated based on the expression of IgG but not IgM to identify a class-switched, antigen-experienced population. Finally, the canonical cell surface markers CD27 and CD21 were used to identify memory B cell subsets, with resting memory (RM) defined by CD27+ CD21+, activated memory (AM) defined by CD27+ CD21- and tissue-like memory (TLM) defined by CD27- CD21-.

In HIV-infected individuals, the proportion of memory B cell subsets is altered, with an increased frequency of AM and TLM B cells and decreased frequency of RM B cells (Moir et al. 2010). TLM B cells have been previously described as having an exhausted phenotype (as discussed in section 1.6.2) and it is

plausible that this may be reflected in the transcriptome with reduced gene expression. In addition, if transcription of the BCR is reduced then this may also impact the output of single B cell cloning. It was therefore important to ensure the compatibility of the pipeline irrespective of cell phenotype. Therefore HIV-negative donor PBMCs from a post-vaccination time point were chosen to validate this pipeline, on the basis that vaccination increases the frequency of both AM and TLM B cells (Andrews et al. 2019; Sutton et al. 2021).

Memory B cells were gated with boxes around each subset to sort cells from well-distinguished populations (Figure 3.2a), rather than using a quadrant that would have had cells at the intersections that are not so clearly defined. A 96 well-plate of single B cells was sorted from each memory subset into individual wells containing lysis buffer and components for reverse transcription. Following cDNA synthesis and pre-amplification using the Smart-Seq2 method (Picelli et al. 2014), the Ig V(D)J genes from each B cell were amplified by nested PCR (described in section 2.3.5). The BCR of each B cell consists of a heavy (IgH) and light chain, of which the latter can be kappa (IgK) or lambda (IgL). Three separate PCRs were therefore conducted to amplify IgH, IgK and IgL variable regions from the cDNA of single B cells in each memory subset (maintaining the same plate layout to trace these back to the original B cell). The amplification of variable regions was analysed by gel electrophoresis and bands observed at the expected size of 350-500bp indicated the recovery of a variable region.

The percentage of IgH, IgK and IgL variable regions recovered from the single B cells in the RM, AM and TLM subsets are shown in Figure 3.2b. Amplification of IgH was found to be lower in the activated subset (58%) than in the resting or tissue-like subsets (68.2% and 70% respectively). It could be speculated that the activated phenotype leads to a signalling cascade that may result in a lower abundance of BCR transcripts. However, this difference may instead be an artefact of the sample size that would not be seen with the inclusion of more cells.

Amplification of the light chain variable region from single B cells was more efficient, with >95% having an IgK and/or IgL recovered by PCR, regardless of the memory subset. This suggests that the primers used in the IgK and IgL PCRs were more compatible and capable of annealing to the template cDNA than primers used for the IgH amplification. Furthermore, when the percentage recovery of IgK and IgL from each memory B cell subset was added together this was >100%. This can be explained by the amplification of both IgK and IgL from a single B cell, which was observed in a small proportion (2-6%) of the memory subsets. The presence of both a kappa and lambda chain has also been previously found in ~5% of single B cells after variable region amplification (Tiller et al. 2008). During B cell development a process known as receptor editing can alter BCRs that exhibit autoreactivity through additional antibody gene rearrangements (Halverson, Torres, and Pelanda 2004). A possible explanation for the recovery of both IgK and IgL is that transcripts from rearranged and pre-existing BCRs exist in these B cells.

Overall the percentage of B cells with an IgH and IgK or IgL variable region for subsequent cloning in each memory subset is reflected by the total pairs and ranged from 58-70% (Figure 3.2b). This recovery was limited by the IgH amplification but is consistent with previous experience of single B cell cloning and was comparable to the PCR amplification described in the original paper, which recovered antibody pairs in 30-60% of single B cells from different populations (Tiller et al. 2008). The higher percentage of total pairs recovered from the HIV-negative donor in this pipeline is likely a result of the higher amount of starting material for PCRs due to differences in the cDNA synthesis. In this pipeline the cDNA was pre-amplified and purified according to the Smart-Seq2 method, however, this is not part of the cDNA generation using the original single B cell cloning method. To summarise, single RM, AM and TLM B cells sorted by FACS from cryopreserved PBMCs were processed using the Smart-Seq2 method to generate cDNA from which antibody variable regions were successfully amplified for subsequent cloning.

A

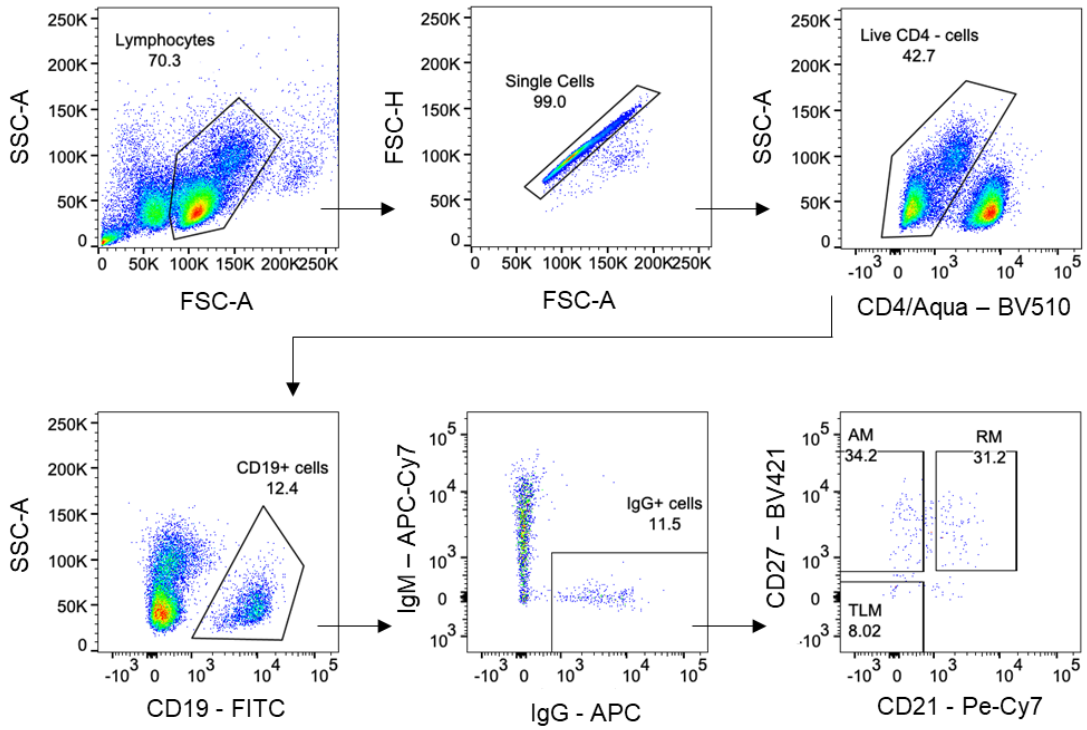

B

B cell subset	PCR Recovery			
	IgH	IgK	IgL	Total pairs
RM	68.2%	55.7%	46.6%	67.0%
AM	58.0%	53.4%	50.0%	58.0%
TLM	70.5%	47.7%	56.8%	70.5%

Figure 3.2 Isolation of single memory B cells from healthy donor PBMCs and recovery of antibody variable regions.

(A) Gating strategy for the isolation of single IgG+ B cells from resting memory (RM), activated memory (AM) and tissue-like memory (TLM) based on the expression of CD21 and CD27. (B) Percentage of B cells with antibody heavy (IgH), kappa (IgK) and lambda (IgL) variable regions amplified by PCR (recovered) from cDNA of RM, AM and TLM subsets. Total pairs reflect the percentage of B cells with both heavy and light chain variable regions recovered.

3.3 Generation of libraries for scRNA-seq from the cDNA of single resting, activated and tissue-like memory B cells

Given that single B cell cloning was found to be compatible with the Smart-Seq2 method, it was necessary to next assess whether the cDNA was also sufficient for the generation of libraries for scRNA-seq. Proceeding with the Smart-Seq2 method was important to ensure the techniques, new to our lab, could be conducted to produce good-quality libraries. In addition, it was necessary to address whether cDNA from memory B cells could be processed and sequenced regardless of phenotype. Therefore, 30 single B cells with paired heavy (IgH) and light (IgK/L) chains from each memory subset were chosen to proceed with, rather than taking forward the cDNA for all cells, for this proof of concept.

The cDNA quality was initially evaluated using an Agilent Tapestation, which is an automated electrophoresis system for high-sensitivity analysis of DNA fragment size. A representative electropherogram generated by the tapestation is shown for single B cells from RM, AM and TLM as well as a negative control (Figure 3.3a). The negative control was subjected to the same processing for cDNA synthesis but intentionally had no RNA input, with no cell sorted into the well, and therefore contained only the lysis and reverse transcription reagents. The electropherogram for this no RNA control showed a single peak at ~150bp representing primer-dimer and had no cDNA peak, indicating that there was no contamination. Electropherograms for the cDNA from single RM, AM and TLM B cells all had a peak consistent with the size of primer-dimer as well as distinct peaks within the range of 1-2 kb reflecting the presence of amplified cDNA (Picelli et al. 2014). The intensity of the cDNA peaks was lowest for RM, reflecting a more quiescent state, and highest in AM, suggesting that these cells have higher transcriptional activity. Yet, this contrasts with the findings in Figure 3.2b which showed that the percentage of B cells with antibody variable regions (total pairs) recovered from AM was lower than in RM.

The cDNA from each B cell was then quantified by Qubit to measure the concentration of double-stranded DNA. Qubit measures the fluorescence of a target-specific dye that is added to the sample and offers a more accurate and sensitive method of quantification than Nanodrop which uses UV absorption. Results from Qubit and tapestation were used to calculate the volume for 1 ng of cDNA required for tagmentation, to fragment the DNA into shorter sections for sequencing. Tagmented DNA was then amplified using an enrichment PCR (as described in section 2.3.3) to add indexes and generate libraries for sequencing. The amplified libraries were purified to remove excess primer before being analysed again by tapestation to check the size of the fragmented DNA. Libraries with an average size of <300bp indicate excessive tagmentation with fragments smaller than required, which would result in inefficient sequencing. However, libraries with an average fragment size >800bp indicate inadequate tagmentation, which would result in DNA fragments that are too large to sequence completely. Representative electropherograms for libraries generated from each memory B cell subset (Figure 3.3b) show that the tagmentation and enrichment PCR were successful, with a broad peak at the expected size of 300-800bp (Picelli et al. 2014). Finally, the concentration of libraries from cells was analysed by Qubit and used in conjunction with the average size of DNA fragments to calculate the molarity of each library. This was essential to allow libraries from each B cell to be normalised to the same molarity (5nM) before being pooled together. The pooled libraries were sequenced by the pathogen genomics unit at UCL using the Illumina NextSeq 500 system with the 2x75 bp Illumina mid-output v2.5 kit. As the flow cell in the Illumina sequencing system preferentially binds to smaller fragments, pooling libraries based on molarity rather than concentration was necessary to achieve the same level of sequencing for each library, also referred to as the read depth. The unique set of indices added to each library during the enrichment PCR enables genes to be tracked back to the original cell after sequencing.

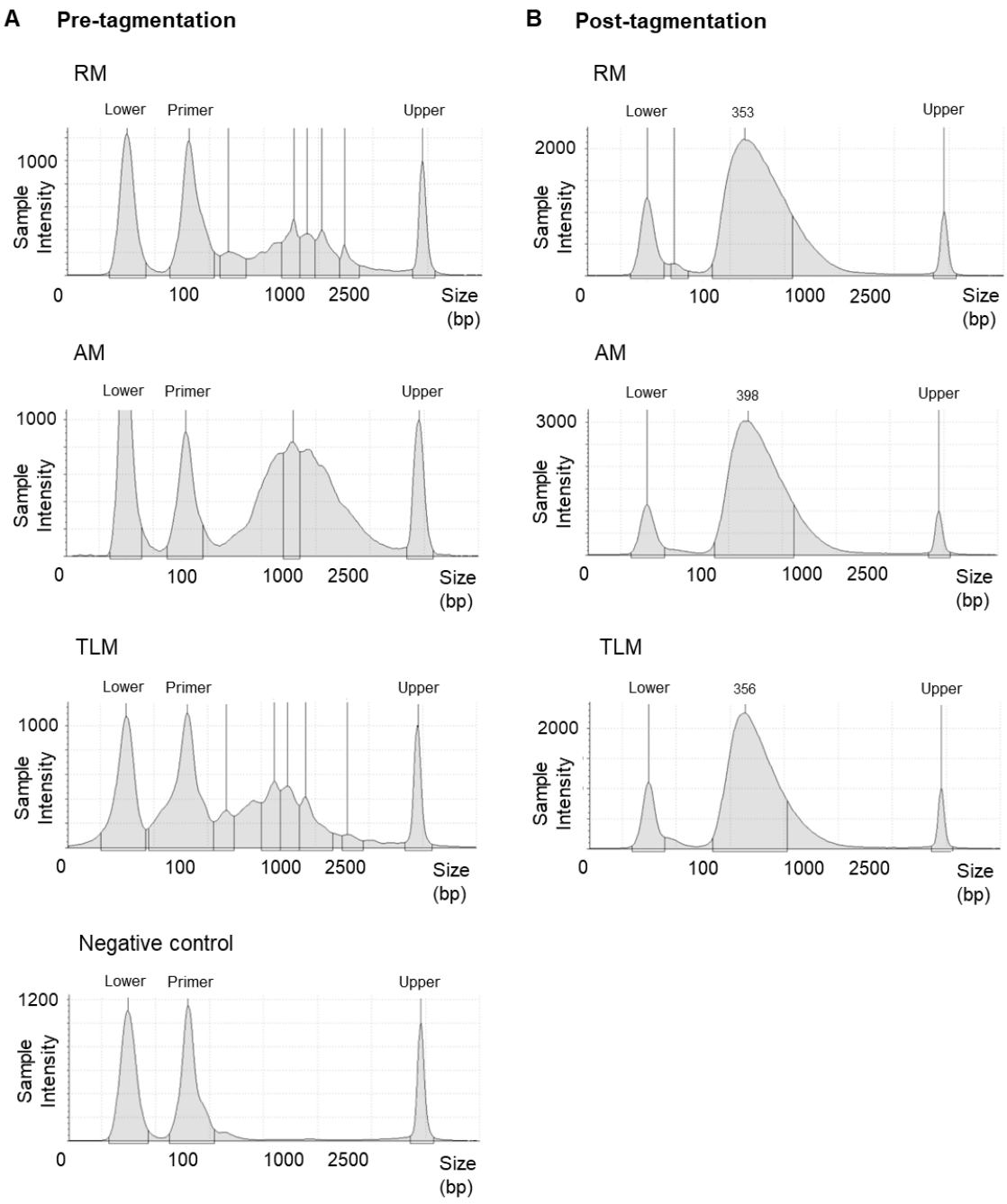

Figure 3.3 Library generation from single memory B cells was successful using the Smart-Seq2 method.

Representative bioanalyser electropherograms of the size distribution in base pairs (bp) and sample intensity (fluorescent units) of cDNA libraries (A) pre-tagmentation, including a negative control (no RNA) and (B) post-tagmentation for resting memory (RM), activated memory (AM) and tissue-like memory (TLM) B cells. Lower and upper markers are indicated on electropherograms and axes are scaled to each sample.

Following Illumina sequencing, the data generated was assessed using three main quality control (QC) measures to ensure that the cells sent for sequencing were viable and libraries were suitable for downstream analysis. First, the library size of B cells was considered and had a median count depth (counts per barcode) of 1.85 million, in keeping with previous B cell libraries of ~1-2 million count depth generated using Smart-Seq2 (Croote et al. 2018). Analysis of outliers in the data identified a minimum count depth threshold of 721,224 (Figure 3.4a) and resulted in three cells (one AM and two TLM) being excluded from further analyses. Second, the number of genes detected in libraries was assessed and found that cells had a median of 893 unique genes. A threshold of 540 genes in a given library was identified by outlier analysis as the lower limit for inclusion in further analyses (Figure 3.4b), identifying two cells (one AM and one TLM) that didn't meet this criterion, which had already been excluded based on library size. Consideration of the gene count per library was necessary to discard outliers with a low number of genes that most likely corresponds to dying cells with a loss of cytoplasmic mRNA due to broken membranes. Although a higher threshold was used by (Croote et al. 2018), discarding cells with fewer than 950 genes, the dataset in this study consisted of naïve B cells and plasmablasts in addition to memory B cells and thus cannot be directly compared as plasmablasts were shown to have a higher gene count than naïve/memory B cells.

Subsequently, the third QC measure used the proportion of mitochondrial genes in libraries as another way to identify non-viable cells, which contain a higher distribution of mitochondrial mRNA that is conserved compared to cytoplasmic mRNA. Outlier analysis of the mitochondrial gene distribution in libraries determined an upper limit of 25%. All cells were below this threshold (Figure 3.4c), showing good viability with a median of 13.6% mitochondrial genes detected. To summarise, libraries from cryopreserved memory B cells were of good quality, with only three cells (two TLM and one AM) that did not pass QC analyses based on library size, due to a low count depth. This indicates that the libraries generated from 97% (87/90) of single memory B cells using the Smart-Seq2 pipeline were suitable for downstream analysis, regardless of whether these were resting, activated or tissue-like.

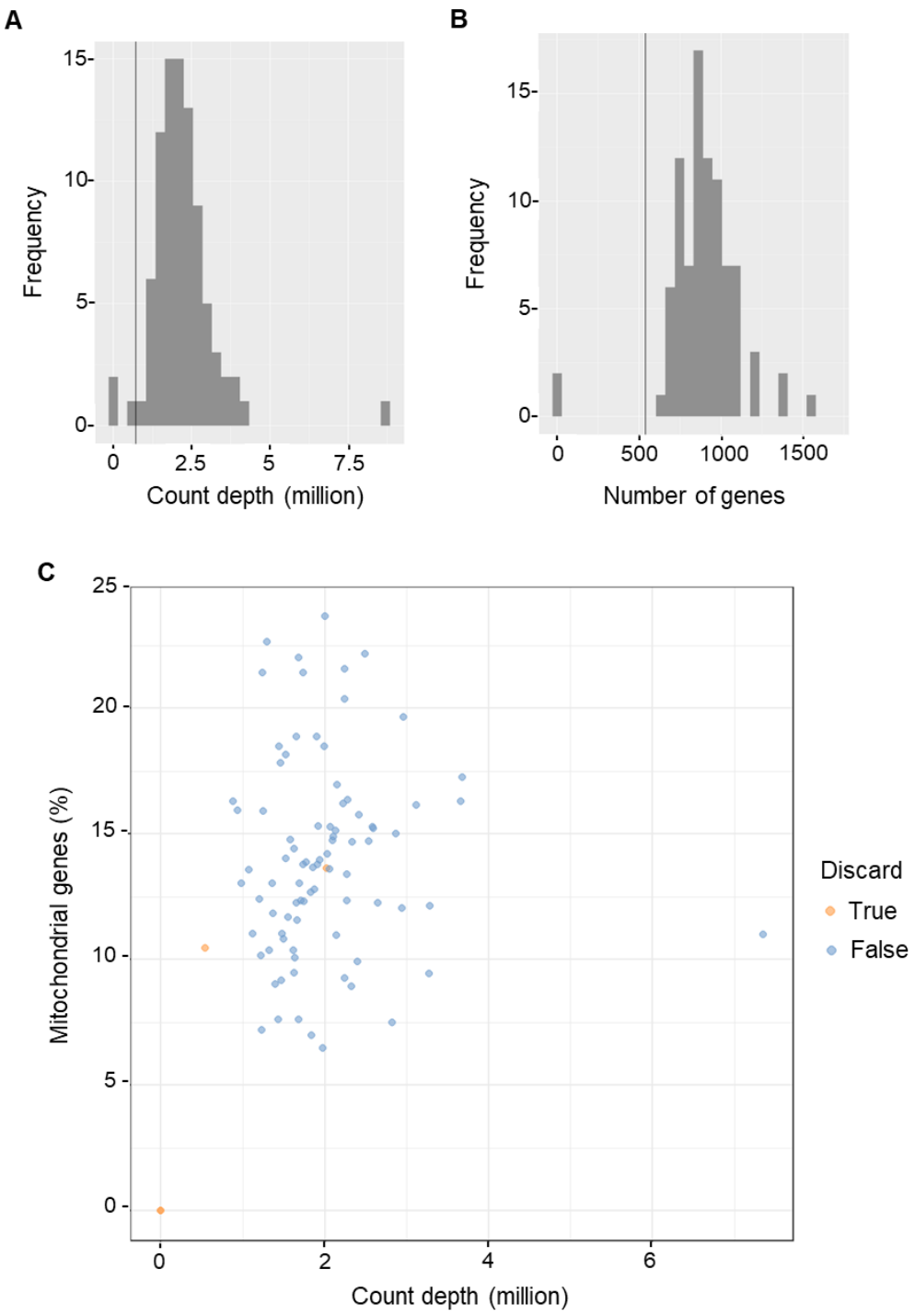

Figure 3.4 Single cell libraries passed quality control checks for downstream analysis.

Outlier analyses were carried out to determine thresholds. (A) Library size based on count depth per cell, with a threshold of 721,224 indicated by the plotted line. (B) Number of genes detected per cell, with a threshold of 540 indicated by the plotted line. (C) Percentage of mitochondrial genes versus count depth, coloured according to if cells passed QC checks (blue) or not (orange).

3.4 BCRs recovered from single memory B cells by scRNA-seq and Ig PCR were comparable

Full-length, paired BCR sequences can be reconstructed from transcriptomic data generated from a plate-based scRNA-seq method by alignment to combinatorial recombinomes using the BraCeR tool, as demonstrated with scRNA-seq data from plasma cells and plasmablasts (Lindeman et al. 2018). The output of BraCeR provides insight into the V(D)J usage, the antibody isotype and reveals the presence of multiple BCRs in a single cell, resulting from non-productive rearrangements of antibody chains or indicating cell multiplets. In addition, clonal relationships between BCRs can be inferred from the V(D)J genes and CDR3 sequences to identify B cell lineages.

The HIV-negative donor scRNA-seq data were subjected to BraCeR analysis to determine whether BCRs could be reconstructed from memory B cells, which have lower BCR transcripts than plasmablasts (Phad et al. 2022). The 90 B cells selected for scRNA-seq were originally chosen, based on the successful PCR amplification of Ig pairs (Figure 3.2b), with an equal number of B cells with an IgH / IgK pairing and an IgH / IgL pairing chosen from each memory subset. As the presence of BCR transcript in these cells was already confirmed, it was expected that BCR reconstruction should be possible from all cells except the two that did not pass scRNA-seq QC analyses based on the low number of genes detected (Figure 3.4b). Indeed, results from BraCeR revealed that a productive IgK or IgL was reconstructed from all but two memory B cells (Figure 3.5a), which were verified as the cells that didn't pass QC. In addition, BraCeR was able to reconstruct IgH from a high proportion of the cells, with 75/88 sequences revealed to be productive (Figure 3.5a). The ability to reconstruct a light chain, but not a heavy chain in all of the cells was also found during the validation of the BraCeR tool (Lindeman et al. 2018). This may be explained by the composition of the heavy chain variable region which is formed of three gene segments (V, D and J), making reconstruction more complex than the light chain which only has two gene segments (V and J). Non-productive sequences were also identified in some cells (Figure 3.5a), which were predominantly IgK or IgL, and likely reflect the presence of BCR

transcripts from previous antibody gene rearrangements. In agreement with this, 13/15 of the single cells with an unproductive light chain (Figure 3.5a) were also found to have a productive light chain. This finding suggests that the ability to produce the mAbs from these B cells may be problematic if the unproductive, instead of the productive, light chain is cloned for expression.

Next, the Ig genes amplified by PCR from these 90 memory B cells were purified and sent for Sanger sequencing to enable comparison to the BraCeR reconstructed BCR sequences. A productive heavy chain sequence was identified in 79 cells, however, nine cells were found to have an unproductive heavy chain sequence and two cells (different from the two cells that didn't pass QC after scRNA-seq) had no heavy chain sequence recovered at all (Figure 3.5b). As mentioned earlier, for the light chain, half of the B cells were IgK and half were IgL. The IgK chain in all 45 B cells was found to be productive, in contrast, the IgL chain in four of the cells was unproductive and in one cell was unable to be sequenced (Figure 3.5b). Comparison to the BraCeR sequences revealed that the cell with no IgL sequence was the same cell that an IgL could not be reconstructed from the scRNA-seq data. In addition, three of the B cells with an unproductive IgL amplified by PCR also had a productive IgL identified by BraCeR, which were not detected upon sequencing after PCR amplification. Nevertheless, when analysed together, 74 of the 90 single B cells had a productive IgH and IgK/L pair amplified by Ig PCR and identified by Sanger sequencing, while 75 of the 90 single B cells had a productive IgH and IgK/L pair identified from scRNA-seq data by BraCeR. Therefore, the number of productive BCR sequences from B cells reconstructed by BraCeR was similar to those amplified for single B cell cloning by PCR. Moreover, this showed that the level of BCR transcript in scRNA-seq libraries of memory B cells is sufficient for reconstruction.

The variable region of productive BCRs identified from scRNA-seq by BraCeR and from Ig PCR by Sanger sequencing of each B cell was then compared. This revealed that heavy, kappa and lambda chains had a range of V-gene and J-gene usage, indicating diversity in the repertoire sampled, which is to be expected even with a limited number of cells. The presence of many similar variants would instead suggest contamination during processing and this was

not found. Moreover, the sequences from BraCeR and Sanger matched, as shown by the same V-gene and J-gene combinations found by both methods (Figure 3.5c). The most frequent heavy chain gene combination was VH3 with JH4 / JH6, which was not surprising considering that the VH3 family has the most alleles and that both VH3 and JH4 genes are the most frequently used in the human repertoire (Volpe and Kepler 2008; Lefranc et al. 2015). For the light chain, the most frequent kappa chain gene combinations were VK1 with JK1/JK2 and VK3 with JK4, while the most frequent lambda chain gene combination was VL1 with JL2. The preferred use of VK1 in the kappa chain of these B cells may be explained by the finding that the VK1 gene family has the highest abundance of alleles (Lefranc et al. 2015). While for the lambda chain, out of the 11 different V-genes, only the VL1, VL2 and VL3 gene families are predominately used (Ignatovich et al. 1997), consistent with the results in Figure 3.5c. It should also be noted that even though not all the possible V-genes and J-genes in the human antibody repertoire were found in these B cells, only a very small proportion of the total B cell population from this HIV-negative donor was sampled, and thus this was not unexpected.

Finally, clonal analysis by BraCeR found only three related sequences in the HIV-negative donor memory B cells, with the same heavy chain (VH4-59 and JH4) and light chain (VL8-61 and JL3) gene usage. The CDR3 sequence of these three B cells was compared to determine their relationship. Two B cells had the same CDRH3 sequence and the CDRL3 sequence varied by one AA, as a consequence, these cells are likely somatic variants. Although only one clonal family was identified, this was expected due to the limited number of cells analysed from this donor. In addition, memory B cells in this trial run were not selected based on antigen specificity during isolation by FACS, and as a result, are unlikely to have been generated during the same immune response. Overall these results confirm that there was no contamination during the processing of single B cells for scRNA-seq or during PCR amplification of Ig, which would have been identified by the presence of only one or a few BCR sequences dominating the results. Instead, B cells exhibited a range of different V-gene and J-gene combinations.

A

	Number of BraCeR sequences		
Productive	IgH	IgK	IgL
Yes	75	44	44
No	1	6	9

B

	Number of Sanger sequences		
Productive	IgH	IgK	IgL
Yes	79	45	40
No	9	0	4

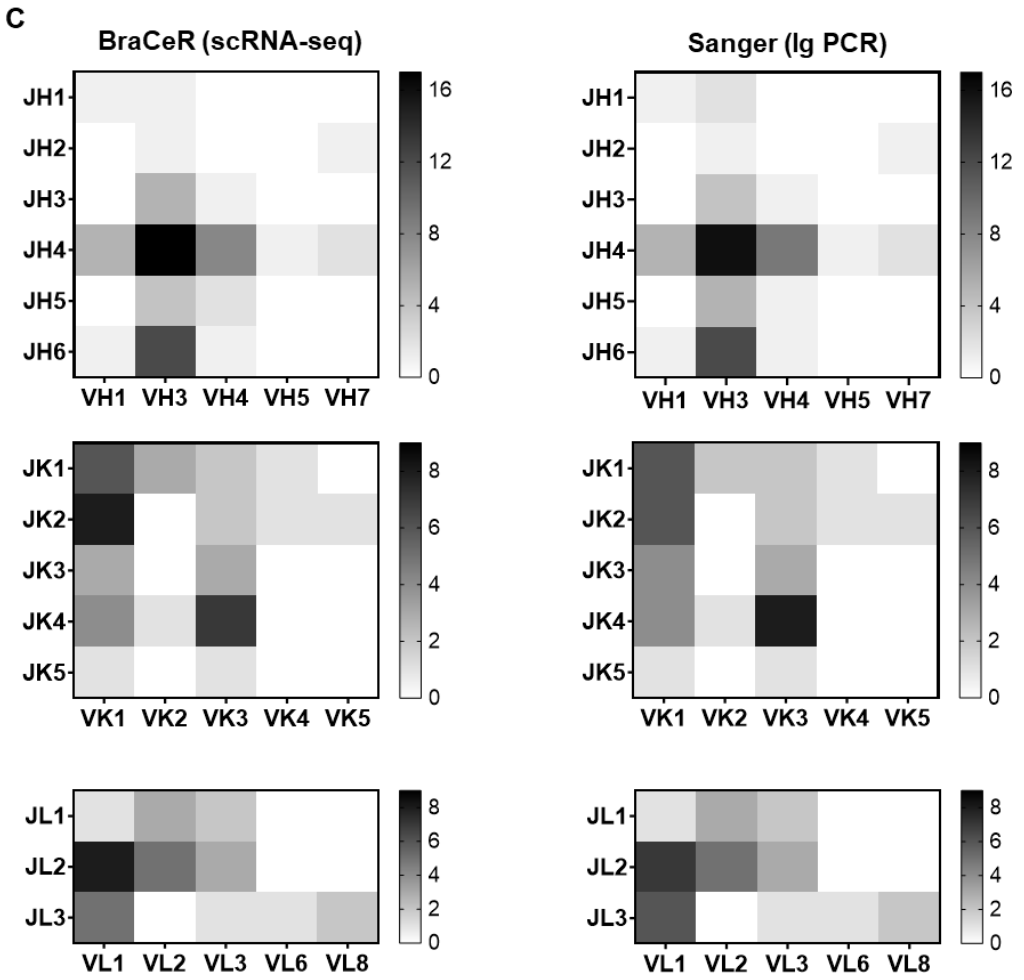

Figure 3.5 Variable region recovery and usage identified from scRNA-seq and Ig PCR were comparable.

(A-B) Frequency of productive and unproductive heavy (IgH), kappa (IgK) and lambda (IgL) chains (A) reconstructed by BraCeR from scRNA-seq data and (B) recovered by Sanger sequencing of Ig PCR products. (C) V-gene and J-gene usage by productive, full-length heavy, kappa and lambda chains identified by BraCeR from scRNA-seq and by Sanger sequencing of Ig PCR products. Sanger sequencing was analysed using IMGT V-Quest to identify V-gene and J-gene usage.

3.5 BCRs from single memory B cells of the HIV-negative donor displayed features consistent with a typical human antibody repertoire

Productive BCR heavy chain sequences identified from the HIV-negative donor B cells by BraCeR were investigated further to compare the main antibody features across each memory subset, specifically the percentage SHM, CDRH3 length and isotype usage. As mentioned in section 1.3.6 B cells that undergo affinity maturation in the germinal centre acquire mutations in the BCR that result in improved binding to antigen. The level of SHM is therefore a reflection of the extent of maturation and can be calculated by comparison to germline reference sequences in IMGT. The V_H sequences from the BCRs in the HIV-negative donor had an average SHM of 6.3%, in keeping with the average SHM of 5.6-9.4% previously identified in a healthy donor cohort (IJspeert et al. 2016). In addition, the BCRs analysed here had a wide range of V_H SHM from 1.4 - 18.5%, although only one of the BCRs exhibited 18.5% SHM and the rest had <15%. A range of SHM in the V_H of BCRs was observed regardless of the memory subset, and when the median SHM for RM (6.1%), AM (7.2%) and TLM (5.1%) was compared this was not significantly different (Figure 3.6a).

Next, the heavy chain CDR3 length in B cells from the three memory subsets was analysed. Although all the CDR loops are important in antigen binding, the CDRH3 confers the most diversity and often has the greatest role in antigen specificity (Xu and Davis 2000). Furthermore, the CDRH3 length can affect the conformation of the antigen-binding site and subsequently, the type of antigen that can be targeted (Collis, Brouwer, and Martin 2003). The CDRH3 length in the BCRs from this HIV-negative donor ranged from 5-23 AAs, falling within the range of 4-36 AAs that have been previously identified in the human antibody repertoire (Shi et al. 2014). Although long CDRH3 regions have been identified in mature B cells, these are less frequent in the repertoire, likely due to the strong association with specific gene combinations (Briney, Willis, and Crowe 2012). The exact definition of a long CDRH3 region is subjective but has been characterised as >21 AAs (Larimore et al. 2012)

and ≥24 AAs (Briney, Willis, and Crowe 2012). While three BCRs in both AM and TLM had a CDRH3 length >21 AAs, none were identified in RM, and none reached 24 AAs (Figure 3.6b). To compare differences between the memory subsets, the median CDRH3 length of BCRs from RM (15 AAs), AM (15 AAs) and TLM (18 AAs) were analysed by Kruskal-Wallis test with Dunn's multiple analysis. Despite TLM BCRs having a higher median CDRH3 length, this difference was not found to be significant. Finally, taking all the CDRH3 sequences together, the average length was 16.1 AAs which is comparable to the average human CDRH3 length of 15.5 (± 3.2) AAs found in public datasets (Shi et al. 2014).

The isotype of BCRs, encoded by the heavy chain constant gene, can also be identified from sequences reconstructed from scRNA-seq data by BraCeR. On the heavy chain locus, the constant region genes IgM and IgD can be rearranged during class-switch recombination to isotypes downstream on the locus, IgG, IgA or IgE, for a different effector function (reviewed in more detail in section 1.3.5). As the single B cells from this donor were isolated by FACS based on their expression of IgG, only the IgG isotypes in each memory subset were considered here (Figure 3.6c). This revealed that RM was predominantly IgG1, followed by IgG2 and rarely IgG3/4. AM was predominantly IgG1 or IgG2, followed by IgG3 and rarely IgG4. In contrast, TLM was predominantly IgG1 or IgG3 and rarely IgG2, with no IgG4 detected. This distribution of IgG isotypes in RM and AM (CD27+) and TLM (CD27-) cells is also consistent with findings in the literature, where CD27- B cells had a preferential use of IgG1 and IgG3 compared to CD27+ B cells that had a dominant IgG1 and IgG2 usage (Berkowska et al. 2011).

Despite the conflicting view of whether TLM cells are an exhausted subset or on the path towards an effector cell at inflammatory sites (reviewed in section 1.6.2), preferential use of IgG3 in TLM cells shown in Figure 3.6c seems logical due to its location within the Ig locus. Considering only the IgG subtypes in the heavy chain constant region locus, these are organised in the following order: IgG3, IgG1, IgG2 and then IgG4. Class-switching occurs sequentially in the order of the locus and is unable to switch back to isotypes upstream. This implies that although IgG3 cells are class-switched these B cells have not been

stimulated to class-switch further, which could be explained by an exhausted state or a fate towards an effector cell rather than continued maturation. Finally, the infrequent use of IgG4 in all memory subsets was expected as IgG4 is further downstream of the locus than the other IgG isotypes and has the lowest proportion (of the IgG isotypes) in human serum (Schroeder and Cavacini 2010). Overall, the features of BCRs from this HIV-negative donor were comparable to those in a typical human antibody repertoire, providing confidence to proceed with the investigation of rare HIV+ samples.

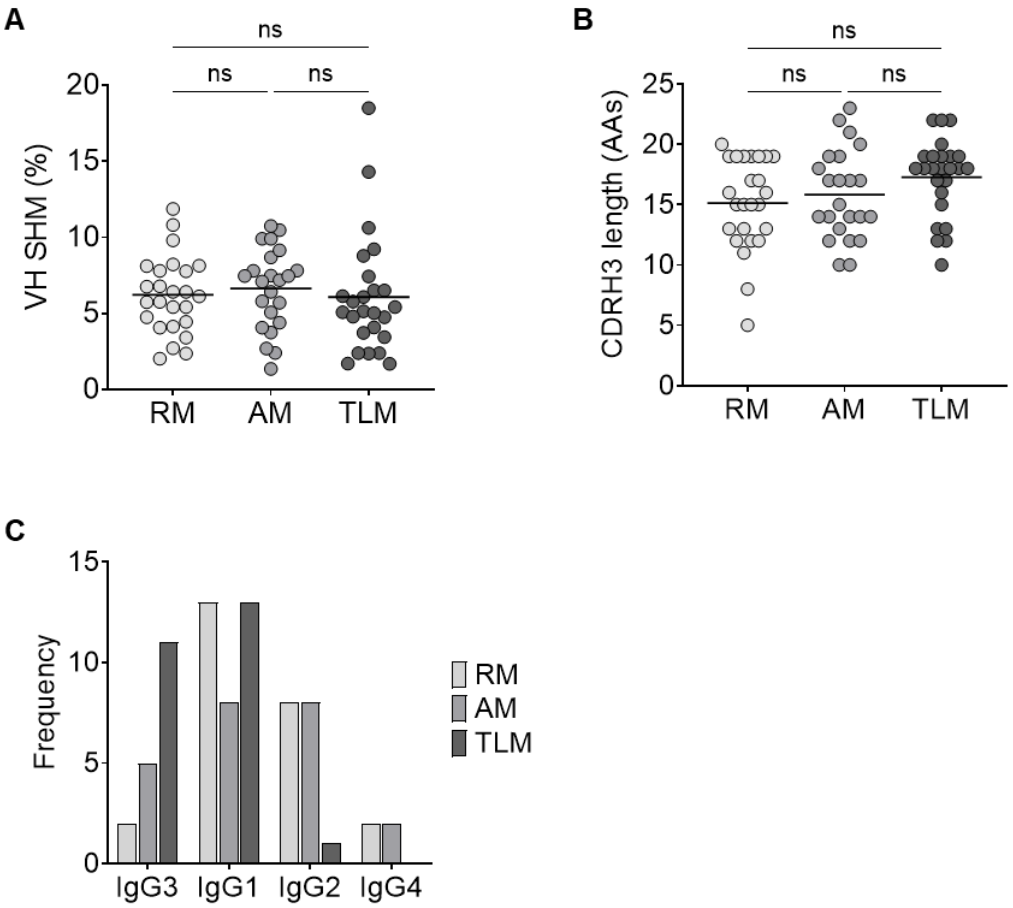

Figure 3.6 Features of antibody heavy chains from memory B cell subsets of a healthy donor.

Heavy chains of resting memory (RM), activated memory (AM) and tissue-like memory (TLM) B cells were analysed based on sequences identified by BraCeR from scRNA-seq data. (A) Percentage somatic hypermutation (SHM) was determined from nucleotide sequences for variable heavy (V_H) genes in each memory B cell subset, with horizontal lines indicating the median. (B) Heavy chain CDR3 length in amino acids (AAs) for each memory B cell subset, with horizontal lines indicating the median. (C) Frequency of IgG isotypes within each memory B cell subset, with isotypes ordered according to the position in the heavy chain locus. Kruskal-Wallis test with Dunn's multiple analysis was conducted in A and B using a *p*-value <0.5, and non-significant (ns) differences are indicated.

3.6 Tissue-like memory B cells were transcriptionally distinct from resting and activated memory B cells

Finally, the scRNA-seq data were analysed to determine how well the pipeline was able to differentiate memory B cell subsets based on their transcriptome. Unsupervised clustering of B cells visualised using principal component analysis (PCA) of normalised gene expression revealed that RM and AM cells had substantial overlap with each other, suggesting highly similar transcriptomes (Figure 3.7a). However, TLM cells showed separation away from the RM and AM cells, indicating that these have a different transcriptional phenotype. This is consistent with existing literature on transcriptomic differences between memory B cell subsets, although precise subset definitions are complicated by non-standard terms across different disease states (Portugal et al. 2017). For instance, TLM cells are also referred to as atypical B cells in malaria research. Findings from bulk RNA-seq analysis of memory B cells from malaria-exposed donors revealed that atypical B cells (CD27-CD21-) have a distinct gene signature compared to classical / resting (CD27+CD21+) and activated (CD27+CD21-) B cells (Holla et al. 2021).

To investigate if similar signatures were observed in the analogous B cell subsets isolated from the HIV-negative donor, memory B cells were assigned gene signature scores based on genes reported to be upregulated in the malaria-exposed atypical B cells from Holla et al. The HIV-negative donor TLM cells achieved the highest score (Figure 3.7b), confirming that these cells are similar to the atypical memory B cell population previously observed in an infection setting, as well as being transcriptionally different from RM and AM cells. However, it is worth considering that several AM cells also had an atypical gene signature score similar to the TLM B cells which ties in with the presence of some AM cells clustering with TLM cells in Figure 3.7a. This likely stems from the fact this data was generated from single B cells yet atypical gene signatures were generated from bulk RNA-seq data (Holla et al. 2021), which likely missed subtle differences / masked the heterogeneity of the population at a single-cell level. In summary, TLM B cells isolated from the HIV-negative donor in this pipeline have a distinct transcriptome that separates

them from RM and AM B cell subsets, similar to previously described atypical B cells as predicted.

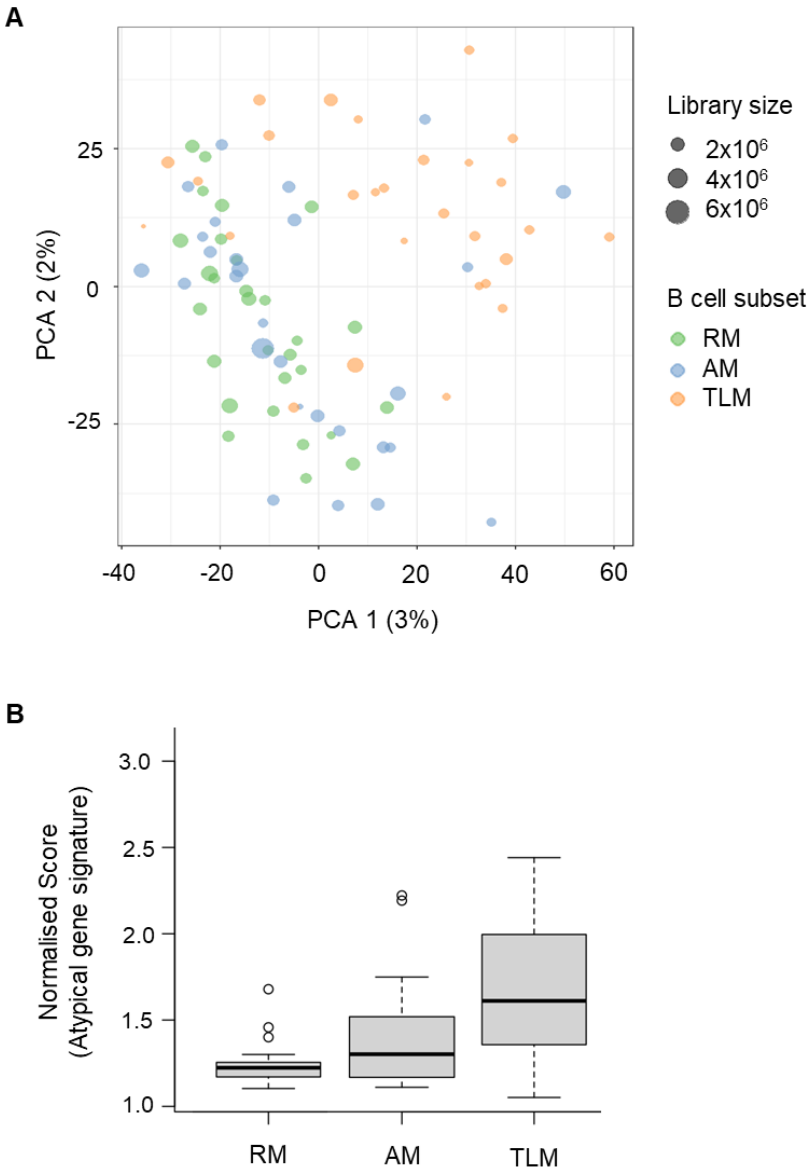

Figure 3.7 Tissue-like memory B cells have a distinct transcriptional phenotype compared to resting and activated memory B cells.

(A) PCA visualisation (after QC) of single-cell transcriptomes of 87 memory B cells from an HIV-negative individual. The size of each circle corresponds to the number of genes per library and the colour corresponds to the original FACS sorting strategy for resting memory (RM, green), activated memory (AM, blue) and tissue-like memory (TLM, orange) B cells. (B) Gene signature score assigned to resting memory (RM), activated memory (AM) and tissue-like memory (TLM) B cells based on upregulated atypical genes identified by (Holla et al. 2021).

Summary

Overall, the ability to combine methods for antibody cloning and Smart-Seq2 transcriptomics was successful and results have shown proof of principle for investigating the phenotype of memory B cell subsets after cryopreservation. This pipeline produced scRNA-seq libraries of the expected size and required quality (for 97% of the cells) necessary for downstream analysis of the transcriptome. There was also sufficient cDNA to amplify V(D)J genes for cloning of antibody heavy and light chain pairs from single B cells. Furthermore, all the productive sequences with a complete variable region were found to match the variable regions of BCRs from the original B cells, which was a requirement to link antibody functionality to the B cell phenotype.

An additional step, to further validate the pipeline, would have been to clone the amplified variable region sequences into full-length IgG vectors, produce purified antibodies and screen their functionality. However, antibody cloning from PCR-amplified variable regions is routinely performed successfully in the lab, and so to validate the pipeline, this step was not deemed necessary. In addition, the PBMCs used were from an HIV-negative donor and although the B cells isolated were class-switched and deemed antigen-experienced, it would not have been feasible or necessary for the overall aims of this research to determine which antigen these were raised against to test for binding. Moreover, analysis of antibody sequences revealed that the V and J gene usage, percentage SHM, CDRH3 length and isotype from the memory B cells of this HIV-negative donor were typical of the human IgG repertoire.

Finally, these results show that this pipeline was suitable for processing cryopreserved memory B cells regardless of whether these were resting, activated or tissue-like (defined based on their cell surface expression of CD27 and CD21). This was important to consider, as this pipeline was established to investigate the phenotype of memory B cells from HIV-infected individuals who have a distorted B cell population, in particular a higher frequency of TLM B cells. Transcriptional analysis using clustering via PCA and assignment of gene signature scores found that consistent with the literature, TLM B cells were distinct from RM and AM B cells. Although the transcriptomic analysis

carried out with the HIV-negative donor cells was not extensive and did not extend far beyond quality control measures, this was due to the relatively small number of cells (30 per memory subset) in the dataset. However, the analysis was sufficient to indicate that the scRNA-seq data produced using this pipeline is suitable for downstream analyses.

In summary, this chapter provides support for the choice of method for generating scRNA-seq libraries with a high recovery rate (by Smart-Seq2) and confirms compatibility with antibody cloning to explore the B cell response in HIV infection using rare patient samples.

Chapter 4: Characterisation of a historic cohort of HIV-1 infected individuals reveals a small subset of elite neutralisers that target a variety of bnAb epitopes

Background

After a few years of HIV-1 infection, a small proportion of individuals (10-30% adults) demonstrate the ability to develop nAbs that exhibit cross-neutralisation of several HIV strains, and an even smaller subset (1-10%) termed elite neutralisers produce broadly neutralising antibodies (bnAbs) against many HIV-1 strains from different clades (McCoy and McKnight 2017). The establishment of standard panels of Env pseudo-typed virus (PV), such as the 6 PV panel and global 12 PV panel (Simek et al. 2009; deCamp et al. 2014), that take the viral tier and clade into consideration has enabled consistent screening for broad antibody neutralisation (as discussed in 1.4.1). In particular, evaluating the neutralisation breadth exhibited by patient plasma or sera against the standard 6 PV panel has been invaluable in identifying elite neutralisers by their ability to neutralise a minimum of one PV across four different clades (Simek et al. 2009). A neutralisation score can also be calculated from the average of log-transformed titres against the PV panel to characterise and compare the breadth of neutralisation, with elite neutralisers classified as having a score >2 (Landais et al. 2016).

Advances in methods have led to many recent HIV bnAbs being isolated from elite neutralisers by single B cell cloning after single B cell culture (Walker et al. 2009; Walker et al. 2011). The use of antigen-specific cell sorting has also been used to identify HIV-reactive B cells based on their BCR specificity, without the need for high-throughput screening of secreted antibodies from cell culture to determine antigen-specificity (McCoy and Burton 2017). In addition, recombinant soluble HIV Env trimers displaying bnAb epitopes have been successfully used as antigen probes in FACS with epitope knockout counter probes to isolate bnAb B cells from PBMCs (Wu, Yang, et al. 2010; Doria-Rose et al. 2016). Therefore, prior knowledge of the epitope(s) on Env targeted by plasma for neutralisation of HIV PVs can be useful to design

antigen probes for use in FACS to identify bnAb and non-bnAb B cells. Previous studies have been able to map broad plasma responses to only one or two bnAb epitopes, in many cases, predominantly through the use of mutant PVs or protein absorption in neutralisation assays (Landais et al. 2016; Walker et al. 2010; Doria-Rose et al. 2017). This method of epitope mapping using mutant PVs is only possible due to the thorough characterisation of previously isolated bnAbs, giving insight into the exact residues targeted within different epitope specificities on HIV Env. In addition, the identification of plasma neutralisation breadth against known bnAb epitopes adds further validation that elite neutralisers are capable of producing individual bnAbs, rather than breadth being attributed to multiple nAbs targeting many different epitopes.

This chapter aimed to identify elite neutralisers from a historic cohort of HIV-infected individuals with the potential to produce bnAbs for evaluation using the single B cell cloning and transcriptomics pipeline validated in chapter 3. In addition, the epitope specificity of neutralising antibodies in the plasma of these individuals was investigated to inform the selection of Env probes for use in FACS to isolate bnAb and non-bnAb B cells.

Results

4.1 Evaluation of neutralisation by the East London cohort identified individuals with the ability to neutralise non-autologous viruses

The use of the TZM-bl assay to evaluate antibody neutralisation by mAbs and polyclonal antibodies in plasma is well-established and validated (Sarzotti-Kelsoe et al. 2014). The TZM-bl cells used in this assay are a modified version of the HeLa cell line that express CD4, CXCR4 and CCR5 (Platt et al. 1998) for HIV-1 entry and contains a firefly luciferase (luc) gene under transcriptional control of a tat-regulated promoter (Wei et al. 2002). Expression of the *Luc* reporter gene is detected by a luminometer following cell lysis and the addition of a luciferase substrate. This enables quantification of the relative light units (RLU) that corresponds to the level of HIV infection (Figure 4.1a). Incubation of the virus with antibodies before the addition of TZM-bl cells allows the neutralisation capacity of mAbs or polyclonal plasma to be assessed (Figure 4.1b). The extent of viral inhibition by neutralising antibodies targeting the Env and thus blocking HIV entry into TZM-bl cells is identified by the reduction in RLU relative to virus-only controls as in Figure 4.1a. In this assay, PVs are typically used to achieve single-round infection of TZM-bl cells and also offer a standardised way to assess antibody neutralisation of different HIV envelope proteins. This is possible because PVs are produced using a two-plasmid expression system, with a backbone plasmid that encodes for the HIV genome but lacks Env and another plasmid for Env expression. As a consequence, different PVs vary only by the Env protein and enable antibody neutralisation to be compared.

To investigate the humoral and B cell response during HIV-1 infection and phenotypes associated with a broadly neutralising response, it was necessary to first identify PLWH in the absence of ART. The East London cohort was originally recruited to study the relationship between viral clade and neutralisation specificity and thus consisted of individuals from geographically diverse regions infected with different clades of HIV-1, determined from sequencing where possible (Dreja et al. 2010). All patients had been infected with HIV-1 for a minimum of one year and recruited before 2010, meaning that

ART was only initiated for those with an AIDS-defining illness or a persisting CD4 cell count <200 cells/µL (Gazzard 2008). Select plasma and PBMC samples from patients in this historic cohort were made available for use here. In addition, data for patients in the cohort regarding the inhibitory dilution of plasma that neutralised 50% of virus input (ID_{50}) of PVs already tested using the TZM-bl assay in the previous study (Dreja et al. 2010) was made available by our collaborators.

An overview of how this data was evaluated to select individuals with the potential to exhibit broadly neutralising antibody responses is shown in Figure 4.2. Neutralisation of a negative control (murine leukaemia virus (MLV)) PV was first considered on the basis that this is an irrelevant (non-HIV) Env that individuals would not have had previous exposure to. Consequently, reactivity against the MLV PV is likely due to the presence of ART in patient samples, which can interfere with the reverse transcription of viral RNA and thus prevent transcription of the tat-regulated luciferase reporter gene (Sarzotti-Kelsoe et al. 2014). As ART can mimic the neutralisation of PVs in the TZM-bl assay, it was important to address whether patients were on ART at the time of sampling to ensure that the neutralisation of HIV PVs was truly a reflection of the antibody response in plasma. Patients that appeared to neutralise the MLV PV, with an ID_{50} titre >200, were therefore excluded (n=9). Next, patients without substantial plasma reactivity against MLV were stratified based on their ability to neutralise HIV PVs that have been previously classified into sensitivity tiers 1, 2 and 3 (Seaman et al. 2010). Tier 1 PVs are considered more sensitive to neutralisation with a predominantly open Env conformation, characteristic of lab-adapted strains. On the other hand, tier 2/3 PVs are more typical of circulating strains with a predominantly closed conformation of the Env trimer that is more resistant to neutralisation (Montefiori et al. 2018; Munro et al. 2014). Plasma samples that were capable of neutralising only tier 1 viruses (n=9) were excluded from further analysis due to the inability to target harder-to-neutralise viruses. A criterion of exhibiting neutralisation against more than one tier 2/3 virus with an ID_{50} titre >100 was then used to select plasma samples for additional screening of neutralisation breadth. Finally, for the purpose of this research, it was necessary to study individuals with both

plasma and PBMC samples available, to investigate the phenotype of B cells (isolated from PBMCs) of individuals confirmed as having broadly neutralising antibody responses (identified from plasma). A total of 22 individuals met this requirement and were chosen to proceed with.

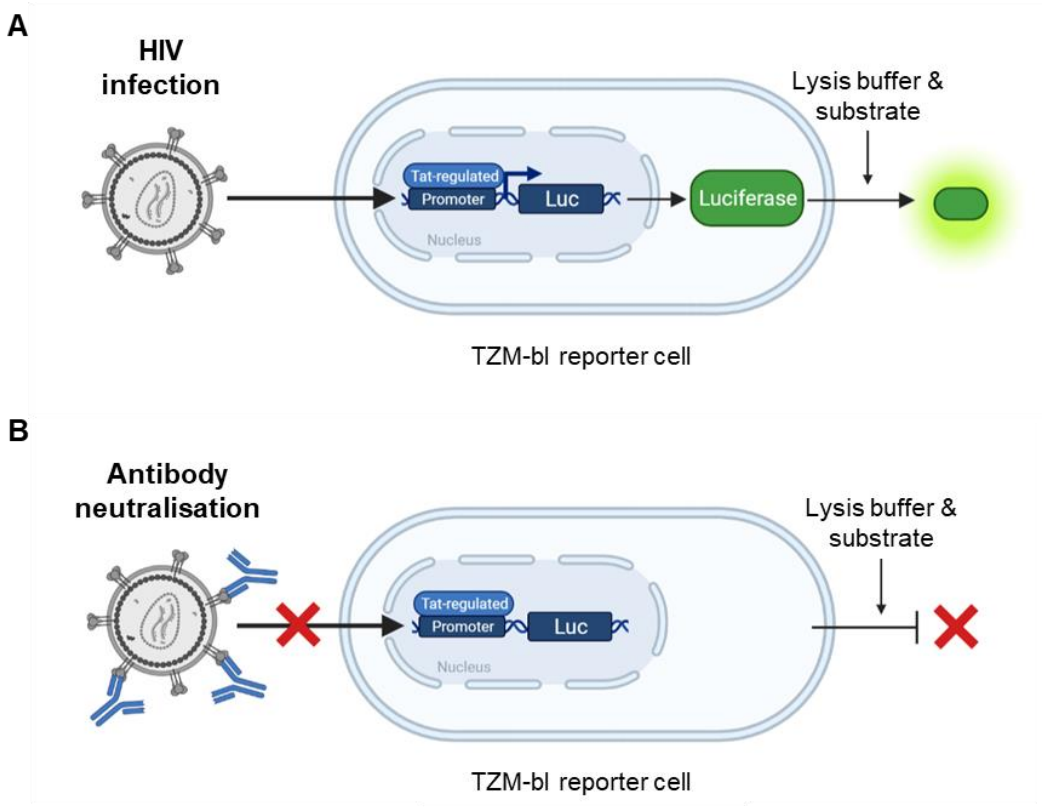

Figure 4.1 TZM-bl cell reporter assay for the detection of HIV infection and antibody neutralisation.

HeLa TZM-bl cells express CD4 as well as CXCR4 and CCR5 for entry of HIV (regardless of tropism) and contain a tat-regulated firefly luciferase gene under the control of an HIV-1 LTR that is transcribed upon HIV infection. (A) Viral infectivity can be measured by the luciferase activity in relative light units (RLU) after lysing the cells and adding a luciferase substrate. (B) Neutralisation of HIV by plasma or monoclonal antibodies can be measured by the reduction in RLU, reflecting the reduction in viral infection, relative to (A). Image made with Biorender.

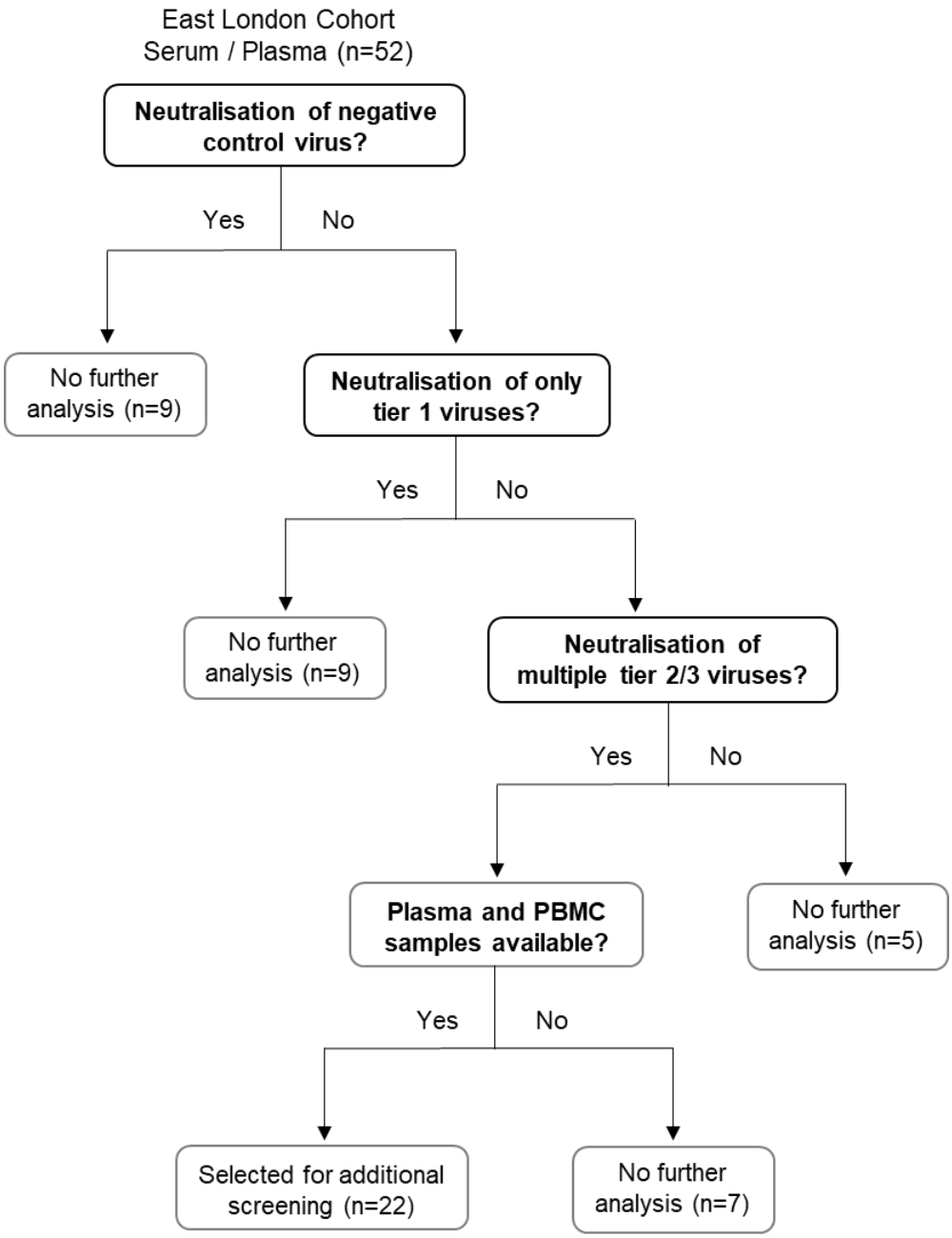

Figure 4.2 Selection of patients from the East London Cohort with the potential for broad neutralisation.

Pre-existing plasma neutralisation data for (n=52) patients was analysed to identify those with the ability to neutralise heterologous viruses, based on neutralising tier 1 and tier 2/3 viruses but not the negative control murine leukaemia virus (MLV).

4.2 Screening plasma from patients against a standard PV panel revealed a range of neutralisation profiles, including elite neutralisation

Standard panels of PVs are frequently used to screen for antibody neutralisation breadth, typically making use of harder-to-neutralise tier 2 viruses from different viral clades. Analysis of large virus panels chosen from globally circulating strains (Simek et al. 2009) identified a minimal set of 6 PVs that could be used to calculate neutralisation breadth with the same degree of confidence as the full panel of viruses. As mentioned earlier, individuals that demonstrate very broad neutralising plasma activity against the 6 PV panel are termed elite neutralisers and can be identified as having a neutralisation score ≥2 (Landais et al. 2016). This scoring system, which takes into consideration the number and potency of viruses neutralised, has proven effective with follow-up studies confirming that bnAbs can be isolated from the PBMCs of donors identified as elite neutralisers (Walker et al. 2009).

The standard 6 PV panel consists of tier 2 PVs expressing Env from multiple clades: 92TH021 (CRF AE), 94UG103 (Clade A), JRCSF (Clade B), 92BR020 (Clade B), C22 (Clade C) and 93IN905 (Clade C). The minimal number of viruses in this panel (compared to the global 12 PV panel) is particularly advantageous, not only for rapid screening but also to reduce the amount of sample required, which is important for samples with limited availability such as those from the East London cohort. The plasma/serum from patients in the East London cohort selected in Figure 4.2 (n=22) was screened against this 6 PV panel to identify those with broad neutralisation. This was achieved by titrating samples against PVs in neutralisation assays using TZM-bl reporter cells to determine the reduction in infectivity (as shown in Figure 4.1 and described in 2.6.3). Plasma/serum that produced a sigmoidal curve with two or more dilutions achieving >50% neutralisation and <50% neutralisation had an appropriate linear range to calculate an ID_{50} from. The ID_{50} titres exhibited by patient samples against the standard 6 PV panel are shown in Figure 4.3 and demonstrate how effective each plasma/serum sample is against each PV, with a higher ID_{50} titre reflecting more potent neutralisation. The starting

dilution of plasma/serum used in assays was 1:100 and hence was the limit of detection, with ID_{50} titres <100 deemed as non-neutralising. In some instances, (sample permitting) the starting dilution of samples was lowered to 1:50 in repeat assays to obtain sigmoidal curves to calculate an accurate ID_{50} titre. Patients demonstrated varying degrees of potency against PVs in the panel (Figure 4.3), ranging from an ID_{50} titre of 102, which was only just above the limit of the detection, to an ID_{50} titre of 4649, which was highly potent. Patients also exhibited a range of neutralisation profiles against the standard 6 PV panel, with some plasma/serum being incapable of neutralising any of the PVs whilst others were able to neutralise all six PVs (Figure 4.3). The most susceptible PV in the panel was 93IN905 (clade C), which was able to be neutralised by plasma from patients with a clade C infection but also those with a non-clade C infection. Conversely, C22, the other clade C PV in the panel was the most resistant to plasma neutralisation (Figure 4.3), signifying that differences in the Env can affect neutralisation despite being from the same clade.

To assess the extent of neutralisation breadth, the ID_{50} titres achieved by patient plasma against each PV in the standard 6 PV panel were log-transformed and then averaged to calculate a neutralisation score (as explained in section 2.6.3). The patients in Figure 4.3 are listed in order of their neutralisation score to rank the neutralisation breadth and identify moderate neutralisers (score ≥0.5), broad neutralisers (score ≥1) and elite neutralisers (score ≥2) (Landais et al. 2016). Despite being selected based on their capacity to neutralise heterologous viruses (Figure 4.2), six patients scored <0.5 and displayed little to no neutralisation breadth against the 6 PV panel. Five patients achieved a score between 0.5 and 1, reflecting moderate breadth of neutralisation and seven displayed broad neutralisation with a score >1. However, of most interest were the four patients (T125, R216, K300c and A260) demonstrating elite neutralisation (with a score >2), indicating the potential to produce bnAbs (Walker et al. 2009; Walker et al. 2011). Indeed, the plasma from patients T125, R216 and A260 were able to neutralise all six PVs in the panel. In particular, T125 exhibited highly potent neutralisation (ID_{50} titre >1000) of four PVs in the panel, from three different clades, and

consequently achieved the highest neutralisation score of 3.19. Plasma from K300c also exhibited elite neutralisation, with only one PV (92BR020) not susceptible. Although plasma/serum from other patients in the cohort also demonstrated the ability to neutralise five PVs in the panel, the ID_{50} titres were not as high and therefore not as potent as K300c, resulting in a neutralisation score of <2. In addition, samples were re-tested against the negative control PV MLV and results confirmed the previous findings that these patients were unable to neutralise MLV, with an ID_{50} titre of <100 (Figure 4.3). This validated that none of the patients were on ART at the time of sampling and that the neutralisation of HIV PVs was a result of the antibody response. Although ideally plasma/serum would have been tested for an n=3 against all PVs, with at least one of these repeats testing plasma in duplicate, the limited amount of sample available restricted this to an n=2 with most individuals only being tested in singlet each time.

As mentioned earlier, neutralisation scores for patient samples were calculated from the ID_{50} titres achieved against the standard 6 PV panel. A representative graph of plasma/serum from each neutralisation score shows the neutralisation curves used to identify these ID_{50} titres (Figure 4.4a). A neutralisation score of 0 reflects the inability of plasma/serum to neutralise any of the PVs tested and is shown by the titration series for patient S162, with only the top dilution close to 50% neutralisation which is insufficient to calculate an ID_{50} titre. Plasma with a neutralisation score <0.5 but >0, e.g. patient G400, neutralised a single PV with a sigmoidal curve consisting of at least two plasma dilutions achieving >50% neutralisation, as shown in the representative graph (Figure 4.4a). In this example, with patient G400 and for patient M210c the neutralisation was found to be clade-specific, with the clade of infection matching the clade of the PV neutralised, although this was not true of the other two patients with a neutralisation score between 0 - 0.5 (Figure 4.3). To be categorised as a moderate neutraliser with a score >0.5 (but <1), plasma either exhibited highly potent neutralisation of a single PV or was capable of neutralising two PVs in the standard panel (Figure 4.3). The latter is shown for patient J520 in the representative graph for a score >0.5 (Figure

4.4a), with two PVs from different clades being neutralised by plasma and therefore demonstrates a level of cross-clade neutralisation.

Broad neutralisation was exhibited by plasma that achieved a score >1, with the ability to neutralise three or more PVs in the standard 6 PV panel. The graph representing a neutralisation score >1 demonstrates the neutralisation of five PVs by patient D650, starting with the plasma dilution of 1:100 dilution but also from 1:50 dilution for 92TH021 and 93IN903 PVs. A lower dilution of plasma was used in this case to obtain a sigmoidal curve and accurate ID_{50} titre for PVs that were susceptible to neutralisation only at 1:100 dilution, which was possible for this patient due to a higher volume of plasma available. However, the need for a lower plasma dilution is reflected by a lower ID_{50} titre (Figure 4.3) and less potent neutralisation of the PV. Finally, a representative graph for a neutralisation score >2 is shown in Figure 4.4a and demonstrates plasma with the most breadth and highest potency. In this example, all six of the PVs in the standard panel were neutralised by patient T125 and only plasma against 94UG103 PV had to be titrated using a lower starting dilution (1:50) to obtain an accurate ID_{50} titre.

In summary, a range of different neutralisation profiles were obtained from plasma tested against the standard 6 PV panel and the proportion of the neutralisation scores achieved by the cohort is illustrated in Figure 4.4b. This revealed that half of the patients tested had a neutralisation score <1, reflecting little to no breadth, and half had a neutralisation score >1, reflecting broad and elite plasma neutralisation. In particular, elite neutralisers with a score >2 were successfully identified and found to represent 18% of the patients. It should be noted that this percentage is higher than the 1-10% of patients that have been found with elite neutralisation in other studies (reviewed in (McCoy and McKnight 2017)) but is likely due to the pre-selection of patients from the East London cohort with neutralisation of heterologous tier 2 PVs (Figure 4.2).

ID_{50} titre 100 >2000		ID_{50} titre in TZM-bl cells							
		CRF AE	Clade A	Clade B	Clade B	Clade C	Clade C	Negative control	
Patient ID	Clade of infection	92TH021	94UG103	JRCSF	92BR020	93IN905	C22	MLV	Neutralisation score
T125	C	1760	226	1336	634	2160	2505	<100	3.19
R216	C	1047	245	623	588	3785	764	<100	2.90
K300c	C	4649	1182	387	<100	474	581	<100	2.50
A260	AE/AI	338	186	421	1204	710	129	<100	2.21
K525	A1	486	287	487	183	865	<100	<100	1.89
D650	-	110	335	1061	805	244	<100	<100	1.84
D600	AE	399	198	352	330	198	<100	<100	1.62
P636	-	<100	<100	<100	1141	292	1509	<100	1.44
T300	AG	<100	293	236	242	168	<100	<100	1.17
E214	-	<100	<100	<100	215	200	925	<100	1.05
B420	CRF02-AG	190	<100	<100	424	450	<100	<100	1.04
K250	D	<100	<100	545	<100	281	<100	<100	0.74
C251	C	<100	<100	<100	<100	102	1359	<100	0.73
B200	-	<100	<100	887	<100	120	<100	<100	0.69
J520	B	<100	<100	<100	366	254	<100	<100	0.67
A320	-	1255	<100	<100	<100	<100	<100	<100	0.54
G400	B	<100	<100	<100	294	<100	<100	<100	0.32
M210c	C	<100	<100	<100	<100	214	<100	<100	0.27
E152	CRF06-CPX	<100	<100	<100	<100	145	<100	<100	0.22
U225	G	142	<100	<100	<100	<100	<100	<100	0.21
E520	-	<100	<100	<100	<100	<100	<100	<100	0.00
S162	-	<100	<100	<100	<100	<100	<100	<100	0.00

Figure 4.3 Identification of elite neutralisers among HIV-1 infected individuals in the East London Cohort using a standard pseudo-typed virus (PV) panel.

Patient plasma/serum neutralisation against the standard 6 PV panel (92TH021, 94UG103, JRCSF, 92BR020, 93IN905 and C22) and negative control murine leukemia virus (MLV) tested in the TZM-bl assay. Plasma/serum neutralisation of PVs reflected by ID_{50} titres are representative of n=2 with a colour gradient from yellow to red for lowest to highest respectively. An ID_{50} titre <100 indicates no neutralisation. Plasma/serum were tested in duplicate, or in singlet where sample was limited. Individuals are referred to by the patient IDs assigned in the original study for anonymity and the clade of viral infection is indicated unless unknown (marked with a hyphen). Neutralisation scores (calculated from log-transformed titres) indicate moderate neutralisers (score ≥0.5), broad neutralisers (score ≥1) and elite neutralisers (score ≥2) (Landais et al. 2016).

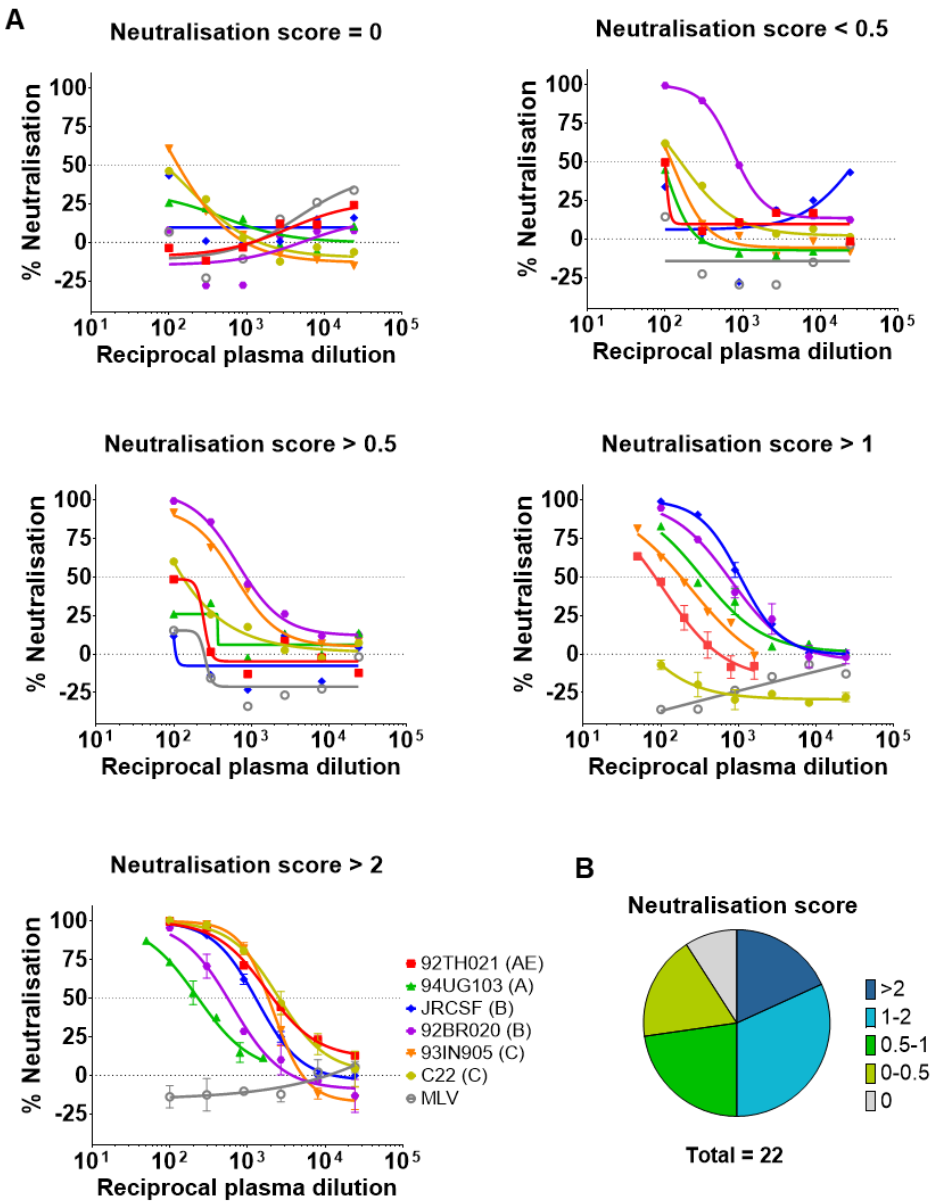

Figure 4.4 HIV-1 infected individuals from the East London Cohort exhibit a range of neutralisation profiles.

(A) Neutralisation curves from serial dilution of patient plasma/serum tested against a negative control PV MLV (grey) and the standard 6 PV panel: 92TH021 (red), 94UG103 (green), JRCSF (blue), 92BR020 (purple), 93IN905 (orange) and C22 (yellow). A representative graph of neutralisation with a score of 0, <0.5, >0.5, >1 and >2 is shown by patients S162, G400, J520, D650 and T125 respectively, with a dotted line plotted at 0% and 50% neutralisation. Patient plasma/serum were tested in singlet (where sample was limited), or in duplicate with the mean and error bars plotted. (B) Summary of neutralisation scores for patient plasma/serum (n=22) screened against the standard 6 PV panel.

4.3 Characterisation of elite neutralisers who have the potential to produce broadly neutralising antibodies

BnAbs have been previously isolated from individuals identified as elite neutralisers, and for this reason, only patients that demonstrated elite neutralisation (score >2) in the East London cohort were considered for further analysis. Neutralisation curves for the four elite neutralisers T125, R216, K300c and A260 are shown in Figure 4.5a and, as mentioned before, were generated by serial titration of plasma to calculate the ID_{50} titres presented in Figure 4.3. These curves illustrate the subtle differences in the ability of each elite neutraliser to target the PVs in the standard panel. For instance, T125 and R216 plasma were the least effective at neutralising 94UG103 PV and A260 had weaker neutralisation of both 94UG103 and C22 PVs, requiring plasma to be tested from a lower starting dilution (1:50) to obtain ID_{50} titres. On the other hand, K300c plasma was classified as non-neutralising against 92BR020 PV with an ID_{50} titre <100 (Figure 4.3) yet exhibited a weak level of neutralisation (63%) just above the 50% threshold against this PV at 1:100 dilution. However, this neutralisation was not sustained in the titration series and dropped down to 12% at the next plasma dilution. As the availability of plasma from K300c was more limited than the other three elite neutralisers, it was not possible to titrate this sample from a lower starting dilution to determine the extent of neutralisation against 92BR020. Despite this, it is clear that the antibodies in K300c plasma were less capable of targeting this clade B PV compared to the other clade B PV in the panel (JRCSF), indicating that the epitope(s) targeted are not as accessible or not present in the 92BR020 PV. It is also worth highlighting that K300c plasma showed the highest level of background against the negative control PV (MLV) out of the four elite neutralisers (Figure 4.5a), although the maximum neutralisation at 1:100 dilution was only 36% and therefore classified as non-neutralising.

As reviewed earlier (section 1.5), studies of HIV-infected individuals categorised according to their plasma neutralisation capacity have previously shown an association between broad neutralisation and high viral load, low CD4 T cell count, length of infection and ethnicity. The demographics and

clinical features of the four elite neutralisers are shown in Figure 4.5b. These patients had an age range of 30-41, were all male except for R216 and were sampled between 2007 and 2009 for recruitment into the East London cohort on the basis of being infected with HIV for at least one year. Regrettably the exact date of HIV acquisition, and therefore the length of infection is unknown for these patients. However, the clade of infection and country of birth for patients were identified where possible from the original study (Dreja et al. 2010). Three of the elite neutralisers (T125, R216 and K300c) had a clade C HIV infection, which was the most prevalent clade circulating at the time of sampling and represented 48% of global infections from 2005-2009 (Hemelaar et al. 2019), while the remaining elite neutraliser (A260) had a CRF_AE infection. Although the country of birth for these patients was presumed to be the location of HIV acquisition, this seems unlikely for A260 who originated from Ghana, located in western Africa where this clade was not widely circulating (<1%) (Hemelaar et al. 2019). Of greater importance was that none of these patients were identified as elite controllers at the time of sampling. While a viraemic controller or long-term non-progressor is capable of limiting the level of viral replication in the absence of ART, an elite controller refers to an individual that is capable of reducing the viral load below the level of detection in the absence of ART (Pereyra et al. 2008). Even though there have been instances where elite neutralisers capable of producing bnAbs have also been found to be elite or viraemic controllers (Scheid et al. 2011; Freund et al. 2017; Sajadi et al. 2018), this is not common and would make investigating the immune response and phenotype specifically associated with a broadly neutralising antibody response difficult. In fact, all of the elite neutralisers with known clinical data in Figure 4.5b were viraemic, with >70,000 c/mL and had a CD4 count <400 cells/µL, indicating a lower level of CD4 T cells than the normal range which is expected during viremia but was not AIDS-defining (<200 cells/µL). Finally, it should be noted that these viral / disease parameters were extracted from publicly available data from the ('LANL Sequence Database') and a previously published paper (Corti et al. 2010) and as a result did not always match the date of samples, as was the case for K300c.

Plasma from the elite neutralisers T125, R216, K300c and A260 were next screened for neutralisation against BG505 (clade A) and CRF250-4 (CRF 02_AG) PVs (Figure 4.6). It was necessary to determine whether BG505 and CRF250-4 Env could be targeted by elite neutralisers for two main reasons. First, the Env from these viruses has been produced successfully as recombinant, soluble, stabilised gp145 'SOSIP' trimers (Sanders et al. 2013; Voss et al. 2017; Pugach et al. 2015) that can be used as antigen probes to isolate HIV-specific B cells without presentation of decoy epitopes found on non-stabilised Env. The rationale was that if antibodies in the plasma are capable of binding and neutralising these PVs, then BCRs on HIV-specific memory B cells in the PBMCs from these patients should also be capable of binding to BG505 and CRF250-4 Env in FACS. Second, the BG505 and CRF250-4 PVs can be used in epitope mapping experiments, with mutations introduced into bnAb epitopes or with soluble protein for absorption of neutralisation to determine which site on the HIV-1 Env is being targeted. The elite neutralisers demonstrated the ability to target both BG505 and CRF250-4 PVs, with serially diluted plasma resulting in two data points both above and below 50% neutralisation (Figure 4.6a), except for A260 which had only 42% neutralisation of BG505 at the second dilution. As this was close to 50%, an ID_{50} titre was still calculated to determine the extent of neutralisation and showed that A260 had an ID_{50} of 275 against the BG505 PV, reflecting relatively weak neutralisation compared to the other elite neutralisers (Figure 4.6b). The ID_{50} titres calculated from the neutralisation curves also revealed that the CRF250-4 PV was more sensitive to plasma neutralisation by all patients, with higher titres achieved, than BG505 PV (Figure 4.6b). Even though both PVs have been classified as harder-to-neutralise tier 2 viruses (Yoon et al. 2015), this indicates that the epitopes targeted on the CRF250-4 PV by T125, R216, K300c and A260 are more accessible than on the BG505 PV. Nonetheless, an ID_{50} titre of >1000 was achieved by T125 against both PVs and thus this elite neutraliser exhibited highly potent neutralisation of both BG505 and CRF250-4 PVs. Furthermore, these results show that both Envs, in particular CRF250-4, would be suitable antigen probes to identify HIV-specific memory B cells from these elite neutralisers.

The standard 6 PV panel used to identify elite neutralisers (Figure 4.3) can also be used to identify potential epitopes targeted. For instance, the inability to neutralise certain PVs in this panel may indicate a particular epitope that is being targeted. Specifically, the resistance of 92TH021 PV to neutralisation can be characteristic of a high mannose patch specificity, as this PV lacks a glycan at position 332 which is required in the epitope of many high mannose patch bnAbs such as 2G12, PGT121-124, PGT127, PGT133, PGDM12 and PGDM21 (Sok, Doores, et al. 2014; Sok et al. 2016; Murin et al. 2014). Meanwhile, the resistance of 92BR020 PV to neutralisation can be indicative of a trimer apex specificity, due to the observation that bnAbs targeting the HIV Env trimer apex such as PG9, PG16, PGDM1400, VRC26.08 and the PCT64 lineage are not able to neutralise this virus (Yoon et al. 2015). All of the elite neutralisers T125, R216, K300c and A260 were capable of neutralising 92TH021 PV (Figure 4.3), suggesting that the high mannose patch is not targeted to achieve neutralisation breath. However, one elite neutraliser (K300c) showed reduced ability to neutralise 92BR020 PV with an ID_{50} titre <100 (Figure 4.3 and 4.5a), indicating that the apex epitope may be targeted. In addition, K300c potently neutralised the CRF250-4 PV with an ID_{50} titre >6000 (Figure 4.6b) and as the CRF250-4 Env is highly sensitive to apex antibodies (Voss et al. 2017) this also suggests an apex specificity. The high potency against CRF250-4 PV also meant that a higher starting dilution (1:400) could be used in neutralisation assays which required less plasma sample for epitope mapping, which was important because the K300c sample was very limited.

A

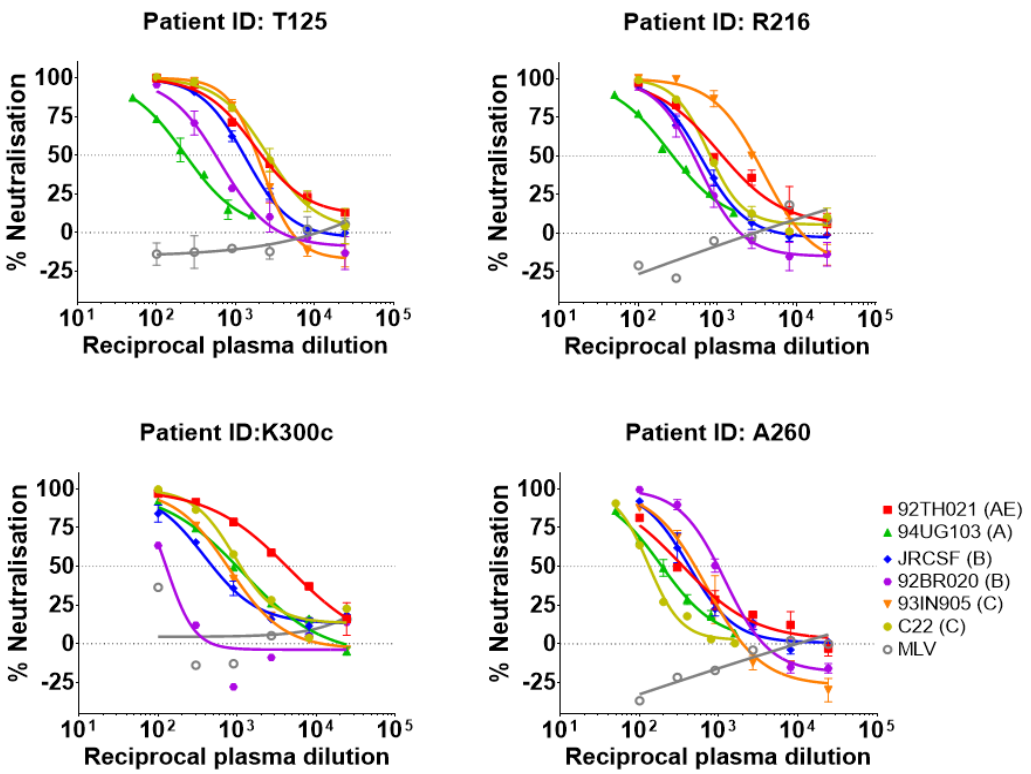

B

	T125	R216	K300c	A260
Gender	Male	Female	Male	Male
Country of birth	Sri Lanka / India	Zimbabwe	Nigeria	Ghana
HIV clade	C	C	C	AE
Elite controller	No	No	No	No
Year of sampling	2009	2009	2007	2008
Age at sampling	37	41	38	30
Viral load	73700	Unknown	72901*	140434
CD4 count	Unknown	Unknown	362*	362
Neutralisation score	3.19	2.90	2.50	2.21

Figure 4.5 Neutralisation profiles, demographic characteristics and clinical features of elite neutralisers.

(A) Neutralisation curves from serial dilution of patient plasma T125, R216, K300c and A260 tested against a negative control PV MLV (grey) and the standard 6 PV panel: 92TH021 (red), 94UG103 (green), JRCSF (blue), 92BR020 (purple), 93IN905 (orange) and C22 (yellow). Patient plasma were tested in duplicate with the mean and error bars plotted, or in singlet where sample was limited. Dotted lines indicate 0% and 50% neutralisation. (B) Demographic characteristics for patients and the clade of infection were provided by collaborators. Clinical features regarding viral load and CD4+ T cell count were sourced from publicly available data online. An asterisk (*) marks information from 2 years before the sampling date. Neutralisation scores achieved by patient plasma tested in (A) reflect elite neutralisation (score >2).

A

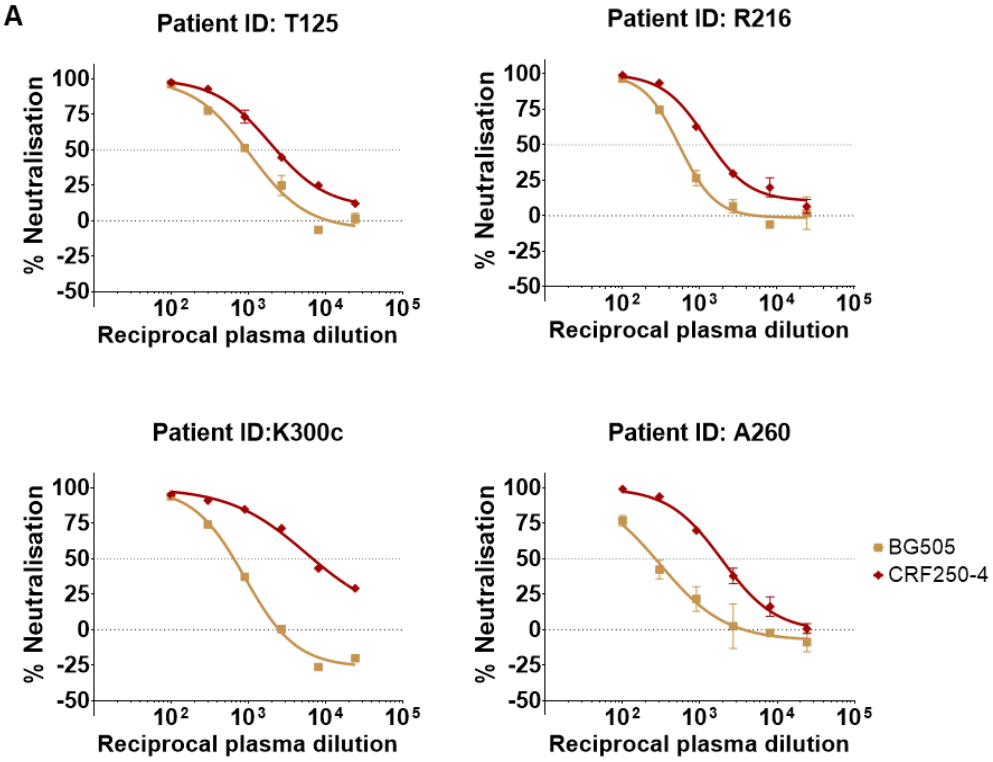

B

ID_{50} titre 100 >2000	ID_{50} titre in TZM-bl cells	
	Clade A	CRF02_AG
Patient ID	BG505	CRF250-4
T125	1049	1934
R216	545	1194
K300c	903	6038
A260	275	1927

Figure 4.6 Elite neutralisers demonstrate neutralisation of PVs that can be used to investigate epitope specificities.

(A) Neutralisation curves from 3-fold serial dilution of patient plasma (starting from 1:100) tested against BG505 and CRF250-4 PV. Plasma was tested in duplicate with the mean and error bars plotted, except for K300c which was tested in singlet due to limited sample available. Dotted lines indicate 0% and 50% neutralisation. (B) ID_{50} titres for patient plasma neutralisation against BG505 and CRF250-4 PV were calculated from neutralisation curves in (A), coloured with a gradient from yellow to red for lowest to highest respectively.

4.4 Plasma neutralisation depends on the trimer apex epitope for patient K300c and partially for patient T125

The potential N-linked glycosylation site (PNGS) at position 160 (HXB2 numbering) in particular has been identified as an essential component of the trimer apex bnAb epitope with mutant viruses lacking N160 becoming partially or completely resistant to neutralisation (Andrabi et al. 2015). A lysine at position 169 is also common in many apex bnAb epitopes and is required for neutralisation by the CAP256 lineage (Andrabi et al. 2015). Therefore, a CRF250-4 Env plasmid already containing mutation of N160 was altered further to mutate K169 by site-directed mutagenesis (SDM) (as described in section 2.6.5), resulting in a CRF250-4 Env with both N160A and K169T mutations. As expected, the double mutant (N160A/K169T) introduced into CRF250-4 PV could knock out neutralisation by the apex bnAb PG9 but did not affect the neutralisation by bnAb PGT121 which targets a different epitope (high mannose patch) on the HIV Env (Figure 4.7a). The CRF250-4 N160A/K169T PV was also found to be completely resistant to plasma neutralisation by K300c (Figure 4.7b), confirming that the trimer apex of the HIV Env is targeted for neutralisation by this patient. Plasma from the other elite neutralisers was also assessed for the presence of trimer apex specific antibodies that may explain their broad neutralisation activity, although this was not expected due to T125, R216 and A260 plasma all showing neutralisation of 92BR020 PV (Figure 4.3). Surprisingly, plasma from T125 showed a decreased ability to neutralise the CRF250-4 N160A/K169T PV, with a shift in the curve down and to the left compared to the wild-type (WT) PV (Figure 4.7b). This shift in the curve to the left indicates that more plasma (a lower dilution) is required to achieve 50% neutralisation and is therefore not as effective against the mutant PV. Indeed, mutations introduced into the apex epitope resulted in an 8-fold decrease in neutralisation (Figure 4.7c), although were not capable of fully knocking out neutralisation as seen with K300c plasma and the bnAb control PG9.

Plasma from R216 and A260 also showed a slight shift in the neutralisation curve to the left when tested against the CRF250-4 N160A/K169T PV,

however, the decrease in neutralisation relative to the WT PV was <3-fold (Figure 4.7b and 4.7c). An acceptable level of variation in neutralisation has been previously established as 3-fold (Sarzotti-Kelsoe et al. 2014), therefore this threshold was used to identify whether an effect on the neutralisation was due to the epitope targeted or not. The decrease in neutralisation against the apex mutant PV by A260 plasma was only 1.9-fold, similar to the 1.6-fold decrease shown by the control bnAb PGT121 that targets a different epitope. For R216, the plasma showed a 2.6-fold decrease in neutralisation against the N160A/K169T mutant PV, which was close to the threshold of 3-fold change but still deemed as not having an apex epitope specificity. In summary, T125 was partially dependent on the N160 glycan site and K169 residue being present for neutralisation, indicating that the apex epitope is targeted by some if not all antibodies in the plasma. In contrast, neutralisation by K300c plasma was mapped entirely to the apex epitope and therefore was not included in further epitope mapping experiments.

A

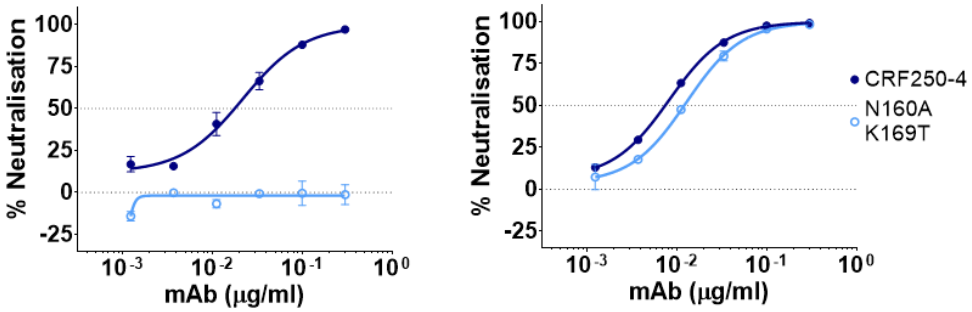

B

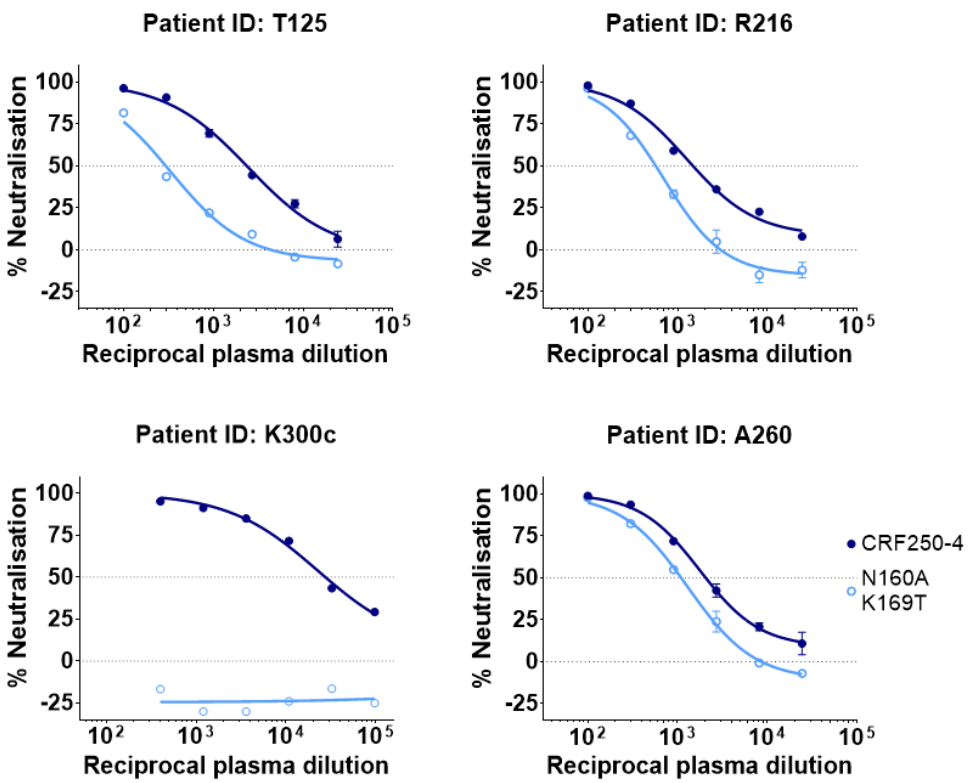

C

Apex mutant N160A / K169T	HIV bnAb		Patient ID			
	PG9	PGT121	T125	R216	K300c	A260
Fold decrease in neutralisation	>16	1.6	8.0	2.6	>200	1.9

Figure legend on next page

Figure 4.7 Plasma neutralisation depends on the trimer apex epitope for patient K300c but only partially for patient T125.

(A-B) Neutralisation of CRF250-4 PV with and without N160A and K169T mutations in the trimer apex epitope. Dotted lines indicate 0% and 50% neutralisation. (A) Neutralisation curves from serial dilution of control HIV bnAbs PG9 (apex-specific) and PGT121 (high mannose patch specific), tested in duplicate with the mean and error bars plotted. (B) Neutralisation curves from serial dilution of patient plasma T125, R216 and A260 tested in duplicate with the mean and error bars plotted. Patient K300c was tested in singlet due to limited plasma. (C) Fold decrease in the neutralisation of CRF250-4 PV as a result of mutations N160A and K169T were based on the change in IC_{50} values for HIV bnAbs in A and ID_{50} titres for patient plasma in B. A decrease in neutralisation of at least 3-fold is highlighted.

4.5 Patient R216 plasma neutralisation is partially absorbed by excess soluble gp120

Plasma was next tested for binding to the (monomeric) gp120 subunit in absorption assays by incubating plasma with excess BG505 D368R gp120 before the addition of BG505 PV and cells. The use of a gp120 with the D368R mutation was necessary to prevent interference with the assay. It is known that the aspartate residue at position 368 interacts with CD4 (Kwong et al. 1998), as such the D368R mutation in gp120 was required to prevent binding to CD4 receptors on cells that would block PV from entering cells and thus mimic neutralisation. A caveat is that this mutation can also affect the binding of antibodies that target the CD4bs (Zhou et al. 2015). Antibodies in the plasma that recognise sites on gp120 (other than the CD4bs) should therefore bind the soluble gp120 and consequently not be capable of neutralising the PV.

The effect of gp120 absorption on the neutralisation was first validated using bnAb controls, PGT121 and VRC01. These bnAbs were chosen on the basis that PGT121 targets the high mannose patch, which is present on the gp120 monomer, while VRC01 targets the CD4bs and therefore should not be able to bind to the gp120 as a result of the D368R mutation. Results show that as

expected PGT121 bound to the soluble gp120 and was no longer capable of neutralising the BG505 PV, however, VRC01 was unaffected (Figure 4.8a). The neutralisation capacity of patient plasma T125 and R216 was then assessed in the absorption assay to identify if plasma antibodies targeted an epitope on the gp120 (Figure 4.8b). Plasma from A260 was not included in the absorption assay with BG505 as this PV was not potently neutralised (Figure 4.6) and it was deemed more appropriate to preserve plasma for use in other epitope mapping assays where an effect on neutralisation would be more prominent.

Patient T125 plasma was still able to neutralise the BG505 PV following pre-incubation with gp120 but the potency was decreased, as shown by the shift in the neutralisation curve to the left. Plasma neutralisation of the BG505 PV by R216 was also decreased following pre-incubation with gp120, resulting in only one plasma dilution (1:100) producing more than 50% neutralisation (Figure 4.8b). The fold-decrease in the neutralisation of BG505 PV after gp120 absorption was calculated and shown in Figure 4.8c. Although R216 had a 3.3-fold decrease in neutralisation and passed the 3-fold threshold, T125 only demonstrated a 2.5-fold decrease in neutralisation and therefore was not deemed a large enough change to be attributed to the epitope targeted. Taking the bnAb controls into consideration, PGT121 showed >17-fold decrease with neutralisation completely absorbed by excess gp120, yet in comparison plasma neutralisation by R216 was only partially absorbed. This partial mapping to the gp120 monomer could be explained by the polyclonal nature of plasma that likely contains antibodies to more than one epitope, or because only part of the epitope is present. For instance, neutralising antibodies targeting the trimer apex, or the gp120-gp41 interface would not be predicted to be fully absorbed by the gp120 subunit alone as they require the trimeric form for the epitope for neutralisation.

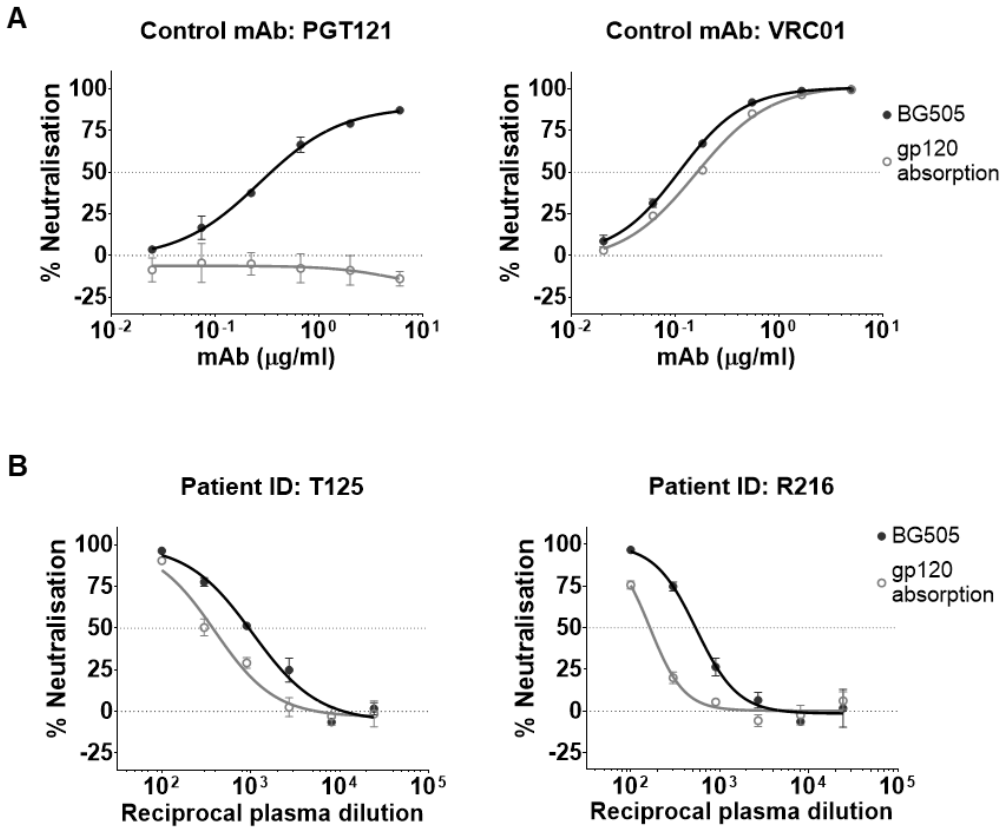

C

gp120 absorption	HIV bnAb		Patient ID	
	PGT121	VRC01	T125	R216
Fold decrease in neutralisation	>17	1.5	2.5	3.3

Figure 4.8 Plasma neutralisation by patient R216 is partially absorbed by monomeric gp120.

(A-B) Neutralisation of BG505 PV with and without prior BG505 D368R gp120 absorption. Dotted lines indicate 0% and 50% neutralisation. (A) Neutralisation curves from serial dilution of HIV bnAbs PGT121 and VRC01, tested in duplicate with the mean and error bars plotted. (B) Neutralisation curves from serial dilution of patient plasma T125 and R216 tested in duplicate with the mean and error bars plotted. (C) Fold decrease in the neutralisation of BG505 PV absorbed by monomeric BG505 D368R gp120 was based on the change in IC_{50} values of HIV bnAbs from (A) and ID_{50} titres of patient plasma from (B). A decrease in neutralisation of at least 3-fold is highlighted.

4.6 Patient T125 and A260 plasma neutralisation is partially enhanced by removing glycans around the CD4bs

Glycans at positions 276 and 462 surround the CD4bs and can limit antibody access to this epitope. Removal of the N276 glycan has been shown to either improve neutralisation by CD4bs bnAbs, such as VRC01, or restrict neutralisation for those that incorporate N276 into their epitope, such as HJ16 (Zhou et al. 2015). The increase in neutralisation by VRC01 against the double glycan mutant N276D / N462D in the BG505 PV was validated in Figure 4.9a, and neutralisation by the bnAb PGT151 that targets a different epitope (gp120-gp41 interface) was found to be unaffected.

To assess whether plasma had a CD4bs specificity, similar to VRC01, neutralisation by T125, R216 and A260 was evaluated against the BG505 N276D / N462D PV. This revealed that both T125 and A260 plasma had a shift in the neutralisation curve to the right (Figure 4.9b), reflecting an increase in neutralisation when glycans surrounding the CD4bs were removed from BG505 PV. In contrast, R216 plasma did not show an increase in the ability to neutralise BG505 N276D / N462D PV and instead had a very slight shift in the curve to the left that resulted in a <1-fold change (Figure 4.9c). The increase in neutralisation was found to be 4.2-fold higher than the WT PV for T125 plasma and 2.9-fold higher than the WT PV for A260 plasma, which meets the 3-fold threshold if rounded up. This indicates that a relatively small proportion of the polyclonal neutralising antibodies are targeting the CD4bs in a manner that doesn't incorporate glycans into the epitope. Moreover, as neither T125 nor A260 plasma exhibited a fold-increase in neutralisation to the same extent as bnAb VRC01 this suggests that the CD4bs is not the only epitope targeted.

A

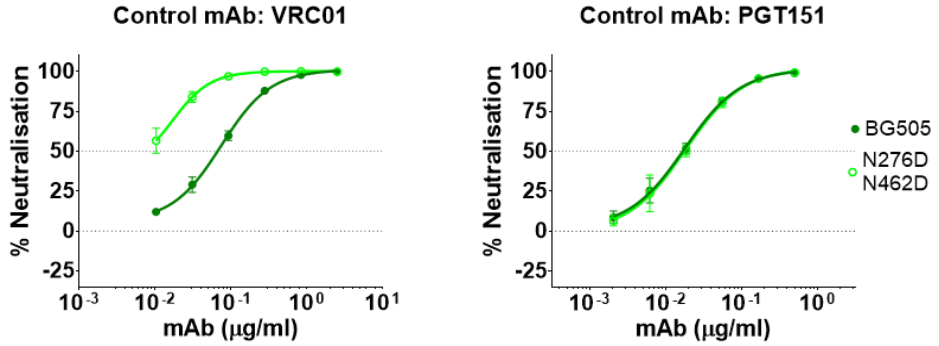

B

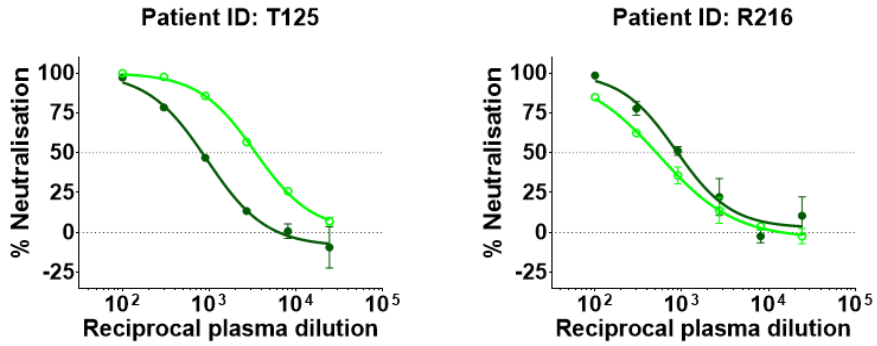

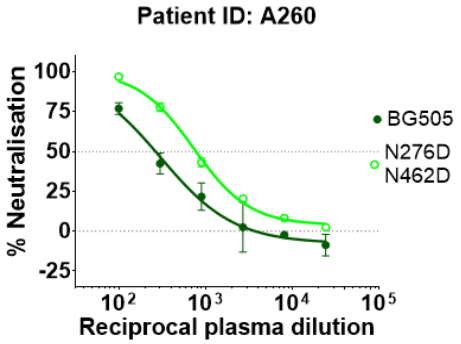

C

CD4bs mutant N276D / N462D	HIV bnAb		Patient ID		
	VRC01	PGT151	T125	R216	A260
Fold increase in neutralisation	9.1	1.0	4.2	0.6	2.9

Figure legend on next page

Figure 4.9 Plasma neutralisation by patient T125 and A260 is enhanced when glycans surrounding the CD4bs are removed.

(A-B) Neutralisation of BG505 PV with and without mutation of glycans N276D and N462D near the CD4bs epitope. Dotted lines indicate 0% and 50% neutralisation. (A) Neutralisation curves from serial dilution of HIV bnAbs targeting the CD4bs (VRC01) and gp120-gp41 interface (PGT151) epitopes, tested in duplicate with the mean and error bars plotted. (B) Neutralisation curves from serial dilution of patient plasma T125, R216 and A260 tested in duplicate with the mean and error bars plotted. (C) Fold increase in the neutralisation of BG505 PV as a result of mutations N276D and N462D were based on the change in IC_{50} values of HIV bnAbs from (A) and ID50 titres of patient plasma from (B). An increase in neutralisation of at least 3-fold is highlighted.

4.7 Elite neutralisers did not show evidence of high mannose patch, fusion peptide or MPER directed neutralisation

The trimer apex (blue), CD4bs (green), high mannose patch (pink), gp120-gp41 interface (red) and MPER (yellow) epitopes known to be targeted by bnAbs (McCoy and Burton 2017) are highlighted on the HIV trimeric Env in Figure 4.10a, comprised of the gp120 (pale grey) and gp41 (dark grey) subunits. As described above, the effect of PV mutation within these epitopes and the effect of protein absorption on patient plasma neutralisation activity was determined in comparison to the WT PV. Due to the inherent variation that is routinely seen between neutralisation assays with polyclonal plasma, only a fold-change in neutralisation ≥3 (Sarzotti-Kelsoe et al. 2014) was considered as a difference due to the epitope targeted and has been highlighted in Figure 4.10b. Results from epitope mapping neutralisation assays that demonstrated a fold-change of ≥3 have already been shown and discussed in Figures 4.7, 4.8, and 4.9, with plasma affected by mutations in the apex and around the CD4bs as well as being absorbed by monomeric gp120 for different patients. Although K300c neutralisation appears to be dominantly targeting the trimer apex, neutralisation by T125, R216 and A260 plasma were only partially mapped and so additional assays were performed in an attempt to fully identify the epitopes targeted.

As mentioned earlier, resistance to 92TH021 PV can indicate targeting of the high mannose patch epitope. Although all the elite neutralisers were capable of neutralising 92TH021 PV (Figure 4.3), only the N332 glycan is absent from this PV. It has previously been shown that mutation of the N332 glycan alone is not necessarily enough to knockout neutralisation for certain high mannose patch bnAbs (PGT125, PGT126, PGT128, PGT130 and PGT131) and instead a double mutant N332A/N295A is required to knock out all neutralisation activity (Sok, Doores, et al. 2014). Therefore, to test if plasma targeted the high mannose patch, neutralisation against a double mutant N332A / N295A was assessed. T125, R216 and A260 plasma had already shown the ability to neutralise JRCSF PV and therefore the double glycan mutant available in this PV was tested. None of the patient plasma were affected by the N332A / N295A mutation, with the fold-change in neutralisation compared to the WT JRCSF PV remaining close to one (Figure 4.10b), indicating that the high mannose patch is not targeted. Another epitope on Env targeted by bnAbs is the fusion peptide at the gp120-gp41 interface, which has been shown to have a reliance on the highly conserved glycan at position 88 on the gp120 for neutralisation (Kong et al. 2016; van Gils et al. 2016). The removal of the N88 glycan using a T90A mutation (to abolish the N-X-S/T glycosylation site required for glycosylation, as explained in 1.2.1) renders JRCSF PV resistant to the bnAb ACS202 (van Gils et al. 2016). This mutant was used to identify whether any of the plasma neutralisation could also be knocked out by altering the fusion peptide epitope, however, no change in neutralisation was observed against JRCSF T90A (Figure 4.10b). Plasma samples were also assessed further for CD4bs specificity using the JRCSF PV with the D279A mutation introduced, as this has been shown to substantially hinder the neutralisation of CD4bs bnAbs VCR01 and PGV04 (Falkowska et al. 2012). Despite T125 and A260 showing a partial CD4bs specificity, with increased neutralisation when glycans surrounding the CD4bs were removed, the D279A mutant did not decrease the neutralisation exhibited by any patient plasma (Figure 4.10b), suggesting that this residue is not targeted and the plasma activity is not VRC01-like.

It was also important to determine whether the plasma response of these elite neutralisers was directed towards the MPER of Env, which is not present on stabilised SOSIP trimers that are often used as Env probes to isolate HIV-specific B cells. To check for this, a linear MPER peptide of JRCSF was synthesised to include residues targeted by a range of MPER bnAbs including 2F5, 4E10 and LN01 (Binley et al. 2008; Pinto et al. 2019). Absorption assays where plasma was pre-incubated with the JRCSF MPER peptide showed that the neutralisation capacity against JRCSF PV was not altered for T125, R216 or A260, as shown by the limited variation in fold-change away from one (Figure 4.10b). While the linear MPER peptide used in this assay absorbed neutralisation by the bnAb 2F5, it was less effective at absorbing 4E10 neutralisation (data not shown) but is likely due to the requirement for a helical conformation found in the native trimer (Cardoso et al. 2005).

A

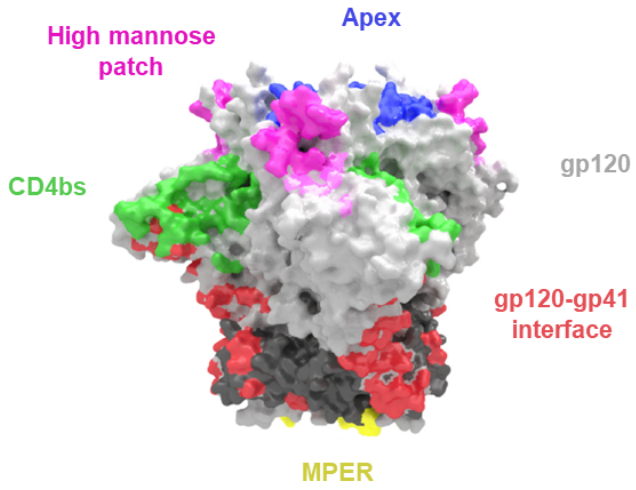

B

Epitope	PV mutation or protein absorption	Fold change in ID_{50} titre			
		T125	R216	K300c	A260
gp120	BG505 gp120 absorption	2.5	**3.3**	ND	ND
High mannose patch	JRCSF N332A/N295A	1.0	0.8	ND	0.4
Trimer apex	CRF250-4 N160A/K169T	**8.0**	2.6	**>200**	1.9
CD4bs	JRCSF D279A	1.0	1.3	ND	0.5
	BG505 N276D/N462D	**4.2**	0.6	ND	**2.9**
Fusion peptide	JRCSF T90A	1.1	1.1	ND	0.6
MPER	JRCSF MPER absorption	0.9	0.8	ND	1.1

Figure 4.10 Plasma from elite neutralisers exhibit different HIV Env epitope specificities.

(A) Model of HIV-1 Env structure adapted from (McCoy and Burton 2017) with bnAb epitopes highlighted: high mannose patch (pink), trimer apex (blue), CD4bs (green), gp120-gp41 interface (red) and MPER (yellow). (B) Effect of PV mutation or protein absorption on plasma neutralisation by elite neutralisers T125, R216, K300c and A260 given as fold-change in ID_{50} titre compared to the wild-type (WT) PV or condition, those with at least a 3 fold-change are highlighted. Effects on plasma that was not determined (ND) due to limited sample is indicated.

4.8 Overview of the epitopes targeted by plasma from elite neutralisers and the implications on the Env probes for FACS

Epitope mapping was successful to varying degrees in identifying regions on the HIV Env targeted by the plasma of elite neutralisers. For T125 plasma, absorption with gp120 resulted in a 2.5-fold change in neutralisation but was just below the 3-fold change cut-off. However, the fact that this effect on neutralisation wasn't very strong may be explained by the finding that the epitope can be mapped by mutagenesis both to the CD4bs and trimer apex. Both of these epitopes are unlikely to be fully blocked by the decoy gp120 because (i) it contained the D368R mutation, which can prevent the binding of CD4bs antibodies and (ii) gp120 is monomeric which can limit the binding capacity of trimer preferring apex antibodies. This partial mapping of the epitopes targeted for neutralisation breadth by T125, along with a dual specificity meant that a single epitope could not be knocked out in an antigen probe to distinguish between bnAb and non-bnAb B cells. Instead, a combination of both BG505 and CRF250-4 Env could be used as probes for FACS because the corresponding PVs were strongly neutralised by T125 plasma. This approach should identify dual binding of both Env probes, expected to be exhibited by bnAb B cells, as well as binding of a single Env probe, likely by non-bnAb B cells.

The R216 plasma neutralisation was partially attributed to an epitope on gp120, however, none of the mutations investigated had a large enough effect on the neutralisation to identify the exact specificity. This may have been due to different residues within these epitopes being targeted, or that a different region on Env was targeted such as the silent face (Schoofs et al. 2019), which was not tested. Further screening would therefore be needed to validate that the neutralisation breadth was attributable to only one or two bnAb epitopes in this elite neutraliser.

In contrast, plasma from K300c had complete knockout of neutralisation against the CRF250-4 N160A / K169T PV, with >200 fold-change, and was therefore mapped to the apex epitope without the need to test plasma against any other mutants or in absorption assays. The CRF250 Env with and without

mutations to N160 and K169 in the apex epitope could therefore be used as antigen probes in FACS for identifying bnAb B cells from K300c that bind only the wild-type CRF250 Env and non-bnAb B cells capable of binding the mutant Env.

Finally, plasma from A260 was partially mapped to the CD4bs with an enhancement in neutralisation upon removal of glycans surrounding this epitope, yet this plasma was not impacted by mutation of D276 in the PV. Therefore, a similar approach could be taken for sorting B cells from A260 as proposed for T125, with two different Envs used as antigen probes to identify HIV-specific B cells. While CRF250 Env would be suitable, the BG505 Env may not be targeted very well as this PV was not potently neutralised by A260 and therefore a more suitable choice would be the use of Env from a PV with a higher ID_{50} titre.

Taken together, these results indicate that T125 and K300c were the most suitable elite neutralisers to investigate the phenotype associated with broadly neutralising antibodies. In particular, T125 achieved the highest neutralisation score reflecting the greatest breadth and potency, yet K300c was able to be mapped solely to one bnAb epitope.

Summary

Patients from the East London cohort, chosen based on the ability to neutralise heterologous tier 2 PVs, showed a wide range of neutralisation profiles when tested against a standard 6 PV panel (Simek et al. 2009). Screening against this standard panel enabled neutralisation scores to be calculated to reflect the breadth and potency of plasma, which has been previously used to identify bnAb donors (Landais et al. 2016). Here, this method was successful in identifying four elite neutralisers with the potential to produce bnAbs, indicated by a neutralisation score >2. However, half of the patient plasma tested were found to have a neutralisation score of <1, reflecting only moderate to limited breadth with two patients demonstrating no plasma neutralisation against the standard 6 PV panel. It could be argued that higher neutralisation scores may have been found across the cohort if a lower starting dilution of plasma had been used to screen patient samples. However, this was not feasible with the volume of plasma available. Indeed, the selection of patients based on their ability to neutralise heterologous PVs was based on pre-existing neutralisation data that started from a 1:20 dilution and this difference in starting dilution may explain why some patients exhibited no/limited neutralisation of the standard 6 PV panel in the present study. Nevertheless, the sole goal of screening this cohort was to identify elite neutralisers with plasma breadth and potency, therefore the more stringent starting dilution of 1:100 ensured that weak neutralisation was not considered and that sufficient sample was preserved for epitope mapping experiments.

Epitope mapping was then carried out to identify bnAb specificities of elite neutralisers and to use this knowledge to inform the choice of antigen probes for single B cell isolation by FACS. This was successful for K300c which was found to have a trimer apex specificity, and for T125 which had a dual specificity for the trimer apex and CD4bs epitopes. Conversely, plasma from A260 was only partially mapped (to the CD4bs) and R216 plasma neutralisation was only found to rely on an epitope within gp120 to a limited degree. As demonstrated by the varying degrees of success, a caveat to the method of epitope mapping using mutated PVs is that bnAb epitopes are targeted in different ways by mAbs and can vary in terms of the residues that

are bound within the general epitope or mAb footprint (McCoy and Burton 2017). In addition, protein absorption was carried out using soluble, monomeric gp120 (with a key residue in the CD4bs mutated) and a soluble, linear MPER peptide. However, these versions of the gp120 and MPER do not reflect the conformation found in the trimeric Env, which neutralising antibodies target, and therefore was a limitation in epitope mapping to these sites. For the MPER epitope, this could have been overcome through the use of HIV-2 chimeric PVs with HIV-1 MPER, as done in other studies (Gray et al. 2009; Landais et al. 2016), although would have also required testing plasma against the HIV-2 WT PV to ensure this was not neutralised.

Overall, the results in this chapter identified four elite neutralisers, with two (T125 and K300c) exhibiting plasma neutralisation targeted towards known bnAb epitopes. In addition, the CRF250 and BG505 Env were also able to be targeted by elite neutralisers. These Envs, which have been previously used with success as antigen probes (van Gils et al. 2016; Voss et al. 2017), would therefore be suitable for isolating HIV Env-specific single B cells from PBMCs by FACS from elite neutralisers. Considering that T125 exhibited the broadest and most potent neutralisation (score of 3.19) and had more PBMCs available to sort B cells from than K300c, this elite neutraliser was chosen to investigate further in chapters 5 and 6 with the pipeline established in chapter 3.

Chapter 5: Memory B cells in the periphery of an elite neutraliser have HIV-specific antibodies with distinct genetic features, neutralisation profiles and epitopes

Background

The single-cell pipeline validated in chapter 3 successfully generates transcriptome data as well as variable regions for antibody cloning to link the phenotype of B cells to the antibody functionality. In chapter 4, screening of plasma from HIV-infected individuals in the East London cohort identified four elite neutralisers, with one in particular (T125) demonstrating exceptional breadth and the ability to target bnAb epitopes on HIV Env. Taken together, this indicated that the elite neutraliser T125 likely has B cells capable of producing bnAbs, and was therefore chosen to investigate whether there are differences in B cells that can produce a bnAb or not. To address this research question, it was necessary to first identify the HIV Env-specific B cell population from T125 PBMCs and conduct single B cell cloning to isolate mAbs for characterisation.

To determine if mAbs could be classified as bnAbs it was important to consider what constitutes a bnAb. So far, the characterisation of mAbs isolated from HIV-infected individuals has predominantly focused on bnAbs, due to interest in their therapeutic potential and ability to provide passive protection in animal models (Gautam et al. 2016; Garber et al. 2020) that is hoped to be elicited by vaccination (as discussed in section 1.4.7). Despite this, a specific criterion of what defines an HIV bnAb has not yet been established (as reviewed by Griffith and McCoy), although evaluation of published data for previously isolated bnAbs found that they commonly exhibit at least 30% breadth against a multi-clade panel of 118 PVs (Griffith and McCoy 2021). In addition, bnAbs have been described as having unusual sequence features such as high levels of SHM in the V_H, which ranges from 9 to 43%, and often have long CDRH3 regions of >20 AAs but can range from 10 to 37 AAs (Griffith and McCoy 2021). Ultimately though, regardless of antibody sequence traits, breadth of

neutralisation is achieved by targeting conserved regions on the functional trimeric Env. These include the CD4 binding site, trimer apex, high-mannose patch, gp120-gp41 interface (including the fusion peptide) and membrane proximal region (MPER), as well as the more recently identified epitope referred to as the ‘silent face’ (McCoy 2018). The use of long CDRH3 regions by many bnAbs is favourable for accessing recessed epitopes on the HIV Env, and extreme SHM is thought to have been acquired over time to cope with a degree of variability within or surrounding the epitopes targeted.

This chapter sought to isolate rare HIV-specific B cells from T125 PBMC samples by FACS with Env probes and use single B cell cloning to express BCRs as soluble mAbs for characterisation. Specifically, mAbs cloned from single T125 B cells will be assessed for their ability to bind Env and known bnAb epitopes by ELISA as well as their capacity to exhibit broad neutralisation of standard PV panels. In addition, sequence features will be evaluated to identify mAbs with high SHM or long CDRH3 regions characteristic of HIV bnAbs. Overall, this chapter aimed to identify bnAb and non-bnAb B cells from T125.

Results

5.1 Recombinant Env conjugated to fluorophores can be recognised by HIV bnAbs and detected during flow cytometry to be used as antigen probes

The original SOSIP trimer was designed using an Env sequence matched to the BG505 virus, however, SOSIP modifications for stabilisation of the Env trimer have also been successfully applied to other isolates such as CRF250-4, which can also be bound by bnAbs (Sanders et al. 2013; Voss et al. 2017; Pugach et al. 2015). As shown in chapter 4, both BG505 and CRF250-4 Env expressed as PVs were potently neutralised by plasma antibodies from elite neutraliser T125 and thus deemed appropriate Env to be used as antigen probes to identify HIV Env-specific B cells from the T125 clade C infected PBMC samples. Epitope mapping also revealed that T125 plasma neutralisation targeted regions on gp120, specifically the trimer apex and CD4bs, indicating that the lack of MPER in SOSIP proteins would not prevent bnAb B cells from being isolated.

For the detection of antigen-specific B cells by flow cytometry, antigen probes first require conjugation to a fluorophore. SOSIP trimers with an avi-tag at the base of the protein enable site-specific addition of biotin, by acting as an acceptor site for the birA ligase, ensuring that none of the epitopes are blocked or altered. Streptavidin-conjugated fluorophores can then bind to the biotinylated SOSIP trimers (Doria-Rose et al. 2016) to form antigen tetramers that can be detected by flow cytometry if bound by the B cell. For this reason, the Env sequence for CRF250 SOSIP in an avi-tagged expression vector was transfected with free biotin and the birA ligase expression vector to facilitate *in vivo* biotinylation (as described in section 2.7.1). Supernatants containing the soluble recombinant SOSIP were harvested and purified by affinity chromatography on a GNL column, to capture Env via interaction with its glycans. As this method of purification does not distinguish between different conformations, the SOSIP proteins were analysed and further purified by size exclusion chromatography (SEC). The CRF250 SOSIP had a strong trimeric peak with a shoulder on the left indicating the presence of aggregates and a

shoulder on the right indicating monomeric protein (Figure 5.1a). Only the fractions eluted between 9 mL and 11.5 mL were selected to exclude the aggregated and monomeric Env protein. Avi-tagged BG505 SOSIP protein had already been produced and purified previously to select for trimeric Env, and therefore only required biotinylation (as described in section 2.7.5) and validation.

First, the CRF250-4 and BG505 SOSIP proteins were validated by SDS-PAGE (Figure 5.1b), which denatures the protein structure. In non-reducing conditions, a band at ~140 kDa can be seen for both proteins, representing the presence of gp140 heterodimers typical of SOSIP proteins that lack MPER. A band at 120 kDa was only observed when the SOSIP proteins were subjected to reducing conditions that break the disulphide bonds between the heterodimer. For the CRF250 SOSIP protein, there was also a band present at ≥250 kDa in non-reducing conditions, suggesting that a small proportion of the protein was still in a higher quaternary structure as this was not seen in the harsher reducing conditions.

Second, effective biotinylation of avi-tagged SOSIP was confirmed by the ability to capture these Env proteins via streptavidin and then detect antibody binding to the captured SOSIP by ELISA (Figure 5.1c). A range of HIV bnAbs targeting the apex (PG9 and VRC26.09), high mannose patch (PGT121 and PGT124), CD4bs (VRC01) and gp120-gp41 interface (3BC315 and PGT151), as well as a CD4bs non-nAb (F105) and a negative control mAb specific for Dengue serotype 3 (Den3) were assayed for the ability to bind the captured SOSIPs. All of the HIV bnAbs tested bound the BG505 SOSIP protein, while the non-nAb F105 did not (Figure 5.1c), which suggests that this non-neutralising epitope is minimally exposed and is consistent with previous characterisation by ELISA (Sanders et al. 2013). The majority of bnAbs also bound the CRF250 SOSIP protein except CD4bs bnAb VRC01, however, this has also been observed previously in Biolayer Interferometry data (Voss et al. 2017) and thus appears to be characteristic of this Env. Instead, the non-nAb F105 which is also specific for the CD4bs was able to bind, suggesting that the epitope of this particular mAb is more accessible on CRF250 than BG505 SOSIP and may be due to differences in the Env conformation or residues

within or around the epitope. In addition, the non-HIV antibody Den3 was unable to bind BG505 or CRF250-4 SOSIP as expected. Ultimately, as both SOSIP proteins were captured onto ELISA plates by streptavidin for the detection of HIV-specific mAb binding to multiple different epitopes, this validated the success of biotinylation and Env conformation.

Third, the biotinylated SOSIP proteins were complexed with streptavidin-conjugated fluorophores to determine whether binding by an HIV-specific mAb presented on the surface of a bead could be detected by flow cytometry (as described in section 2.7.7). This system aimed to mimic the binding of antigen probes by HIV-specific BCRs on the surface of a B cell for isolation by FACS. The high mannose patch bnAb PGT121 was used to coat beads on the basis that this mAb had already demonstrated the ability to bind to both CRF250-4 and BG505 SOSIP proteins in Figure 5.1c. Biotinylated CRF250-4 SOSIP was conjugated to strep-PE, while biotinylated BG505 SOSIP was conjugated to strep-BV786 before incubating with PGT121-coated beads. Results from flow cytometry demonstrated the ability of CRF250-4 and BG505 SOSIP binding to be detected, with 95% of beads showing positivity for PE and BV786 respectively (Figure 5.1d). It was also possible to detect the dual binding of CRF250-4 and BG505 SOSIP proteins by PGT121-coated beads when incubated with both antigen probes, as shown by the positivity for both PE and BV786 by 91% of beads. Finally, beads were coated with a non-HIV (Den3) mAb and incubated with both SOSIP proteins. This demonstrated that there was a very low level of background binding (<0.2%) and that the detection of antigen probes by PGT121-coated beads was a result of binding by the HIV bnAb. This validation was necessary to confirm that both CRF250-4 and BG505 SOSIP proteins could be used to isolate HIV-specific B cells from elite neutraliser T125.

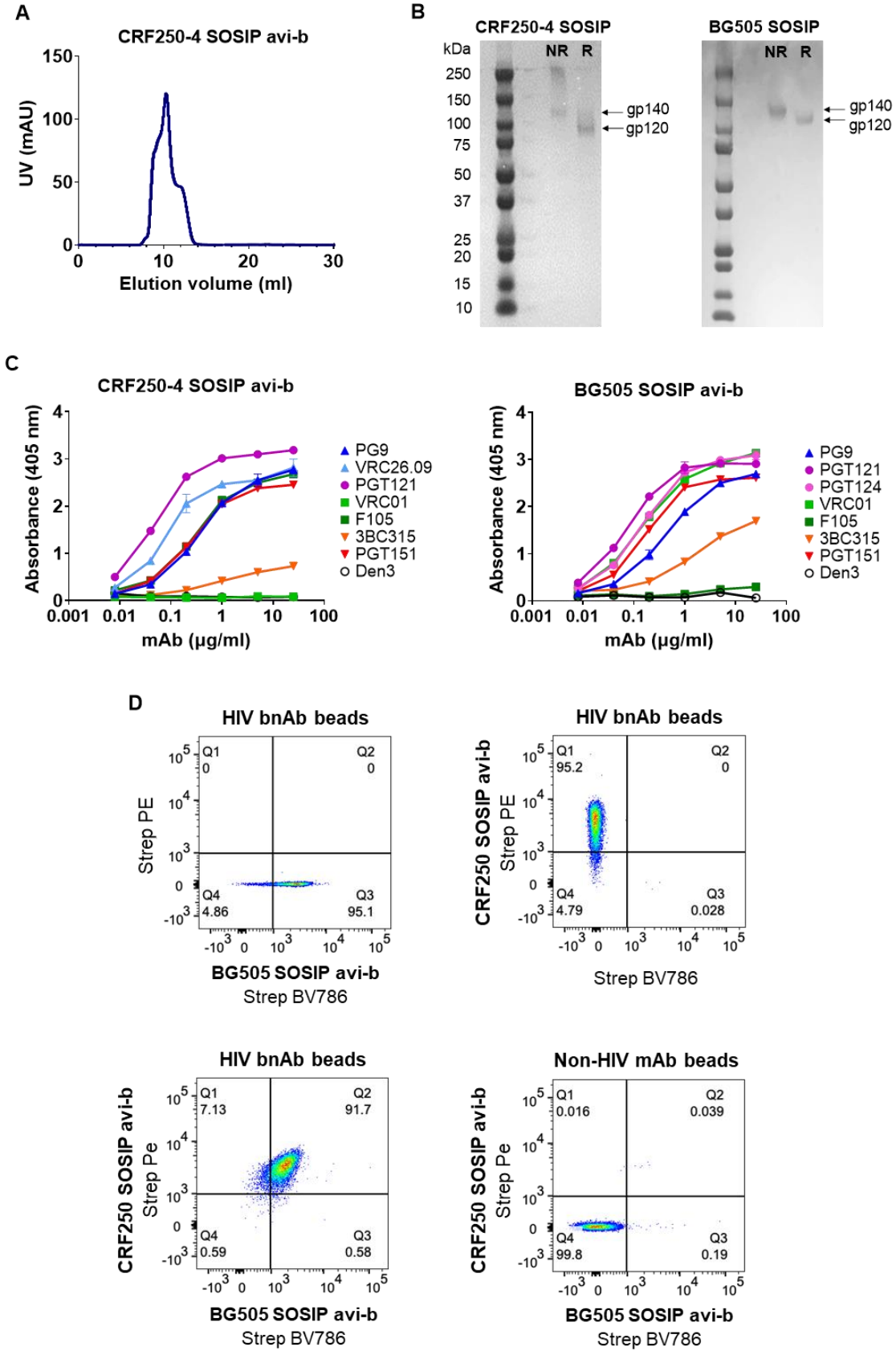

Figure legend on next page

Figure 5.1 Purification and validation of Env probes to isolate HIV+ B cells by FACS.

Stabilised recombinant trimeric Env protein (SOSIP) with a biotinylated avi-tag (avi-b) were chosen as antigen probes. (A) Size exclusion chromatography (SEC) to purify CRF250 SOSIP protein trimers. (B) SDS-PAGE of CRF250 and BG505 SOSIP proteins in non-reducing (NR) and reducing (R) conditions. (C) Binding of HIV mAbs specific for the apex (blue), high mannose patch (pink), CD4bs (green) and gp120-gp41 interface (orange / red) and non-HIV mAb Den3 to biotinylated CRF250 and BG505 SOSIP proteins in a streptavidin-capture ELISA, tested in duplicate with the mean and error bars plotted. (D) Flow cytometry to detect biotinylated CRF250 and BG505 SOSIP avi-tagged (avi-b) proteins complexed with streptavidin-conjugated fluorophores (PE and BV786 respectively) using HIV bnAb PGT121 coated beads or non-HIV mAb Den3 coated beads.

5.2 Isolation of single HIV-Env reactive IgG B cells from elite neutraliser T125 PBMCs was achieved by FACS using antigen probes

The PBMCs from two timepoints for elite neutraliser T125 were thawed and stained according to methods in section 2.7.8 for analysis and separation by FACS. In addition, the PBMCs from an HIV-negative donor were also included as a control for staining. First, the lymphocyte population and single cells were identified based on size, using FSC and SSC (as in chapter 3, Figure 3.2a). The gating strategy that was then used to identify HIV-specific memory B cells is shown in Figure 5.2. Viable B cells were selected based on the cell surface expression of CD19 but not CD4 and a live-dead aqua stain was used on the same laser as the fluorophore conjugated to CD4 to also exclude dead cells. The IgG+ B cell population was then selected based on the presence of surface IgG and the absence of IgM to identify the class-switched population. Finally, HIV Env+ B cells were identified based on IgG binding to BG505 SOSIP and/or CRF250 SOSIP conjugated to fluorophores. Importantly, the inclusion of PBMCs from an HIV-negative donor showed that there was minimal background binding to the HIV Env probes (0.28%) as expected (Figure 5.2a).

From this HIV-negative donor, the total viable B cell population was 4.36% (Figure 5.2a), which was lower than the 12.4% that was observed in the HIV-negative donor PBMCs analysed in chapter 3 (Figure 3.2a), but the latter was following vaccination and both are in line with the proportion of B cells previously reported in healthy controls (4-15%) (Wang et al. 2020). In contrast, the first T125 timepoint PBMCs had 23.2% viable B cells (Figure 5.2b), which is consistent with the percentage of total B cells observed in other HIV-infected donors (22-34%) (Wang et al. 2020). Yet, in the second T125 timepoint PBMCs sampled four months later, the viable B cell population was lower at 11.2% (Figure 5.2c), but this may be a result of the PBMCs not having optimal preservation, as cell clumping was observed following thawing which can reflect cell lysis and thus fewer viable cells. Indeed only 2.5 million PBMCs were recovered from the second timepoint in comparison to 7.5 million PBMCs from the first timepoint. Despite this, the percentage of IgG+ B cells between the two timepoints was comparable, with 5.6% from the first timepoint (Figure 5.2b) and 6.2% from the second timepoint (Figure 5.2c). Of the IgG+ B cell population, 1.5% were specific for HIV Env from the first timepoint (Figure 5.2b) and 1.12% were specific for HIV Env from the second timepoint (Figure 5.2c). Single HIV Env+ IgG+ B cells from this final gate were sorted by FACS into individual wells of a 96-well plate, isolating a total of 67 cells from the first timepoint and 62 cells from the second timepoint. Although FACS is capable of dispensing droplets containing individual cells, the high purity required to ensure that only single cells are dispensed can result in some cells being discarded if they are too close together. This was observed during sorting from the first timepoint PBMCs and explains why there are more events in the HIV Env+ B cell plot identified by the flow cytometer than the number of cells that were isolated.

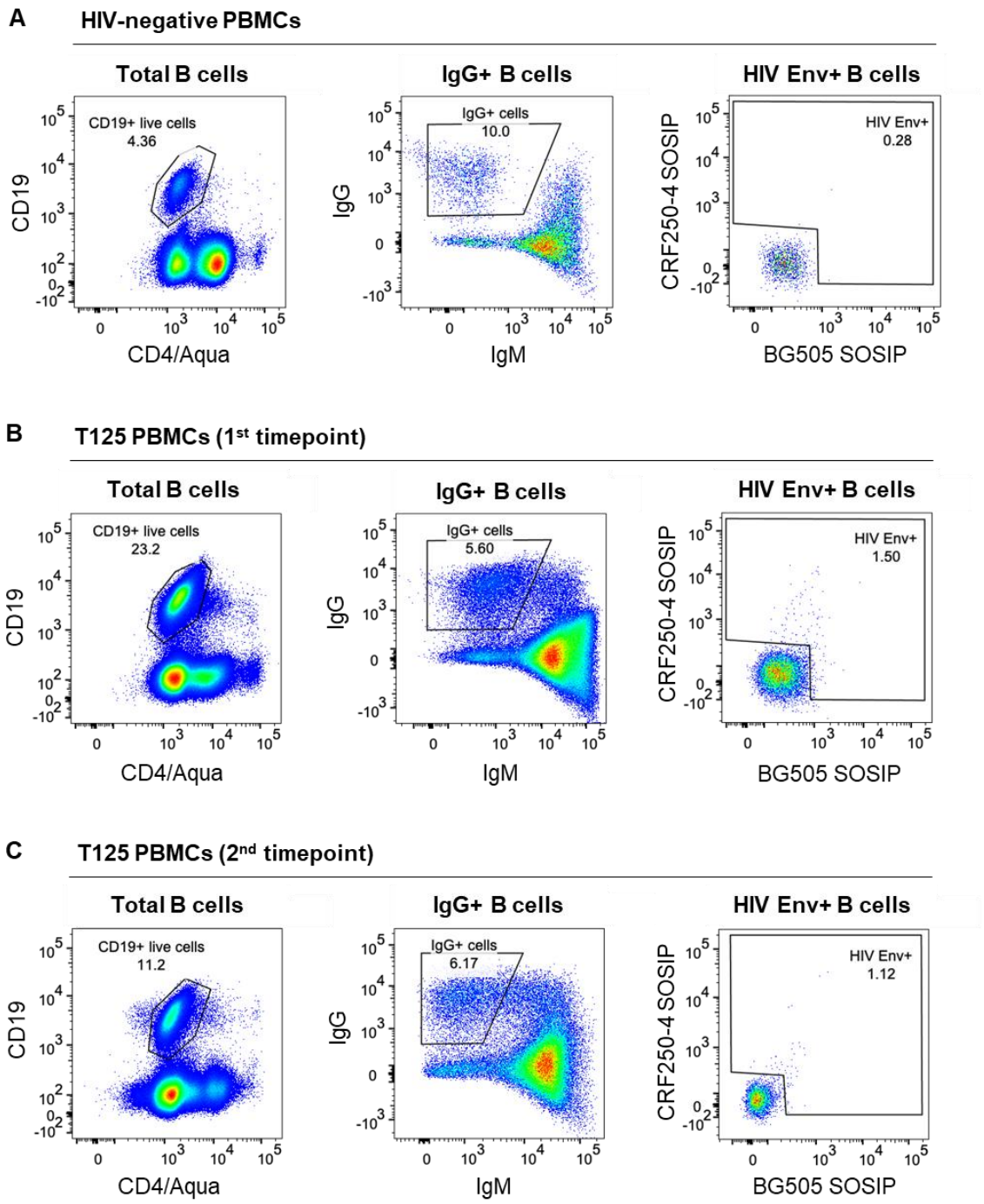

Figure 5.2 Gating strategy for the isolation of single HIV Env+ B cells from elite neutraliser T125.

(A-C) Identification of single IgG+ HIV Env+ B cells from (A) HIV-negative PBMCs, (B) T125 1st timepoint PBMCs and (C) T125 2nd timepoint PBMCs by flow cytometry, based on the surface expression of CD19+ and IgG+ followed by the ability to bind fluorescently labelled HIV Env probes, CRF250-4 and/or BG505 SOSIP.

5.3 Single B cell cloning successfully recovered Ig variable regions for mAb expression, with almost half demonstrating the ability to bind trimeric HIV Env

The 129 single HIV Env+ memory B cells that were sorted from elite neutraliser T125 were then processed in individual wells according to the pipeline validated in chapter 3 for scRNA-seq and antibody cloning. First, the mRNA from lysed cells was reverse transcribed to generate cDNA according to the Smart-Seq2 method and evaluated using an Agilent Tapestation, to check for DNA at the expected size of 1-2kb by high-sensitivity electrophoresis. Regrettably, this revealed that some of the wells (n=19) did not contain any cDNA and were therefore excluded from downstream processing.

Next, antibody variable regions were amplified from the cDNA of single B cells by individual nested PCRs for IgH, IgK and IgL. Gel electrophoresis was used to assess the amplification (recovery) of Ig variable regions, identified by the presence of a band at the expected size of 350-500bp. The percentage of single B cells from each timepoint with an IgH, IgK or IgL variable region band is shown in Figure 5.3a. Although the percentage of cells with an IgH variable region band was higher from the second timepoint (77.8%) than the first timepoint (67.7%), the percentage of cells with an IgK or IgL variable region band was lower in the second timepoint (57.8% and 22.3% respectively) compared to the first timepoint (72.3% and 49.2% respectively). As both are required to form an antibody pair, this meant a similar percentage of total pairs of IgH and IgK/IgL variable regions was recovered from B cells from both timepoints (62.2% and 66.2%) for cloning into expression vectors. Moreover, these percentages were consistent with the PCR recovery of antibody pairs (58-70%) identified in chapter 3 from the different memory B cell subsets of the HIV-negative donor.

Ig variable regions were then amplified using primers that added overhangs complementary to expression vectors to clone the IgH, IgK and IgL variable region PCR products into vectors containing the heavy chain, kappa light chain and lambda light chain constant regions respectively (as described in section 2.8.3). Recombinant-based cloning was attempted for 95 and 58 variable

region bands from the first and second timepoints respectively. Following this, each newly assembled plasmid was transformed into chemically competent *E. coli* for amplification of the DNA. The success of cloning was assessed by lysing a sample of the *E. coli* culture grown from a single colony and performing a PCR to amplify the Ig variable region, with primers specific for the vector on either side of the cloning site. Observation of a band at ~350-500bp after gel electrophoresis of the PCR products indicated successful insertion of the variable region into the expression vector. This was achieved for all of the IgH, IgK and IgL variable region bands from the first timepoint resulting in 100% cloning efficiency (Figure 5.3b) and 43 potential mAbs. From the second timepoint all but one of the IgH variable regions was successfully cloned, thus resulting in 96.3% cloning efficiency of antibody pairs (Figure 5.3b) and 26 potential mAbs. Finally, to achieve expression of each mAb, the heavy and light chain vectors from all 69 antibody pairs were co-transfected into HEK-293T cells (as described in section 2.9.1). The cell supernatant was collected 3 days later and screened by ELISA (as described in section 2.9.2) to detect the presence of secreted mAb. It should be noted that some of the transfections did not initially yield mAb expression as a result of one of the chains being unproductive (as identified in chapter 3), however, this was often rectified by picking a different colony containing a productive sequence. As a consequence, almost all the cloned antibody pairs were expressed from the first (93%) and second (88.5%) timepoint (Figure 5.3b).

The cDNA from the single B cells from both timepoints was also processed for scRNA-seq. Initial analyses revealed that 15% of cells did not pass QC checks based on the library quality (to be discussed more in chapter 6). In addition, the reconstruction of BCR sequences from transcriptomic data by BraCeR highlighted three cells with a non-IgG isotype that may bias analyses, as well as six cells with multiple antibodies suggesting that these were not single cells. For these reasons, mAbs cloned from these B cells were not characterised further. However, as identified in chapter 3, there were also instances where a heavy or light chain for an antibody was able to be reconstructed by BraCeR from the transcriptomics data that was not amplified by Ig PCR. The variable regions from these sequences were commercially synthesised as genestrings

with overhangs required for cloning into vectors and inserted into antibody expression vectors as described above. This resulted in the expression of four additional mAbs. Overall, a total of 50 antibodies from single IgG B cells isolated from elite neutraliser T125 were successfully cloned and expressed, enabling the investigation of their sequence features and ability to bind HIV Env by ELISA.

Initially, the mAb-containing cell supernatants were screened by ELISA (as described in section 2.9.3) to identify binding to the HIV Env probes (BG505 and CRF250-4 SOSIP proteins) used in FACS. A threshold of 3 times the background absorbance was used to distinguish mAbs in supernatants capable of binding to at least one SOSIP protein and identified 24 out of 50 mAbs (48%) bound Env (shown in Table 1). This proportion was slightly lower than expected compared to previous experience by our lab for cloning mAbs from antigen-specific B cells and a similar prior study that reported 17 out of 29 mAbs (59%) cloned from HIV Env+ B cells showed binding to BG505 SOSIP by ELISA (van Gils et al. 2016). The ability to bind Env by ELISA was tested by incubating soluble mAbs with SOSIP protein captured on the surface of a plate. However, HIV Env+ B cells were identified by FACS through the binding of membrane-bound BCRs to SOSIP protein displayed as a tetramer on a streptavidin fluorophore. Therefore, it is plausible that these differences may impact the sensitivity to detect mAb binding in ELISA, and will be discussed in more detail later.

T125 mAbs that displayed convincing Env binding were produced on a larger scale by transient transfection of 293F suspension cells and subsequently purified from supernatants using protein G beads (as outlined in section 2.9.4). Purified mAbs were then tested at a known concentration (25 µg/mL) to confirm binding to BG505 and CRF250-4 SOSIP proteins (Figure 5.3c). The majority of mAbs demonstrated differential binding of the two SOSIP proteins, with a preference for CRF250-4 as shown by a higher absorbance. Only one mAb (7E7) exhibited considerably higher binding of the BG505 SOSIP protein. The difference in the ability to target each SOSIP may be a result of variation in the Env itself or due to the Env conformation. For instance, the SOSIP mutations to stabilise the trimer in a closed conformation and occlude non-nAb

epitopes were designed specifically for BG505 and are not as effective for CRF250, as demonstrated earlier by the stronger binding of the non-nAb F105 and weaker binding of gp120-gp41 (trimeric) specific mAb 3BC315 (Figure 5.1c).

A

HIV Env+ B cells	Ig PCR Recovery			
	IgH	IgK	IgL	Total Pairs
1st TP	67.7%	72.3%	49.2%	66.2%
2nd TP	77.8%	57.8%	22.2%	60.0%

B

Ig PCR Pairs	mAb production	
	Cloning	Expression
1st TP	100.0%	93.0%
2nd TP	96.3%	88.5%

C

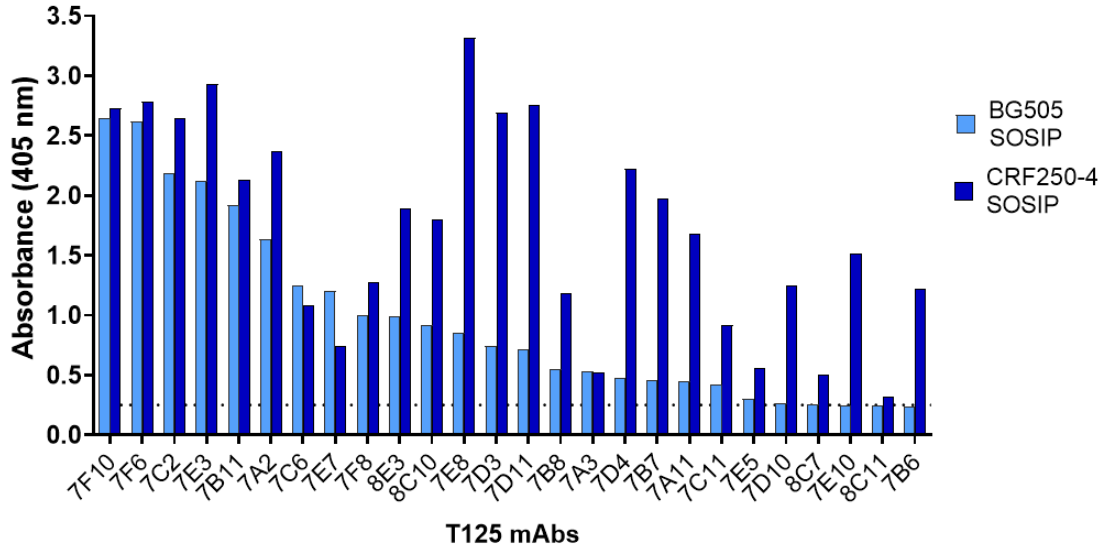

Figure 5.3 Antibody variable regions recovered from single HIV Env+ B cells of elite neutraliser T125 were able to be expressed as mAbs and displayed different binding profiles.

(A) Percentage of B cells with antibody heavy (IgH), kappa (IgK) and lambda (IgL) variable regions amplified by PCR (recovered) from the cDNA of HIV Env+ B cells isolated from two timepoints (TP) of the elite neutraliser T125. Total pairs reflect the percentage of B cells with both a heavy and kappa or lambda variable region recovered by Ig PCR. (B) Percentage of Ig pairs with variable regions (amplified by PCR) successfully cloned into expression vectors containing the constant region and expressed as the complete mAb. (C) Binding of mAbs cloned from HIV Env+ B cells to CRF250 and BG505 SOSIP (trimeric HIV Env) proteins. The strength of binding, measured by ELISA, is indicated by the level of absorbance at 405nm for mAbs tested at 25 µg/mL. The threshold for binding was determined as 3-fold background, indicated by the dotted line.

5.4 HIV Env-specific mAbs isolated from elite neutraliser T125 had higher levels of SHM and different isotype usage compared to non-Env mAbs

The variable regions within the heavy and light chain plasmids, used to produce mAbs, were sequenced to characterise T125 mAbs at the nucleotide and amino acid level. Analysis of sequences by IMGT V-Quest was first used to identify the V-gene and J-gene usage selected during B cell development. This revealed that T125 mAbs utilised a variety of genes, although identification of the exact gene was not always conclusive due to similarities in homology as is commonly the case for mAbs (Table 1). The most common gene used was VH3-30, which is one of the most frequently recombined V-genes in the antibody repertoire (Yang et al. 2021). However, among the mAbs which bound Env in ELISA, the gene most frequently used was VH5-51, while mAbs with undetectable Env binding had more frequent use of the VH3-23 gene. In the light chain, the gene usage was more diverse although the VK3-15 and VK3-20 genes were most commonly used by mAbs, regardless of Env binding. While the majority of sequences were unique, there were a few exceptions where mAbs shared the same V-gene and J-gene in both the heavy and light chains (Table 1). Construction of a guide tree using only the CDRH3 sequence from mAbs revealed that three pairs (7B7 and 7D4, 7E3 and 7E8 as well as 7F6 and 7F10) were clonally related (Figure 5.4). As these mAb pairs also had the same heavy and light chain V-gene usage (Table 1) they are likely somatic variants. However, most sequences were singletons belonging to a few V_H families as seen in a previous study (van Gils et al. 2016).

The features of mAb sequences cloned from elite neutraliser T125 were investigated further by considering the level of SHM and CDRH3 lengths (Table 1). These were of particular interest because extensive SHM (up to 43%) and/or long CDRH3 loops (up to 37 AAs) are features of previously isolated HIV bnAbs (Griffith and McCoy 2021), as mentioned earlier. The sequences from mAbs had a wide range of V_H SHM from 1% to 23.7%, with an average of 9.1% SHM, which was higher than the level of SHM seen in the

HIV-negative donor (1.4-18.5% SHM, with an average of 6.3%) analysed in chapter 3. To put this into a wider context, the average SHM (9.1%) in T125 mAbs still fell within the range of average SHM (5.6-9.4%) previously identified in a healthy donor cohort (IJspeert et al. 2016). However, when only the mAbs that showed Env binding (in ELISA) were considered this revealed that the V_H SHM was higher with an average of 11.23%. Furthermore, comparison of the T125 mAbs based on their specificity for Env found that the median SHM was significantly higher in the V_H of mAbs that bound Env (10.53%) than those that did not (6.94%), as shown in Figure 5.5a. In addition, the level of SHM in the V_K or V_L of mAbs ranged from 0.3 to 21.6% and mAbs specific for Env had a higher mean of 8.4% SHM compared to non-Env mAbs which had a mean of 3.8% SHM (Table 1). Overall, this suggests that the IgG+ B cells in elite neutraliser T125 with soluble mAbs capable of binding Env have undergone greater affinity maturation than IgG+ B cells with mAbs that had undetectable Env binding by ELISA.

Next, the CDRH3 of mAbs was assessed, which found that the length ranged from 9 to 20 AAs (Table 1), with an average of 15.7 AAs. This was a narrower range than the HIV-negative donor, which had CDRH3 sequences from 5-23 AAs in length (chapter 3). However, the average CDRH3 length of T125 mAbs was comparable to the 15.5 (± 3.2) AAs length identified from public datasets (Shi et al. 2014). Interestingly, none of the mAbs displayed a long CDRH3 of >20 AAs, which can be characteristic of HIV bnAbs such as those targeting the trimer apex on Env (Griffith and McCoy 2021). To determine if there was a difference in the CDRH3 of mAbs capable of binding to Env or not, the median length was compared but this was not significantly different (Figure 5.5b). Finally, the CDRL3 length of mAbs ranged from 8 to 12 AAs (Table 1), showing that none exhibited a short CDRL3 of 5 or 6 AAs characteristic of VRC01-like CD4bs bnAbs, to prevent steric clashing (Zhou et al. 2013).

Single B cell cloning, which amplifies antibody variable regions but not the constant regions from B cells, has been predominantly used to isolate HIV bnAbs. Consequently, the isotype usage is not determined, and instead, the amplified heavy chain variable region is typically cloned into an expression vector containing the IgG1 constant region. Although single B cell cloning was

also used here to isolate mAbs from elite neutraliser T125, these B cells were also processed for scRNA-seq. Reconstruction of antibody sequences from the transcriptomics data using BraCeR (Lindeman et al. 2018) enabled the isotype to be determined from the heavy chain constant region. As the single B cells from T125 were isolated based on their IgG expression, only the distribution of the four IgG isotypes was assessed (Figure 5.5c). This revealed that there was a stark contrast between the isotype of mAbs that were capable of binding Env compared to those that did not. Env-specific mAbs were found to be predominantly IgG1 (Figure 5.5c), which are typically induced in response to protein antigens from viral infections (Ferrante, Beard, and Feldman 1990). While non-Env mAbs were predominantly IgG2 (Figure 5.5c), which has more of an association with polysaccharide antigens from bacterial infections (Vidarsson, Dekkers, and Rispens 2014). However, it was observed that regardless of Env-specificity very few mAbs were IgG3 and none were IgG4 (Figure 5.5c). Furthermore, the overall distribution of isotypes was most similar to the RM subset in the HIV-negative donor (chapter 3), which was predominantly IgG1, followed by IgG2 and rarely IgG3 or IgG4. In summary, the HIV mAbs capable of binding Env displayed higher levels of V_H SHM and had a predominant use of IgG1 compared to mAbs with undetectable Env binding, but had no difference in the CDRH3 length.

Table 1 Genetic features and characteristics of antibodies cloned from elite neutraliser T125

	Heavy chain				Light chain				
mAb	V-gene	SHM (%)	J-gene	CDR3 length	V-gene	SHM (%)	J-gene	CDR3 length	Env binding
7B8	VH1-18*01	9.8	JH6*02	18	VK3-20*01	5.2	JK5*01	9	+
7E7	VH1-69*01	18.4	JH6*01	20	VK1-5*01	18.6	JK1*01 / 2*02	9	+
7B11	VH1-69*01	10.5	JH4*02 / 5*02	18	VK1-39*01	9.1	JK5*01	9	+
7A3	VH1-69*01	10.1	JH5*02	18	VL10-54*01/*02	15.7	JL1*01	11	+
7E10	VH1-69*04	10.8	JH4*02	15	VK3-11*01/*02	6.7	JK3*01	8	+
8E3	VH3-11*03	5.9	JH4*02	15	VK1-12*01/*02	2.8	JK4*01	9	+
7D11	VH3-11*05	7.8	JH1*01 / 4*02	17	VK1-12*01/*02	5.6	JK4*01	9	+
7D3	VH3-21*01	14.6	JH4*02	18	VL3-21*02	6.6	JL1*01	11	+
7D10	VH3-23*04	16.0	JH4*02	15	VL2-11*01	11.5	JL1*01	12	+
7B7	VH3-30 / 3-30-3	18.4	JH1*01	15	VK3-15*01	7.7	JK4*01/*02	10	+
7D4	VH3-30 / 3-30-3	19.1	JH1*01	15	VK3-15*01	8.4	JK4*01/*02	10	+
7C11	VH3-30*10	15.9	JH1*01	15	VK1-16*01/*02 / 1-5*01	21.6	JK4*01/*02	9	+
7E3	VH3-30*18 / 3-30-5*01	7.1	JH4*02 / 5*02	9	VK1-33*01	8.1	JK3*01	8	+
7E8	VH3-30*18 / 3-30-5*01	7.1	JH4*02 / 5*02	9	VK1-33*01	8.1	JK3*01	8	+
7F8	VH3-74*01	6.3	JH4*02 / 5*02	13	VK3-15*01	5.2	JK4*01	9	+
8C7	VH3-74*01	2.0	JH4*02	13	VL2-14*03	1.4	JL3*02	10	+
7C6	VH4-31*03	8.4	JH3*01/*02	15	VL2-8*01	6.1	JL2*01 / 3*01/*02	10	+
8C11	VH4-39*07	8.1	JH4*02	15	VL2-8*01	4.7	JL2*01 / 3*01	10	+
7E5	VH5-51*01/*02/*03	4.7	JH4*02	16	VK3-20*01	4.2	JK5*01	9	+
7F6	VH5-51*01	14.9	JH5*02	18	VL3-1*01	9.9	JL1*01	9	+
7F10	VH5-51*01	14.6	JH3*02	18	VL3-1*01	9.9	JL1*01	9	+
8C10	VH5-51*01	12.9	JH3*02	20	VL3-10*01	10.3	JL2*01 / 3*01	11	+
7A2	VH5-51*01	15.2	JH3*02	17	VL6-57*01/*02	8.5	JL3*02	10	+
7C2	VH5-51*01/*02/*03	10.6	JH3*02	16	VL6-57*01/*02	5.9	JL3*02	10	+
7A8	VH1-18*01	10.4	JH4*02	17	VL10-54*01	5.1	JL2*01 / 3*01	11	-
8F3	VH1-46*01	6.1	JH6*03	20	VL1-40*01	4.4	JL3*02	11	-
7F2	VH1-46*01	7.1	JH4*02	12	VL2-8*01	3.1	JL1*01	10	-
7C4	VH3-11*01	3.7	JH4*01/*02	18	VK4-1*01	3.6	JK1*01	9	-
7E4	VH3-15*01	5.3	JH5*02	11	VL1-44*01	2.8	JL2*01 / 3*01	11	-
7D7	VH3-21*01	1.7	JH4*02	12	VL2-14*01	0.7	JL1*01	10	-
8E8	VH3-23*01	5.1	JH6*02	16	VK2-28*01	3.0	JL1*01	9	-
8A10	VH3-23*01	9.8	JH5*02	16	VK3-20*01	1.8	JK2*01	8	-
8E10	VH3-23*01	6.5	JH4*02	16	VK3-20*01	2.4	JK4*01	9	-
8D11	VH3-23*01	10.1	JH3*02	16	VK3-20*01	3.5	JK2*01	11	-
7F5	VH3-23*01	2.7	JH6*02	19	VL2-23*02	3.2	JL1*01	10	-
7A5	VH3-23*01	8.2	JH4*02	16	VL8-61*01	10.0	JL2*01 / 3*01/*02	10	-
8C8	VH3-23*03	5.4	JH4*02	17	VL4-69*01	1.7	JL1*01	9	-
8D7	VH3-30*18 / 3-30-5*01	8.5	JH4*02	16	VK2-28*01	4.0	JK5*01	9	-
7C3	VH3-30*18 / 3-30-5*01	7.4	JH4*02	17	VK3-11*01	4.9	JK3*01	10	-
8B6	VH3-30*18 / 3-30-5*01	6.8	JH5*02	15	VK3D-15*01	4.9	JK5*01	9	-
8F7	VH3-30*18 / 3-30-5*01	3.0	JH5*02	19	VK4-1*01	1.0	JK2*01	9	-
8A7	VH3-30-3*01	6.8	JH4*02	15	VK3-11*01	2.1	JK4*01	10	-
7B4	VH3-33*01	2.7	JH3*02	20	VK1-27*01	1.4	JK1*01	9	-
7A7	VH3-33*01/*05	8.4	JH4*02 / 5*02	13	VL2-23*02	3.1	JL3*02	11	-
7B9	VH3-48*02	23.7	JH4*02	14	VK3-15*01	9.0	JK4*01	8	-
8C9	VH3-66*01	1.0	JH4*02	12	VL2-11*01	0.3	JL3*02	11	-
8D10	VH3-72*01	3.0	JH5*02	15	VK1-9*01	3.2	JK4*01	9	-
8F5	VH3-74*01	7.4	JH5*02	17	VK1-39*01	6.0	JK5*01	9	-
8F4	VH4-30-4*03	15.2	JH3*02	15	VK3-15*01	5.2	JK3*01	9	-
7E2	VH5-51*01	7.8	JH4*02	12	VK1-5*03	8.5	JK2*01/*02	8	-

V-gene and J-gene assignment for antibody heavy and light chain sequences was performed using IMGT (Brochet, Lefranc, and Giudicelli 2008). The percentage somatic hypermutation (SHM) was determined from the V-gene nucleotide sequence and CDR3 length from the amino acid sequence. Binding to HIV-1 Env by monoclonal antibodies (mAbs) was determined by ELISA using BG505 and CRF250 SOSIP proteins, with a threshold of 3-fold background used to determine binding (+) or not (-).

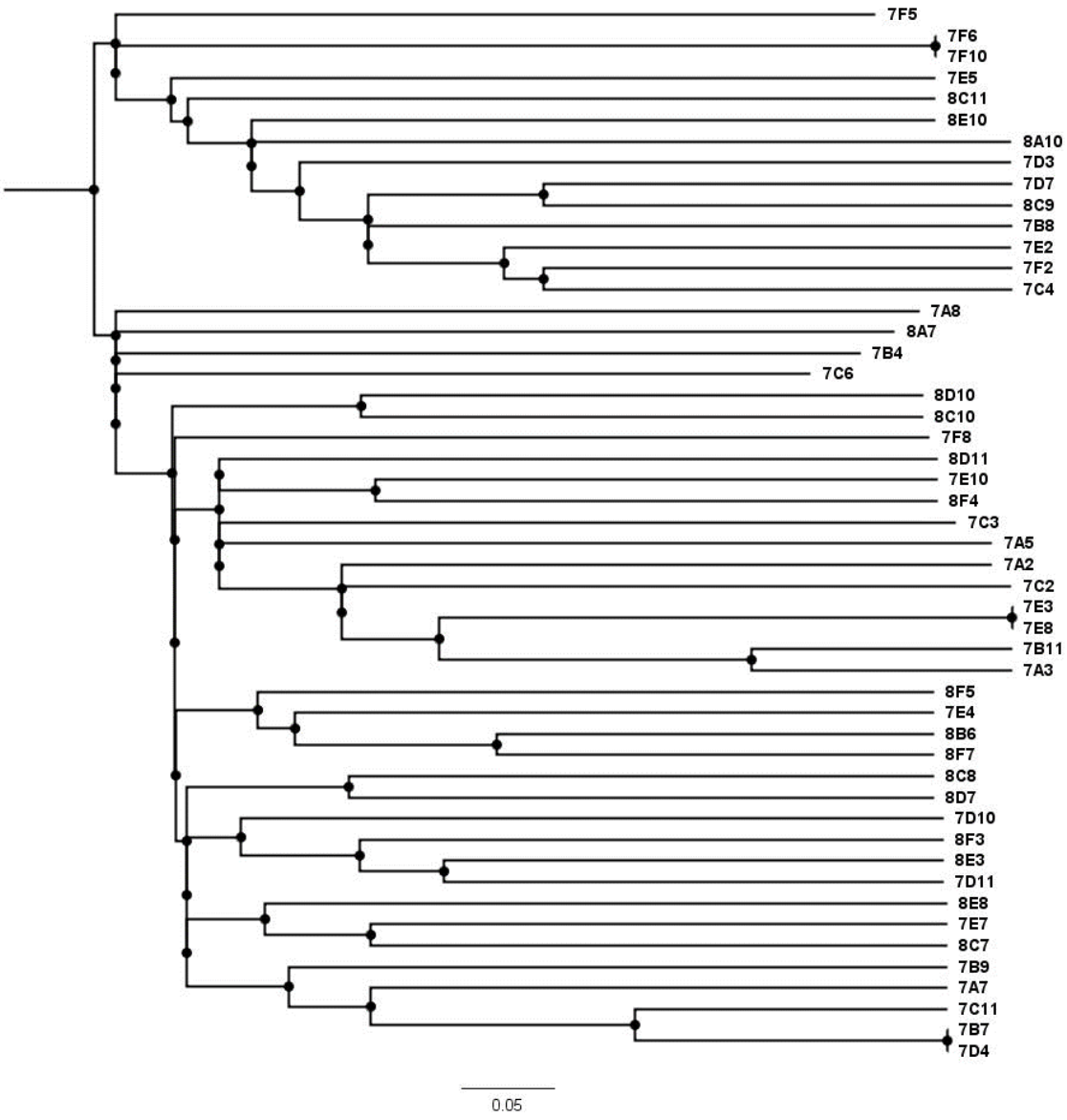

Figure 5.4 Clonal analysis of antibody CDRH3 sequences from elite neutraliser T125 revealed few that were related.

The Clustal Omega multiple sequence alignment tool was used to analyse the CDRH3 amino acid sequences from antibodies and generate a guide tree that was visualised using FigTree. The scale shows the phylogenetic distance of 0.05 substitutions per site.

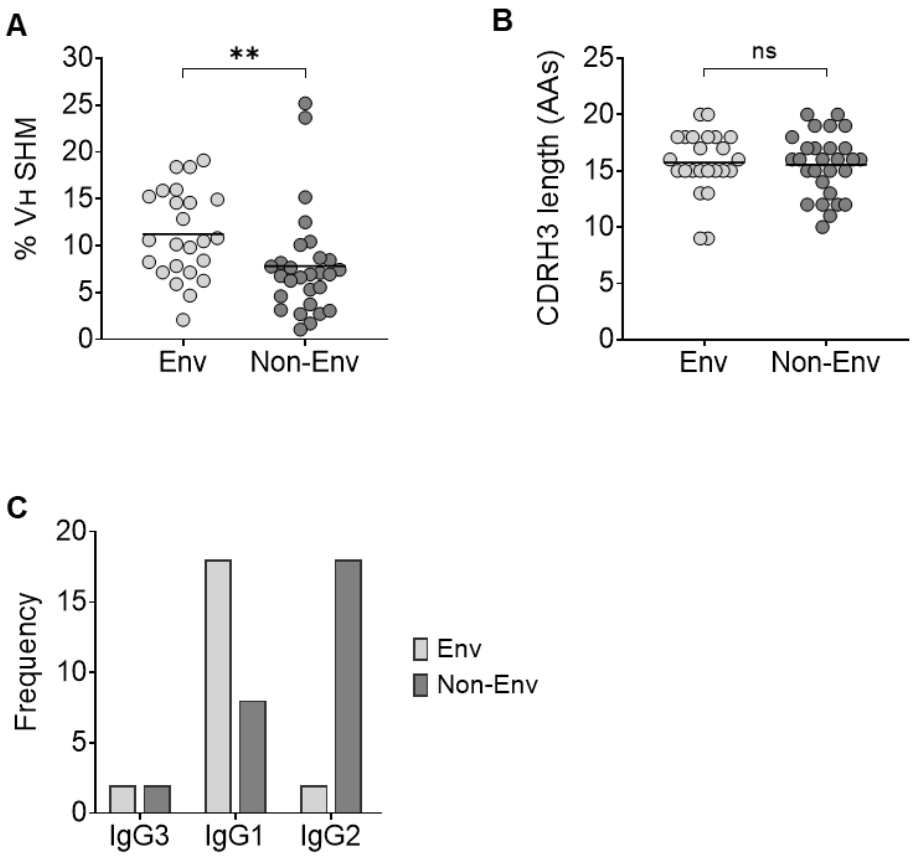

Figure 5.5 HIV Env-specific mAbs have higher levels of somatic hypermutation and predominant use of IgG1 compared to non-specific mAbs, but had no difference in CDRH3 length.

(A) Percentage somatic hypermutation (SHM) in V_H of HIV Env-specific and non-specific mAbs, with a significant difference between the groups (p=0.003) marked by an asterisk. (B) Length of CDRH3 in amino acids (AAs) of HIV Env-specific and non-specific mAbs. (A-B) Black horizontal lines indicate the median and a Mann-Whitney U-test was used to determine the difference between groups. P values >0.05 were deemed non-significant (ns). (C) Frequency of IgG isotypes for HIV Env-specific and non-specific mAbs, with isotypes ordered according to the position in the locus. Isotypes were identified from scRNA-seq data by BraCeR.

5.5 HIV Env-specific mAbs from elite neutraliser T125 exhibited a range of neutralisation profiles, with the identification of a bnAb

Although some HIV-1 bnAbs have similarities in genetic features, such as long CDRH3 regions for targeting the trimer apex or common use of the VH1-2 gene for targeting the CD4bs (West et al. 2014), unfortunately, the V(D)J gene sequence alone is not enough to identify nAbs or bnAbs (Griffith and McCoy 2021). Therefore, the Env-specific mAbs cloned from T125 were first screened for neutralisation against the standard 6 PV panel (Figure 5.6a), which is the same panel that was used to identify plasma neutralisation breadth in chapter 4. The concentration required for 50% viral inhibition (IC_{50}) is shown for each mAb in Figure 5.6a and reflects the potency of neutralisation. As the starting concentration of mAbs was 50 µg/mL this was used as the limit of detection, and any mAbs with an IC_{50} >50 were classed as non-neutralising. This revealed that 10 of the 24 mAbs were incapable of neutralising any of the PVs in the panel. However, nine mAbs neutralised a single clade C PV, 93IN905, with an IC_{50} in the range of 0.22 to 3.56 µg/mL, which was highly potent. The elite neutraliser T125 had a clade C infection, and so this suggests that these mAbs have a degree of clade-specific neutralisation, due to the fact they were able to neutralise 93IN905 but not the other clade C PV (C22) in the panel. This highlights the differences between Env even within the same clade and thus indicates that 93IN905 is likely to be more similar to the Env on the autologous virus that T125 was infected with. Of greater interest were the four mAbs 7F10, 7A2, 7F6 and 7C2 that were able to neutralise 94UG103 (clade A) as well as potently neutralise 93IN905 (clade C), exhibiting a degree of cross-clade neutralisation. The mAbs 7F6 and 7F10 were identified earlier as somatic variants (Figure 5.4) and thus it is unsurprising that these mAbs exhibited the same neutralisation profile. The other two mAbs 7A2 and 7C2 with cross-clade neutralisation also had the same gene usage as each other but had subtly different CDRH3 regions (Table 1 and Figure 5.4) which may explain the difference in neutralisation potency against 94UG103. Intriguingly, all four of these mAbs use VH5-51, however, this did not always result in cross-clade neutralisation as demonstrated by the other Env-specific mAbs (7E5 and

8C10) identified from T125 that had this V-gene usage yet only exhibited clade-specific neutralisation. Finally, the mAb with the greatest neutralisation breadth was 7E7, which was capable of targeting three PVs from different clades: 92TH021 (clade AE), 94UG103 (clade A) and C22 (clade C) and thus displayed 50% breadth of the standard 6 PV panel (Figure 5.6a). This level of neutralisation breadth exceeds the bnAb threshold of 30% mentioned earlier, and as the standard 6 PV panel is representative of larger panels of PVs (Landais et al. 2016) this indicates that the T125 mAb 7E7 is likely a bnAb.

The neutralisation curves for the bnAb 7E7 are shown in Figure 5.6b and revealed that in addition to neutralising 92TH021, 94UG103 and C22, there was also weak neutralisation of two additional PVs (92BR020 and 93IN905) at the top concentration (50 µg/mL). However, an IC_{50} value was only calculated for mAbs against a given PV if there were at least two values >50% neutralisation to generate a sigmoidal curve and enable an accurate IC_{50} value to be calculated. Representative curves for mAbs with cross-clade neutralisation (7F6), clade-specific neutralisation (7D11) and no neutralisation (7C6) against the standard 6 PV panel and a negative control PV (MLV) are also shown in Figure 5.6b. This demonstrates the differences in neutralisation capacity by T125 mAbs and shows that none had reactivity against a non-HIV PV (MLV). In summary, none of the mAbs isolated were capable of neutralising all of the PVs in the standard 6 PV panel and thus did not recapitulate the neutralisation breadth exhibited by antibodies in the plasma from T125. However, a range of neutralisation profiles was exhibited by mAbs, with the identification of non-bnAbs and one bnAb with neutralisation of 50% of the standard 6 PV panel. Thus, this allows the phenotype of B cells with different neutralisation capacities including bnAb B cells to be explored transcriptomically.

The neutralisation breadth of mAbs that exhibited cross-clade or broad neutralisation was investigated further against a larger panel of PVs (Figure 5.7a). This global PV panel was chosen on the basis that this is another standard panel that has been used frequently in the HIV field to screen for neutralisation breadth, consisting of 12 tier 2 PVs from six different clades that are representative of a 219 PV panel (deCamp et al. 2014). Cross-clade

neutralisation was demonstrated again by mAbs 7F10, 7A2, 7F6 and 7C2 which were able to target a clade G PV (X1632), and mAb 7A2 was also able to neutralise one of the clade C PVs in the panel (25710), with modest potency. However, these four mAbs only exhibited 8-17% neutralisation breadth against the global panel (Figure 5.7a) compared to 33% neutralisation breadth against the standard 6 PV panel (Figure 5.6a). In contrast, bnAb 7E7 was able to neutralise six of the PVs in the 12 PV global panel, from five different clades, and thus exhibited reproducible neutralisation breadth of 50% (Figure 5.7a). The neutralisation curves for 7E7 highlight the differences in its ability to neutralise 398, 246, TRO11, 25710, Ce1176 and X1632 (Figure 5.7b), with the most potent neutralisation exhibited against one of the clade C PVs (25710).

A

		mAb IC_{50} (µg/mL)											
Virus	**Clade**	**7E7**	**7F10**	**7A2**	**7F6**	**7C2**	**7E8**	**7E3**	**8C10**	**7B8**	**7D3**	**7D11**	**8E3**
92TH021	AE	3.57	>50	>50	>50	>50	>50	>50	>50	>50	>50	>50	>50
94UG103	A	3.15	3.27	4.26	5.49	16.44	>50	>50	>50	>50	>50	>50	>50
JRCSF	B	>50	>50	>50	>50	>50	>50	>50	>50	>50	>50	>50	>50
92BR020	B	>50	>50	>50	>50	>50	>50	>50	>50	>50	>50	>50	>50
93IN905	C	>50	0.30	0.24	0.52	0.51	0.22	0.27	0.53	1.38	2.15	2.66	3.12
C22	C	3.56	>50	>50	>50	>50	>50	>50	>50	>50	>50	>50	>50
Breadth %		50%	33%	33%	33%	33%	17%	17%	17%	17%	17%	17%	17%

		mAb IC_{50} (µg/mL)											
Virus	**Clade**	**7B11**	**7E5**	**7A3**	**7B7**	**7C6**	**7C11**	**7D4**	**7D10**	**7E10**	**7F8**	**8C7**	**8C11**
92TH021	AE	>50	>50	>50	>50	>50	>50	>50	>50	>50	>50	>50	>50
94UG103	A	>50	>50	>50	>50	>50	>50	>50	>50	>50	>50	>50	>50
JRCSF	B	>50	>50	>50	>50	>50	>50	>50	>50	>50	>50	>50	>50
92BR020	B	>50	>50	>50	>50	>50	>50	>50	>50	>50	>50	>50	>50
93IN905	C	3.16	3.56	>50	>50	>50	>50	>50	>50	>50	>50	>50	>50
C22	C	>50	>50	>50	>50	>50	>50	>50	>50	>50	>50	>50	>50
Breadth %		17%	17%	0%	0%	0%	0%	0%	0%	0%	0%	0%	0%

B

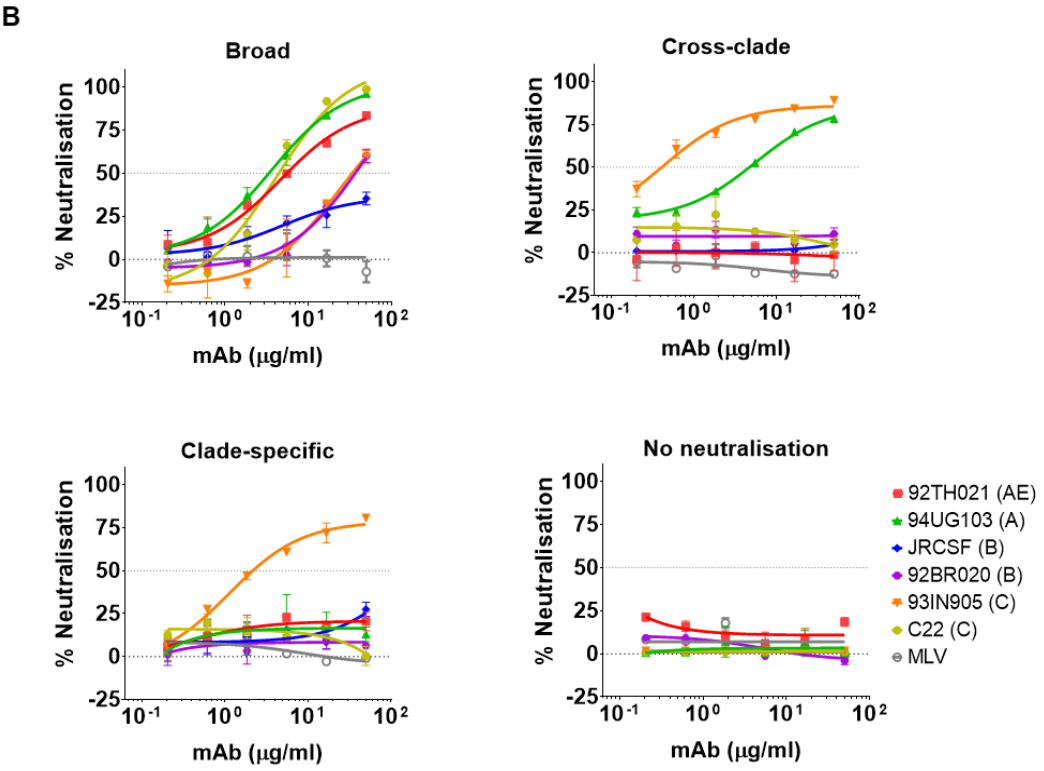

Figure legend on next page

Figure 5.6 HIV Env-specific mAbs demonstrated a range of neutralisation profiles against the standard 6 PV panel.

(A) Neutralisation of the standard 6 PV panel by HIV Env-specific mAbs, with IC_{50} titres reflecting an average of two repeats and an IC_{50} >50 indicates no neutralisation. (B) Representative graphs of mAbs with broad (7E7), cross-clade (7F6), clade-specific (7D11) and no neutralisation (7C6) against the standard 6 PV panel: 92TH021 (red), 94UG103 (green), JRCSF (blue), 92BR020 (purple), 93IN905 (orange) and C22 (yellow) and a negative control PV MLV (grey). Neutralisation curves were generated from the serial titration of mAbs tested in duplicate with the mean and error bars plotted and dotted lines at 0% and 50% neutralisation. The clade of each virus in the panel is shown in brackets.

A

		IC_{50} (µg/mL)				
		bnAb	Cross-clade nAbs			
Virus	Clade	7E7	7F10	7A2	7F6	7C2
398	A	1.80	>50	>50	>50	>50
246	AC	1.73	>50	>50	>50	>50
CNE8	AE	>50	>50	>50	>50	>50
CNE55	AE	>50	>50	>50	>50	>50
TRO11	B	1.75	>50	>50	>50	>50
X2278	B	>50	>50	>50	>50	>50
CH119	BC	>50	>50	>50	>50	>50
BJ0X002	BC	>50	>50	>50	>50	>50
25710	C	0.21	>50	13.23	>50	>50
Ce1176	C	2.33	>50	>50	>50	>50
CE0217	C	>50	>50	>50	>50	>50
X1632	G	3.42	4.04	5.53	9.77	8.51
Breadth %		50%	8%	17%	8%	8%

B

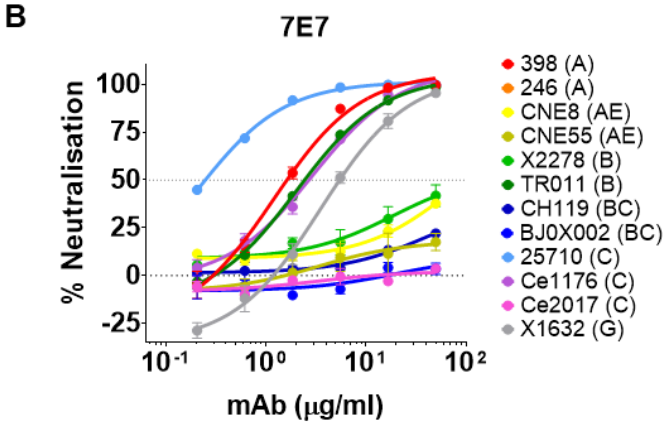

Figure 5.7 Broad neutralisation exhibited by mAb 7E7 was reproducible against a larger global PV panel.

(A) Neutralisation of the global 12 PV panel by broad and cross-clade nAbs, with IC_{50} titres reflecting an average of two repeats and an IC_{50} >50 indicates no neutralisation. (B) Representative graph of broad neutralisation by mAb 7E7 against the global 12 PV panel, with the clade of each virus shown in brackets. Neutralisation curves were generated from the serial titration of 7E7 tested in duplicate with the mean and error bars plotted and dotted lines at 0% and 50% neutralisation.

5.6 Antibodies with limited neutralisation against a multi-clade PV panel did not exhibit breadth against viruses from the clade of infection

To address whether any of the neutralising mAbs had breadth across different clade C viruses (the clade of T125 infection), rather than across different viral clades, a standard panel consisting entirely of clade C PVs was tested. This revealed that the broad neutralisation by 7E7 was enhanced against the Clade C PV panel, exhibiting 67% breadth (8/12 PVs), although the IC_{50} values which reflect the potency of neutralisation varied depending on the PV (Figure 5.8a). The range of IC_{50} values is emphasised in the neutralisation curves of bnAb 7E7 against the PVs in the panel (Figure 5.8b), with Du422.1 being the most susceptible to neutralisation (IC_{50} 0.49 µg/mL) and CAP210.2 being the most resistant (IC_{50} 11.94 µg/mL). This additionally showed that neutralisation of ZM233 was close to 50% at the highest concentration of 7E7 (Figure 5.8b), but was not enough to be classed as neutralising, with an IC_{50} >50 µg/mL (Figure 5.8a). Conversely, only one PV (ZM109) was susceptible to neutralisation by the cross-clade nAbs 7A2, 7F6, 7C2 and 7F10, which resulted in limited breadth (8%) against the clade C panel (Figure 5.8a). Finally, the nine clade-specific nAbs, (identified in Figure 5.6a), were only capable of neutralising a single additional PV or none of the PVs in the clade C panel (Figure 5.8a). Specifically, six mAbs were able to neutralise ZM109 in addition to 93IN905 in the initial 6 PV panel, suggesting they have a level of clade C specific neutralisation. Interestingly, ZM109 was the same PV neutralised by the cross-clade nAbs, suggesting that the Env of ZM109 is most similar to the autologous T125 Env out of the clade C PVs tested here.

A

		IC_{50} (µg/mL)				
		bnAb	Cross-clade nAbs			
Virus	Clade	7E7	7A2	7F6	7C2	7F10
Du156.12	C	>50	>50	>50	>50	>50
Du172.17	C	>50	>50	>50	>50	>50
Du422.1	C	0.49	>50	>50	>50	>50
ZM197	C	2.84	>50	>50	>50	>50
ZM214	C	2.68	>50	>50	>50	>50
ZM233	C	>50	>50	>50	>50	>50
ZM249	C	4.33	>50	>50	>50	>50
ZM53	C	>50	>50	>50	>50	>50
ZM109	C	1.37	4.72	5.13	5.20	5.74
ZM135	C	4.85	>50	>50	>50	>50
CAP45.2	C	1.32	>50	>50	>50	>50
CAP210.2	C	11.94	>50	>50	>50	>50
Breadth %		**67%**	**8%**	**8%**	**8%**	**8%**

		IC_{50} (µg/mL)								
		Clade-specific nAbs								
Virus	Clade	7B8	7E8	7E3	7B11	7D11	8E3	8C10	7D3	7E5
Du156.12	C	>50	>50	>50	>50	>50	>50	>50	>50	>50
Du172.17	C	>50	>50	>50	>50	>50	>50	>50	>50	>50
Du422.1	C	>50	>50	>50	>50	>50	>50	>50	>50	>50
ZM197	C	>50	>50	>50	>50	>50	>50	>50	>50	>50
ZM214	C	>50	>50	>50	>50	>50	>50	>50	>50	>50
ZM233	C	>50	>50	>50	>50	>50	>50	>50	>50	>50
ZM249	C	>50	>50	>50	>50	>50	>50	>50	>50	>50
ZM53	C	>50	>50	>50	>50	>50	>50	>50	>50	>50
ZM109	C	5.25	6.92	6.00	9.39	25.47	41.41	>50	>50	>50
ZM135	C	>50	>50	>50	>50	>50	>50	>50	>50	>50
CAP45.2	C	>50	>50	>50	>50	>50	>50	>50	>50	>50
CAP210.2	C	>50	>50	>50	>50	>50	>50	>50	>50	>50
Breadth %		**8%**	**8%**	**8%**	**8%**	**8%**	**8%**	**0%**	**0%**	**0%**

B

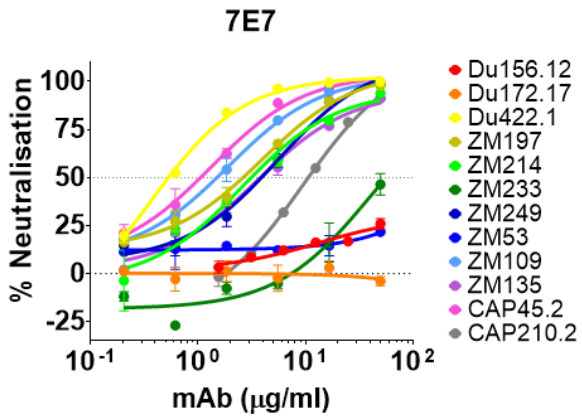

Figure legend on next page

Figure 5.8 Neutralisation breadth against viruses from the clade of infection was exhibited by bnAb 7E7 but not cross-clade or clade-specific nAbs.

(A) Neutralisation of a standard 12 Clade C PV panel by broad and cross-clade nAbs as well as clade-specific nAbs. IC_{50} titres reflect an average of two repeats and >50 indicates no neutralisation. (B) Neutralisation curves were generated from the serial titration of bnAb 7E7 tested in duplicate against the 12 Clade C PV panel, with the mean and error bars plotted and dotted lines at 0% and 50% neutralisation.

5.7 Production of three infectious T125 autologous PV

Next, it was of interest to determine if any of the mAbs isolated from T125 were able to neutralise the donor's own (autologous) virus. While elite neutralisers can produce bnAbs that neutralise heterologous viruses, this does not necessarily result in the capacity to neutralise autologous viruses, due to ongoing viral escape (as discussed in section 1.2.3).

Sequence information for HIV isolates previously identified from T125 plasma was found in an HIV database ('LANL Sequence Database') from the same timepoint examined in this study. Of particular interest were the *env* gene sequences from viral isolates (n=32) that were publicly available on GenBank and used to construct a maximum likelihood phylogenetic tree to predict evolutionary pathways (Figure 5.9). Reference sequences from the *env* of two clade B viruses (NL4.3 and Ba-L) and two C viruses (Du156.12 and 93IN905) were also included. As expected the clade B *env* formed a separate branch from the clade C *env* and additionally showed that the clade C *env* 93IN905 was most similar to the autologous T125 clade C *env* sequences. This mirrors the finding that the majority of the mAbs cloned from T125 could target 93IN905 (Figure 5.6a) but not Du156.12 (Figure 5.8a) for neutralisation. Furthermore, this analysis revealed the high diversity of autologous *env* within T125 at the time of sampling and had two main branch points (nodes) that represent divergence events. While one node led to *env* sequences with the same branch length reflecting high similarity, the other node gave rise to multiple branches with varying lengths, reflecting different levels of mutation

and diversity in the *env* sequences (Figure 5.9). Overall, the shape of the tree is distinct from an HIV patient with low viral diversity, where the majority of *env* sequences stem from the same node and all have the same branch length (Gupta et al. 2019).

Additional analysis to identify differences in glycan holes (as outlined in 2.10.2) revealed that all of the *env* sequences on the branch with the least variation lacked five conserved PNGS, while *env* sequences on the branch with more diversity had no, one, two or three PNGS missing. It was decided that three *env* sequences would be produced as PVs to test T125 mAbs for autologous neutralisation to try and cover the diversity of the viruses in circulation. Consequently, two *env* sequences (2139_e21 and 2139_e9 with no or two PNGS missing respectively) were chosen from the branch with the most variation, and one (2139_e7, with five PNGS missing) from the branch with the least variation (marked with an asterisk, Figure 5.9).

The selected T125 *env* gp160 sequences 2139_e7, 2139_e9 and 2139_e21 were first synthesised with overhangs to enable cloning into an expression vector, which was verified by PCR using primers on either side of the cloning sites (as described in section 2.10.4). PCR amplification of a band (~2kb) was visualised by gel electrophoresis to confirm successful cloning of the gp160 *env* sequences. These T125 Env plasmids were then co-transfected with an HIV backbone plasmid into 293T cells as per previous production of PVs (outlined in section 2.6.1) and titrated against TZM-bl cells to check for infectivity (as in section 2.6.2). All three T125 PVs were infectious and thus able to be used in neutralisation assays to test susceptibility to mAbs cloned from T125.

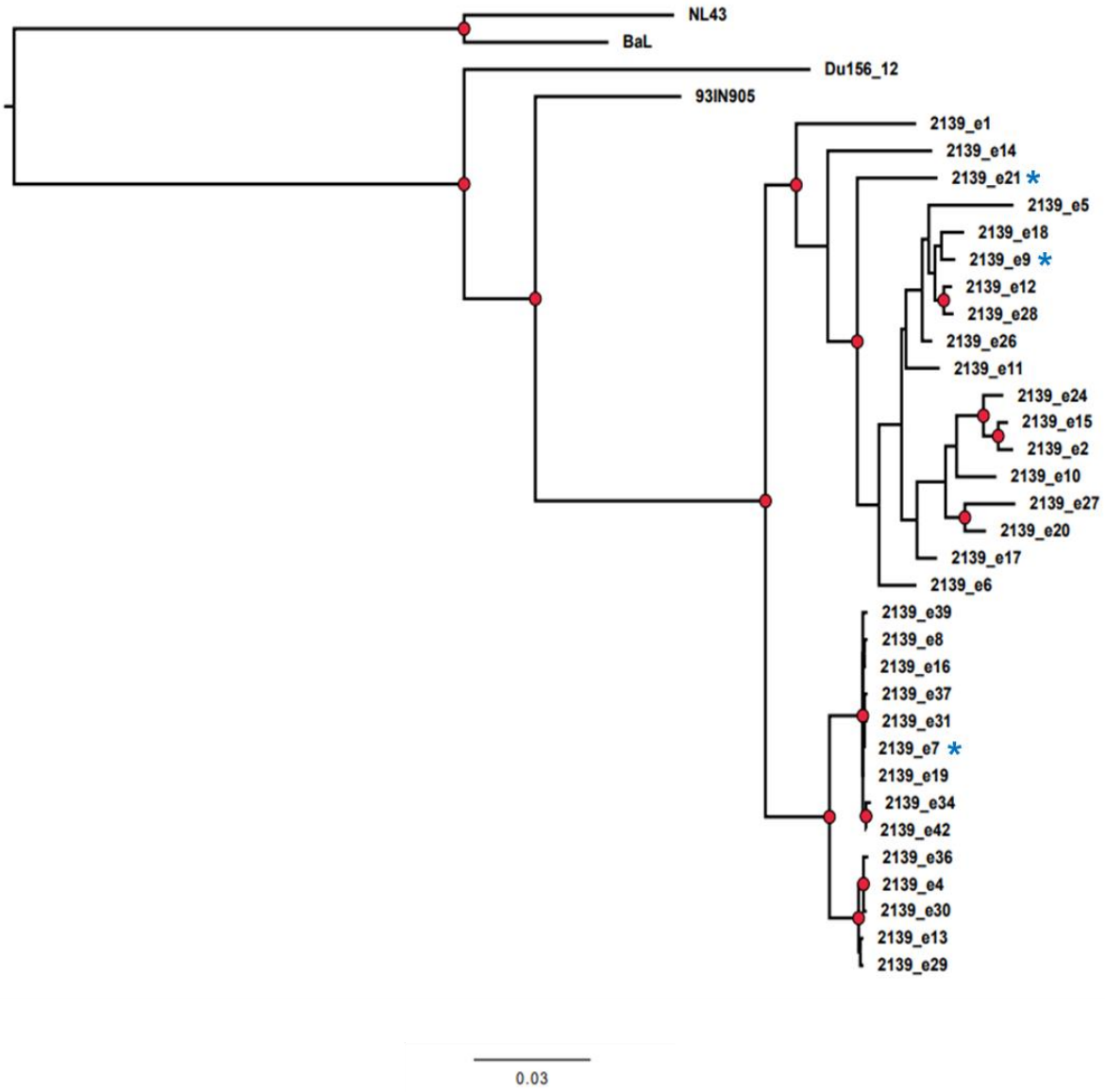

Figure 5.9.Autologous *env* from elite neutraliser T125 at a single timepoint showed high diversity.

Maximum likelihood phylogenetic tree of T125 *env* sequences from GenBank (KC156146-64, KC156166-78) trimmed to the start and end of gp160 based on the HXB2 *env* sequence. Two clade B *env* sequences (NL4.3 and Ba-L) and two clade C *env* sequences (93IN905 and Du156.12) from GenBank were also included in the tree for reference. Nodes in red indicate >70% bootstrap support. The scale bar indicates nucleotide substitutions per site. T125 *env* sequences marked with an asterisk (*) were synthesised and cloned into an Env expression plasmid.

5.8 T125 bnAb 7E7 was encoded to use the IgG3 isotype

Unlike most of the Env-specific mAbs that were predominantly IgG1 (Figure 5.5c), the isotype of the bnAb 7E7 was IgG3. However, during single B cell cloning, the 7E7 Ig variable regions were cloned into an IgG1 expression vector meaning that all of the characterisation up until this point was in the IgG1 format. While the isotype of an antibody is not often considered in mAb neutralisation studies, due to its predominant role in Fc effector functions, the structural differences between isotypes such as the long, flexible hinge of IgG3 can influence binding and neutralisation. For instance, IgG3 versions of HIV bnAbs targeting the trimer apex displayed enhanced neutralisation potency compared to IgG1 counterparts and were shown to be modulated by the hinge length (Richardson et al. 2019). HIV bnAbs against other epitopes have also shown increased neutralisation potency, although this was virus-dependent (Richardson et al. 2021). Additionally, IgG3 versions of mAbs have demonstrated more effective autologous neutralisation compared to IgG1 versions, with greater breadth in the viruses targeted and/or improved potency of neutralisation (Scheepers et al. 2020). Therefore, to evaluate if the difference in isotype had an impact on neutralisation by 7E7, in particular for autologous PV, the heavy chain variable region was cloned into an IgG3 constant region vector (as described in section 2.8.3) and included alongside the IgG1 version in neutralisation assays.

5.9 T125 mAbs frequently exhibit incomplete neutralisation against autologous PV with limited bnAb neutralisation

Notably, the maximum percentage neutralisation (MPN) exhibited by mAbs at 50 µg/mL against autologous T125 PVs was frequently low, and as such can be described as incomplete neutralisation (McCoy et al. 2015) (Figure 5.10). This phenomenon has previously been seen across many virus/mAb combinations and attributed to a proportion of viral particles being resistant to a given mAb, such that only 70% MPN is achieved as 30% of virions are resistant. This effect makes it hard to quantify neutralisation titres, especially

when MPN plateaus as low as 50% have been observed (van Gils et al. 2016) as this is the cut-off for neutralisation. Therefore, for many T125 mAbs although a trend towards neutralisation was observed it is not possible to define these mAbs as neutralising against these autologous viruses, as the plateau was <50%. Moreover, for many of the mAbs, only one concentration gave neutralisation of >50% making the calculation of IC_{50} values less accurate than those generated thus far, but can still indicate the neutralisation potency. With this caveat, the PV most susceptible to neutralisation was T125 2139_e21, with 12 out of 24 mAbs exhibiting >50% neutralisation with IC_{50} values ranging widely from 2.57 to 39.79 µg/mL. These mAbs were previously identified as clade-specific or cross-clade neutralisation but did not include the bnAb 7E7. Only poor autologous neutralisation was achieved by the bnAb 7E7, in line with previous observations on autologous neutralisation by bnAbs (Liao, Lynch, et al. 2013; MacLeod et al. 2016; Doria-Rose et al. 2014). However, the MPN revealed subtle differences between 7E7 expressed as IgG1 and IgG3, with enhanced potency exhibited by the IgG3 version that resulted in >50% neutralisation against the T125 2139_e9 PV (Figure 5.10). Moreover, when expressed as IgG3 the bnAb 7E7 exhibited modest neutralisation (IC_{50} of 23.07 µg/mL) against T125 2139_e9, which none of the other mAbs were able to target. Interestingly, analysis of the position of these *env* sequences on the phylogenetic tree showed that 2139_e9 was on a branch downstream of 2139_e21 (Figure 5.9), which suggests that 2139_e9 evolved from 2139_e21. Since most T125 nAbs could neutralise 2139_e21 but not 2139_e9, it could be speculated that this evolution is a result of escape from neutralisation. Finally, the T125 2139_e7 PV which was on a different branch in the phylogenetic tree and thus unrelated to the other two *env* sequences, also showed resistance to autologous mAbs, with none displaying strong enough neutralisation to calculate an IC_{50} value. It was also observed that mAbs unable to neutralise any heterologous PVs (Figure 5.6) were also unable to neutralise any of the autologous T125 viruses tested (Figure 5.10) and thus can be classed as non-neutralising. In summary, Env-specific mAbs isolated from the single B cells of T125 tested in neutralisation assays against heterologous and autologous viruses identified 10 non-nAbs, nine clade-

specific nAbs, four cross-clade nAbs and one bnAb. The variety of neutralisation capacities exhibited by mAbs suggests differences in their binding to Env and thus the epitopes targeted.

		MPN against T125 PV			IC_{50} (µg/mL) against T125 PV		
	T125 mAb	2139_e21	2139_e9	2139_e7	2139_e21	2139_e9	2139_e7
Broad nAb	7E7 IgG1	<50%	<50%	<50%	>50	>50	>50
	7E7 IgG3	<50%	58%	<50%	>50	23.07	>50
Cross clade nAb	7A2	74%	<50%	<50%	5.72	>50	>50
	7C2	71%	<50%	<50%	12.50	>50	>50
	7F6	57%	<50%	<50%	22.79	>50	>50
	7F10	56%	<50%	<50%	30.09	>50	>50
Clade specific nAb	7B8	80%	<50%	<50%	2.57	>50	>50
	7B11	77%	<50%	<50%	4.81	>50	>50
	7D11	73%	<50%	<50%	7.04	>50	>50
	7E3	72%	<50%	<50%	5.94	>50	>50
	7E8	67%	<50%	<50%	15.34	>50	>50
	7D3	59%	<50%	<50%	19.39	>50	>50
	8E3	60%	<50%	<50%	21.50	>50	>50
	8C10	53%	<50%	<50%	39.79	>50	>50
	7E5	<50%	<50%	<50%	>50	>50	>50
Non-nAb	7A3	<50%	<50%	<50%	>50	>50	>50
	7B7	<50%	<50%	<50%	>50	>50	>50
	7C6	<50%	<50%	<50%	>50	>50	>50
	7C11	<50%	<50%	<50%	>50	>50	>50
	7D4	<50%	<50%	<50%	>50	>50	>50
	7D10	<50%	<50%	<50%	>50	>50	>50
	7E10	<50%	<50%	<50%	>50	>50	>50
	7F8	<50%	<50%	<50%	>50	>50	>50
	8C7	<50%	<50%	<50%	>50	>50	>50
	8C11	<50%	<50%	<50%	>50	>50	>50

Figure 5.10 HIV Env-specific mAbs demonstrated limited neutralisation of autologous virus.

Maximum percentage neutralisation (MPN) of three autologous T125 PVs by HIV Env-specific mAbs at 50 µg/mL. IC_{50} titres were calculated from the neutralisation curves of mAbs titrated in duplicate, for those that demonstrated >50% maximum neutralisation. A colour gradient of red to yellow reflects the neutralisation capacity from highest to lowest respectively, with less than 30% neutralisation and an IC_{50} >50 in grey reflecting no neutralisation. T125 mAbs were grouped according to neutralisation profiles exhibited previously against the standard 6 PV panel.

5.10 Neutralising antibodies with limited breadth target the V3 loop and CD4bs

To investigate the epitope specificity, the binding profiles of mAbs were tested in ELISAs using different versions of the Env protein or in the presence of other mAbs to identify competitive binding to the same region on Env. The gp120 subunit of HIV Env is comprised of five conserved regions separated by five variable loops, V1, V2, V3, V4 and V5. The tip of the V3 loop in particular is more conserved than the other variable loops due to its role in co-receptor binding, but in trimeric Env, the V3 is concealed beneath the V1/V2 and only exposed upon conformational changes following engagement of CD4 (Mbah et al. 2001; Julien et al. 2013). As a result, antibodies that target the V3 loop can block viral entry and thus are capable of neutralisation, although are often limited to tier 1 viruses that have a predominantly open conformation, similar to the CD4-bound state. An ELISA to test for binding to a peptide containing the V3 loop from BG505 was used to determine if any of the neutralising antibodies from T125 targeted this region. In total, seven nAbs (7A2, 7C2, 7E3, 7E8, 7F6, 7F10 and 8C10) were capable of binding to the V3 peptide (Figure 5.11a), with an absorbance higher than the negative control SARS-CoV mAb CR3018 (van den Brink et al. 2005) and comparable to the positive control mAb ACS221 that is specific for the V3 loop (van Gils et al. 2016). Five nAbs that bound the V3 had VH5-51 gene usage, although two (7F6 and 7F10) were somatic variants, and the other two nAbs (7E3 and 7E8) were also a pair of somatic variants that instead used VH3-30/3-30-5. Interestingly, mAbs with VH5-51 gene usage have been identified as V3-dependant in previous studies, and appear to require pairing with a lambda light chain (van Gils et al. 2016; Gorny et al. 2011; Gorny et al. 2009). This may explain why the mAb 7E5 which also has VH5-51 gene usage but paired with a kappa light chain (Table 1), did not bind to the V3 peptide (Figure 5.11a).

Another neutralising epitope cluster located on the gp120 subunit is the CD4bs, which is conserved to enable interaction with CD4 on the host cell for entry. In particular, the residue D368 on the CD4 binding loop is highly conserved and is targeted by the majority of antibodies elicited against the

CD4bs (Zhou et al. 2015). Therefore, the T125 nAbs were next tested for their ability to bind to BG505 gp120 lacking this residue (D368R), to determine if any of the nAbs were affected and thus specific for the CD4bs. This revealed that three nAbs (7D11, 7E5 and 8E3) had a reduction in binding to gp120 when the D368R point mutation was introduced, with a fold-decrease that was even higher than the positive control VRC01 (Figure 5.11b), indicating that these nAbs target the CD4bs. On the basis that not all CD4bs-specific mAbs are dependent on D368 (Wibmer et al. 2016; Balla-Jhagjhoorsingh et al. 2013; Freund et al. 2015), the remaining T125 nAbs were then assessed for CD4bs specificity using a competition ELISA with the CD4bs bnAb VRC01. Competition ELISAs can be used to determine whether two mAbs bind to the same region on a given protein and have been used in previous studies to map the site of HIV mAb binding (McCoy et al. 2016; van Gils et al. 2016). This involves allowing the first mAb to bind to the protein before the addition of a second (biotinylated) mAb, and a reduction in binding by the second mAb is detected if there is an overlap in the binding footprint and thus competition for the same epitope. Here, BG505 gp120 was used to assess whether binding by T125 nAbs blocked the biotinylated VRC01 bnAb from binding to the CD4bs (Figure 5.11c). This revealed that 7B8, 7B11 and 7D3 were all able to compete with VRC01 for the CD4bs epitope by reducing VRC01 binding to <50%, unlike the negative control HIV bnAb PGT151 which does not target the CD4bs. VRC01 was also included as a positive control to show self-competition and resulted in <20% binding of the biotinylated version of itself (Figure 5.11c). To summarise, six T125 nAbs were found to target the CD4bs epitope, yet only three were affected by the D368R mutation. These CD4bs nAbs each had different gene usage, except 7D11 and 8E3 which differed only in the allele of the VH gene, but none used the VH1-2 gene characteristic of the VRC01-class of antibodies (Zhou et al. 2013) and may explain why none achieved neutralisation breadth.

Next, the epitopes of non-nAbs from T125 were investigated using competition ELISAs to identify changes in binding to BG505 SOSIP. Competitive binding by T125 non-nAbs revealed that 7B7, 7D4, 7C11 and 7D10 had an overlapping epitope, with binding reduced from 100% to below 50% (Figure

5.12a). An exception to this was 7D10 which did not prevent the binding of biotinylated mAbs, even when tested against itself this was only partially blocked (65%). A second epitope in common was shown by the reduced binding of biotinylated 7E10 (63%) as a result of partial blocking by 7C6, although the inverse binding of biotinylated 7C6 was not blocked by 7E10 (Figure 5.12a). This finding suggests that there may be a difference in the angle of approach or affinity for Env as there was some overlap in the binding footprint yet competition was only seen in one direction. Finally, non-nAbs 7A3, 7F8, 8C7 and 8C11 did not demonstrate any competitive binding, not even self-competition, and thus were not included in further competition ELISAs. In addition, as the non-nAbs 7B7 and 7D4 were shown earlier to be somatic variants (Figure 5.4) and had overlapping epitopes (Figure 5.12a), only one was included in further analysis. The non-nAbs that were found to target overlapping regions on Env were then tested in competition ELISAs using HIV mAbs targeting known epitopes on Env. Specifically, CD4bs, high mannose patch, trimer apex and gp120-gp41 interface antibodies were used to block these epitopes on Env, however, all of the T125 non-nAbs were still capable of at least 70% binding (Figure 5.12b). Even though all of the HIV mAbs used in this ELISA were bnAbs, these should still be capable of limiting access by non-nAbs if this region on Env was targeted. Therefore it can be concluded that the non-nAbs do not overlap with the known bnAb epitopes tested here and likely target other regions on the trimeric Env that are not as well characterised.

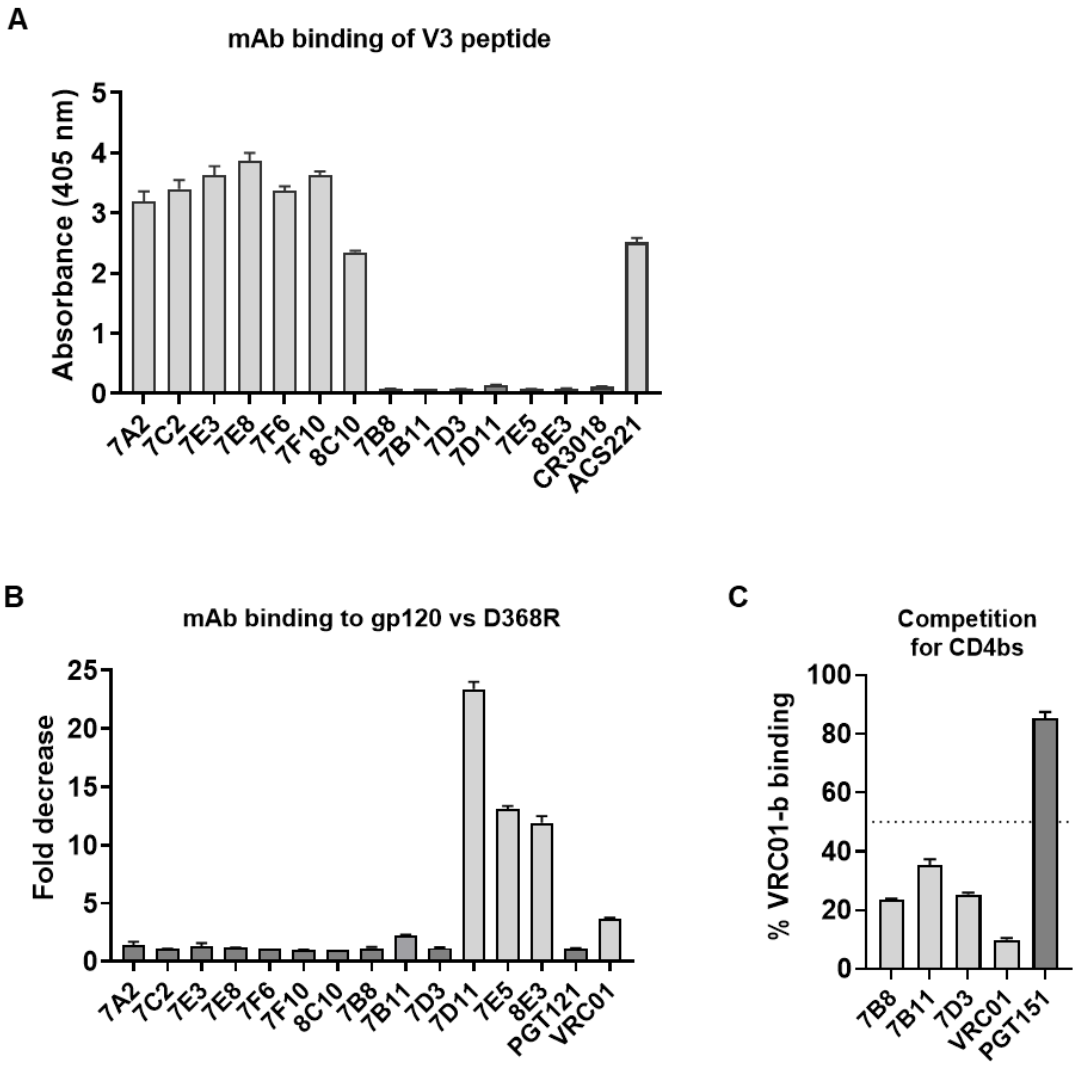

Figure 5.11 Neutralising antibodies target the V3 or CD4bs on HIV-1 Env.

(A-C) Epitope mapping ELISAs of mAbs tested in duplicate, with the mean and error bars shown. (A) Binding of mAbs to the V3 peptide of BG505 was shown by absorbance at 405nm, with ACS221 a V3 mAb isolated from a different bnAb donor (van Gils et al. 2016) as a positive control and non-HIV mAb CR3018 as a negative control. (B) Effect of the D368R mutation (in the CD4bs) on mAb binding of BG505 gp120, shown by fold-decrease in binding, with the CD4bs mAb VRC01 as a positive control and high mannose patch mAb PGT121 as a negative control. (C) Percentage binding of biotinylated VRC01 (VRC01-b) mAb to BG505 gp120 in the presence of non-biotinylated mAbs 7B8, 7B11, 7D3 and control HIV mAbs VRC01 (for self-competition) and PGT151 (for a negative control), assessed in a competition ELISA. Competitive mAb binding for the CD4bs epitope was identified by a reduction from 100% binding of VRC01-b to 50% binding or lower as highlighted by the gradient from white to blue.

A

	% binding of biotinylated competitor mAb									
mAb	**7A3-b**	**7B7-b**	**7D4-b**	**7C11-b**	**7D10-b**	**7C6-b**	**7E10-b**	**7F8-b**	**8C7-b**	**8C11-b**
7A3	101	97	103	103	103	94	93	108	98	98
7B7	96	19	32	24	28	97	91	111	100	99
7D4	97	19	29	25	30	99	92	101	97	97
7C11	97	27	38	25	27	98	94	105	98	96
7D10	98	73	77	76	65	99	95	104	100	97
7C6	101	99	97	96	96	14	63	103	115	103
7E10	102	96	100	100	99	93	11	100	100	99
7F8	99	98	104	100	102	96	101	84	104	100
8C7	97	99	102	100	98	95	95	101	94	98
8C11	96	97	101	96	92	95	100	106	94	92
CR3018	100	100	100	100	100	100	100	100	100	100

B

		% binding of biotinylated competitor mAb				
Epitope	**mAb**	**7B7-b**	**7C11-b**	**7D10-b**	**7C6-b**	**7E10-b**
CD4bs	**PGV04**	82	88	103	91	100
	b12	95	114	92	84	81
High mannose patch	**PGT121**	93	103	94	77	102
	PGT135	92	102	90	92	90
	2G12	82	91	73	83	82
Trimer Apex	**PG9**	93	109	104	95	96
	CAP256.09	94	101	97	100	85
	PGT145	96	96	93	95	86
gp120-gp41 interface	**ACS202**	86	119	96	81	77
	35O22	91	122	91	80	79
	3BC315	92	101	93	83	104
Non-HIV	**CR3018**	100	100	100	100	100

Figure 5.12 Non-neutralising antibodies show some overlap in the epitopes targeted on HIV-1 Env but do not compete with previously characterised HIV mAbs.

(A-B) Percentage binding of biotinylated competitor mAbs to BG505 SOSIP in the presence of non-biotinylated mAbs, assessed by competition ELISA, with the inclusion of a non-HIV mAb (CR3018) as a negative control. Competitive mAb binding was identified by a reduction from 100% binding of biotinylated mAbs to 50% binding or lower as highlighted by the gradient from white to blue. (A) Competition of non-neutralising mAbs with self and other non-neutralising mAbs isolated from elite neutraliser T125. (B) Competition of non-neutralising mAbs with previously characterised HIV Env-specific mAbs that target the CD4bs, high mannose patch, trimer apex or gp120-gp41 interface.

5.11 Broadly neutralising antibody 7E7 targets a gp120-gp41 epitope similar to the bnAb 3BC315, that is independent of the surrounding glycans

To epitope map the bnAb 7E7, the same approach was taken to screen for competitive binding using a range of HIV bnAbs that target different epitopes on Env. The results from the competition ELISA uncovered that 7E7 binding to BG505 SOSIP was reduced the most in the presence of gp120-gp41 interface specific bnAbs (Figure 5.13a), suggesting that 7E7 competed for binding to this epitope. In particular, competition with bnAb 3BC315 resulted in <25% binding by 7E7. Differences in the blocking of 7E7 binding by the three gp120-gp41 interface bnAbs reflect the differences between their modes of binding and footprints on this broad epitope. For instance, ACS202 is capable of targeting the gp41 fusion peptide (van Gils et al. 2016), unlike 35O22 or 3BC315. Instead, 3BC315 binds between the two gp41 subunits near the base of the trimer with a partial overlap in the epitope bound by 35O22 (Lee et al. 2015). As the T125 bnAb 7E7 had the least competition with ACS202, retaining 84% binding (Figure 5.13a), this suggests that the fusion peptide is not part of its epitope. The competitive binding of 7E7 and 3BC315 is shown in more detail in Figure 5.13b, and when 3BC315 was allowed to bind to BG505 SOSIP first, this bnAb blocked the binding of biotinylated 7E7 to a greater extent than 7E7 itself. However, when 7E7 was allowed to bind first, this did not prevent binding by biotinylated 3BC315 which retained 92% binding, similar to the negative control mAb CR3018, yet self-competition by the bnAb 3BC315 was observed (Figure 5.13b). This one-way competition suggests that 7E7 has a similar footprint to the gp120-gp41 interface bnAb 3BC315, but the angle of approach is not the same or that binding induces a conformational change in the Env protein that effects binding of the second mAb.

To investigate the similarity between 7E7 and 3BC315 these bnAbs were next compared in neutralisation assays. It has previously been demonstrated that 3BC315 has enhanced neutralisation when the glycan at position 88 in the gp120 subunit is removed (Lee et al. 2015). Therefore the JRCSF Env plasmid

was mutated using SDM to disrupt the glycosylation site (T90A). Neutralisation against JRCSF WT and T90A PVs was tested in parallel and showed that both 7E7 and 3BC315 gained the ability to neutralise JRCSF when the N88 glycan site was mutated (Figure 5.13c). Specifically, 7E7 demonstrated weak neutralisation of JRCSF, with the highest mAb concentration exhibiting 50% neutralisation, yet was enhanced to >90% when tested against the T90A PV. In contrast, 3BC315 was unable to neutralise JRCSF until the N88 glycan was removed by the T90A PV and exhibited more potent neutralisation than 7E7 to this mutant PV. The PGT121 bnAb that targets the high mannose patch was used as a negative control and was unaffected by the T90A mutation, as expected (Figure 5.13c). This result suggests that the epitope targeted by 7E7 does not include the N88 glycan and is more accessible when this glycan is not present. The dependency on glycans in or around the epitope of 7E7 was explored further by producing the PV 94UG103, neutralised by 7E7 and 3BC315, in the presence of kifunensine, which is a mannosidase inhibitor that prevents the processing of high mannose glycans into complex glycans. Neutralisation of 94UG103 PV produced in the presence of kifunensine was not largely affected by 7E7 or 3BC315 (Figure 5.13d), in contrast to PG9 that binds to complex glycans at the trimer apex and was therefore no longer able to neutralise this PV. Taken together, these results indicate that the T125 bnAb 7E7 binds to a gp120-gp41 epitope that does not include glycans and is similar to the epitope targeted by 3BC315 as both can be partially obstructed by the N88 glycan.

The sequence features of T125 bnAb 7E7 were then compared to 3BC315. This revealed that although both had VH1 gene usage, the VH1-69*01 gene was used by 7E7 while the VH1-2*02 gene was used by 3BC315 (Klein et al. 2012). For the light chain, the gene usage was very different, with the VK1-5*01 gene used by 7E7 and VL-23*02 used by 3BC315 (Klein et al. 2012). It has already been shown for 3BC315 that aromatic residues in the CDRL1 and CDRH3 allow hydrophobic interactions with gp41 (Lee et al. 2015). To determine if similar residues were also found in 7E7, a 2D graphical representation of the variable region structure (generated by IMGT) for the heavy and light chains of 3BC315 and 7E7 was compared (Figure 5.14).

Hydrophobic residues classified by IMGT include: isoleucine (I), valine (V), leucine (L), phenylalanine (F), cysteine (C), methionine (M), alanine (A) and tryptophan (W) and those that are commonly found in antibody sequences are highlighted in blue. Of these, phenylalanine (F) is also recognised as an aromatic residue, along with tyrosine (Y) and tryptophan (W) which can facilitate non-covalent antibody-antigen interactions and thus occur more frequently at the binding sites (Wu, Sun, et al. 2010). The 7E7 variable heavy chain structure showed the positioning of an 8 AA CDRH1 and CDRH2 as well as the 20 AA CDRH3, in which four residues were aromatic (Figure 5.14a). The variable light chain of 7E7 was shown to have a 6 AA CDRL1, a 3 AA CDRL2 and a 9 AA CDRL3, with aromatic residues only present in the CDRL3 (Figure 5.14b). This suggests that the CDRH3 and CDRL3 of the T125 bnAb 7E7 facilitate binding, although without structural studies this observation is only speculative. The variable heavy chain of 3BC315 was similar to 7E7 with the same length CDRH1 and CDRH2 as well as a CDRH3, which was longer by only one AA and contained four aromatic residues, although only one of these was in the same position as in the 7E7 CDRH3 (Figure 5.14c). In addition, the 3BC315 CDRH3 had the presence of two prolines in close succession that were not observed in the 7E7 CDRH3. As prolines are often associated with protein folding this finding was unexpected but may contribute to the angle of approach by the CDRH3 of 3BC315 for antigen binding. Finally, the variable light chain of 3BC315 was evaluated and showed that the CDRL2 and CDRL3 lengths were the same as 7E7, however, the 9 AA CDRL1 length (Figure 5.14d) was longer and had aromatic residues that were not present in the 6 AA CDRL1 of 7E7 (Figure 5.14b). Considering that aromatic residues in the CDRL1 of 3BC315 have been found to interact with gp41 (Lee et al. 2015), this suggests that the involvement of the light chain CDRs in 7E7 binding differs from 3BC315. In summary, both 7E7 and 3BC315 target the gp120-gp41 epitope on the HIV trimer and share some structural similarities, such as CDR lengths, despite distinct gene usage. Nevertheless, the differences shown by one-way competitive binding and neutralisation of JRCSF in Figure 5.13 imply that the angle of approach and specific residues in CDRs used to target the gp120-gp41 interface vary.

A

Epitope	mAb	% binding 7E7-b
CD4bs	PGV04	94
	b12	103
High mannose patch	PGT121	87
	PGT135	105
	2G12	79
Trimer Apex	PG9	100
	CAP256.09	93
	PGT145	93
gp120-gp41 interface	ACS202	84
	35O22	62
	3BC315	23
Non-HIV	CR3018	100

B

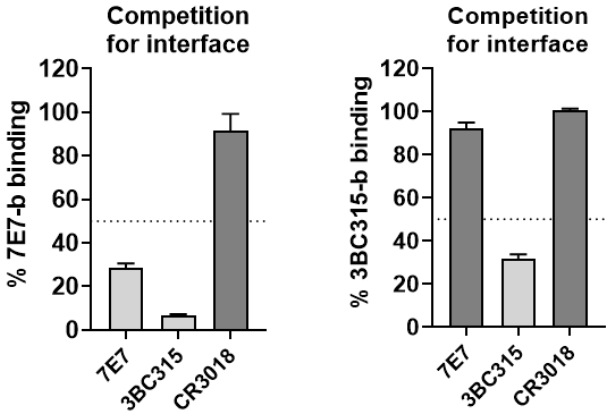

C

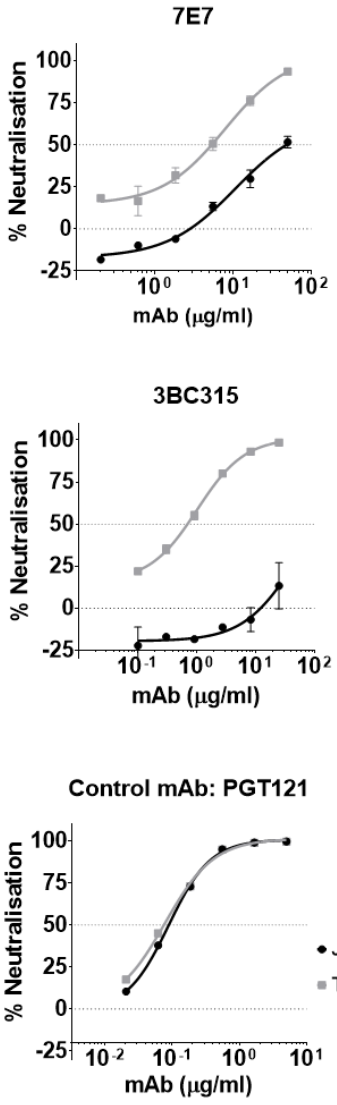

D

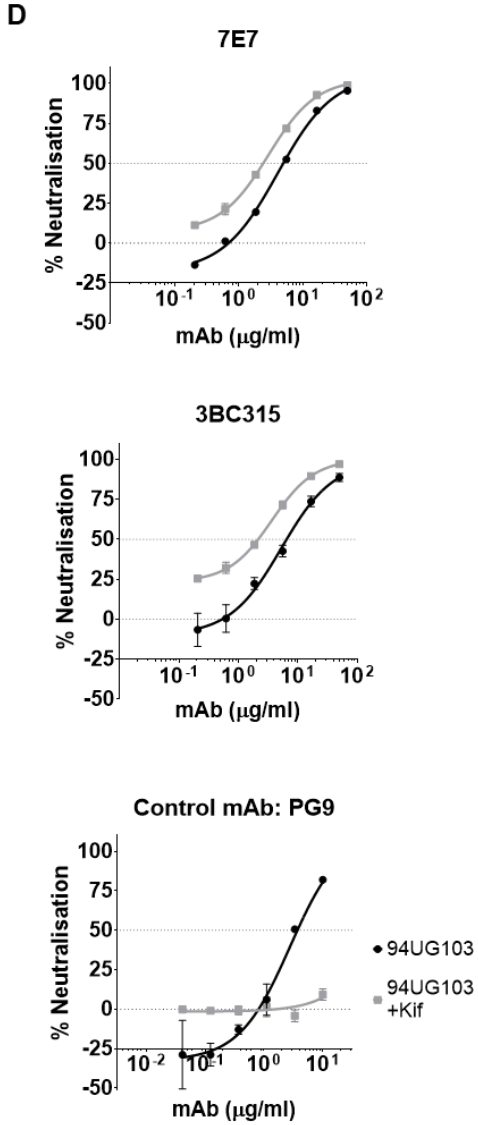

Figure legend on next page

Figure 5.13 Broadly neutralising antibody 7E7 targets the gp120-gp41 interface of HIV Env, with an epitope independent of the surrounding glycans.

(A) Competition of biotinylated 7E7 mAb (7E7-b) with previously characterised HIV mAbs specific for the CD4bs, high mannose patch, trimer apex or gp120-gp41 interface and a negative control (non-HIV) mAb CR3018. Competitive mAb binding to BG505 SOSIP was identified by a reduction from 100% binding of 7E7-b mAb to 50% binding or lower as highlighted by the gradient from white to blue. (B) Percentage binding of 7E7-b and 3BC315-b to the gp120-gp41 interface of BG505 SOSIP in reciprocal competition ELISAs, with the mean and error bars shown for mAbs tested in duplicate. A negative control (non-HIV) mAb CR3018 was included and a dotted line at 50% shows the threshold for competitive binding. (C-D) Neutralisation curves of mAbs titrated in duplicate against (C) JRCSF PV and a T90A mutated version, to remove the glycan site at position 88, and (D) 94UG103 PV produced in the presence and absence of kifunensine (kif), with the mean and error bars shown along with dotted lines to indicate 0% and 50% neutralisation.

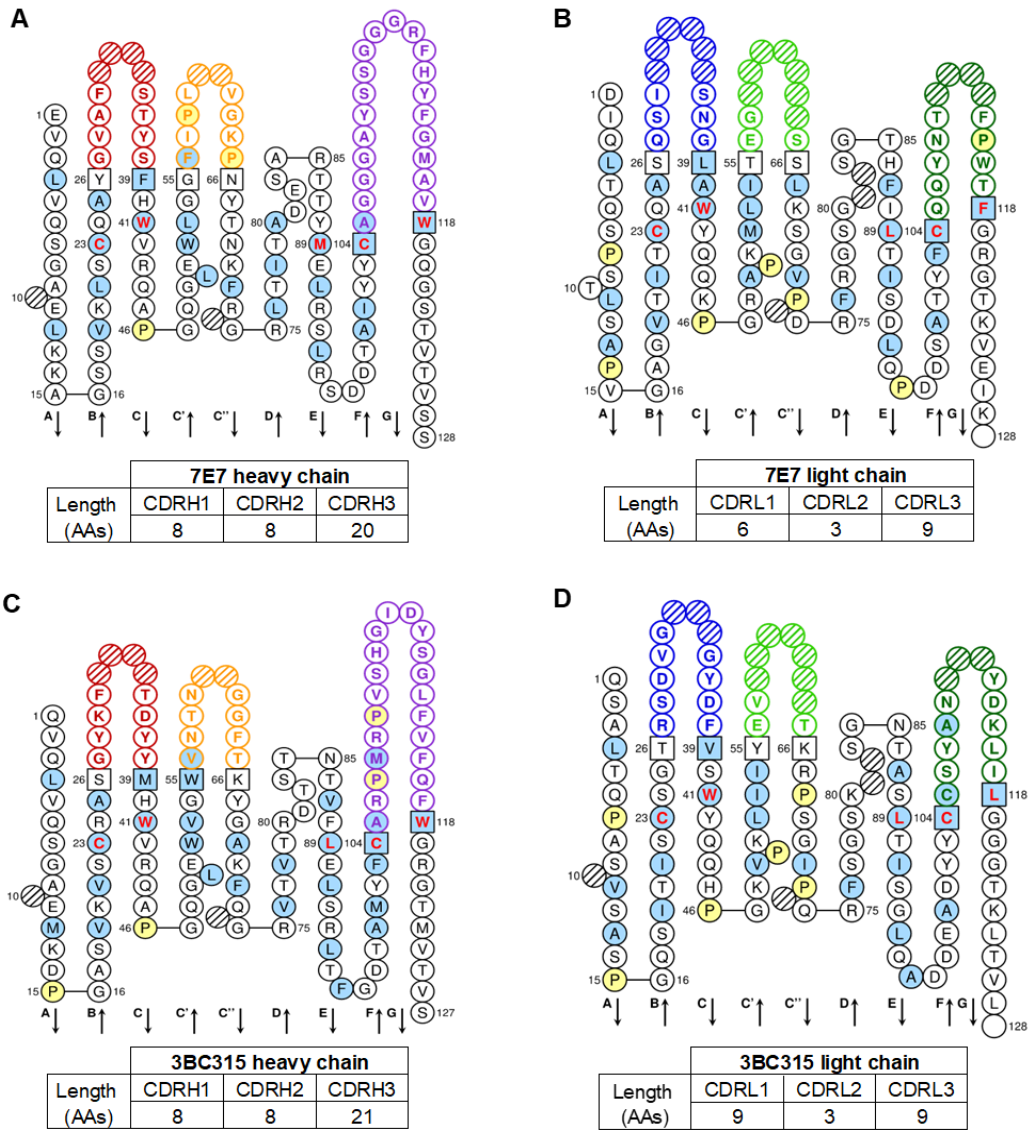

Figure 5.14 Graphical representation of antibody variable regions reveals similarity between the amino acid positioning in heavy chains of 7E7 and gp120-gp41 interface bnAb 3BC315.

(A-D) Amino acid (AA) sequence of Ig variable regions visualised using IMGT Collier de Perles (Brochet, Lefranc, and Giudicelli 2008) for (A) 7E7 heavy chain, (B) 7E7 light chain, (C) 3BC315 heavy chain and (D) 3BC315 light chain. (A, C) The CDRH1 (red), CDRH2 (orange) and CDRH3 (purple) lengths are specified based on the amino acid (AA) sequence. (B, D) The light chain CDR1 (blue), CDR2 (light green) and CDR3 (dark green) lengths are specified based on the AA sequence. Hydrophobic AAs (I, V, L, F, C, M and A) and all tryptophan (W) were highlighted (light blue) if present in more than 50% of analysed Ig sequences at that position, all prolines (yellow) and positions missing based on the IMGT numbering (hashed shapes) were also highlighted and the direction of beta sheets are indicated by arrows.

5.12 Neutralisation breadth exhibited by 7E7 was comparable to previously isolated gp120-gp41 interface specific bnAbs

To compare differences between 3BC315 and 7E7 in terms of their neutralisation, and put the breadth of 7E7 into the wider context of all bnAbs it was necessary to test the T125 bnAb 7E7 against a larger panel of PVs. The most commonly used standard panel to assess neutralisation breadth is the 118 multi-clade PV panel (Griffith and McCoy 2021), therefore PVs from this panel were used in neutralisation assays with 7E7. A total of 103 PVs from the 118 PV panel were successfully produced (plasmids for the remaining 15 PVs either could not be sourced or did not yield infectious PV). The percentage of viruses neutralised and potency of neutralisation within each clade are stated as the neutralisation breadth and the geomean IC_{50} respectively for 7E7 expressed as IgG1 and IgG3 (Figure 5.15a). This showed that 7E7 was capable of neutralising 9 out of 11 clades in the panel, with only clade D and clade CD PVs being completely resistant. The breadth of neutralisation against clade AE PVs was also low, with only 25% of viruses being susceptible to 7E7. Surprisingly, the greatest neutralisation breadth by 7E7 was not achieved against the clade of infection (clade C), but rather AC/ACD recombinants. Overall, the neutralisation by IgG1 and IgG3 versions of 7E7 was comparable, with 53% breadth and 56% breadth respectively. In addition, the potency of 7E7 as IgG1 and IgG3 was also comparable with an overall geomean IC_{50} of 2.93 µg/mL and 2.73 µg/mL respectively. Furthermore, these findings are consistent with the 50% breadth exhibited by 7E7 against both the standard 6 PV panel (Figure 5.6a) and the global 12 PV panel (Figure 5.7a). Neutralisation by T125 bnAb 7E7 was visualised using a dendrogram in Figure 5.15b to highlight the different clades targeted and the potency of PV neutralisation, which is represented by the length of each line.

Publicly available neutralisation data for previously characterised gp120-gp41 interface bnAbs was then extracted from the LANL database. First, the neutralisation profile of 7E7 was compared to 3BC315 by using the same set of PVs (n=21) that both bnAbs had been tested against. This revealed that, despite having an overlapping footprint on Env, 7E7 had slightly broader and

more potent neutralisation than 3BC315 (Figure 5.15c). The 3BC315 somatic variant 3BC176 was also included in this analysis and showed the same neutralisation breadth as 3BC315 but was more potent, with a geomean IC_{50} comparable to 7E7. Neutralisation by other gp120-gp41 bnAbs PGT151, 35O22 and 8ANC195 that have been tested against more PVs was also compared to 7E7 using the same set of PVs (n=103) from the 118 multi-clade PV panel (Figure 5.15c). The 53% neutralisation breadth exhibited by 7E7 was found to be in the range of 50-73% exhibited by other interface bnAbs yet these had a geomean IC_{50} of 0.03-1.54 µg/mL, which is more potent than 7E7 neutralisation (geomean IC_{50} of 2.93 µg/mL). This difference in potency likely reflects differences in the residues contacted in the gp120-gp41 interface, for instance, PGT151, 35O22 and 8ANC195 have neutralisation that requires interaction with glycans (Scharf et al. 2015; Huang et al. 2014; Falkowska et al. 2014) while 7E7 does not. Overall, these findings demonstrate that the elite neutraliser T125 was capable of producing bnAbs against HIV, with the isolation of the bnAb 7E7 that had at least 50% neutralisation breadth against over 100 PVs from the 118 multi-clade PV panel. Furthermore, the T125 bnAb 7E7 was found to target the gp120-gp41 interface, a known bnAb epitope on Env, and had comparable neutralisation breadth to previously characterised bnAbs against the gp120-gp41 interface.

A

Clade	# of viruses	7E7 bnAb Neutralisation Breadth IgG1	7E7 bnAb Neutralisation Breadth IgG3	7E7 bnAb Geomean IC_{50} (µg/mL) IgG1	7E7 bnAb Geomean IC_{50} (µg/mL) IgG3
AE	12	25%	25%	2.74	2.73
AG	9	44%	33%	2.62	1.25
A	7	71%	71%	2.24	2.16
B	21	52%	57%	3.49	3.53
C	27	59%	67%	2.07	2.50
D	2	0%	0%	>50	>50
G	6	67%	67%	2.99	2.95
AC	4	100%	100%	6.12	5.34
ACD	2	100%	100%	3.20	3.11
CD	5	0%	0%	>50	>50
BC	8	75%	88%	2.30	2.66
Total	**103**	**53%**	**56%**	**2.93**	**2.73**

B

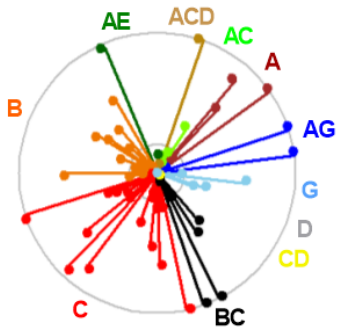

7E7 Breadth	7E7 IC_{50} (µg/mL)
53%	2.93

C

HIV bnAb	21 PVs tested 3BC315	21 PVs tested 3BC176	21 PVs tested 7E7	103 PVs tested PGT151	103 PVs tested 35O22	103 PVs tested 8ANC195	103 PVs tested 7E7
Neutralisation breadth	39%	39%	43%	73%	50%	66%	53%
Geomean IC_{50} (µg/mL)	6.31	2.14	2.11	0.03	0.30	1.54	2.93

Figure 5.15 Broad neutralisation was exhibited by 7E7 expressed as IgG1 or IgG3, and was similar to the breadth of previously isolated gp120-gp41 interface bnAbs.

(A) Percentage neutralisation of 103 PVs from the standard 118 multi-clade PV panel by the T125 bnAb 7E7, expressed as IgG1 and IgG3, with PVs grouped by clade and the geomean of IC_{50} titres reflecting the potency. An IC_{50} >50 indicates no neutralisation. (B) Dendrogram of the neutralisation breadth and potency achieved by T125 7E7 expressed as IgG1 against 103 PVs in the standard 118 multi-clade PV panel, with lines coloured according to the clade of PV neutralised. Longer lines indicate more potent neutralisation and reflect the IC_{50} titre achieved against each PV. (C) Published neutralisation data for HIV gp120-gp41 interface bnAbs 3BC315, 3BC176, PGT151 and 35O22 against the 118 multi-clade PV panel was extracted from LANL (Yoon et al. 2015) for comparison to T125 bnAb 7E7 neutralisation, using data for viruses in common. The potency of neutralisation is given as the geomean IC_{50} and the neutralisation breadth reflects the percentage of viruses neutralised from those tested.

Table 2 Summary of T125 HIV Env-specific antibodies and their functionality

					Standard 6 PV multi-clade panel		Standard Clade C PV panel		Autologous T125 Clade C PVs	
Epitope	**T125 mAb**	**V_H gene**	**V_H SHM (%)**	**CDRH3 length**	**Viruses neutralised**	**IC_{50} (µg/mL)**	**Viruses neutralised**	**IC_{50} (µg/mL)**	**Viruses neutralised**	**IC_{50} (µg/mL)**
CD4bs	**7B8**	1-18*01	9.80	18	1/6	1.38	1/12	5.25	1/3	2.57
	7B11	1-69	10.47	18	1/6	3.16	1/12	9.39	1/3	4.81
	7D3	3-21*01	14.58	18	1/6	2.15	0/12	>50	1/3	19.39
	8E3	3-11*03	5.90	15	1/6	3.12	1/12	41.41	1/3	21.5
	7D11	3-11*05	7.82	17	1/6	2.66	1/12	25.47	1/3	7.04
	7E5	5-51	4.67	16	1/6	3.56	0/12	>50	0/3	>50
V3 peptide	**7E3**	3-30 or 3-30-5	7.14	9	1/6	0.27	1/12	6.00	1/3	5.94
	7E8	3-30 or 3-30-5	7.14	9	1/6	0.22	1/12	6.92	1/3	15.34
	8C10	5-51*01	12.85	20	1/6	0.53	0/12	>50	1/3	39.79
	7A2	5-51*01	15.24	17	2/6	1.01	1/12	4.72	1/3	5.72
	7C2	5-51	10.59	16	2/6	2.88	1/12	5.20	1/3	12.5
	7F6	5-51*01	14.92	18	2/6	1.69	1/12	5.13	1/3	22.79
	7F10	5-51*01	14.58	18	2/6	0.99	1/12	5.74	1/3	30.09
Interface	**7E7**	1-69	18.40	20	3/6	3.42	8/12	2.53	0/3	>50
Non neutralising	**7A3**	1-69	10.14	18	0/6	>50	ND	ND	0/3	>50
	7E10	1-69*04	10.81	15	0/6	>50	ND	ND	0/3	>50
	7D10	3-23*04	15.97	15	0/6	>50	ND	ND	0/3	>50
	7B7	3-30	18.40	15	0/6	>50	ND	ND	0/3	>50
	7D4	3-30	19.10	15	0/6	>50	ND	ND	0/3	>50
	7C11	3-30*10	15.88	15	0/6	>50	ND	ND	0/3	>50
	8C7	3-74*01	2.03	13	0/6	>50	ND	ND	0/3	>50
	7F8	3-74*01	6.25	13	0/6	>50	ND	ND	0/3	>50
	7C6	4-31*03	8.42	15	0/6	>50	ND	ND	0/3	>50
	8C11	4-39*07	8.11	15	0/6	>50	ND	ND	0/3	>50

The percentage SHM in the heavy chain V-gene (V_H) was determined from nucleotide sequences and the CDRH3 length was determined from amino acid sequences. Neutralisation was determined by serial dilution of mAbs in the TZM-bl neutralisation assay, with a cut off of 50 µg/mL. The potency of neutralisation is given as the average geomean of IC_{50} values from n=2.

Summary

Recombinant trimeric HIV Env protein, BG505 and CRF250-4 SOSIP, were validated as antigen probes for detection of mAb binding by flow and subsequently used to isolate single HIV Env reactive B cells from the elite neutraliser T125. Single B cell cloning of the HIV Env+ IgG+ B cells successfully amplified Ig variable region pairs within the same range of efficiency as from the HIV-negative donor single IgG+ B cells in chapter 3. Cloning of Ig variable regions into vectors, followed by transfection of Ig heavy and light chain pairs resulted in the expression of 50 mAbs that were characterised further in terms of their functionality and sequence features. As summarised in Table 2, 24 mAbs demonstrated binding of trimeric Env (BG505 and/or CRF250-4 SOSIP) by ELISA and were subsequently tested for their neutralisation capacity, as well as the epitopes targeted. In total, 14 mAbs displayed neutralisation of heterologous and/or autologous PV by targeting three distinct epitopes on the HIV Env, with a V_H SHM in the range of 4.67-18.40% and a CDRH3 length of 9-20 AAs (Table 2). The sequence features of nine T125 nAbs were consistent with those of previously characterised HIV bnAbs, falling in the range of 9-43% V_H SHM and a CDRH3 of 10-37 AAs (Griffith and McCoy 2021), yet only one exhibited neutralisation breadth.

To epitope map the region on Env targeted by T125 mAbs, competition ELISAs were primarily used, however, a limitation is that this approach only provides insight into the footprint on Env using previously characterised mAbs, rather than the exact residues targeted. Instead, the use of mutated Env proteins, with AA changes in epitopes, can be more informative but is not a quick screening tool unless a specific residue is required for binding by the majority of mAbs, such as CD4bs mAbs dependency on D368. Of the T125 mAbs that demonstrated neutralisation, six were found to target the CD4bs with half having a dependency on D368, but neutralisation was restricted to a limited number of clade C viruses. Seven mAbs were found to bind the V3 loop and exhibited clade C specific neutralisation or cross-clade neutralisation against PVs in the standard 6 PV panel. Yet, only one mAb, 7E7 had a gp120-gp41 interface specificity and exhibited neutralisation of ≥50% breadth against

multi-clade and clade C specific panels of PVs, and thus was identified as a bnAb. Furthermore, bnAb 7E7 displayed neutralisation breadth within the same range as previously identified gp120-gp41 interface bnAbs. Although, in line with previous reports on minimal/no autologous neutralisation by bnAbs, 7E7 was only capable of weak autologous neutralisation when expressed as its original IgG3 but not as IgG1.

In conclusion, a variety of mAbs with different sequence features, functionality and epitopes were isolated from the single B cells of elite neutraliser T125, demonstrating the diversity of the humoral response. The identification of an HIV bnAb further validates the reasoning for selecting this individual to study the phenotype associated with bnAb development. Yet, unfortunately, none of the other nAbs were clonally related to the bnAb 7E7. As the original research aim was to investigate bnAb vs non-bnAb B cells within patient at the transcriptomic level, the isolation of only a single bnAb will limit this analysis in the next chapter. However, the characterisation of the T125 mAbs isolated here can still be linked back to their original B cells to give insight into the phenotype associated with functionality.

Chapter 6: Preservation of memory B cell homeostasis may facilitate the development of broadly neutralising antibodies against HIV

Background

The indirect effect of HIV infection on the B cell population results in altered frequencies of subsets circulating in the periphery. In particular, an increase in immature/transitional and terminally differentiated B cells, as well as activated memory (AM) and tissue-like memory (TLM) B cells are observed compared to HIV-negative individuals, at the expense of fewer naïve B cells and resting memory (RM) B cells (Moir et al. 2010). The downregulation of both CD27 and CD21 on the cell surface of class-switched B cells is used to characterise the TLM subset, which have increased expression of inhibitory receptors and receptors for migration to inflammatory sites yet downregulation of receptors for homing to lymph nodes (Moir et al. 2008). This phenotype suggests that the TLM subset does not participate in further germinal centre reactions, which may restrict the humoral response. An increase in this subset, also referred to as atypical cells, has also been observed in other chronic infections such as Hepatitis B (Burton et al. 2018) and malaria (Portugal et al. 2017). It is thought that ongoing viral infection leads to persistent antigen-driven activation and inflammation that contributes to the expansion of TLM / atypical B cells. Indeed, in HIV infection, the perturbation of the B cell population increases from early to chronic infection, yet is reduced following the initiation of ART which brings the viral load below the limit of detection (Moir et al. 2010). Given that the majority of bnAbs have been isolated from individuals infected with uncontrolled HIV for a minimum of two years it is logical to presume that this perturbation is also present in these individuals, although this is yet to be explored. While many factors have been associated with the development of neutralisation breadth (as discussed in section 1.5), none are predictive and there is limited data on the B cell phenotypes in bnAb donors. Moreover, the phenotype of the individual B cells that produce nAbs of varying breadth has not been investigated.

In the previous chapter, the characterisation of antibodies cloned from single HIV Env+ IgG+ B cells confirmed that elite neutraliser T125 was capable of producing bnAbs, with the identification of an interface bnAb that demonstrated 53% breadth against a multi-clade panel of over 100 PVs, similar to other bnAbs in this class. In addition, mAbs with limited or no neutralisation breadth were also identified from single T125 B cells. This final results chapter aimed to investigate the cell surface and transcriptomic phenotype of B cells from the bnAb donor, incorporating information on the mAb functionality to try and identify phenotypes associated with the development of bnAbs.

Results

6.1 Cell surface profiles of the viraemic bnAb donor T125 did not show expected perturbation of B cell subsets associated with HIV infection

Cell surface markers CD27 and CD21 can be used during flow cytometry to identify B cell phenotypes (as described in section 1.6.2). Inclusion of these markers during staining of bnAb donor T125 PBMCs for the isolation of HIV-specific B cells by FACS, as described in chapter 5, revealed that subsets within the total B cell, IgG+ B cell and HIV Env+ B cell populations were comparable between the first (Figure 6.1a) and second timepoint (Figure 6.1b). The inclusion of IgG in analyses was used to identify class-switched, bona fide memory. As mentioned earlier, untreated HIV infection distorts the memory B cell population, with a decrease in resting memory (RM; CD27+ CD21+) and a notable increase in tissue-like memory (TLM; CD27- CD21-) as well as activated memory (AM; CD27+ CD21-) (Moir et al. 2010), yet this was not observed in the PBMCs from T125, despite detectable viraemia. Instead, both the total IgG+ and HIV Env+ B cell populations in T125 were predominantly RM (CD27+ CD21+), whereas TLM (CD27- CD21-) was the most infrequent phenotype of both populations across the two timepoints. In particular, 84% and 94.6% of the HIV Env+ B cells had a RM phenotype at the first timepoint (Figure 6.1a) and second timepoint (Figure 6.1b) respectively, while <1% were identified as TLM in either timepoint. On the contrary, findings in a previous study showed that IgG+ Env+ (gp140) B cells from 42 HIV viraemic individuals were mostly AM (48.8%), with lower levels of RM (37%) and elevated TLM (11.6%) (Kardava et al. 2014).

As a result of these unexpected observations, the B cell subsets from two HIV-infected donors not on ART were assessed. The first was viraemic with a relatively high VL (110,000 c/mL) and the second was an elite controller, with a low VL just above the current detection threshold (100 c/mL). PBMC from these two donors and an HIV-negative donor were analysed by flow cytometry using the same cell surface markers to directly compare to the B cells from the

bnAb donor T125 (Figure 6.2). This revealed that consistent with the literature, in the total B cell population (CD19+) there was a higher percentage of AM (8.5%) and TLM (10.8%) in the viraemic donor than the HIV elite controller (3.9% AM, 2.8% TLM) and the HIV-negative donor (4.6% AM, 3.7% TLM) (Figure 6.2a). In the IgG+ B cell population, there was an even more striking increase in the percentage of TLM in the viraemic donor (22.4%) as compared to the elite controller (3.1%) or HIV-negative donor (4.9%) (Figure 6.2b). In addition, the percentage of IgG+ B cells with a RM phenotype was reduced in the viraemic donor (49.9%) compared to both the elite control donor (82.4%) and HIV-negative donor (74.6%) (Figure 6.2b).

Finally, a direct comparison of the subsets showed that T125 had a lower proportion of TLM compared to the HIV viraemic donor in both the total B cell population (shown in black, Figure 6.2c) and the IgG+ B cell population (Figure 6.2d). The total B cell population was considered here on the basis that memory can exist as isotypes other than IgG, for instance IgM, which can also be RM, AM or TLM. Although IgM was included in the staining panel, IgD was not, and thus it was not possible to identify IgM only B cells. Furthermore, analysis of the IgG+ B cell population indicated that the proportion of subsets in both timepoints from T125 was most similar to the elite controller with low VL and/or the HIV-negative donor, with higher RM and lower TLM than the HIV viraemic donor (Figure 6.2d). Taken together, these results imply that the bnAb donor T125 did not have the disturbances in the B cell population normally associated with HIV viraemia. These novel observations will be investigated further in this chapter by considering the transcriptomic phenotype of the bnAb donor memory B cells.

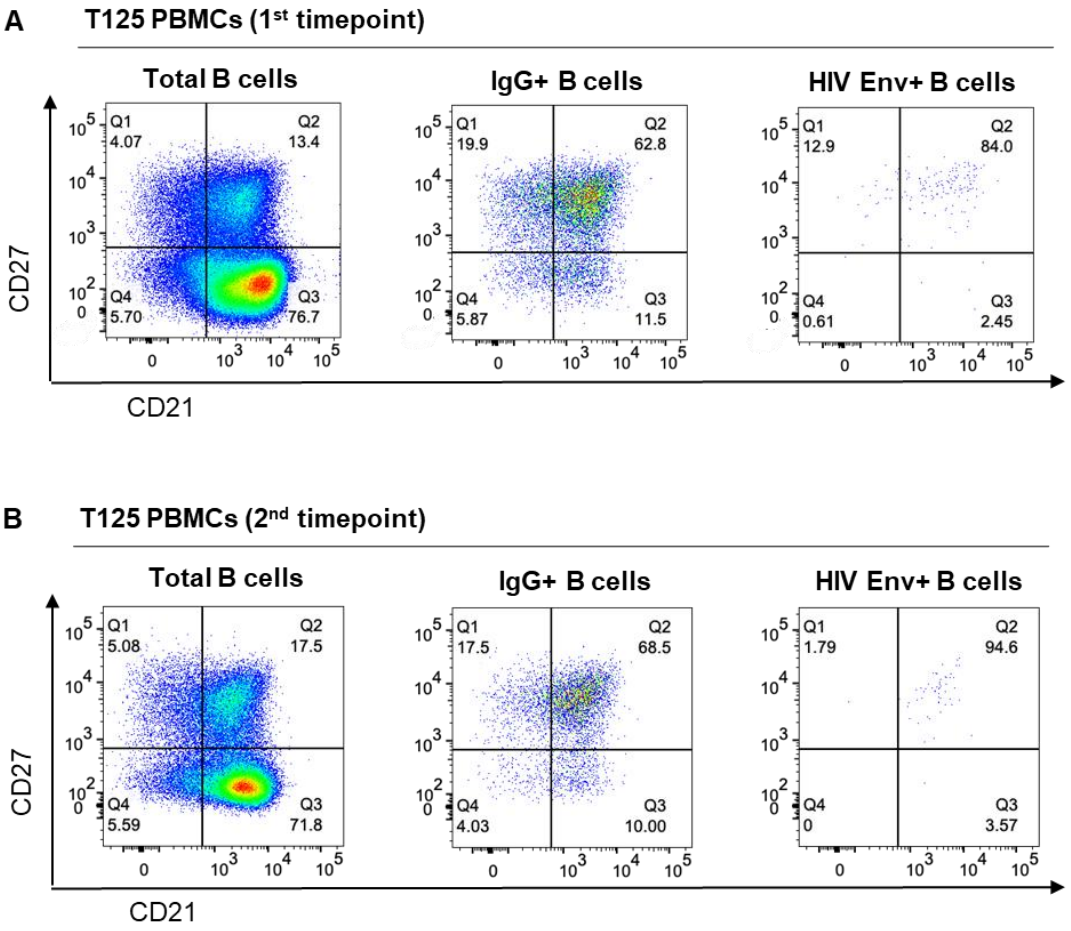

Figure 6.1 B cell subsets are comparable between two timepoints from the bnAb donor T125.

(A-B) FACS analysis of total B cells (CD19+ CD4-), IgG+ B cells (CD19+ IgG+ IgM-) and HIV Env+ (CD19+ IgG+ SOSIP+) B cells based on the surface expression of CD27 and CD21 from (A) 1st timepoint T125 PBMCs and (B) 2nd timepoint T125 PBMCs, sampled four months apart.

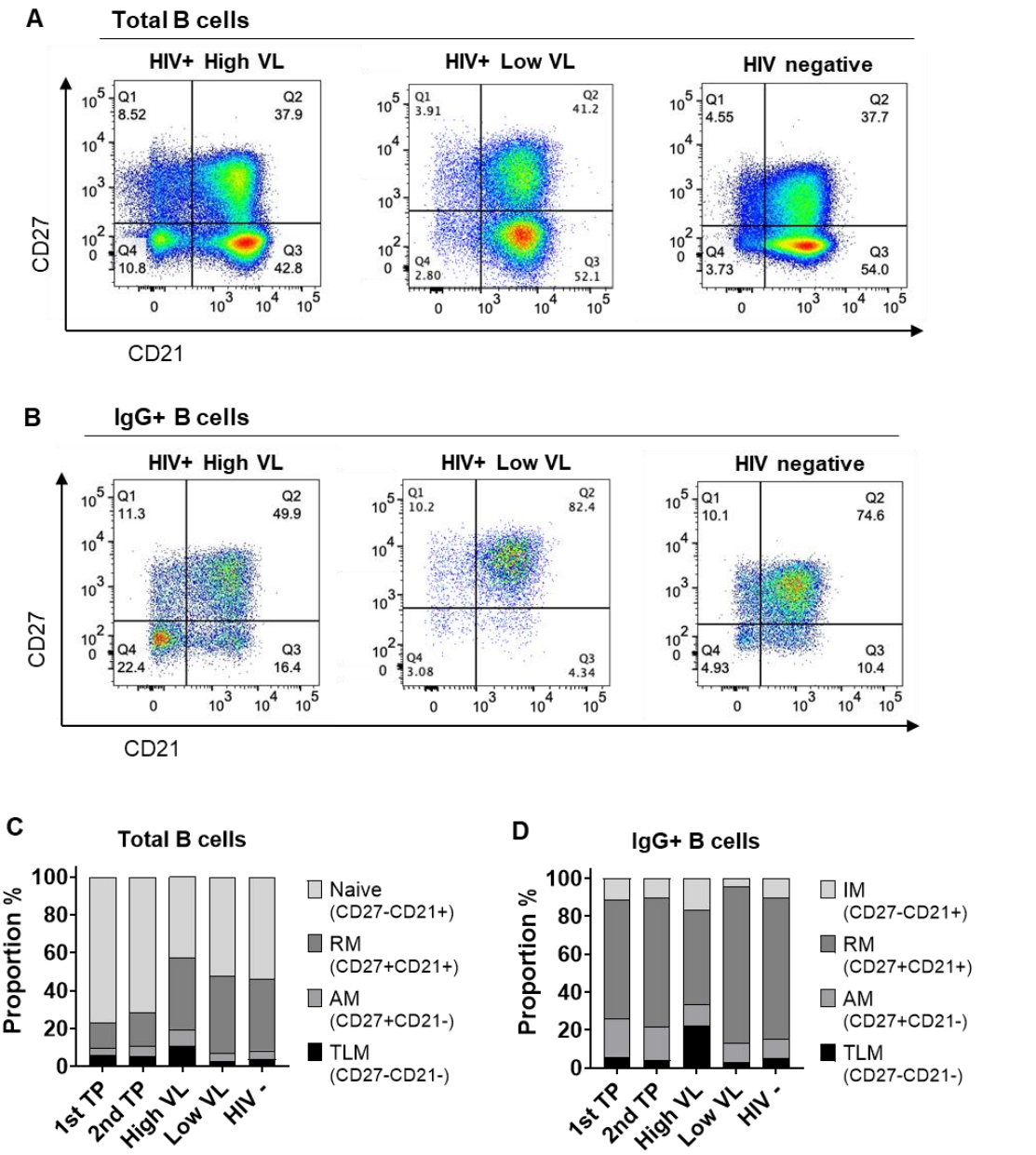

Figure 6.2 HIV-associated dysfunction is not seen in the B cell population of bnAb donor T125, based on cell surface markers.

(A-B) FACS analysis of B cell subsets based on the surface expression of CD27 and CD21 within the (A) total B cell population (CD19+ CD4-) and (B) IgG+ B cell population (CD19+ IgG+ IgM-) from an HIV-infected donor with high viral load (VL) of 110,000 c/mL, low viral load (VL) of 100 c/mL and an uninfected HIV-negative donor. (C-D) Percentage of naïve, intermediate memory (IM), resting memory (RM), activated memory (AM) and tissue-like memory (TLM) B cells observed in T125 PBMCs from the 1st and 2nd timepoint (TP) compared to the HIV-infected donor with high VL, low VL and an uninfected (HIV-) donor based on the CD27 and CD21 expression within the (C) total B cell population and (D) IgG+ B cell population.

6.2 Libraries generated for scRNA-seq from the majority of bnAb donor HIV-Env reactive memory B cells passed quality control checks

As discussed in chapter 5, single IgG+ HIV Env+ B cells were isolated from T125 and processed according to the Smart-Seq2 method to produce cDNA that was validated by electrophoresis using an Agilent tapestation, and then used for antibody cloning. Next, cDNA from the same single B cells (n=110) was processed further using the Smart-Seq2 method (as described in section 2.3.3) to generate libraries for scRNA-seq and transcriptional analysis. To begin with, the cDNA from single B cells was quantified by Qubit to calculate the volume required (for 1.5 ng) for tagmentation, to fragment the DNA into shorter sections for Illumina sequencing. Unique indices were then added to the fragmented DNA from each B cell by PCR. The resulting libraries were purified and the fragment size was assessed again by electrophoresis (using an Agilent Tapestation), which showed the required size of 300-800bp. Finally, libraries were quantified again by Qubit, for normalisation to 5 ng before pooling together for sequencing.

The scRNA-seq data generated from T125 B cells were first assessed, as in chapter 3, using quality control measures to ensure that libraries were suitable for downstream transcriptomics analysis. The library size of T125 B cells from both the first and second timepoint was initially assessed and had a median count depth of 1.3 million. Although this was lower than the 1.85 million count depth of the HIV-negative memory B cells in chapter 3, this was still in line with previous B cell libraries (~1-2 million count depth) generated using Smart-Seq2 (Croote et al. 2018). Analysis of outliers identified a minimum library count depth threshold of 348,862 (Figure 6.3a) and resulted in nine cells (one from the first timepoint and eight from the second timepoint) being excluded from further analyses. Next, the number of genes detected in libraries was considered and found that cells had a median of 1370 unique genes, which was higher than the genes detected (median of 893) in the HIV-negative donor memory B cells (chapter 3). Outlier analysis of libraries identified a threshold of 708 genes as the lower limit for inclusion in further analyses (Figure 6.3b) and found that nine of the ten cells that didn’t meet this criterion had already

been excluded based on library size. In addition, the proportion of mitochondrial genes in libraries can identify non-viable cells, as dying cells have broken membranes that result in the loss of cytoplasmic mRNA but not mitochondrial mRNA. An upper limit of 30% mitochondrial genes was determined from outlier analysis of the libraries and revealed that six cells from the first timepoint and three cells from the second timepoint exceeded this threshold (Figure 6.3c) and thus were discarded. However, considering all of the libraries together the viability was good, with a median of 12.7% mitochondrial genes.

Overall, the majority of libraries from single T125 B cells were of good quality, however, 16 cells (seven from the first timepoint and nine from the second timepoint) did not pass one of the three QC measures. Nevertheless, the libraries generated from 85% (94/110) of single B cells from the bnAb donor T125 were suitable for downstream analysis based on outlier analyses.

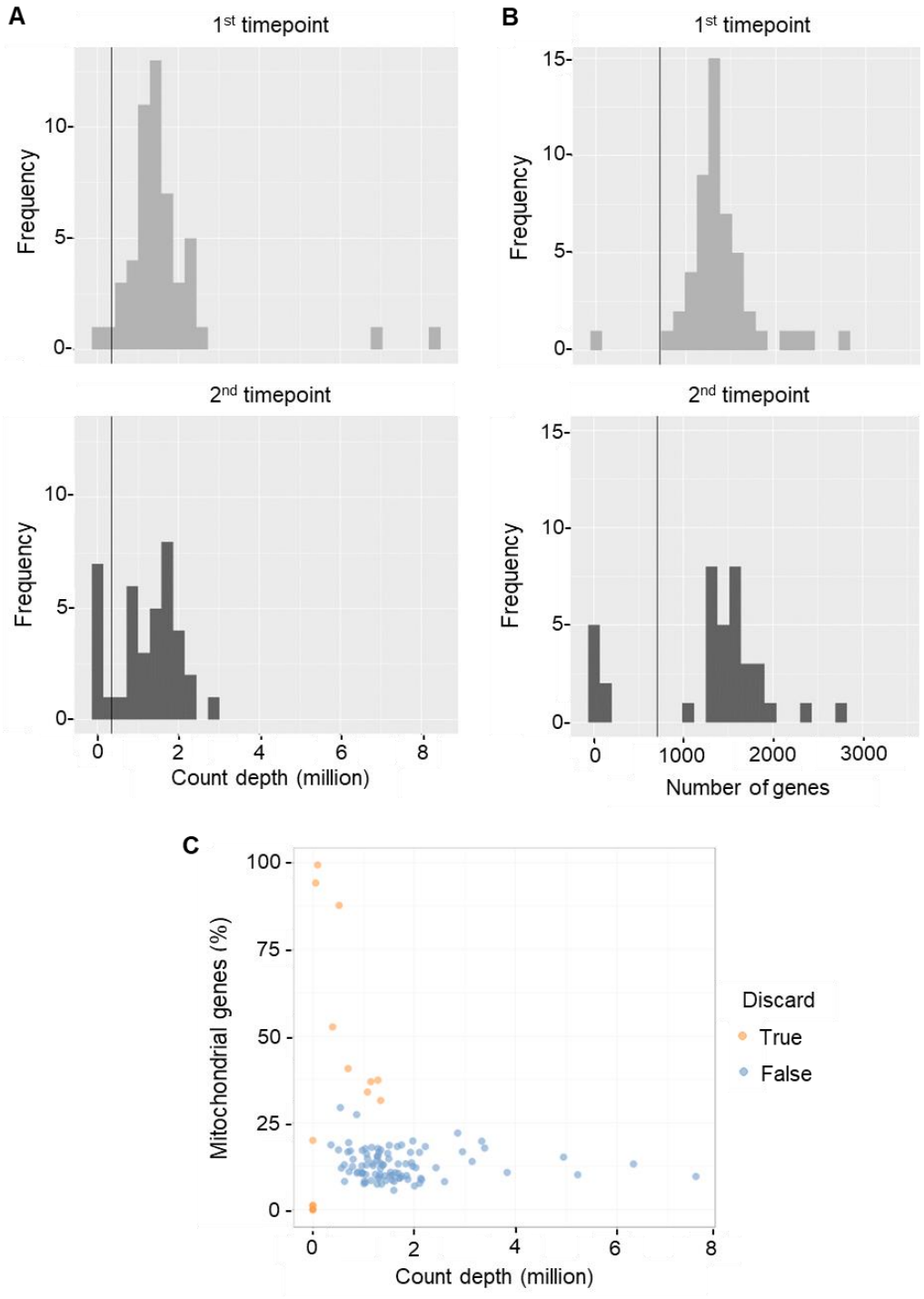

Figure 6.3 Quality control of single B cell libraries generated from bnAb donor T125.

(A) Library size based on count depth per cell, with a threshold of 348,862 indicated by the plotted line. (B) Number of genes detected per cell, with a threshold of 708 indicated by the plotted line. (C) Percentage of mitochondrial genes versus count depth, coloured according to if cells passed QC checks (blue) or not (orange), including an upper limit of 30% mitochondrial genes. Thresholds were determined from outlier analyses.

6.3 HIV-Env reactive B cells from the viraemic bnAb donor had a transcriptional phenotype most similar to resting memory B cells

As shown earlier, the cell surface phenotype of single memory B cells from the bnAb donor T125, in particular the HIV-Env reactive IgG+ B cells, were predominantly RM (CD27+ CD21+) by flow cytometry (Figure 6.1). However, without index sorting (which was not feasible on the BD Melody sorter), it was impossible to identify which specific B cells related to those seen in each quadrant for CD27 and CD21 expression. It was therefore of interest to explore whether a resting phenotype was also observed at the transcriptome level and if this related to the functionality of the encoded antibody. To achieve this, additional scRNA-seq datasets were needed to put the bnAb donor T125 B cells into context. Fortunately, a Smart-Seq2 dataset was generated contemporaneously by Dr Luke Muir in our lab and consisted of 253 single memory B cells (CD19+ IgG+) isolated based on differential expression of CD27 and CD21 from an HIV-infected donor with long-term elite control of their virus (VL of 100 c/mL at the timepoint sampled). Consequently, this provided pre-defined RM (CD27+ CD21+), AM (CD27+ CD21-) and TLM (CD27- CD21-) B cell transcriptomes for inclusion in analyses.

Memory subsets from the HIV elite controller were first visualised by UMAP and annotated according to the flow cytometry phenotype which revealed that TLM B cells clustered away from the RM and AM B cells (Figure 6.4a), similar to the HIV-negative memory B cell data in chapter 3. This indicates that TLM B cells have a distinct transcriptome, while RM and AM B cells have more transcriptional overlap in the genes expressed. Next, the single B cells in these memory subsets were used in Glmnet analysis to predict the maximum likelihood for each bnAb donor B cell from T125 for each of the three phenotypes. The probability of each single T125 B cell being RM, AM or TLM is shown in Figure 6.4b and indicated that the majority were most like RM, with some showing similarity to AM and very few having a high probability of a TLM phenotype. The specificity and functionality of the T125 B cells were then considered, based on the behaviour of the BCR expressed as soluble mAb (assessed in chapter 5). This revealed that, regardless of the ability to bind

Env or not, the phenotype of T125 bnAb donor B cells was most similar to RM, and unlike AM or TLM (Figure 6.4c). Analysis of T125 B cells based on their neutralisation capacity also showed that the phenotype was closest to RM, although non-nAb B cells had the highest probability of a RM phenotype, followed by cross-clade nAb B cells and then clade-specific B cells which also showed a low probability (<0.5) of having an AM phenotype (Figure 6.4d). Investigation of B cells based on the epitope targeted on HIV Env was considered next. Interestingly, the one B cell with a BCR that targeted the Env interface was the T125 bnAb 7E7 and this B cell was found to have the highest probability of being RM (Figure 6.4e). The B cells with BCRs targeting CD4bs and non-nAb epitopes also had a phenotype most similar to RM, yet those targeting the V3 had a similar probability for RM and AM (Figure 6.4e).

Finally, the T125 B cells were assessed based on their BCR isotype and found that all IgG subtypes were most like RM, except a single B cell whose isotype was unable to be determined (either IgG1 or IgG2) which had a high probability for a TLM phenotype. In summary, single B cells from the T125 bnAb donor had a transcriptional phenotype comparable to RM B cells from an HIV-infected donor who had minimal/no viraemia over 19 years of infection (sampled here at year 15), and consequently had very little of the B cell dysfunction associated with uncontrolled HIV (Figure 6.2). In addition, B cells where the specificity and functionality of their BCR was characterised were also most similar to RM B cells, although the probability of a RM phenotype was lower for B cells with clade-specific neutralisation or V3 specificity which had some overlap with an AM phenotype.

The differentially expressed genes (DEG) in the transcriptome of single B cells from bnAb donor T125 as compared to the RM, AM and TLM B cells of the HIV elite controller were then investigated to assess how they differed. This first required integration of the bnAb donor B cells with the memory B cell dataset from the elite controller. Visualisation by PCA showed that the bnAb donor B cells clustered predominantly with RM B cells, with some overlap with AM B cells, but not TLM B cells as expected (Figure 6.5a). In line with this, bnAb donor B cells had the fewest significant DEGs when compared to RM B cells (Figure 6.5b), with a similar number of significant DEGs when compared

to AM B cells (Figure 6.5c) yet had the highest number of significant DEGs when compared to TLM B cells (Figure 6.5d).

In particular, genes previously associated with a TLM phenotype in HIV or an atypical phenotype in malaria (FCRL5, ITGAX, EZR, LITAF, NR4A2, ENC1, RGS2, CEMIP2 and ZNF331) (Holla et al. 2021; Sutton et al. 2021; Moir et al. 2008; Kardava et al. 2014) were among those that had significantly higher expression in the TLM B cells compared to the bnAb donor B cells (Figure 6.5d). Increased expression of B cell surface markers CD19 and CD20 (MS4A1) has also been previously observed in TLM / atypical B cells (Holla et al. 2021; Andrews et al. 2019), and although CD19 had higher expression in TLM compared to the bnAb donor cells, CD20 did not (Figure 6.5d). The transcription factor T-bet (TBX21) is often also highly expressed in TLM and atypical B cells (Knox et al. 2017; Obeng-Adjei et al. 2017), however, this gene was not detected in many of the cells from either dataset and thus was not identified as a DEG. Similarly, the differential expression of T-bet was not identified in another Smart-Seq2 dataset, despite the detection of many other genes associated with an atypical phenotype, yet was in a larger 10x dataset (Sutton et al. 2021). Finally, the cell surface 'memory' marker CD27 was significantly higher in bnAb donor B cells compared to TLM B cells (Figure 6.5d), consistent with a lack of CD27 on TLM B cells observed by flow cytometry.

While T125 bnAb donor cells were most similar to RM B cells, this subset had higher expression of LTB, CXCR4 and DUSP1 than the T125 B cells (Figure 6.5b). These genes are involved in the organisation of secondary lymphoid organs (Tumanov et al. 2002), recruitment to the GC dark zone (Allen et al. 2004) and negatively regulating proliferation respectively. Moreover, in both the RM and AM B cells, there was higher expression than in T125 cells of the following genes: JUN which is an oncogene, ZFP36 which inhibits cytokine expression (Makita, Takatori, and Nakajima 2021), KLF6 which inhibits cell proliferation (Slavin et al. 2004) and TXNIP which can suppress BCL-6 in the GC (Shao et al. 2010) (Figure 6.5b,c). On the other hand, expression of MALAT1 (also known as NEAT2) and IFITM3 were significantly higher in the bnAb donor cells compared to RM and AM B cells (Figure 6.5b,c). While it is

known that MALAT1 is a long non-coding RNA its role in B cells has not been previously studied, however, IFITM3 has recently been discovered to be induced by BCR engagement of antigen to amplify PI3K signalling (Lee et al. 2020). Consideration of other genes associated with BCR signalling revealed that despite the differences listed, T125 bnAb donor cells were most like RM B cells, with the differential expression of CD79A, Syk and Lyn below the threshold of significance (Figure 6.5b), while AM and TLM both had higher expression of CD79A and Syk (Figure 6.5c,d) than the T125 B cells. In contrast, the expression of a single gene, TWIST2, was significantly higher in the bnAb donor B cells compared to all three memory B cell subsets (Figure 6.5b-d) and encodes a transcription factor to regulate inflammatory cytokines and induce anti-apoptotic genes (Merindol et al. 2014). Curiously, TWIST2 expression was only just above the significance threshold yet had the largest fold-change, which may be explained by the detection of this gene in cells only from the second T125 timepoint.

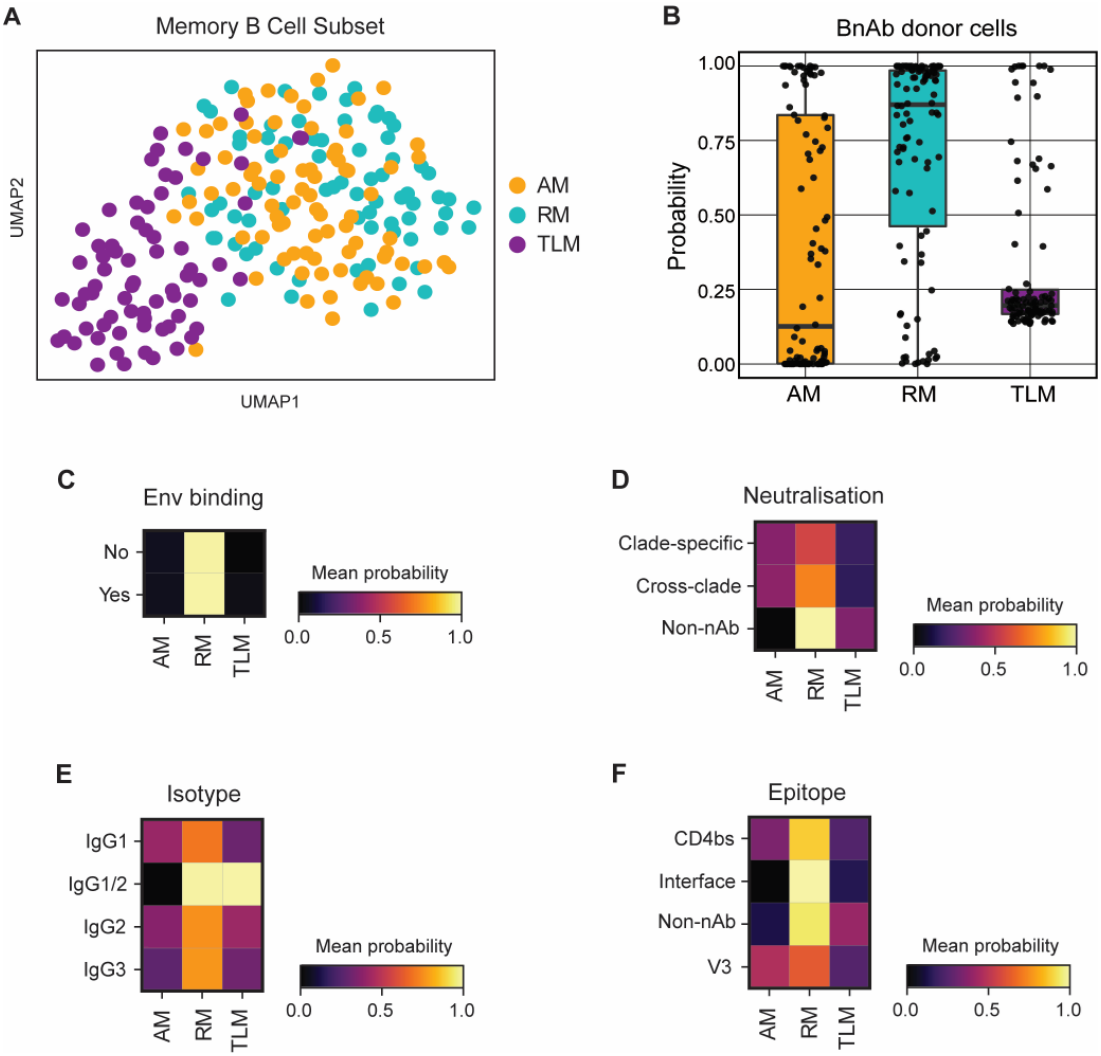

Figure 6.4 B cells from bnAb donor T125 have a transcriptional phenotype most similar to resting memory, irrespective of their BCR specificity or functionality.

(A) UMAP visualisation (after QC) of single-cell transcriptomes (Smart-Seq2) of 223 memory B cells from an HIV-infected donor with low VL. Coloured by their original FACS sorting strategy as resting memory (RM; cyan), activated memory (AM; orange) and tissue-like memory (TLM; purple). (B) Similarity of single B cell transcriptomes (from the bnAb donor) with RM, AM and TLM B cell subsets from the low VL donor, calculated as a probability using the Glmnet algorithm. (C-F) Heatmaps showing the mean probability (as calculated in B) of bnAb donor B cells for memory subsets based on BCR (C) binding of Env, (D) neutralisation of clade C specific or cross-clade HIV PVs or no neutralisation (non-nAb), (E) epitope targeted on Env and (F) IgG isotype. BCR specificity and functionality were characterised based on the behaviour of soluble mAb cloned and expressed from single T125 B cells.

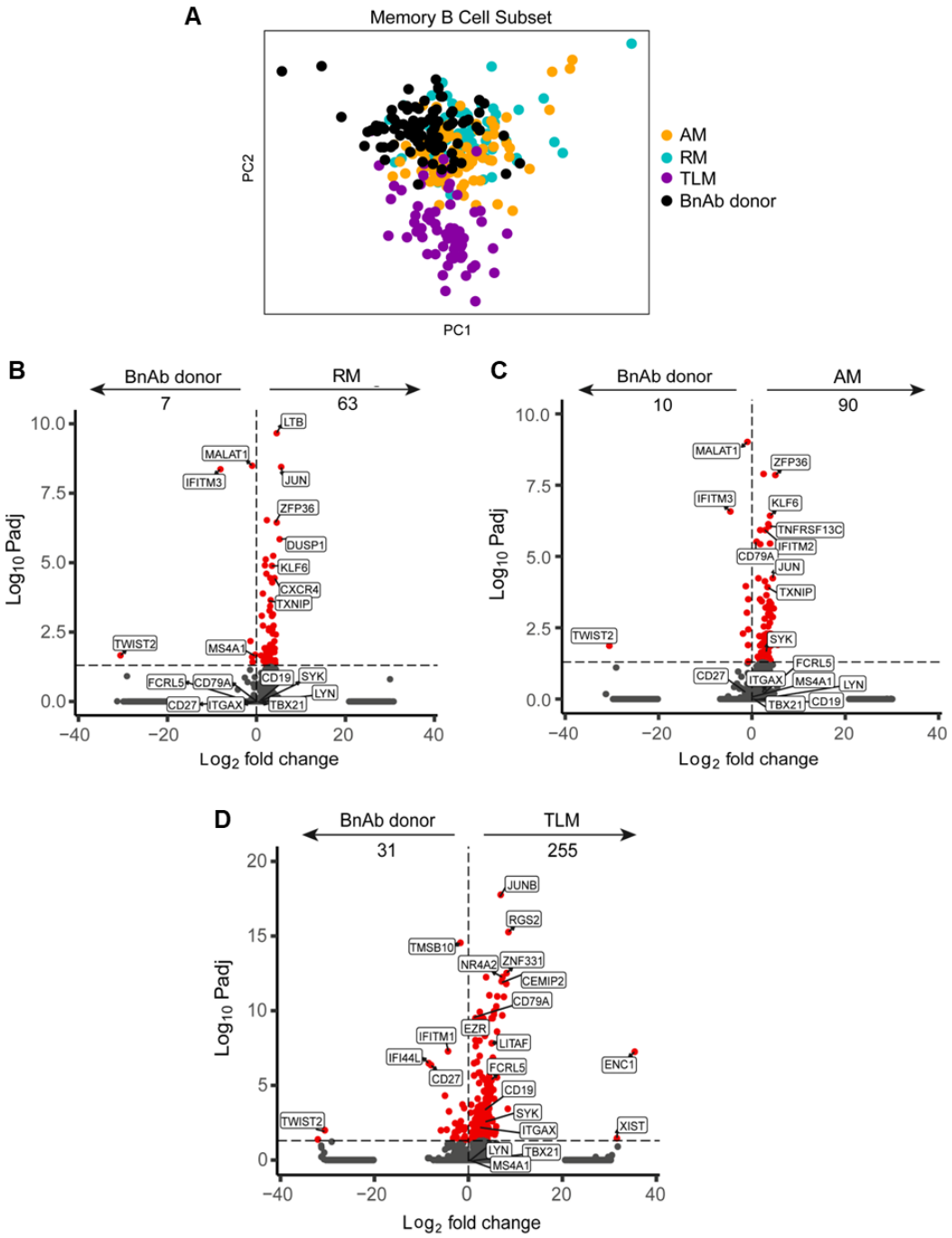

Figure 6.5 Differential gene expression revealed that single B cells from bnAb donor T125 are most distinct from TLM B cells.

(A) PCA visualisation of bnAb donor cells (black) after integration with resting memory (RM; cyan), activated memory (AM; orange) and tissue-like memory (TLM; purple) B cells from an HIV-infected donor with low VL. (B-D) Volcano plots of DEG between bnAb donor cells and (B) RM (C) AM and (D) TLM B cells. The adjusted p-value threshold for significant DEG is indicated by the horizontal dotted line, with significant DEGs highlighted in red and their total number stated underneath each arrow. The top DEGs, as well as genes of interest, are annotated.

6.4 Transcriptomic profiles of HIV-Env reactive B cells from a viraemic bnAb donor showed minimal HIV-associated dysfunction

On the basis that the HIV-Env reactive, memory B cells from the bnAb donor T125 had a cell surface and transcriptome similar to a resting phenotype, which is normally distorted in the presence of viraemia, it seems there was minimal HIV-associated dysfunction within the T125 B cell population despite a viral load of 73,700 c/mL. To address this fully and consider what impact uncontrolled HIV normally has on B cells, single B cells from healthy control donors and HIV-infected donors with viraemia or on suppressive ART were assessed. A previously published scRNA-seq 10x study was identified that had sequenced PBMCs from chronically infected HIV viraemic donors (PID529 and PID717), as well as those on ART which were suppressed to <20 c/mL (PID630 and PID876) (Wang et al. 2020). In addition, this study also included analysis of PBMCs from healthy donors, although only one (HD1) was sequenced by the group and included in the dataset available online. Therefore, to increase the number of healthy donors included in analyses, PBMC data from another scRNA-seq 10x study were included, specifically, 11 healthy donors recruited in Cambridge (CV0902, 04, 11, 15, 17, 26, 29, 34, 39, 40 and 44) (Stephenson et al. 2021).

To begin with, the transcriptomes of B cells from the different donors were extracted from each dataset and integrated, as shown by the UMAP in Figure 6.6a. These cells were then annotated according to the donor group which revealed that B cells from control donors largely formed a separate cluster that only partially overlapped with HIV-suppressed donors and had the least overlap with HIV viraemic donors (Figure 6.6b). Next, the B cells were analysed using Cell Typist to predict the identity of a given cell by employing an existing model based on a pre-defined dataset of different immune cells (as described in section 2.11.2). Classification of the B cells based on the greatest probability for a cell type identified three main subsets: naïve, memory and age-associated B cells which were visualised again by UMAP for comparison (Figure 6.6c). The position of B cells in the naïve subset showed that these were largely from control donors, in contrast, the age-associated subset was

mainly from the viraemic donors, while the memory subset was comprised of B cells from all donor groups (Figure 6.6b,c). In addition, when the T125 bnAb donor cells were classified by Cell Typist they were designated as memory B cells, not naïve or age-associated, as expected given they were sorted as memory (IgG+) cells (Figure 6.6d). The top DEGs from each subset are shown in Figure 6.6e and revealed that the memory subset was characterised by higher expression of genes such as CD27, the classical memory marker, and TNFRSF13B (also known as TACI), which is one of the receptors for the B cell survival factor BAFF. Conversely, the age-associated subset had DEGs related to an atypical phenotype, including RGS2 and SAT1 (Sutton et al. 2021), while the naïve subset had DEGs including TCL1A, FCER2 and IL4R consistent with previously characterised naïve B cells (Stewart et al. 2021).

Successful identification of the memory subset across all donors made it possible to compare differences between these B cells from each donor group with the memory B cells isolated from the bnAb donor T125. As shown in Figure 6.7a, the transcriptome of memory B cells from HIV-suppressed and viraemic individuals was distinct from the majority of memory B cells from healthy control donors. Specifically, memory B cells from viraemic individuals showed DEGs associated with interferon stimulation, IFI44L and ISG15, as well as XAF1, associated with apoptosis (Jeong et al. 2018) (Figure 6.7b). In contrast, DEGs in memory B cells from healthy control donors had higher expression of genes such as CD79A, which is involved in BCR signalling (Figure 6.7b). Further analysis was carried out to investigate genes associated with specific phenotypes. This showed that memory B cells from control donors had higher expression of the memory marker CD27 than the HIV suppressed or viraemic donors (Figure 6.7c), consistent with HIV-negative individuals having a higher proportion of resting (CD27+) memory B cells. Similarly, there was high expression of SELL in control memory B cells, which facilitates entry into secondary lymph nodes (Venturi et al. 2003) and BACH2, which is required for GC regulation (Hu et al. 2022) (Figure 6.7c). Moreover, expression of the chemokine receptor CCR7, which is linked to GC retention (Reif et al. 2002), was detected in memory B cells from control and suppressed individuals, but not memory B cells from viraemic donors (Figure 6.7c). This is

logical given the higher levels of TLM in viraemic individuals and that TLM cells have low CCR7 expression (Moir et al. 2008; Kardava et al. 2014).

Activation markers associated with HIV viraemia, FAS and CD86 (Moir et al. 2004; Nicholas et al. 2013), were also expressed in a small fraction of the memory B cells from viraemic donors, but not in those from suppressed or control donors (Figure 6.7c). As a result of these differences in gene expression, in particular the signs of dysfunction in the HIV viraemic donors, it was of interest to determine which transcriptomic profile was the closest match to the bnAb donor B cells. To do this, Cell Typist was trained using the memory B cell transcriptomes from the viraemic, suppressed and control donors. This revealed that the Env-reactive memory B cells isolated from the bnAb donor T125 were most similar to memory B cells from healthy control donors, and unlike the HIV suppressed or viraemic donors (Figure 6.7d). In conclusion, this finding confirmed the lack of HIV-associated dysfunction in the bnAb donor B cells, consistent with the predominantly resting memory phenotype observed at the cell surface level and at the transcriptomic level when compared to distinct memory B cell subsets.

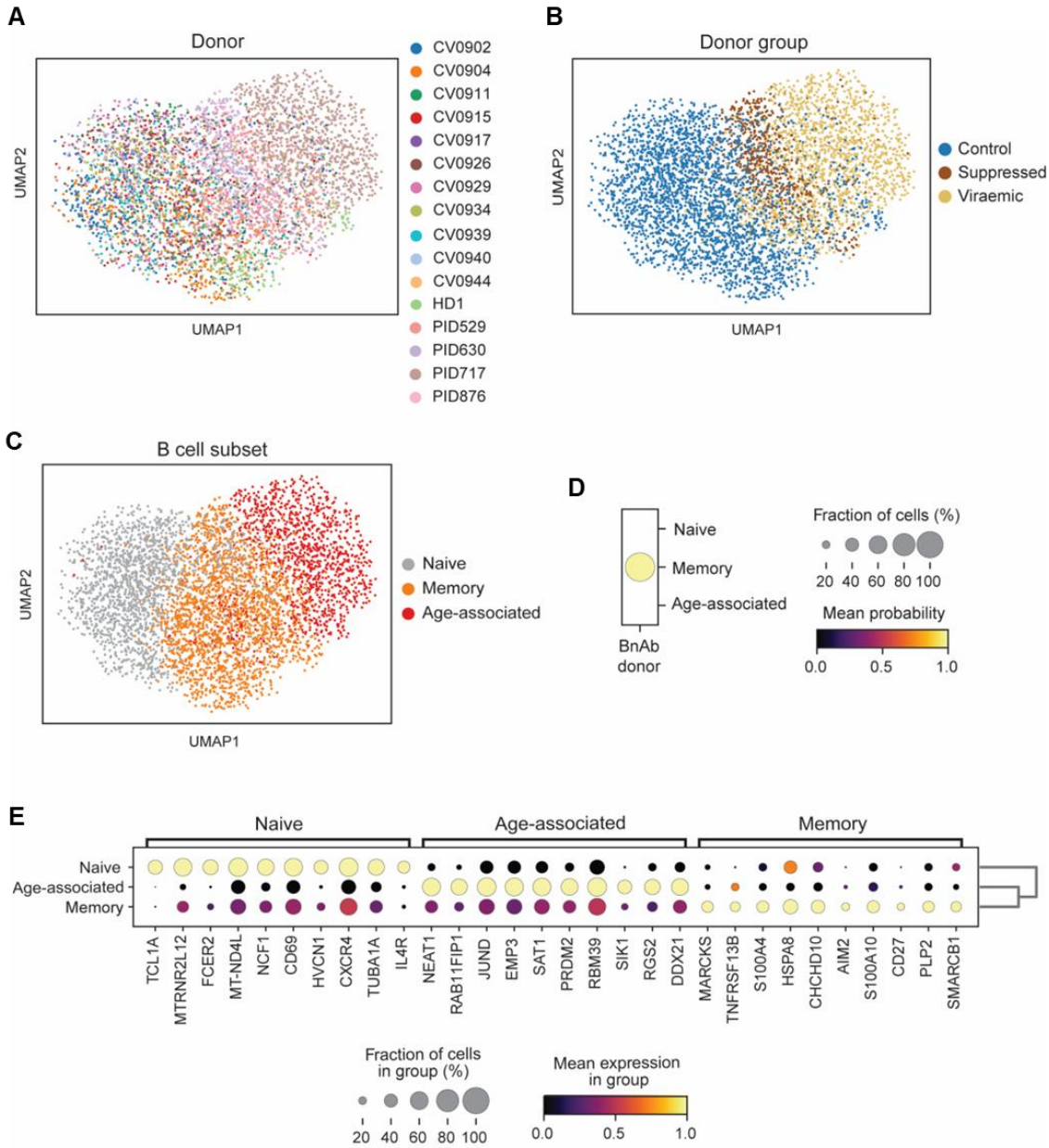

Figure 6.6 B cells from HIV-infected donors are transcriptionally distinct from healthy control donors.

(A-C) UMAP visualisation of B cells from two integrated publicly available scRNA-seq (10x) datasets taken from 11 healthy donors (Stephenson et al. 2021) and 2 HIV viraemic donors, 2 HIV suppressed donors and 1 healthy donor (Wang et al. 2020). Coloured by (A) donor ID, (B) donor group or (C) Celltypist annotation. (D) Dot plot showing Celltypist based mean probability of bnAb donor B cells belonging to naïve, memory or age-associated B cell subsets. (E) Expression of the top 10 DEGs for each B cell subset annotated by Celltypist in C. The dot size indicates the fraction of cells expressing each particular gene, the dot colour indicates mean gene expression.

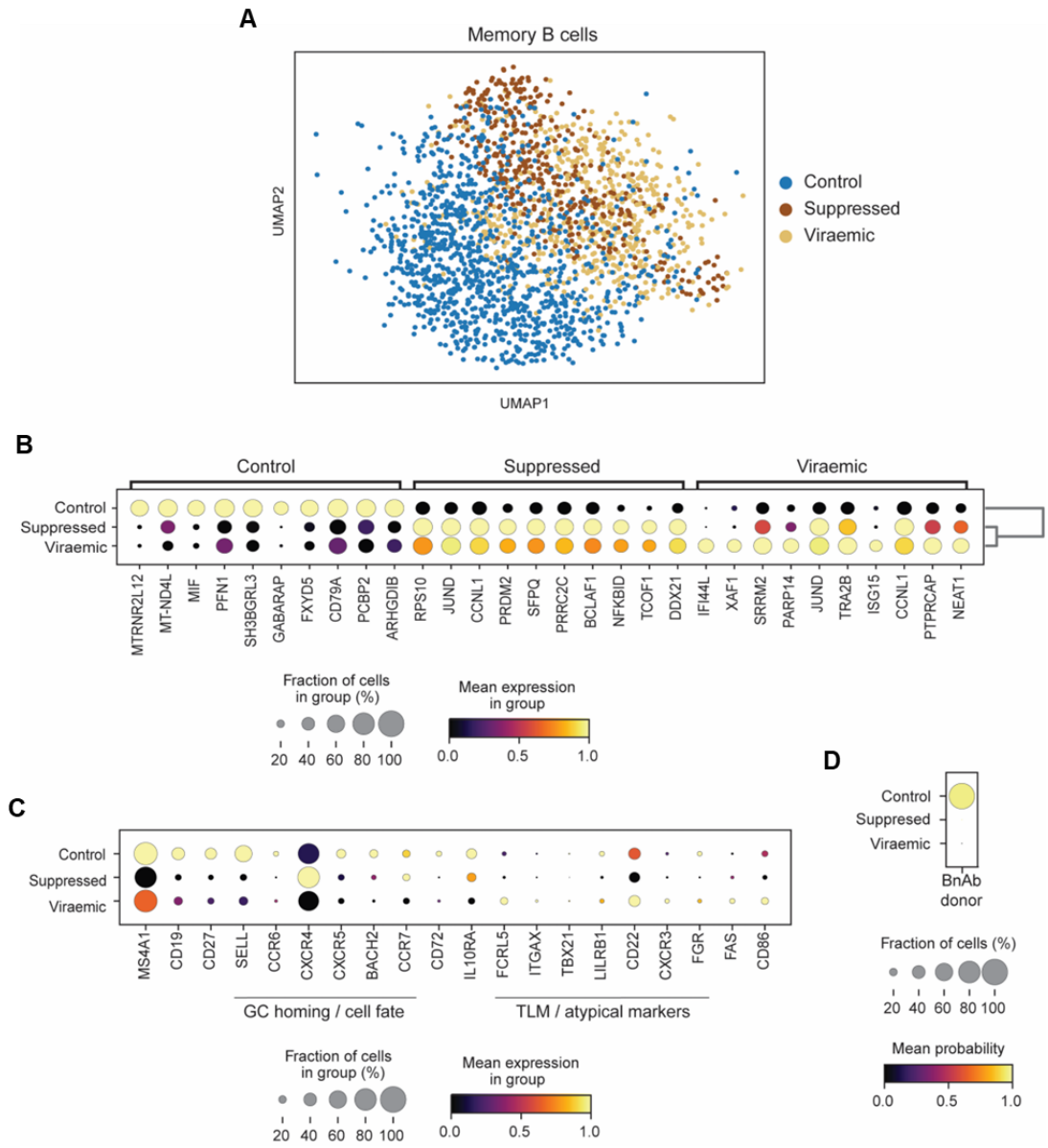

Figure 6.7 Transcriptomic profiles of single memory B cells from the viraemic bnAb donor T125 mirror memory B cells from healthy control donors but not from other HIV-infected donors.

(A) UMAP visualisation of memory B cell transcriptomes extracted from the B cell datasets analysed in Figure 6.6A, coloured by their donor group. (B) Expression of top 10 DEGs for each donor group. (C) Expression of selected genes (associated with B cell phenotypes) in each donor group. The fraction of cells is shown by the dot size and the mean gene expression is reflected by the colour. (D) Dot plot showing Celltypist probability of bnAb donor B cells being similar to memory B cells from control, suppressed or viraemic donors.

6.5 Suppression of IFN responses normally found in vireamia may have facilitated the preservation of memory B cell homeostasis

Ongoing HIV infection leads to chronic immune activation and inflammation (as discussed in section 1.6), resulting in the upregulation of ISGs in B cells (Moir et al. 2004; Wang et al. 2020). Guided by the observation that the bnAb donor B cells did not show signs of viraemia-associated dysfunction and instead had transcriptomes most similar to healthy control donors, it was postulated that the IFN response and thus the level of ISGs within the B cells may also be reduced.

The expression of hallmarks associated with an IFN-α response and IFN-γ response (Liberzon et al. 2015) was initially assessed within the memory subsets across the different donor groups. This showed that the mean expression of genes in response to both IFN-α and IFN-γ was highest in the memory B cells from viraemic donors, as expected (Figure 6.8a). Gene set enrichment analysis (GSEA) was then used to compare the memory B cells from HIV suppressed and viraemic donors to the healthy control donors. The normalised enrichment score (NES) for hallmark IFN-α and IFN-γ responses was significantly higher in viraemic donor memory B cells (Figure 6.8b). However, for the suppressed donors, the NES for the memory B cell IFN-α response was found to be significantly lower than the control donors, yet the IFN-γ response was not significantly different (Figure 6.8b). The expression of 27 unique leading-edge genes from the hallmark IFN-α and IFN-γ GSEA were then explored across the different donor groups (Figure 6.8c). Overall, the level of ISG expression in memory B cells from the control donors was lower than the viraemic donors (Figure 6.8c). Most striking was the low expression of IFI44L in the B cells from both the control and suppressed donors, yet this gene was strongly expressed in most B cells from viraemic donors. In addition, the expression levels of other ISGs including PARP14, ISG15 and EIF2AK2 were reduced in most B cells from the control and suppressed donors compared to the viraemic donor (Figure 6.8c). While it would have also been interesting to see how the bnAb donor B cells vary in terms of ISG expression

as compared to these controls, the integration of data to allow this was not of sufficient quality to enable robust conclusions to be drawn.

However, markers of systemic inflammation and infection can also be detected in patient plasma/serum. Specifically, the presence of cytokines mediating an anti-viral response can be quantified using bead-based methods such as LegendPLEX (as described in section 2.12.1). Therefore, this technique was employed to analyse the levels of 13 different cytokines, including type I, type II and type III IFNs in the plasma of the bnAb donor T125 as well as other HIV-infected and uninfected patients, although very few of the cytokines were detected at levels higher than the cut-off (Figure 6.9). Plasma/serum from viraemic patients in the East London cohort evaluated in chapter 4 were also included to identify if there was an association between the cytokine profiles and HIV neutralisation breadth, yet no obvious trend was observed. While the presence of IP-10, IFN-γ, IFN-α2, IL-8 and IL-10 was detected in the plasma of bnAb donor T125, these same cytokines at similar concentrations were also present in patients with a lower neutralisation score (Figure 6.9). In addition, plasma from the two HIV-infected donors with known VL analysed earlier for differences in the B cell subsets (Figure 6.2) were included. The low VL donor was an elite controller, without perturbations to the B cell subsets, and had quantifiable levels of IP-10, TNF-α, IL-8, IL-10 and IL-12p70, although the concentration of the three interleukins was only just above the threshold of detection (Figure 6.9). The donor with relatively high VL, and an increased TLM B cell subset, instead had detectable levels of IP-10, IFN-ʎ2/3, IFN-α2, IL-6 and IL-10. In contrast, only a single cytokine (IFN-β or IL-1β) was identified in the plasma of uninfected (HIV-negative) donors (Figure 6.9). Overall, the cytokine profiles varied between the different HIV-infected donors, although one cytokine IP-10 (also known as CXCL10), which is induced by IFN-γ, was detected in the plasma/serum of all 24 HIV-infected donors, but not the HIV-negative donors. Levels of IP-10 have previously been associated with plasma viraemia (Cohen et al. 2014), even low-level viraemia which along with TNF-α was also associated with the development of cross-neutralisation (Dugast et al. 2017), which will be discussed more in section 7.5.

The presence of IFN-α2 and IFN-γ in the plasma of the bnAb donor, despite memory B cell transcriptomes having most similarity to control donor memory B cells with reduced ISGs suggested that the effects of circulating IFN were somehow being blocked. It was therefore hypothesised that this could be mediated by auto-antibodies capable of neutralising IFN, similar to the blocking of IFN-α by auto-nAbs in lupus patients that leads to the normalisation of B cell subsets (Bradford et al. 2023). To test this theory, it was necessary to establish a system to quantify the stimulation induced by different IFNs and the ability to block or neutralise this effect. HEK293 cells transiently transfected with a plasmid containing a luciferase gene under the control of a human interferon-stimulated response element (ISRE) promoter have been used previously by another research group to evaluate functional blocking of type I IFN (Bastard et al. 2021). Similar to this published approach, expression of the *luc* reporter gene in permanently modified HEK293 ISRE cells can be detected using a luminometer, after cell lysis and the addition of a luciferase substrate, allowing measurement of the level of IFN stimulation based on the RLU (Figure 6.10a). The addition of IFN to HEK ISRE cells in the presence of mAbs or polyclonal plasma allows the neutralisation capacity of antibodies to be assessed (Figure 6.10b), with the extent of stimulation blocking identified by the reduction in RLU relative to IFN-only controls.

As this system had not been used by our lab before, it was necessary to first establish the HEK ISRE assay. A serial titration of IFN-α2 starting from 10 ng/mL and IFN-γ starting from 150 ng/mL demonstrated ISRE stimulation in a dose-dependent manner (Figure 6.11a). The requirement for a higher concentration of IFN-γ to induce ISRE was expected given that different receptors are bound by IFN-α2 and IFN-γ, which both activate JAK/STAT signalling pathways but use different components (Walter 2020). A concentration of 0.1 ng/mL IFN-α2 was chosen to proceed with on the basis that this concentration had been used previously in assays to detect the presence of auto-nAbs against IFN (Bastard et al. 2021). A concentration of 5 ng/mL IFN-γ was then chosen on the basis that this achieved an RLU for at least 5 fold-background, and the use of a concentration higher than this was deemed physiologically irrelevant. The ability of commercial antibodies to

block ISRE stimulation by IFN-α2 and IFN-γ was then tested. As shown in Figure 6.11b, a mAb specific for the IFN-α receptor (MMHAR-2) was capable of potently blocking IFN-α2 stimulation of the ISRE cells but not IFN-γ stimulation, as expected. A nAb specific for IFN-γ (B27) was able to block IFN-γ stimulation and to a lesser extent IFN-α2 stimulation (Figure 6.11b). This finding suggests that there may be a similarity in the epitopes targeted on IFN-α2 and IFN-γ to enable cross-reactivity by B27. Finally, a non-nAb against IFN-γ (MMHGR-2) did not block ISRE stimulation by IFN-α2 or IFN-γ, with at least 80% ISRE stimulation detected, and an IgG standard used as a negative control retained close to 100% ISRE stimulation by both IFNs (Figure 6.11b).

The HEK293 ISRE assay was further validated using plasma samples from HIV-infected individuals on ART or individuals from an elite control cohort with variable levels of viraemic control but low VL (<500 c/mL). This revealed that in the presence of plasma from individuals on ART, the ISRE stimulation by IFN-α2 was maintained at 70-115% (Figure 6.12a) and thus was similar to if plasma hadn't been added. In contrast, the plasma from all but one of the individuals with low VL reduced the ISRE stimulation by IFN-α2 to below 65%, with some capable of blocking IFN-α2 stimulation to almost 20%, although none reduced ISRE stimulation to as low a level as the nAb (MMHAR-2) control (Figure 6.12a). Plasma from the same individuals were also tested in the presence of IFN-γ, which showed that those on ART slightly enhanced the ISRE stimulation by IFN-γ resulting in between 100-160% stimulation (Figure 6.12b). Yet the plasma from most individuals from the elite control cohort with low/undetectable VL reduced ISRE stimulation by IFN-γ to <60%, and almost down to 20% in some cases, although none were as low as the nAb (B27) control (Figure 6.12b). In summary, this suggests that the plasma from untreated HIV infection but with low/undetectable VL due to immunological control mechanisms was capable of partially blocking IFN-α2 and/or IFN-γ. However, this was not observed with plasma from HIV-infected individuals suppressed by ART.

Finally, the established HEK ISRE assay was used to test the hypothesis that bnAb donors can restrict the effects of IFN-driven activation. Plasma/serum from all of the HIV-infected patients in the East London cohort, including the

bnAb donor T125, were therefore tested in this assay. The ISRE stimulation by IFN-α2 was reduced to <60% in the presence of plasma/serum from all HIV-infected individuals in the cohort, although none blocked the stimulation to <20% (Figure 6.13a). This range of IFN-α2 blocking by plasma was similar to the HIV controllers with low/undetectable VL (Figure 6.12a). In addition, there was no correlation between the patient plasma/serum neutralisation score and the ISRE stimulation by IFN-α2, determined using Spearman's rank correlation coefficient (r=-0.172, *p*=0.432). There was also no significant difference between patients with elite neutralisation (score >2) and those with no HIV neutralisation breadth (score = 0) and the ISRE stimulation by IFN-α2 (Figure 6.13a). The nAb control showed blocking of IFN-α2 as expected, with <5% ISRE stimulation, and plasma from HIV-negative donors did not affect the ISRE stimulation, remaining close to 100% (Figure 6.13a).

When plasma/serum from individuals in the cohort were tested against IFN-γ, the level of ISRE stimulation was reduced to <35%, and in some cases to <20%, although none blocked IFN-γ stimulation to the same extent as the nAb (B27) (Figure 6.13b). Nevertheless, a correlation between the patient plasma/serum neutralisation score and the ISRE stimulation by IFN-γ was identified by Spearman's rank correlation coefficient (r=-0.578, *p*=0.004). The decrease in IFN-γ stimulation mediated by plasma from elite neutralisers (score >2) compared to patients with no HIV neutralisation breadth (score = 0) was also found to be significantly different (Figure 6.13b). In contrast, plasma from HIV-negative donors did not alter/slightly increased the ISRE stimulation by IFN-γ resulting in 100-160% stimulation (Figure 6.13b). Overall, this indicates that plasma from untreated HIV-infected individuals were capable of partially blocking the effects of IFN. In particular, more potent blocking of IFN-γ was associated with greater neutralisation breadth against HIV.

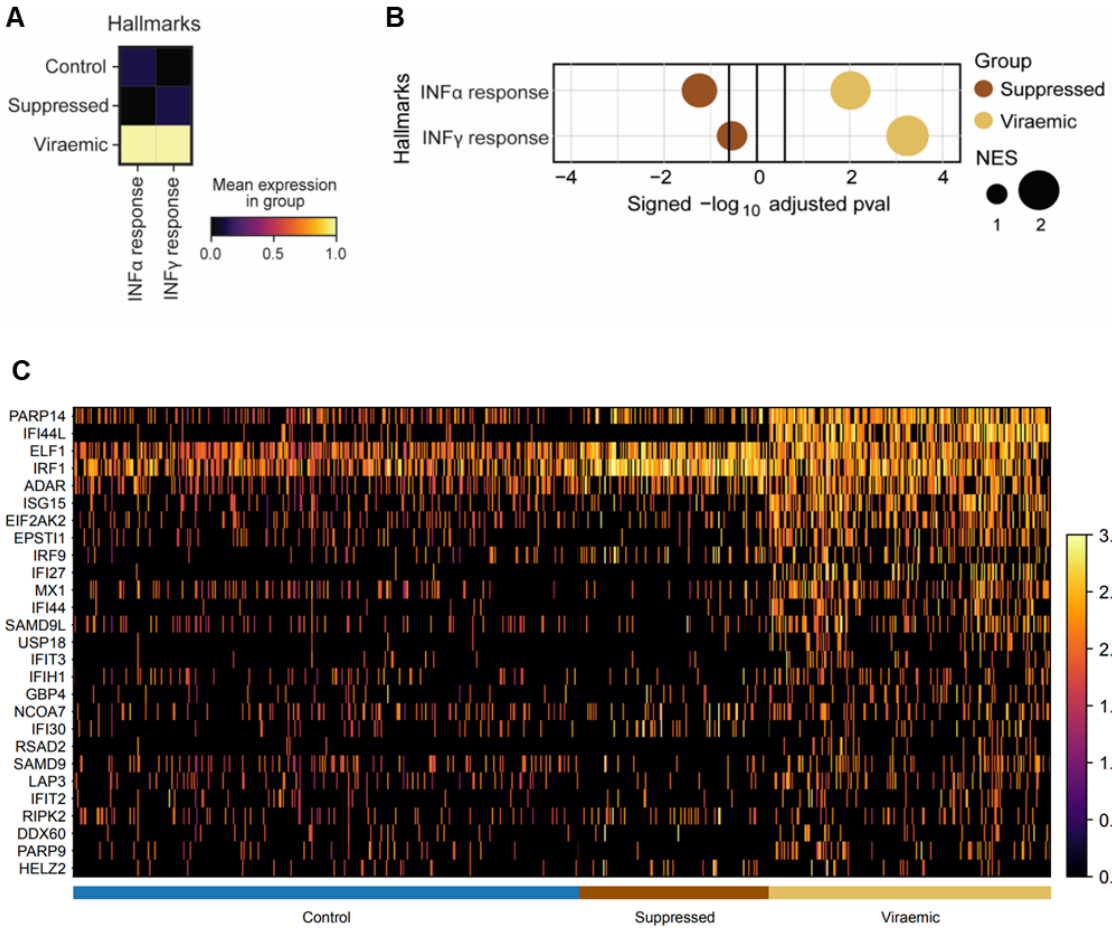

Figure 6.8 IFN responses are suppressed in the viraemic bnAb donor T125. (A) Hallmark IFN-α and IFN-γ response signature scores in memory B cells of control, suppressed and viraemic donors scaled by column. (B) GSEA for a hallmark IFN-α and IFN-γ response based on pre-ranked DEGs in suppressed or viraemic vs. control memory B cells respectively. Normalised enrichment score (NES) reflects the circle size. Vertical black lines indicate the threshold of significance. (C) Expression heatmap of unique leading edge genes from the GSEA for hallmark IFN pathways (as shown in B) by control, suppressed and viraemic memory B cells.

	Patient ID	Cytokine (pg/mL)												
		IP-10	IFN-λ1	IFN-λ2/3	IFN-γ	IFN-α2	TNF-α	IFN-β	IL-1β	IL-6	IL-8	IL-10	IL-12p70	GM-CSF
Score >2	T125	720.2	<49.3	<169.7	141.1	15.0	<15.8	<20.8	<6.15	<2.5	8.4	2.4	<1.8	<4.0
	R216	260.0	168.0	<169.7	<91.4	<2.6	<15.8	<20.8	13.9	<2.5	8.8	5.9	2.4	<4.0
	K300c	276.2	<49.3	<169.7	<91.4	<2.6	<15.8	<20.8	<6.15	<2.5	12.8	<1.6	<1.8	<4.0
	A260	578.6	161.1	<169.7	106.6	9.0	34.1	<20.8	29.0	7.8	10.6	16.8	5.6	6.3
Score 1-2	K525	1426.3	146.7	593.6	<91.4	<2.6	27.8	<20.8	<6.15	<2.5	21.5	<1.6	<1.8	<4.0
	D650	196.2	58.2	<169.7	<91.4	<2.6	<15.8	<20.8	<6.15	<2.5	5.0	4.9	<1.8	<4.0
	D600	873.3	125.5	<169.7	<91.4	<2.6	<15.8	<20.8	<6.15	<2.5	9.2	<1.6	<1.8	<4.0
	P636	145.7	224.4	208.7	<91.4	10.2	<15.8	<20.8	11.0	<2.5	20.8	<1.6	<1.8	<4.0
	T300	1016.5	51.5	<169.7	421.9	7.9	<15.8	<20.8	<6.15	<2.5	14.6	6.2	1.9	<4.0
	E214	499.2	<49.3	<169.7	<91.4	<2.6	<15.8	<20.8	7.2	<2.5	5.9	1.9	<1.8	<4.0
	B420	1392.6	345.2	514.7	266.9	<2.6	<15.8	<20.8	24.4	21.3	4.6	11.9	7.8	5.5
Score 0.5-1	K250	510.3	<49.3	<169.7	<91.4	<2.6	<15.8	<20.8	<6.15	<2.5	7.1	<1.6	<1.8	<4.0
	C251	749.8	209.5	<169.7	<91.4	18.0	<15.8	<20.8	9.4	4.5	31.9	3.4	6.9	<4.0
	B200	541.3	51.5	<169.7	<91.4	<2.6	<15.8	<20.8	<6.15	<2.5	<4.0	<1.6	<1.8	<4.0
	J520	331.2	79.3	<169.7	<91.4	<2.6	<15.8	<20.8	<6.15	<2.5	<4.0	<1.6	<1.8	<4.0
	A320	251.0	181.2	473.9	263.7	19.3	37.2	<20.8	38.0	14.7	7.5	15.2	9.8	9.8
Score 0-0.5	G400	785.2	60.2	317.1	<91.4	<2.6	<15.8	<20.8	33.8	3.7	31.9	1.7	<1.8	<4.0
	M210c	268.4	<49.3	<169.7	<91.4	3.6	<15.8	<20.8	<6.15	<2.5	5.4	<1.6	<1.8	<4.0
	E152	285.3	<49.3	421.9	<91.4	<2.6	<15.8	<20.8	27.9	<2.5	<4.0	<1.6	<1.8	<4.0
	U225	1113.0	161.4	525.5	<91.4	16.1	<15.8	<20.8	10.5	4.5	4.5	8.2	<1.8	<4.0
Score 0	E520	294.3	<49.3	<169.7	<91.4	<2.6	<15.8	<20.8	<6.15	<2.5	22.9	<1.6	3.8	<4.0
	S162	470.3	51.5	<169.7	<91.4	<2.6	<15.8	<20.8	<6.15	6.8	10.6	3.1	<1.8	<4.0
HIV+	High VL	224.2	<49.3	295.2	<91.4	5.8	<15.8	<20.8	<6.15	2.7	<4.0	2.4	<1.8	<4.0
	Low VL	559.0	<49.3	<169.7	<91.4	<2.6	20.2	<20.8	<6.15	<2.5	4.5	2.0	1.9	<4.0
HIV-	D1	<48.7	<49.3	<169.7	<91.4	<2.6	<15.8	22.1	<6.15	<2.5	<4.0	<1.6	<1.8	<4.0
	D2	<48.7	<49.3	<169.7	<91.4	<2.6	<15.8	<20.8	9.5	<2.5	<4.0	<1.6	<1.8	<4.0

Figure 6.9 Cytokine levels detected in the periphery of HIV-infected individuals do not appear to have association with HIV neutralisation breadth.

Concentration of 13 cytokines (IP-10, IFN-ʎ1, IFN-ʎ2/3, IFN-γ, IFN-α2, TNF-α, IFN-β, IL-1β, IL-6, IL-8, IL-10, IL-12p70 and GM-CSF) in patient plasma/serum, detected by flow cytometry using the LegendPLEX human anti-viral response panel. Cytokines concentrations reflect the mean of samples tested in duplicated and are highlighted from highest to lowest with a colour gradient from red to yellow respectively, those below the limit of detection are shown in grey. Patients are listed in order of the neutralisation score achieved against the standard 6 PV panel and are grouped as elite neutralisers (score ≥ 2), broad neutralisers (score 1-2), moderate neutralisers (score 0.5-1), weak neutralisers (0-0.5) and no neutralisation (score = 0). HIV-infected donors with high VL (110,000 c/mL) and low VL (100 c/mL) as well as uninfected (HIV-) donors were included as controls.

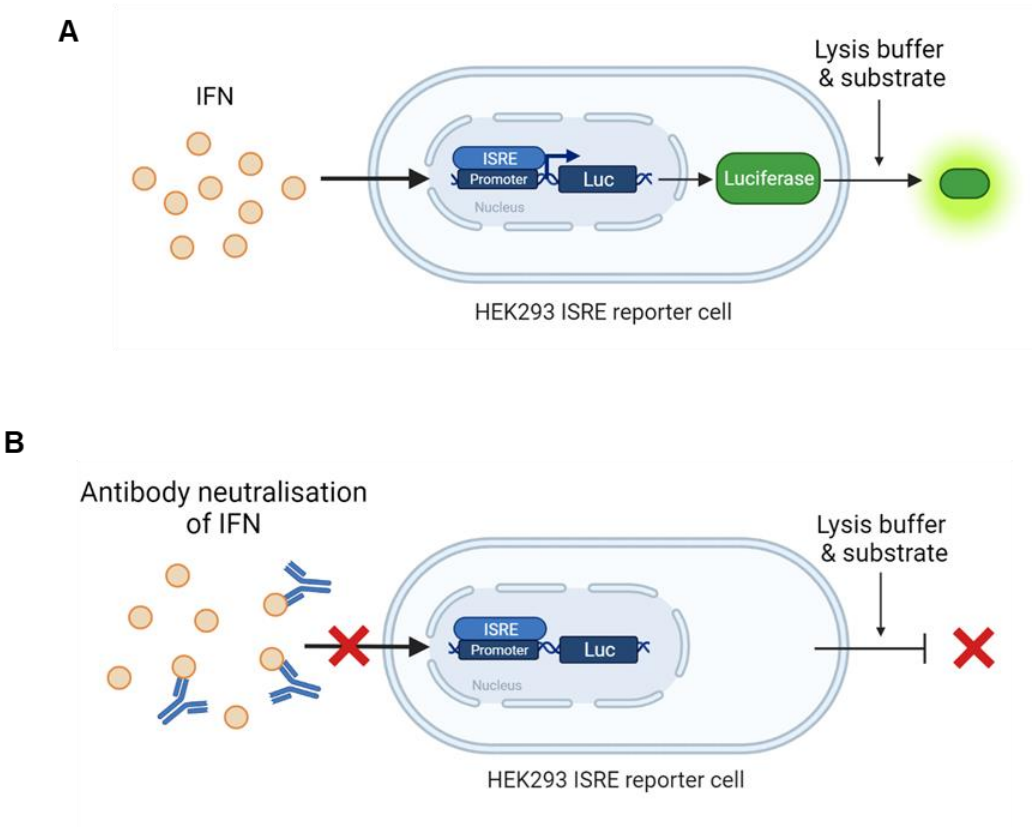

Figure 6.10 HEK293 ISRE assay to detect interferon (IFN) induced stimulation and neutralising antibodies against IFN.

Receptors on the surface of the HEK293 ISRE reporter cells bind IFN and induce JAK/STAT signalling that results in transcription of the firefly luciferase gene which is under the control of an interferon-stimulated response element (ISRE). (A) The level of IFN-induced stimulation can be measured by the luciferase activity in relative light units (RLU) after lysing the cells and adding a luciferase substrate (B) Neutralisation of IFN by plasma or monoclonal antibodies can be measured by the reduction in RLU, reflecting the reduction in IFN-induced stimulation, relative to (A). Image made with Biorender.

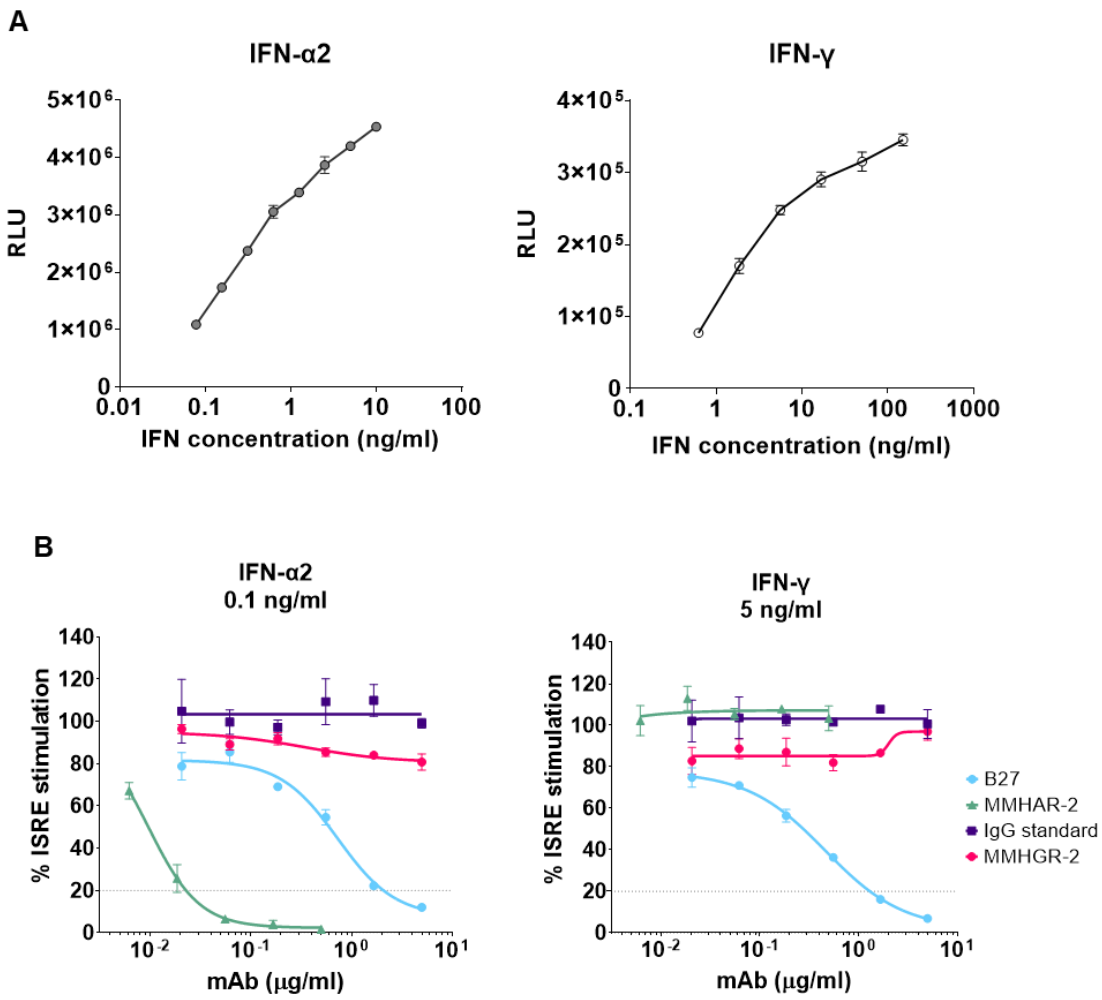

Figure 6.11 Validation of the HEK293 ISRE assay was successful in detecting neutralisation by commercial mAbs against IFN.

(A) Stimulation of HEK293 ISRE reporter cells using a 3-fold titration series of IFN-α2 and IFN-γ starting from 10 ng/mL and 150 ng/mL respectively. (B) Serial titration of mAbs B27 (blue), MMHAR-2 (green), IgG standard (navy) and MMHGR-2 (pink) tested in duplicate against a set concentration of IFN-α2 (0.1 ng/mL) or IFN-γ (5 ng/mL) in the HEK293 ISRE assay, with the mean and error bars plotted as well as a dotted line indicating 20% IFN-induced stimulation.

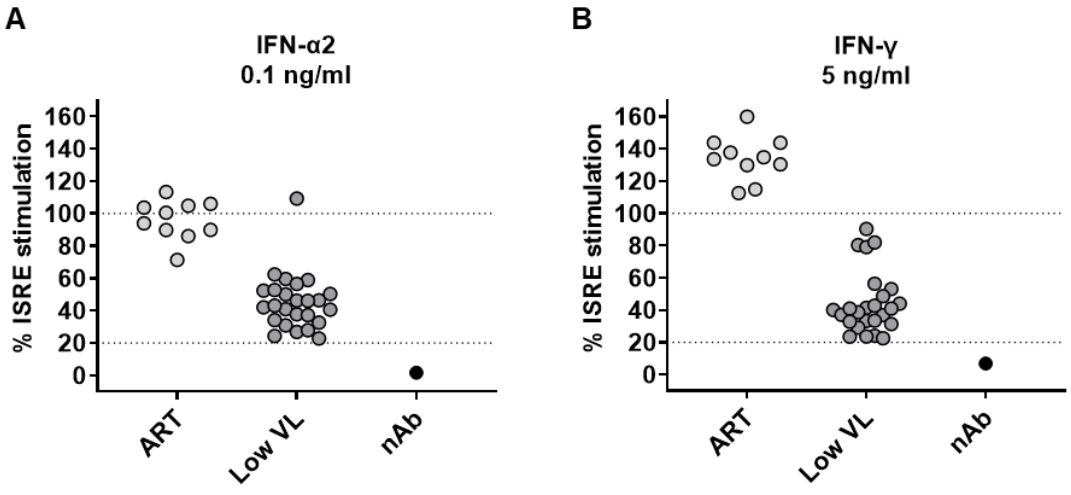

Figure 6.12 Stimulation of ISRE by IFN-α2 and IFN-γ was reduced in the presence of plasma/serum from HIV-infected individuals with low VL, but not from individuals on ART.

(A-B) The percentage ISRE stimulation by IFN was measured using the HEK293 ISRE assay. ISRE stimulation by (A) 0.1 ng/mL IFN-α2 and (B) 5 ng/mL IFN-γ in the presence of plasma/serum from HIV-infected individuals with low VL (< 500 c/mL) or on ART (undetectable VL) tested in duplicate at 1:10 dilution with the mean plotted. A commercial mAb capable of neutralising IFN-α2 (MMHAR-2, tested at 0.5 µg/mL) and IFN-γ (B27, tested at 5 µg/mL) was also included as a positive control in (A) and (B) respectively. Dotted lines show 20% and 100% ISRE stimulation.

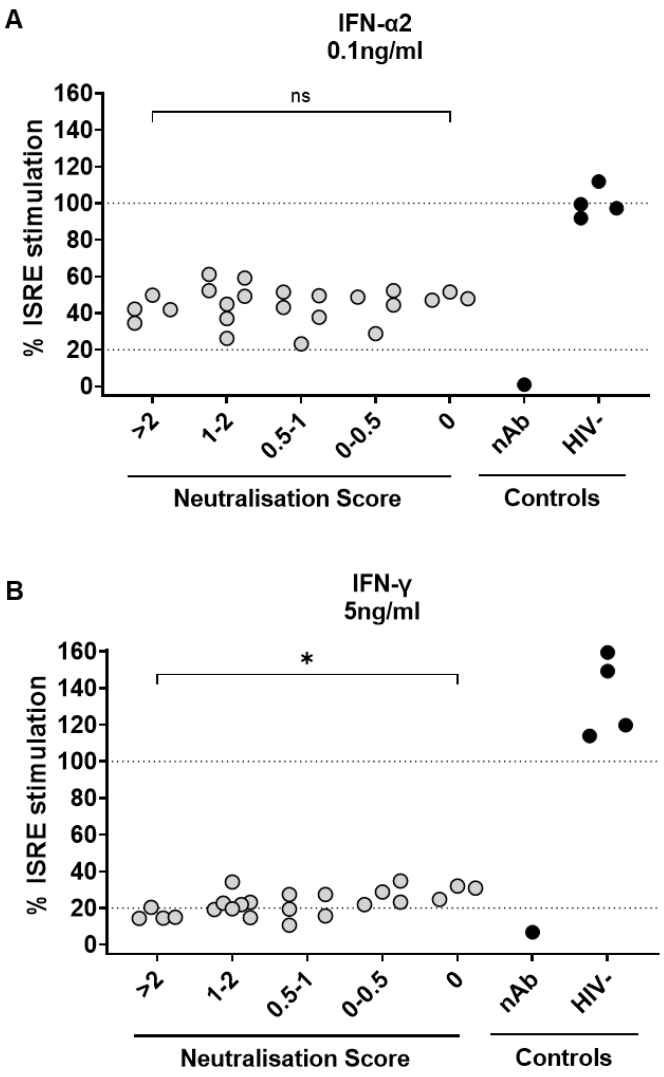

Figure 6.13 HIV neutralisation breadth was associated with enhanced blocking of IFN-γ mediated ISRE stimulation, but not IFN-α2.

(A-B) ISRE stimulation was measured using the HEK293 ISRE assay. Patient plasma/serum blocking of (A) 0.1 ng/mL IFN-α2 and (B) 5ng/mL IFN-γ was tested at 1:10 dilution, in duplicate with the mean plotted. Patients from the East London cohort were plotted according to their plasma/serum neutralisation score. The Kruskal-Wallis test was used to compare differences in ISRE stimulation between groups. Only the difference between patients with a neutralisation score >2 (elite neutralisation) and score=0 (no neutralisation breadth) was significant (p=0.048) for IFN-γ, shown by an asterisk, but non-significant (ns) for IFN-α2 (p >0.05). Plasma from uninfected (HIV-) donors were included as negative controls, and a commercial mAb capable of neutralising IFN-α2 (MMHAR-2, tested at 0.5 µg/mL) and IFN-γ (B27, tested at 5 µg/mL) was used as a positive control in (A) and (B) respectively. Dotted lines show 20% and 100% ISRE stimulation.

Summary

The inclusion of cell surface markers CD27 and CD21 during FACS provided the first insight into the phenotype of bnAb donor T125 B cells, revealing that IgG+ and HIV Env+ B cells were predominantly RM (CD27+ CD21+). This was unexpected given the concurrent viral load of 73,700 c/mL and the known impact of HIV viraemia on decreasing RM B cells and increasing TLM B cells. Overall, the distribution of the bnAb donor memory B cell subsets (based on the cell surface expression of CD27 and CD21) was most similar to both an HIV-negative donor and an HIV-infected donor with only 100 c/mL (undetectable at the time of sampling), rather than an HIV-infected donor with a VL similar in magnitude to that of the bnAb donor T125. Specifically, a higher frequency of TLM B cells and a lower frequency of RM B cells were observed in the high VL donor, consistent with the literature, which was not seen in either timepoint for T125. This indicated that the bnAb donor T125 did not display perturbation of the B cell subset distribution that is associated with uncontrolled HIV infection.

This novel finding was then investigated at the transcriptome level for single HIV Env+ IgG+ B cells that had been isolated from T125. This showed that the B cells from the bnAb donor T125 also had a transcriptional phenotype most similar to RM B cells and least like TLM B cells, regardless of the BCR specificity. Furthermore, the transcriptomic profile of bnAb donor B cells was unlike memory B cells from other HIV viraemic donors and instead had a phenotype most similar to healthy control donors. Findings from early transcriptomic analysis by microarray identified that the B cells from viraemic donors had upregulation of ISGs (Moir et al. 2004), consistent with findings from analyses conducted here. Additionally, the stimulation of B cells by IFN-γ *in vitro* has led to an increase in cells with a TLM phenotype (Ambegaonkar et al. 2019). Strikingly, memory B cells from control and suppressed individuals had reduced expression of ISGs compared to the viraemic donors, suggesting that lower levels of IFNs may explain the limited frequencies of TLM B cells in the bnAb donor.

However, a lower level of inflammatory cytokines was not observed in the bnAb donor plasma compared to other HIV-infected individuals. A caveat to this result is that the levels of cytokines quantified by the bead assay were very low and thus this approach may not have been sensitive enough to detect subtle differences. Observations of restored B cell populations in lupus (Bradford et al. 2023) support the hypothesis that preservation of a resting B cell phenotype achieved by the bnAb donor T125 could plausibly be explained by auto-antibodies restricting the effects of IFN that are induced during chronic HIV infection. In support of this, a weak but significant association was found between the ability to block IFN-γ stimulation and HIV neutralisation breadth, which suggests that preservation of the B cell population may also be identified in other broad and elite neutralisers. Finally, although a reduction in the downstream effects of IFN-γ was detected in the presence of plasma from these individuals, it is yet to be confirmed whether this was mediated by auto-antibodies.

Chapter 7: Discussion and future directions

Thesis summary

In chapter 3, I found that the Smart-Seq2 method was successful in generating cDNA from cryopreserved memory B cells, regardless of the subset, and was compatible with both antibody cloning and generating libraries for scRNA-seq. This work also showed that single resting memory (RM), activated memory (AM) and tissue-like memory (TLM) B cells were transcriptionally distinct, consistent with previous studies (Holla et al. 2021; Portugal et al. 2015; Kardava et al. 2014). The validation of this method meant that I had a system to address my research question of whether the phenotype of B cells is associated with the development of bnAbs. To do this, I aimed to investigate single memory B cells from rare HIV elite neutralisers at the cell surface and transcriptional level.

To identify samples with sufficient neutralisation potency and breadth I then evaluated plasma/serum from patients in the East London cohort in chapter 4. This revealed 50% had broad reactivity, with four (18%) being elite neutralisers obtaining a score of 2.21-3.19 in line with previous studies (Landais et al. 2016). I found that neutralisation by patient T125, who had the highest neutralisation score, was partially abrogated by occluding the trimer apex and partially enhanced by removing glycans around the CD4bs, consistent with the behaviour of previously isolated bnAbs against the apex and CD4bs epitopes. However, as the bnAb epitope targeted was not mapped completely/involved two independent epitopes, this precluded the use of antigen probes with and without the bnAb epitope to specifically isolate bnAb and non-bnAb B cells during FACS. Nevertheless, previous studies of donors with elite, but unmapped, neutralisation have demonstrated that bnAbs can be successfully isolated (McCoy and Burton 2017; van Gils et al. 2016), and thus FACS-based single B cell cloning was carried out using two Env baits in an epitope agnostic manner.

In chapter 5, a total of 24 Env-specific antibodies were isolated from donor T125, and although most had limited/no neutralisation against a multi-clade

PV panel, one bnAb was identified. The bnAb 7E7 targets a gp120-gp41 interface epitope independent of the surrounding glycans, similar to a previously isolated bnAb 3BC315 (Lee et al. 2015), and exhibits neutralisation breadth comparable to other gp120-gp41 interface specific bnAbs. While the identification of 7E7 enabled bnAb and non-bnAb B cells to be compared, analysis was limited by the identification of a single bnAb without any clonally related antibodies, and only a few that exhibited a level of cross-clade neutralisation. However, a striking observation during FACS was that the T125 bnAb donor did not show perturbation of B cell subsets associated with HIV infection, despite having uncontrolled viraemia. This unexpected finding suggested that instead of a difference between B cells within a donor based on each cell's neutralisation capacity there may be a difference in the B cell population of bnAb donors as a whole.

This hypothesis was explored in chapter 6 and I found that HIV Env-reactive B cells from the bnAb donor had a transcriptional phenotype most similar to RM B cells with minimal HIV-associated dysfunction. De novo analysis of memory B cells from a published dataset of HIV viraemic, HIV treatment-suppressed and uninfected controls also suggested a strong IFN signature in B cells from viraemic individuals, in contrast to suppressed individuals and uninfected controls. Additional analysis revealed that bnAb donor B cells were predicted to be most similar to memory B cells from uninfected controls than viraemic donors. This led to the proposal of a model where suppression of IFN responses in the bnAb donor may have facilitated the preservation of memory B cell homeostasis, for sustained affinity maturation during ongoing HIV infection. However, the major caveat to the analyses conducted is that data from non-bnAb donors were used to identify changes in the IFN responses of memory B cells, and these comparator data were generated by a different scRNA-seq method in a different study and full integration with my data to allow direct comparison to bnAb donor B cells was not possible. Therefore, to fully elucidate the importance of memory B cell homeostasis in the development of bnAbs, multiple HIV-infected individuals with bnAb-like serum and minimal cross-neutralisation would need to be evaluated in parallel. Overall, there were several limitations and challenges during this project as

well as caveats to how strongly the data supported the proposed model. These will now be discussed in turn to clarify the strength of the conclusions and outline future directions.

7.1 A major challenge in identifying phenotypes associated with bnAbs was the exact definition of a bnAb or bnAb-producing individual and accessing suitable samples

Until now, studies investigating factors associated with the development of bnAbs have typically used plasma/serum neutralisation breadth as a proxy for classifying bnAb and non-bnAb donors (Simek et al. 2009; Landais et al. 2016). However, the PVs used to screen for neutralisation breadth against HIV-1 vary between studies and in some cases originate from a single clade, rather than across multiple different clades, which can bias the breadth achieved (McCoy and McKnight 2017). In addition, most serological studies have not confirmed that these donors can produce individual bnAbs rather than their serum containing a multitude of different nAbs (Scheid et al. 2009), as this is a time-consuming and labour-intensive process. Nevertheless, it has been shown that bnAbs can be isolated from individuals with elite plasma neutralisation (Walker et al. 2009) (Walker et al. 2011) and can be defined by calculating a neutralisation score (Simek et al. 2009; Landais et al. 2016), yet none of these studies have focused on the B cell response or more specifically the B cells that produce bnAbs

Before conducting the research presented in this thesis, it was hypothesised that there would be a phenotypic difference in the B cells capable of producing bnAbs compared to B cells that produced mAbs with limited/no breadth. This hypothesis was based on the observation that most of the bnAbs isolated from HIV-infected individuals have high levels of SHM and/or long CDRH3s, which are features infrequently found in the human antibody repertoire (Griffith and McCoy 2021). However, the extent of SHM and the length of CDRH3 to be classed as unusual were not clearly or consistently defined. In addition, the neutralisation breadth and potency achieved by antibodies classified as

broadly neutralising had not yet been established. As a result, a review of existing HIV bnAbs was conducted to identify the current criteria that these met (Griffith and McCoy 2021), to apply this to the antibodies isolated in this study. The precise amount of V_H SHM and CDRH3 length in different bnAbs varied depending on the epitope targeted on Env and neither of these features enabled the prediction of breadth from sequence criteria alone. However, this review did provide crucial thresholds for the neutralisation breadth and potency of bnAbs against a standard panel of HIV PVs, which was particularly important for this project to distinguish between bnAb and non-bnAbs. This enabled the functionality of the isolated antibodies to be linked to their original B cells for investigation of associated phenotypes.

Interestingly, two studies that have been published since starting the research in this project explored the antibody repertoire in HIV infection and showed a correlation between higher SHM and broad neutralisation, yet this was based on the neutralisation capacity of plasma which is polyclonal (Roskin et al. 2020; Cizmeci et al. 2021). Moreover, plasma neutralisation breadth was determined using a panel of 12 HIV PVs consisting of only two different clades in the 2020 study (Roskin et al. 2020) or a panel of nine HIV PVs consisting of a single clade that was presumed to be the same as the HIV infection of patients in the 2021 study (Cizmeci et al. 2021). As it has been demonstrated that neutralisation is often higher when the clade of the PV matches the autologous virus (Simek et al. 2009; Seaman et al. 2010; Hraber et al. 2014), this is arguably an inadequate reflection of neutralisation breadth. Nevertheless, this does indicate an association between increasing affinity maturation to acquire more SHM and more effective neutralisation, even if this is breadth within a clade rather than across clades. As individual bnAbs often have particularly high SHM this could imply that the B cells capable of producing them are primed for multiple rounds of affinity maturation, and thus may differ from non-bnAb B cells.

On the other hand, a long CDRH3 is acquired during B cell development (Briney, Willis, and Crowe 2012) and is often associated with autoreactivity (Wardemann et al. 2003), therefore, bnAbs with long CDRH3s may indicate that self-tolerance is lower to allow these B cells to pass checkpoints for entry

into the periphery. This suggests that there could be an alteration to the overall immune response in bnAb donors rather than differences between the individual B cells. In agreement with this, the 2020 antibody repertoire study mentioned above found that the average CDRH3 length in individuals with plasma neutralisation breadth negatively correlated with the frequency of CTLA-4 Treg cells (Roskin et al. 2020), suggesting less regulation. However, when only the antibodies with a long CDRH3 of >19 AAs were considered there was no significant difference between donors with and without broad plasma neutralisation (Roskin et al. 2020). Furthermore, although long CDRH3s are infrequent in the human antibody repertoire these can also be found in HIV-negative individuals (Willis et al. 2016). Consequently, a long CDRH3 does not necessarily indicate lower tolerance and is only unusual because this feature is common to many HIV bnAbs, suggesting that a long CDRH3 is selected due to being beneficial for binding Env (Johnson and Wu 1998) (Yu and Guan 2014).

The next challenge in assessing how B cell phenotypes contribute to the development of bnAbs was to identify individuals with bnAb-like sera and available PBMC. Access to the East London cohort, which had both plasma and PBMCs from patients sampled before 2010 (Dreja et al. 2010) provided a unique opportunity to study the humoral and B cell response during HIV infection in the absence of treatment. However, the availability of these samples was limited, with very few vials of plasma and PBMCs remaining per patient and often from only a single timepoint, as the original study was not longitudinal. It was also not possible to study certain individuals as no PBMCs were available and as this was a historic cohort it was not feasible to re-sample these patients. Additionally, the clinical information and demographics obtained for patients in the East London cohort was minimal. While patients were recruited into the cohort based on being infected for at least one year, the exact length of infection, the viral load and CD4+ T cell count was unknown for the majority of patients. This makes it hard to compare this cohort to other cohorts where the development of breadth has been assessed in terms of these parameters. For example, prior associations with neutralisation breadth

include high VL and diversity, high frequency of circulating Tfh cells and longer HIV infection (Landais et al. 2016; Rusert et al. 2016; Moody et al. 2016).

Furthermore, changes in the UK guidance over time have resulted in the immediate initiation of ART upon detection of HIV infection, which as a consequence has made access to samples from untreated PLWH unviable. For this project, the availability of patient samples was compounded by the fact that only a small proportion of PLWH develop bnAbs. The first objective was therefore to identify patients in the East London cohort who had acquired neutralisation breadth. Although the limited availability of plasma restricted the characterisation of the neutralisation capacity to a small panel of HIV PVs, the standard 6 PV panel chosen is representative of larger panels of PVs from all major clades in circulation and thus is a good indicator of breadth(Simek et al. 2009). In addition, access to pre-existing plasma neutralisation data enabled patients with a level of cross-neutralisation to be selected before screening for breadth using the standard 6 PV panel, and this increased the proportion of elite neutralisers that were identified to 18% compared to other cohorts where this is ~1-10% (McCoy and McKnight 2017). In summary, while access to samples from the East London cohort was invaluable for this research project, there were many limitations such as poor clinical data, minimal longitudinal sampling and constraints resulting from sample availability.

Ideally, access to a cohort of HIV-infected individuals already identified as having neutralisation breadth with bnAb(s) previously isolated would have been a better starting point. Yet, without proof of concept for this line of research, it would have been challenging to justify the use of such rare PBMC samples. However, this would have prevented the requirement to spend time characterising donors based on their plasma neutralisation, as well as avoiding the need to clone and characterise antibodies to identify bnAb-producing B cells. Indeed, prior knowledge of antibody sequences and their functionality may have also led to a different scRNA-seq approach being taken that could have provided more insight into bnAb development, which will be discussed later in more detail in section 7.3. More importantly, though, this would have enabled the B cell phenotype of additional bnAb donors to be investigated as this initial characterisation was more time-consuming than

anticipated. Finally, a cohort with longitudinal PBMC sampling could have enabled the tracking of bnAb and non-bnAb lineages over time and whether B cell phenotypes changed during bnAb development.

7.2 The quality and quantity of bnAb-producing B cells sampled was lower than anticipated

Plasma from patient T125 exhibited highly potent neutralisation of all six PVs in the standard multi-clade panel tested, resulting in the highest neutralisation score in the East London cohort and was identified as an elite neutraliser. In addition, the inability to neutralise the negative control PV, which had an irrelevant Env, provided evidence that this neutralisation breadth was antibody-mediated and not a result of being on treatment. Indeed, single B cell cloning was successful in isolating a bnAb from T125 that exhibited ~50% neutralisation of multiple standard PV panels in line with other bnAbs against the interface epitope (as shown in section 5.2.12), confirming that this elite neutraliser was capable of producing bnAbs. However, the rest of the mAbs isolated had limited or no neutralisation. In total 50 mAbs were isolated and characterised for functionality, yet only 24 mAbs demonstrated detectable Env binding and 10 of these were non-neutralising. Of the 14 mAbs capable of neutralisation only one was identified as a bnAb and four had minimal cross-clade neutralisation, which restricted the ability to compare bnAb and non-bnAb B cells from the same donor. Moreover, even in combination, these nAbs would only be capable of neutralising four of the six PVs in the standard panel and thus did not recapitulate the 100% breadth of plasma neutralisation against this panel. This finding suggests that additional nAbs or even multiple bnAbs, as seen in other donors (Walker et al. 2011; Walker et al. 2009; Doria-Rose et al. 2014; Gao et al. 2014; Sok, van Gils, et al. 2014), must be present in the polyclonal plasma and thus the B cells responsible were not recovered using this approach.

The neutralisation by T125 plasma was not only broad but also able to be partially mapped to known bnAb epitopes, which further indicated that this

donor was a good candidate to study. Specifically, T125 plasma neutralisation was knocked down by removing residues within the apex epitope (N160A/K169T) and enhanced upon the removal of glycans surrounding the CD4bs (N276D/N462D). As the aim of epitope mapping the plasma neutralisation was to identify specificities targeted for breadth, many of the PVs used were chosen based on having mutation of residues typically found in bnAb epitopes. However, the predominant use of mutant PVs may explain why it was not possible to entirely epitope map the breadth of T125 plasma, as the dependency on certain residues can vary between bnAbs even if they target the same region on Env (McCoy and Burton 2017). Another limitation of epitope mapping the plasma specificity was that effects on neutralisation were tested with only a single PV. To show that epitopes were truly responsible for neutralisation breadth a more thorough approach could have been taken to introduce mutations into all of the PVs in the standard 6 PV panel, yet this would have been highly time-consuming and required a large quantity of plasma sample. Moreover, the challenges of working with polyclonal plasma mean that a complete knockout of neutralisation due to the alteration of one epitope is often hard to achieve (Landais et al. 2016). An alternative method to determine epitope specificities is to screen plasma against a panel of PVs capable of predicting the bnAb specificity that plasma neutralisation is most similar to (Doria-Rose et al. 2017). While this approach may have been more conclusive, this fingerprinting panel consists of 20 PVs which was too many to test for the amount of plasma available. In addition, predictions based on the neutralisation of this fingerprinting panel rely on the behaviour of previously isolated bnAbs and thus would have been unable to identify if novel epitopes are targeted.

Conversely, the individual nAbs isolated from T125 were mapped to three known neutralising epitopes on Env. While six nAbs targeted the CD4bs and thus were consistent with the partial CD4b specificity of the plasma, these nAbs were limited to clade-specific neutralisation. Another region targeted by seven nAbs was the V3 peptide which was not included in the epitope mapping of the plasma neutralisation as this is not a bnAb epitope, but four of these nAbs did exhibit a level of cross-clade neutralisation. The final epitope targeted

was the gp120-gp41 interface which was unique to the bnAb 7E7 isolated from T125, however, this specificity was only able to be identified using competition ELISAs with bnAbs of known epitope specificity which cannot be conclusively assessed with polyclonal plasma. In addition, the exact residues bound by 7E7 were unable to be determined in the ELISAs and neutralisation assays used. As the gp120-gp41 interface is a large, continuous area the use of electron microscopy (EM) methods, such as negative-stain EM or cryogenic EM, would likely be required to identify the exact bnAb contacts with the HIV Env. Nevertheless, mutation of the glycan at position 88 led to enhanced neutralisation by the bnAb 7E7 and this same mutant PV was used during epitope mapping of the plasma, but a change in neutralisation was not observed. This suggests that the bnAb 7E7 was either not prevalent in the plasma or that the enhancement in neutralisation may have been masked by other antibodies, highlighting the difficult task of epitope mapping polyclonal plasma.

Finally, none of the nAbs isolated from T125 targeted the trimer apex which was an epitope specificity identified based on the plasma neutralisation. This suggests that apex-specific memory B cells were not present in the periphery at the time of sampling, or were missed during isolation. As the majority of antibodies in plasma derive from long-lived plasma cells in the bone marrow (Montezuma-Rusca et al. 2015) this is perhaps not surprising. Indeed, while antibodies isolated from circulating memory B cells are found in plasma cells from the bone marrow there are also many additional variants in the bone marrow (Scheid et al. 2011). Therefore, a caveat to the single B cell cloning approach from PBMCs is that this relies upon memory B cells circulating in the periphery being clonally related to the plasma cells or plasmablasts that secrete the antibodies found in plasma. While single B cell cloning and scRNA-seq can be conducted with antibody-secreting cells, it is not possible to identify those that are HIV-specific by flow cytometry with antigen probes as the BCR is no longer present on the cell surface. Furthermore, long-lived plasma cells reside in the bone marrow making these cells difficult to obtain due to the invasive nature of sampling.

Ultimately, only a single bnAb was isolated from T125. This bnAb originated from a memory B cell identified from the first timepoint PBMCs but disappointingly no clonally related memory B cells were identified in the first or second timepoint PBMC samples. This likely stems from the small number of Env+ IgG+ B cells that were isolated by FACS, which despite sorting from two PBMC samples only amounted to a total of 110 cells with cDNA. It could be argued that the use of different antigen probes, such as autologous Env, may have yielded a higher number of Env+ memory B cells although the production of stabilised trimers from the autologous Env of elite neutralisers has rarely been done (van Gils et al. 2016). Moreover, it had already been demonstrated that the Env used as probes in FACS were capable of being targeted by nAbs in the T125 plasma and thus the use of heterologous Env designed to occlude non-neutralising epitopes (Sanders et al. 2013; Voss et al. 2017) was deemed appropriate for maximising the identification of bnAb B cells. Although the antigen-specific population in HIV-infected individuals is incredibly rare and constitutes <1.5% of IgG+ B cells (van Gils et al. 2016; Freund et al. 2017; Schommers et al. 2020; Sok, van Gils, et al. 2014), the low number of Env+ IgG+ B cells isolated from T125 was not due to any deficiency in the Env+ IgG+ population with 1.5% at the first timepoint and 1.1% at the second timepoint. Nevertheless, problems that arose during FACS with the BD Melody upon index sorting by purity from the first timepoint meant that many of these rare cells were discarded due to being in close proximity to another cell. Sorting of single B cells was trialled during method validation but this was conducted using a BD FACS-Aria, which was different to the BD FACS-Melody that had to be used to sort HIV PBMC samples in a CL3 facility at another university (KCL), and thus this was an unforeseen problem. Therefore, sorting based on yield without index sorting was used during FACS from the second timepoint to try and prevent loss of cells, yet the number of viable PBMCs from this timepoint was drastically lower (~2.5 million compared to ~7.5million in the first PBMC timepoint sample) and thus limited the number of Env+ IgG+ B cells that could be recovered.

The low number of Env+ IgG+ B cells was compounded by the fact that not all of these B cells had antibodies that were capable of binding Env by ELISA.

This further reduced the number of HIV-specific mAbs isolated as well as the probability of identifying bnAbs, which impacted the number of B cells that could be compared based on functionality. It is plausible that the poor recovery of Env-specific mAbs may be a result of differences in the avidity of binding, as BCRs on the surface of a B cell are more likely to display bivalent binding which would produce a stronger signal than monovalent binding in ELISA. In addition, the SOSIP protein used to detect Env binding in flow cytometry was complexed into a tetramer, resulting in higher valency than the SOSIP used in ELISAs. This is similar to the requirement of immune complexes between mAb and antigen for detecting binding affinity reported in a recent Sars-Cov2 paper (Robbiani et al. 2020). Taken together, this may explain the difference between BCRs displaying Env-reactivity during flow cytometry but not as soluble mAbs assessed by ELISA and may have meant that low-affinity antibodies were missed. On the contrary, it is also possible that reactivity to the SOSIP protein probes during flow cytometry may have been non-specific and hence not the result of binding by the BCR on the B cell surface. In particular, this may have been the case with cells isolated from the second timepoint PBMCs which had lower cell viability and visible clumping upon thawing, indicating the release of viscous DNA and thus may have led to non-specific association of Env with cells upon staining. Additionally, it has been reported that Env can bind to non-BCR elements on the surface of B cells, such as C-type lectin receptors, although these are typically on IgD+ IgM+ B cells and can be minimised by co-staining with IgG (He et al. 2006; Kardava et al. 2014), as was performed here. Another consideration is that there may have been non-specific binding to the fluorophore, streptavidin or biotin as this can be observed with HIV naïve PBMC samples, although this is usually minimal and a contemporaneous HIV naïve control was used to define the Env+ sort gate at each sort.

As mentioned above, PBMCs from T125 at the first timepoint were initially used to isolate Env+ IgG+ B cells and were processed to generate cDNA and clone mAbs to confirm the presence of bnAb B cells before investigating the second timepoint PBMCs. Therefore at this stage, it would have been possible to have taken an alternative approach to identify more bnAb B cells, especially

considering that only a single bnAb was isolated from the first timepoint. For instance, the use of a different scRNA-seq method such as 10x, which has a higher throughput to sequence more B cells and the use of this method will be discussed more in section 7.3, although this would have lost information on which cells were Env+. Moreover, the Smart-Seq2 method and compatibility with single B cell cloning had already been validated and having experienced how to improve the yield of single cells isolated by FACS it was decided that it would be best to continue with this approach.

Overall, the isolation of bnAbs is challenging and in previous studies initial single B cell cloning has led to the identification of only 1-6 bnAbs per elite neutraliser (Walker et al. 2011; Wu, Yang, et al. 2010; van Gils et al. 2016). However, by conducting single B cell cloning from two PBMC samples it was expected that it would be possible to identify more bnAbs and clonally related lineages from elite neutraliser T125 than the single bnAb that was isolated. Consequently, there were not enough bnAbs identified to test the original hypothesis and compare whether there is a difference in phenotype between bnAb and non-bnAb B cells. However, the novel finding of a non-perturbed memory B cell population at the cell surface level, identified by flow cytometry from both T125 timepoints, enabled the research into B cell phenotypes associated with the development of bnAbs to take a different direction. Specifically, the bnAb donor T125 did not have a high percentage of CD27-CD21- TLM B cells typically found in viraemic patients (Moir et al. 2010). This was a striking finding as TLM B cells express homing receptors to inflammatory sites rather than the GC (Wherry et al. 2007) and the antibodies from Env-specific TLM B cells display lower SHM than RM B cells (Meffre et al. 2016). In addition, most of the Env+ IgG+ B cells were found to express both CD27 and CD21, characteristic of RM that is reduced in other viraemic individuals (Kardava et al. 2014). Therefore, a lower proportion of TLM B cells in the bnAb donor and preservation of a resting phenotype by Env-reactive memory B cells suggests that broader neutralisation may have developed due to the ability to continue to mature in response to the ongoing HIV infection. Furthermore, as most of the Env-reactive memory B cells had the same cell surface phenotype this implies that there is not a difference between bnAb and

non-bnAb B cells, but rather a difference between bnAb and non-bnAb donors. In agreement with this, when B cell subsets were compared based on the cell surface expression of CD27 and CD21 this showed that the T125 bnAb donor was more similar to HIV-suppressed and HIV-negative donors than a typical viraemic donor (as shown in section 6.2.1). As a consequence, the transcriptomic phenotype of bnAb donor B cells was instead investigated in the context of other HIV-infected and uninfected donors to explore this novel finding.

7.3 Plate-based Smart-Seq2 transcriptomics enabled antibody and cell phenotypes to be linked for investigation of rare Env-reactive cells, but at the expense of gaining higher numbers of total B cell transcriptomes

There were several reasons to have a high level of confidence in the applicability of the pipeline chosen for studying Env-specific B cells from bnAb donors, which was incredibly important given the rarity of elite neutralisers samples. First, the use of the plate-based Smart-Seq2 method to generate cDNA sufficient for both scRNA-seq and antibody cloning was validated as part of this project with a healthy control and shown to be compatible with cryopreserved cells. This meant that the functionality of mAbs, such as neutralisation capacity, could be characterised and linked to the phenotype of single B cells. Notably, this pipeline had only previously been used with fresh PBMCs (Croote et al. 2018), yet access to fresh PBMC samples from HIV-infected individuals off-treatment is difficult to obtain and so compatibility with cryopreserved cells was vital. Second, there is evidence that cryopreservation does not alter the signalling in B cells (Hermansen et al. 2018), and thus the transcriptome should reflect the phenotype of B cells at the time of sampling. Third, comparative analysis has shown that the full-length Smart-Seq2 method has higher sensitivity, detecting the highest amount of genes per cell and thus greater sequencing depth, than other methods such as 10x, Drop-Seq and MARS-Seq that use UMIs (Ziegenhain et al. 2017; Wang et al. 2021), which is essential for accurate annotation of single-cell transcriptomes. In addition, it

was known that the number of Env-specific memory B cells for investigation would be low and thus another advantage of using the Smart-Seq2 method was that there was no minimum number of cells required for scRNA-seq. Indeed, at the time of conducting this research, the Smart-Seq2 approach had already been applied to study rare populations of single B cells based on isotype in the context of allergy (Croote et al. 2018) and has since been used to study antigen-specific memory populations in the context of influenza (Andrews et al. 2019; Burton et al. 2022).

Although this approach was the most suitable at the time to address whether there was a difference between bnAb and non-bnAb B cells, scRNA-seq analysis was limited by cell numbers and on reflection it would have also been interesting to explore the phenotype of additional cells. For instance, only a very small fraction of the B cell population was sampled to obtain Env-specific IgG+ memory B cells, yet lineage members in other subsets may have been identified if the entire B cell population had been considered. Additionally, other immune populations such as CD4+ T cells could have provided further insight into bnAb development as these cells facilitate the selection of B cells in response to antigens. To be able to do this, a more high throughput approach such as using 10x Genomics would have been required to conduct scRNA-seq with a higher number and diversity of cells. While the droplet-based approach of 10x allows a higher number of single cells to be processed, this comes at the expense of a lower sequencing depth and recovery than Smart-Seq2 (Picelli et al. 2014), yet is being used for scRNA-seq in an increasing number of published studies to gain a broader perspective of the immune response.

An advantage of high throughput scRNA-seq by 10x is that cells can be loaded straight onto the machine without prior processing which reduces potential transcriptome alterations and enables sequencing of total PBMCs. Although, where cell types of interest are minority populations, such as total B cells, they can be first isolated from PBMCs in bulk using magnetic-activated cell sorting (MACS) which is also much faster than staining cells and conducting FACS. Yet the use of FACS provides phenotypic information of cell surface protein

expression, which in this case was the first indication that there was preservation of the memory B cell population in the bnAb donor. To overcome this, the use of cellular indexing of transcriptomes and epitopes by sequencing (CITE-seq) can be conducted which uses barcoded antibodies to detect the expression of specific proteins (Stoeckius et al. 2017). However, the identification of antigen-specific cells by 10x is very challenging as compared to FACS and was only made possible recently by linking the BCR to antigen specificity through sequencing (LIBRA-seq) using barcoded antigens (Setliff et al. 2019) and is yet to be widely adopted. Alternatively, a pure population of antigen-specific B cells identified by flow-cytometry could have been used as input into 10x for scRNA-seq, however, obtaining a high enough number of cells from such a rare subset, as already demonstrated, would require sorting from lots of PBMC samples which was not possible from this cohort. Furthermore, antibody cloning would still have been necessary following scRNA-seq by 10x to test the mAb functionality and address the research question in this project, which would have been unfeasible as each Ig chain would need to be synthesised based on the sequencing information. This would have meant synthesising thousands of antibodies as discerning which BCRs encode bnAbs is not feasible from sequence traits alone as discussed in section 7.2.

Another approach could have been to use the Smart-Seq2 method followed by 10x, as done in a recent study to investigate both antigen-specific and total B cells in malaria-exposed individuals (Sutton et al. 2021). By taking advantage of both scRNA-seq methods the mAb sequence and functionality identified from the Env-specific B cells using the Smart-Seq2 pipeline with the first timepoint PBMCs from the bnAb donor could then have been applied to investigate the total B cells in the second timepoint PBMCs using 10x. The generation of a V(D)J library in addition to a gene expression library could have enabled clonally related BCRs to those already characterised to be identified from any B cell subset in the PBMC sample. However, this would have relied on the presence of the same lineages in circulation during the sampling of PBMCs at the second timepoint four months later or multiple vials

of PBMCs at each timepoint which were not available. Moreover, this would not have enabled any additional Env-specific B cells to be identified as the 10x data would have been filtered for BCRs that were clonal relatives of those identified by FACS sorting.

To make the most informed decision it would have been beneficial to have initially trialled both the 10x approach and the Smart-Seq2 method, however, this was not feasible due to the high expense of processing and sequencing cells for transcriptomic analysis and limited sample availability. Additionally, at the beginning of this research, the main aim was to focus on the antigen-specific B cell population and for reasons already discussed the Smart-Seq2 method appeared to be more suitable than 10x. Nevertheless, this approach still required optimisation and validation to adapt the Smart-Seq2 method to investigate cryopreserved memory B cells in conjunction with single B cell cloning. This was necessary because a previous study had only shown that this approach was viable using B cells from fresh PBMCs and that the gene count in naïve/memory B cells is lower than plasmablasts which were the primary focus of their study (Croote et al. 2018). Therefore it was unknown if cDNA could be generated from cryopreserved B cells, especially those from the more quiescent memory B cell subsets, and be sufficient for both scRNA-seq and antibody cloning.

It should be noted that the validation of this methodology was conducted with a small set of single memory B cells from healthy donor PBMCs to minimise costs and prove proof of concept in our lab, thus was never intended to be used as a comparator dataset to the HIV-infected donors. Consequently, a total of only 30 memory B cells per subset were processed for scRNA-seq, which was not high enough to conduct powerful analyses. Additionally, consideration of the date of sampling to have the same length of time in cryopreservation as well as the age and gender of the donor would need to have been accounted for to best match the HIV bnAb donors. While a more comprehensive dataset of memory B cell subsets from a sample matched uninfected control processed using the same scRNA-seq method as the bnAb

donor B cells may have been useful, a better control would have been a donor with HIV infection. Fortunately, this was possible to obtain as a post-doc in the lab was contemporaneously using Smart-Seq2 to study untreated HIV infection and although this was in an elite controller with low VL it did provide an opportunity to compare the bnAb donor B cells to different memory B cell subsets in the context of HIV infection.

Finally, a different technique that is still in its infancy is the use of proteomic and genomic approaches to deconvolute the plethora of the mAbs in polyclonal plasma to isolate antigen-specific mAbs (Wine et al. 2015). This system has already been employed to identify a pool of nAbs responsible for plasma breadth against HIV along with the nAb sequences for the isolation of bnAbs, although so far has only been done by one research group (Sajadi et al. 2018). In the future, this approach could be used to characterise plasma from elite neutralisers to provide knowledge of mAb sequences and functionality for investigating large scRNA-seq libraries to identify Env-specific nAb B cells without the need for antibody cloning or being limited by the antigen-specific subsets that can be isolated by flow cytometry. For instance, gene expression and VDJ libraries could be generated by 10x of total B cells to identify lineages of memory and antigen-secreting cells with BCRs that match proteomic data indicating Env specificity.

7.4 Additional datasets were required to act as comparators for single memory B cell transcriptomes from a bnAb donor

RM, AM and TLM can be distinguished at the cell surface level by the differential expression of CD27 and CD21, however, transcriptional analysis of these B cell subsets has revealed a more complex phenotype. Differences in the gene expression of different memory subsets were initially characterised in HIV infection studies by microarray (Moir et al. 2004) and later showed that while TLM B cells were distinct, RM and AM B cells had substantial overlap (Kardava et al. 2014). More comprehensive analysis of these memory subsets in malaria-exposed individuals by RNA-seq revealed a unique gene signature

for each memory subset (Holla et al. 2021), yet scRNA-seq has also identified a level of heterogeneity within each memory subset that likely stems from transitioning between phenotypes (Sutton et al. 2021; Andrews et al. 2019).

As mentioned earlier, most of the Env+ IgG+ B cells from both timepoints of the T125 bnAb donor displayed cell surface expression of both CD27 and CD21 in flow cytometry, and therefore had a predominantly resting phenotype. Transcriptional analysis mirrored this finding, with the majority of these Env-reactive B cells having the highest probability of being RM based on a memory B cell scRNA-seq dataset generated by our lab from an HIV-infected donor with elite control. Analysis also showed that the T125 Env-reactive B cells had the highest probability for a resting phenotype regardless of their mAb neutralisation capacity, indicating that there may not be a difference between bnAb and non-bnAb B cells, although again this is caveated by the finding of only one bnAb and a few cross-clade nAbs. Importantly, the Glmnet analysis conducted considers the probability of each cell for a phenotype in turn, and thus a single B cell can have a high probability for more than one phenotype if there are high similarities in the transcriptome.

This dataset was then used to explore DEG between the bnAb donor B cells and memory subsets from the HIV-infected donor with elite control. Given each memory subset had a similar sample size to the B cells from the bnAb donor this enabled comparative analysis without introducing bias. The DEG analysis gave further support that the Env-reactive B cells from the bnAb donor were least like TLM and most like RM, validating the novel finding observed from the cell surface phenotype that the memory B cell population was not perturbed. It was also revealed that a single gene, TWIST2, had significantly higher expression in the Env-reactive B cells from the bnAb donor regardless of which memory subset was the comparator. Interestingly, this gene was only found in B cells from the second T125 timepoint and is responsible for regulating inflammatory cytokines and inducing anti-apoptotic genes (Merindol et al. 2014). Comparison of the memory population from the two T125 timepoints by flow cytometry showed that the subsets from the second timepoint had a distribution even more similar to an HIV-negative individual than the first timepoint. Although this difference was subtle, there was a higher

proportion of RM and a lower proportion of AM and TLM in the IgG+ population in the second timepoint, which was reflected in the Env-reactive population and may have resulted from the upregulation of TWIST2. Therefore it could be speculated that B cells from the bnAb donor had a high propensity for survival and maintenance of homeostasis.

A potential limitation of these analyses was the comparison of the T125 Env-reactive B cells to memory B cells from a different donor for the identification of the transcriptional phenotype and DEG. However, it would have been unfeasible to isolate single memory B cells from each subset before isolating single antigen-specific B cells from T125 PBMCs due to the risk of lowering the number of cells in this rare population and the availability of only one vial of PBMC. Equally, it was not possible to isolate single B cells from different memory subsets after the antigen-specific B cell sort as this required all of the PBMC sample to be screened. Instead, the use of index-sorting could have enabled single Env-specific B cells within the different memory B cell subsets to be identified, however, the BD Melody FACS machine was incompatible with this function without the loss of many cells, which was discovered during the first single B cell sort from T125 PBMCs. Additionally, there were no pre-infection PBMCs from this donor to compare to. Hence it was necessary to employ a scRNA-seq memory B cell dataset from another donor for phenotypic analysis, and this was selected based on being generated from an HIV-infected individual using the same Smart-Seq2 method. Although this HIV-infected donor was an elite controller with low VL, unlike the viraemic bnAb donor, I had already shown that the cell surface phenotype of the bnAb donor memory B cell population was more similar to this elite controller rather than that of a typical viraemic donor, and thus was deemed a suitable dataset for comparison.

As already mentioned, the distribution of the bnAb donor memory B cell subsets based on CD27 and CD21 cell surface expression was also comparable to an HIV-negative donor, and thus indicated that the memory B cell population was not perturbed in the bnAb donor despite being viraemic. However, comparator data of memory B cells from other viraemic donors, those suppressed on ART and uninfected controls were lacking. Therefore,

two 10x scRNA-seq datasets (Wang et al. 2020; Stephenson et al. 2021) were analysed to compare memory B cells from multiple HIV-infected and uninfected donors. The Wang et al. study in 2020 sequenced PBMCs from six HIV-infected individuals with high viraemia (>185,000 c/mL) or suppressed viraemia (<20 c/mL) as a result of treatment (not elite control) as well as one uninfected control, which provided a relatively unexplored B cell dataset (Wang et al. 2020). A caveat to this was that the HIV-infected individuals were presumed to be non-bnAb donors, however, the neutralisation capacity of these individuals was not tested in the original study but this is a reasonable assumption based on the low prevalence (1-10%) of bnAb-like sera. It should also be noted that one of the three donors with viraemia was removed from analysis on the basis that the CD4+ T cell count was extremely low (AIDS-defining), to prevent the cells from this donor skewing analysis. Furthermore, the Wang et al. study only conducted scRNA-seq of one uninfected control and so to overcome this limitation PBMCs from additional uninfected controls from a different 10x scRNA-seq study by (Stephenson et al. 2021) were also included.

Although the 10x and Smart-Seq2 scRNA-seq methods both generate cDNA from poly-A mRNA, differences in the generation of libraries lead to different read depths (as reviewed in section 1.7.2) and thus additional steps are required for normalisation to enable integration of the datasets, which can be challenging. Indeed, this prevented the direct comparison of transcriptomes from the bnAb donor B cells generated by Smart-Seq2 to the memory B cells identified in the 10x datasets. Another limitation of working with data from multiple studies is that these have been processed and sequenced at different times. However, this can usually be accounted for using batch correction as done for the data obtained from the two previously published 10x scRNA-seq studies and thus enabled de novo analysis to make comparisons between memory B cells from different donor groups.

Our initial analysis by Celltypist classified B cells from the HIV-infected, HIV-suppressed and uninfected control donors as naïve, memory or age-associated. In particular, the age-associated subset has shown high similarity to the TLM and atypical B cell subset, which is expanded upon viral infection

or vaccination and characterised by low expression of CD27 and CD21, with high expression of T-bet and CD11c (Mouat and Horwitz 2022). Indeed, DEGs related to an atypical phenotype, although not T-bet (TBX21) or CD11c (ITGAX), were identified in this age-associated subset and these cells were primarily found in the viraemic donors. However, the key population under investigation in the bnAb donor was memory B cells, and therefore these age-associated B cells as well as naïve B cells were removed from further analysis. In support of this choice, even after the removal of age-associated B cells from subsequent analysis, the expression of other genes previously observed in a TLM / atypical phenotype (FCRL5, CD22 and CXCR3) were still observed in a small proportion of cells and were highest in the memory cells from viraemic donors. There were also differences in the expression of genes associated with GC entry and retention that were higher in the memory B cells from control donors than viraemic donors. Taken together, this suggests a fundamental difference in the memory B cell population of HIV-viraemic donors when compared to control donors, which appeared to be only partially restored by treatment in the suppressed donors. Additionally, this analysis enabled Celltypist classification of the Env-reactive memory B cells from the bnAb donor, which revealed these were most similar to memory B cells from uninfected controls. This implied that the bnAb donor B cells were unlike those in typical viraemic donors and instead primed for continued maturation that may have contributed to bnAb development.

It was also found that the type I IFN-α and type II IFN-γ response was higher in the memory B cells from viraemic donors than control donors, suggesting higher inflammation as a result of HIV infection, consistent with previous literature (Moir et al. 2004; Wang et al. 2020). Conversely, the IFN-α response of HIV-suppressed donor memory B cells was significantly lower compared to those from the control donors. While it is assumed that control donors are ‘healthy’ and do not have other infections at the time of sampling, in reality, these donors were selected based only on being HIV-negative in the Wang et al. study or COVID-negative based on serology in the Stephenson et al. study and therefore may explain this difference. It would have also been interesting to directly compare the IFN signature of the Env-reactive memory B cells from

the bnAb donor, but this was not feasible as the integration required to perform this analysis did not meet acceptable quality control standards. However, it seems likely from the Celltypist classification of the bnAb donor B cells as most similar to memory B cells from uninfected controls that a similar weak IFN signature would be observed. Unfortunately, without longitudinal sampling of this bnAb donor, it is impossible to know how the memory B cell population changed over the course of infection or whether this predominantly resting phenotype was maintained throughout infection. In particular, access to samples prior to infection and during acute infection as well as the isolation of more single B cells may have enabled pseudotime analysis to be conducted to track subsets or even B cell lineages over time.

7.5 Model: Preservation of memory B cell homeostasis in the face of chronic infection can promote the generation of bnAbs

Overall, in the bnAb donor, a predominantly RM B cell phenotype comparable to that of HIV-negative donors was observed at both the cell surface and transcriptomic level. Yet, this bnAb donor had a substantial level of viraemia at the first timepoint with a viral load of 73,700 c/mL, and although the viral load at the second timepoint is unknown, this sample was taken only four months later and hence is unlikely to be drastically different. A largely resting phenotype without signs of dysfunction was highly unexpected due to multiple previous observations showing that viraemia is associated with a reduced frequency of RM B cells (Moir et al. 2010; Kardava et al. 2014) and increased expression of ISGs or genes involved in terminal differentiation (Moir et al. 2004). Although analyses are caveated by the investigation of only a single bnAb donor, the consistency of findings in the Env-reactive memory B cells across the different transcriptional analyses conducted with different datasets adds support to the validity of these findings.

The identification of a normalised B cell population and inhibition of type I IFN gene signature has also been reported recently in lupus and was shown to be a result of neutralising auto-Abs against IFN-α2 (Bradford et al. 2023).

Therefore, it was proposed that the effects of type I, or even type II, IFN may be blocked in a similar manner in the HIV bnAb donor. Yet, it was also plausible that the preserved homeostasis of memory B cells despite ongoing viraemia may instead be a result of lower levels of inflammatory cytokines, mediated by other immune mechanisms such as the action of IL-10 secreted by regulatory B cells (Catalán et al. 2021). Both of these possibilities were tested using plasma from the bnAb donor and revealed that while there were only minimally quantifiable levels of IFN-α2 and IFN-γ, the effects of both IFNs were capable of being restricted by component(s) in the plasma, although this was more prominent against IFN-γ. Unfortunately, sufficient plasma remained only from the first timepoint from the bnAb donor and thus it was not possible to determine if this was also true of the second timepoint. Nevertheless, plasma from patients in the East London cohort with known neutralisation capacity, including the other three elite neutralisers identified, were included in analyses and identified a link between neutralisation breadth and a higher percentage of blocking IFN-γ, but not IFN-α2. These findings, therefore, support a model in which a suppressed type II inflammatory response during HIV infection allows the humoral response to develop neutralisation breadth, although further evidence is needed to confirm this model as discussed below.

While it remains to be explored whether the memory B cell phenotype in other elite neutralisers is also preserved, which would be an essential future experiment, the ability to block IFN-γ was consistent in the elite neutralisers and the bnAb donor, suggesting a similar mechanism for the development of breadth. Plasma from other patients in the cohort with less neutralisation breadth also demonstrated the ability to block IFN-γ, although this was often not as potent. It is plausible that some of these patients may not have been infected for long enough to acquire elite neutralisation but that the suppression of IFN-γ precedes this. For instance, although the patients in this cohort had been infected for at least one year, the exact length of infection was unknown, and it has been shown that neutralisation breadth is often acquired incrementally over the course of at least 2 years to develop (Landais et al. 2016). However, without access to longitudinal sampling from these donors it

was not possible to address whether those with comparable blocking of IFN-γ to elite neutralisers developed elite neutralisation over time.

The HEK-ISRE assay used to quantify the blocking of IFN-γ by patient plasma has been previously used to identify the presence of auto-antibodies against IFN-α and IFN-ω in Sars-Cov2 infection (Bastard et al. 2021). As plasma consists of many components, not just antibodies, the next step would have been to carry out IgG purification before conducting the HEK-ISRE assay to validate that the blocking of IFN-γ was antibody-mediated, but unfortunately, there was not enough time to do this. Alternatively, an IgG-specific ELISA could have been used to confirm the presence of auto-IFN-γ mAbs, but there was not enough sample to do this (required 50 µl of the original 200 µl). Furthermore, if the activity is indeed antibody-mediated, then there may be two possible mechanisms of blocking IFN mAbs, as demonstrated by the mAb controls used in the ISRE assay which either target the IFN molecules themselves or the IFN receptors, although this is yet to be validated. Another possibility is that a component of the plasma may have been killing the cells in the assay, which would also prevent expression of the ISRE-reporter and thus mimic IFN blocking. However, precautions were taken to avoid this, such as sterile filtering and heat inactivation of the samples to remove complement proteins before use, as well as cell viability assessment after the assay. In addition, if cell death was occurring as a result of the plasma then it would be expected that the same level of blocking would be observed across multiple assays, yet there was a difference in the percentage blocking of IFN-α2 and IFN-γ.

Unlike type I IFNs, which have direct antiviral activity, type II IFN (IFN-γ) is a proinflammatory cytokine and is involved in establishing and maintaining immune activation (Roff, Noon-Song, and Yamamoto 2014). In addition, it has recently been shown that IFN-γ could also have a negative impact on the adaptive response to infections as demonstrated by the potential to disrupt pre-existing GCs (Biram et al. 2022). Of particular interest however is the specific effect of IFN-γ on B cells, which has been demonstrated in recent *in vitro* studies to play a role in the stimulation of B cells towards an atypical/TLM phenotype following BCR engagement (Ambegaonkar et al. 2019; Obeng-

Adjei et al. 2017; Austin et al. 2019). This ties in with early microarray data of B cells from HIV-viraemic donors, which found increased ISGs in $CD21^{low}$ B cells (Moir et al. 2004), which consists of both AM and TLM B cells. Given the findings presented in this thesis, this suggests that the blocking of IFN-γ could prevent B cells from a TLM fate in the face of viraemia, as a potential mechanism for the preservation of the memory phenotype, which in turn allows the development of neutralisation breadth given the concurrent high antigen burden. As it is currently hypothesised but not yet confirmed that the blocking of IFN-γ is antibody-mediated, a future experiment should be to investigate whether auto-IFN-γ nAbs are capable of blocking the induction of a TLM phenotype *in vitro*.

So far there has been minimal investigation into features associated with the development of bnAbs in HIV at the single-cell transcriptomic level, with only one study that focused on the NK response (Bradley et al. 2018). Nevertheless, this identified that NK cells had an altered phenotype, with impaired effector functions including reduced secretion of IFN-γ, which was proposed to prevent the reduction of CD4+ T cells for improved B cell help. Based on the findings in this research, this altered NK function may also assist in the maintenance of a RM B cell phenotype for an improved humoral response. Although the concentration of IFN-γ in plasma samples from the East London cohort was investigated this showed no trend with the neutralisation capacity, but the sensitivity of LegendPLEX may have been too low to identify subtle differences. It could be speculated that a lower level of IFN-γ may instead be more localised and thus detected in the tissue rather than in circulation, but this is yet to be explored.

Other factors previously associated with, but not predictive of, broadly neutralising plasma include a low CD4+ T cell count (Landais et al. 2016; van Gils et al. 2009; Euler et al. 2010; Gray et al. 2011), and conversely higher levels of circulating Tfh cells (Locci et al. 2013; Moody et al. 2016; Yamamoto et al. 2015) which are a subset of CD4+ T cells. Unfortunately, the CD4+ T cell count for the bnAb donor was unknown and so couldn't be compared, but it is known that this donor was not on ART and at the time therapy was only initiated if the CD4+ T cell count was <200 cells/μl (Gazzard 2008). However,

two of the other three elite neutralisers in the East London cohort did have a known CD4+ T cell count of ~360 cells/μL but the frequency of circulating Tfh cells was not available to compare. In addition, the bnAb donor and two of the other three elite neutralisers which had known VL showed that these all had viraemia with >70,000 c/mL. A high VL has also been one of the most consistently associated features with the development of breadth and is thought to be linked to the level of viral diversity (Doria-Rose et al. 2010; Landais et al. 2016; Rusert et al. 2016), although it is not predictive of breadth. Moreover, this is caveated by the finding that some elite controllers with low VL are also capable of producing bnAbs (Sajadi et al. 2018; Scheid et al. 2011; Freund et al. 2017). However, in the context of the data presented here, a low VL also suggests a lower level of inflammation that likely results in a preserved memory B cell response. Indeed, this was observed in the elite controller included in flow cytometry analysis and a previous study where the proportion of TLM B cells was not elevated (Rouers et al. 2017). Furthermore, it is known that despite elite control these individuals have untreated infection and can experience viral blips, which over long periods may provide enough antigenic stimulation and diversity for bnAb development. When this was investigated, it was instead found that low but persistent viral replication was observed in controllers with limited clade B neutralisation breadth as well as a unique inflammatory cytokine profile, although this may only be a biomarker rather than contributing to breadth as multi-clade bnAb activity was not detected (Dugast et al. 2017).

It has also been previously reported that higher SHM in the HIV Env-specific repertoire correlated with broader serum neutralisation (Cizmeci et al. 2021). Although bnAbs are often described as having high levels of SHM, as was the case with the T125 bnAb, some of the non-nAbs from this donor were also found to have comparable SHM. This is consistent with previous findings of mAbs with restricted neutralisation but similar levels of SHM to bnAbs (Bhiman et al. 2015; Sok, van Gils, et al. 2014). It is already known that mutations acquired in the germinal centre are selected based on improved affinity for binding to antigen (Victora et al. 2010), however, these findings suggest that higher SHM is an acquired feature in response to ongoing HIV infection rather

than being directly linked to the acquisition of neutralisation breadth as previously proposed (Cizmeci et al. 2021). Indeed, mAbs isolated from the bnAb donor with detectable Env binding were found to have higher SHM in the V_H than those incapable of binding Env, indicating increased affinity maturation to HIV. In agreement with this, other studies have also shown that Env-reactive mAbs from HIV-infected individuals have significantly higher levels of V_H SHM than non-reactive mAbs (Scheid et al. 2009; Schommers et al. 2020). Yet, if directed towards conserved neutralising epitopes on the Env trimer, the ability to mature and gain beneficial mutations for binding or improving the angle of approach may lead to the development of a bnAb (Liao, Lynch, et al. 2013; MacLeod et al. 2016; Bonsignori, Kreider, et al. 2017; Bonsignori et al. 2016).

In summary, the discovery of a preserved memory B cell population in a bnAb donor was potentially linked to lower type II IFN-γ responses and suggests that bnAb development is associated with the maintenance of B cell homeostasis in the face of chronic HIV infection. However, additional experiments are needed to confirm this finding in other donors with elite neutralisation and whether this is also seen in donors as they progress towards elite neutralisation. As already discussed, this could be achieved by using a more high throughput approach such as 10x to explore the B cell phenotype in longitudinal cohorts. In addition, although it has been proposed that blocking IFN-γ leads to the preservation of a resting B cell phenotype, this has not been directly proven and the exact mechanism is still unclear. While it is currently thought that this is mediated by auto-nAbs against IFN-γ, future experiments will be needed to characterise the IgG component of plasma from elite neutralisers to confirm if this is capable of neutralising IFN-γ and whether this can prevent B cells from a TLM fate *in vitro*. Alternatively, or additionally, there may be an intrinsic difference in the B cells of bnAb donors such as the ability to downregulate IFN receptors, which was not explored, or upregulate TWIST2, as seen in the second timepoint, for the regulation of inflammatory cytokines and maintenance of a resting phenotype. The role of TWIST2 could be studied using a B cell CRISPR knock-in experiment to determine whether upregulation of this gene is involved in the preservation of a resting B cell phenotype. Furthermore, at this stage, it can only be speculated that

preserving memory B cell homeostasis assists the development of bnAbs, but it seems logical that this is associated with the ability to sustain affinity maturation to emerging viral variants during infection. Once it is established how the memory phenotype is preserved, this could be explored using a chronic infection animal model to determine whether this results in increasing SHM and an improved B cell response. A recent immunisation study that primed with HIV Env for a long period has shown that the duration of GCs can persist for up to 6 months and has resulted in improved memory B cell responses with higher SHM (Lee et al. 2022). Therefore, this system could be used as a model to test the effects of adding in IFN-γ and whether these can be reversed by anti-IFN antibodies.

Final remarks

The data presented in this thesis explored the phenotype of B cells in a bnAb donor, which has previously been overlooked, but indicated that differences between individual B cells based on their neutralisation capacity are unlikely. As only one bnAb donor was investigated and only a single bnAb B cell was identified, further analyses would be needed to thoroughly disprove the original hypothesis that there is a difference between bnAb and non-bnAb B cells. Nevertheless, this research also led to the observation of a surprisingly “normal” global memory B cell phenotype in the bnAb donor despite a substantial viral load, which is usually accompanied by widespread disruption of the B cell compartment. BnAb donor memory B cell transcriptomes were found to be unaffected by the functionality of the antibody encoded and were most similar to those from uninfected controls. In particular, memory B cells from uninfected controls had experienced less IFN stimulation and preliminary experiments indicate that bnAb-like serum can block type II IFN that has been previously linked to disruption of memory B cell subsets. Further work will be required to establish how widespread the preservation of memory B cell homeostasis is in individuals who make bnAbs and the potential mechanistic role of IFN.

References

Aalberse, R. C., S. O. Stapel, J. Schuurman, and T. Rispens. 2009. 'Immunoglobulin G4: an odd antibody', *Clin Exp Allergy*, 39: 469-77.

Alam, S. M., M. McAdams, D. Boren, M. Rak, R. M. Scearce, F. Gao, Z. T. Camacho, D. Gewirth, G. Kelsoe, P. Chen, and B. F. Haynes. 2007. 'The role of antibody polyspecificity and lipid reactivity in binding of broadly neutralizing anti-HIV-1 envelope human monoclonal antibodies 2F5 and 4E10 to glycoprotein 41 membrane proximal envelope epitopes', *J Immunol*, 178: 4424-35.

Alam, S. M., M. Morelli, S. M. Dennison, H. X. Liao, R. Zhang, S. M. Xia, S. Rits-Volloch, L. Sun, S. C. Harrison, B. F. Haynes, and B. Chen. 2009. 'Role of HIV membrane in neutralization by two broadly neutralizing antibodies', *Proc Natl Acad Sci U S A*, 106: 20234-9.

Alberts B, Johnson A, Lewis J, et al. 2002. 'The Generation of Antibody Diversity', Molecular Biology of the Cell. 4th edition. New York: Garland Science.

Allen, C. D., T. Okada, and J. G. Cyster. 2007. 'Germinal-center organization and cellular dynamics', *Immunity*, 27: 190-202.

Allen, Christopher D. C., K. Mark Ansel, Caroline Low, Robin Lesley, Hirokazu Tamamura, Nobutaka Fujii, and Jason G. Cyster. 2004. 'Germinal center dark and light zone organization is mediated by CXCR4 and CXCR5', *Nature Immunology*, 5: 943-52.

Allers, K., G. Hütter, J. Hofmann, C. Loddenkemper, K. Rieger, E. Thiel, and T. Schneider. 2011. 'Evidence for the cure of HIV infection by CCR5Δ32/Δ32 stem cell transplantation', *Blood*, 117: 2791-9.

Ambegaonkar, A. A., S. Nagata, S. K. Pierce, and H. Sohn. 2019. 'The Differentiation in vitro of Human Tonsil B Cells With the Phenotypic and Functional Characteristics of T-bet+ Atypical Memory B Cells in Malaria', *Front Immunol*, 10: 852.

Andrabi, R., J. E. Voss, C. H. Liang, B. Briney, L. E. McCoy, C. Y. Wu, C. H. Wong, P. Poignard, and D. R. Burton. 2015. 'Identification of Common Features in Prototype Broadly Neutralizing Antibodies to HIV Envelope V2 Apex to Facilitate Vaccine Design', *Immunity*, 43: 959-73.

Andrews, Sarah F., Michael J. Chambers, Chaim A. Schramm, Jason Plyler, Julie E. Raab, Masaru Kanekiyo, Rebecca A. Gillespie, Amy Ransier, Sam Darko, Jianfei Hu, Xuejun Chen, Hadi M. Yassine, Jeffrey C. Boyington, Michelle C. Crank, Grace L. Chen, Emily Coates, John R. Mascola, Daniel C. Douek, Barney S. Graham, Julie E. Ledgerwood, and Adrian B. McDermott. 2019. 'Activation Dynamics and Immunoglobulin Evolution of Pre-existing and Newly Generated Human Memory B cell Responses to Influenza Hemagglutinin', *Immunity*, 51: 398-410.e5.

Ansel, K. M., L. J. McHeyzer-Williams, V. N. Ngo, M. G. McHeyzer-Williams, and J. G. Cyster. 1999. 'In vivo-activated CD4 T cells upregulate CXC chemokine receptor 5 and reprogram their response to lymphoid chemokines', *J Exp Med*, 190: 1123-34.

Antanasijevic, Aleksandar, Leigh M. Sewall, Christopher A. Cottrell, Diane G. Carnathan, Luis E. Jimenez, Julia T. Ngo, Jennifer B. Silverman,

Bettina Groschel, Erik Georgeson, Jinal Bhiman, Raiza Bastidas, Celia LaBranche, Joel D. Allen, Jeffrey Copps, Hailee R. Perrett, Kimmo Rantalainen, Fabien Cannac, Yuhe R. Yang, Alba Torrents de la Peña, Rebeca Froes Rocha, Zachary T. Berndsen, David Baker, Neil P. King, Rogier W. Sanders, John P. Moore, Shane Crotty, Max Crispin, David C. Montefiori, Dennis R. Burton, William R. Schief, Guido Silvestri, and Andrew B. Ward. 2021. 'Polyclonal antibody responses to HIV Env immunogens resolved using cryoEM', *Nature Communications*, 12: 4817.

'Antibody infusions prevent acquisition of some HIV strains, NIH studies find'. 2021. National Institutes of Health, Accessed 04 May. https://www.nih.gov/news-events/news-releases/antibody-infusions-prevent-acquisition-some-hiv-strains-nih-studies-find.

Arnaout, R., W. Lee, P. Cahill, T. Honan, T. Sparrow, M. Weiand, C. Nusbaum, K. Rajewsky, and S. B. Koralov. 2011. 'High-resolution description of antibody heavy-chain repertoires in humans', *PLoS One*, 6: e22365.

Arts, E. J., and D. J. Hazuda. 2012. 'HIV-1 antiretroviral drug therapy', *Cold Spring Harb Perspect Med*, 2: a007161.

Austin, James W., Clarisa M. Buckner, Lela Kardava, Wei Wang, Xiaozhen Zhang, Valerie A. Melson, Ryan G. Swanson, Andrew J. Martins, Julian Q. Zhou, Kenneth B. Hoehn, J. Nicholas Fisk, Yiannis Dimopoulos, Alexander Chassiakos, Sijy O'Dell, Margery G. Smelkinson, Catherine A. Seamon, Richard W. Kwan, Michael C. Sneller, Stefania Pittaluga, Nicole A. Doria-Rose, Adrian McDermott, Yuxing Li, Tae-Wook Chun, Steven H. Kleinstein, John S. Tsang, Constantinos Petrovas, and Susan Moir. 2019. 'Overexpression of T-bet in HIV infection is associated with accumulation of B cells outside germinal centers and poor affinity maturation', *Science Translational Medicine*, 11: eaax0904.

Bailey, J. R., T. M. Williams, R. F. Siliciano, and J. N. Blankson. 2006. 'Maintenance of viral suppression in HIV-1-infected HLA-B*57+ elite suppressors despite CTL escape mutations', *J Exp Med*, 203: 1357-69.

Balla-Jhagjhoorsingh, S. S., D. Corti, L. Heyndrickx, E. Willems, K. Vereecken, D. Davis, and G. Vanham. 2013. 'The N276 glycosylation site is required for HIV-1 neutralization by the CD4 binding site specific HJ16 monoclonal antibody', *PLoS One*, 8: e68863.

Bar, K. J., M. C. Sneller, L. J. Harrison, J. S. Justement, E. T. Overton, M. E. Petrone, D. B. Salantes, C. A. Seamon, B. Scheinfeld, R. W. Kwan, G. H. Learn, M. A. Proschan, E. F. Kreider, J. Blazkova, M. Bardsley, E. W. Refsland, M. Messer, K. E. Clarridge, N. B. Tustin, P. J. Madden, K. Oden, S. J. O'Dell, B. Jarocki, A. R. Shiakolas, R. L. Tressler, N. A. Doria-Rose, R. T. Bailer, J. E. Ledgerwood, E. V. Capparelli, R. M. Lynch, B. S. Graham, S. Moir, R. A. Koup, J. R. Mascola, J. A. Hoxie, A. S. Fauci, P. Tebas, and T. W. Chun. 2016. 'Effect of HIV Antibody VRC01 on Viral Rebound after Treatment Interruption', *N Engl J Med*, 375: 2037-50.

Bar, K. J., C. Y. Tsao, S. S. Iyer, J. M. Decker, Y. Yang, M. Bonsignori, X. Chen, K. K. Hwang, D. C. Montefiori, H. X. Liao, P. Hraber, W. Fischer, H. Li, S. Wang, S. Sterrett, B. F. Keele, V. V. Ganusov, A. S. Perelson,

B. T. Korber, I. Georgiev, J. S. McLellan, J. W. Pavlicek, F. Gao, B. F. Haynes, B. H. Hahn, P. D. Kwong, and G. M. Shaw. 2012. 'Early low-titer neutralizing antibodies impede HIV-1 replication and select for virus escape', *PLoS Pathog*, 8: e1002721.

Barnes, C. O., H. B. Gristick, N. T. Freund, A. Escolano, A. Y. Lyubimov, H. Hartweger, A. P. West, Jr., A. E. Cohen, M. C. Nussenzweig, and P. J. Bjorkman. 2018. 'Structural characterization of a highly-potent V3-glycan broadly neutralizing antibody bound to natively-glycosylated HIV-1 envelope', *Nat Commun*, 9: 1251.

Barouch, D. H., F. L. Tomaka, F. Wegmann, D. J. Stieh, G. Alter, M. L. Robb, N. L. Michael, L. Peter, J. P. Nkolola, E. N. Borducchi, A. Chandrashekar, D. Jetton, K. E. Stephenson, W. Li, B. Korber, G. D. Tomaras, D. C. Montefiori, G. Gray, N. Frahm, M. J. McElrath, L. Baden, J. Johnson, J. Hutter, E. Swann, E. Karita, H. Kibuuka, J. Mpendo, N. Garrett, K. Mngadi, K. Chinyenze, F. Priddy, E. Lazarus, F. Laher, S. Nitayapan, P. Pitisuttithum, S. Bart, T. Campbell, R. Feldman, G. Lucksinger, C. Borremans, K. Callewaert, R. Roten, J. Sadoff, L. Scheppler, M. Weijtens, K. Feddes-de Boer, D. van Manen, J. Vreugdenhil, R. Zahn, L. Lavreys, S. Nijs, J. Tolboom, J. Hendriks, Z. Euler, M. G. Pau, and H. Schuitemaker. 2018. 'Evaluation of a mosaic HIV-1 vaccine in a multicentre, randomised, double-blind, placebo-controlled, phase 1/2a clinical trial (APPROACH) and in rhesus monkeys (NHP 13-19)', *Lancet*, 392: 232-43.

Barré-Sinoussi, F., J. C. Chermann, F. Rey, M. T. Nugeyre, S. Chamaret, J. Gruest, C. Dauguet, C. Axler-Blin, F. Vézinet-Brun, C. Rouzioux, W. Rozenbaum, and L. Montagnier. 1983. 'Isolation of a T-Lymphotropic Retrovirus from a Patient at Risk for Acquired Immune Deficiency Syndrome (AIDS)', *Science*, 220: 868-71.

Barton, John P., Nilu Goonetilleke, Thomas C. Butler, Bruce D. Walker, Andrew J. McMichael, and Arup K. Chakraborty. 2016. 'Relative rate and location of intra-host HIV evolution to evade cellular immunity are predictable', *Nature Communications*, 7: 11660.

Bastard, P., A. Gervais, T. Le Voyer, J. Rosain, Q. Philippot, J. Manry, E. Michailidis, H. H. Hoffmann, S. Eto, M. Garcia-Prat, L. Bizien, A. Parra-Martínez, R. Yang, L. Haljasmägi, M. Migaud, K. Särekannu, J. Maslovskaja, N. de Prost, Y. Tandjaoui-Lambiotte, C. E. Luyt, B. Amador-Borrero, A. Gaudet, J. Poissy, P. Morel, P. Richard, F. Cognasse, J. Troya, S. Trouillet-Assant, A. Belot, K. Saker, P. Garçon, J. G. Rivière, J. C. Lagier, S. Gentile, L. B. Rosen, E. Shaw, T. Morio, J. Tanaka, D. Dalmau, P. L. Tharaux, D. Sene, A. Stepanian, B. Megarbane, V. Triantafyllia, A. Fekkar, J. R. Heath, J. L. Franco, J. M. Anaya, J. Solé-Violán, L. Imberti, A. Biondi, P. Bonfanti, R. Castagnoli, O. M. Delmonte, Y. Zhang, A. L. Snow, S. M. Holland, C. Biggs, M. Moncada-Vélez, A. A. Arias, L. Lorenzo, S. Boucherit, B. Coulibaly, D. Anglicheau, A. M. Planas, F. Haerynck, S. Duvlis, R. L. Nussbaum, T. Ozcelik, S. Keles, A. A. Bousfiha, J. El Bakkouri, C. Ramirez-Santana, S. Paul, Q. Pan-Hammarström, L. Hammarström, A. Dupont, A. Kurolap, C. N. Metz, A. Aiuti, G. Casari, V. Lampasona, F. Ciceri, L. A. Barreiros, E. Dominguez-Garrido, M. Vidigal, M. Zatz, D. van de Beek,

S. Sahanic, I. Tancevski, Y. Stepanovskyy, O. Boyarchuk, Y. Nukui, M. Tsumura, L. Vidaur, S. G. Tangye, S. Burrel, D. Duffy, L. Quintana-Murci, A. Klocperk, N. Y. Kann, A. Shcherbina, Y. L. Lau, D. Leung, M. Coulongeat, J. Marlet, R. Koning, L. F. Reyes, A. Chauvineau-Grenier, F. Venet, G. Monneret, M. C. Nussenzweig, R. Arrestier, I. Boudhabhay, H. Baris-Feldman, D. Hagin, J. Wauters, I. Meyts, A. H. Dyer, S. P. Kennelly, N. M. Bourke, R. Halwani, N. S. Sharif-Askari, K. Dorgham, J. Sallette, S. M. Sedkaoui, S. AlKhater, R. Rigo-Bonnin, F. Morandeira, L. Roussel, D. C. Vinh, S. R. Ostrowski, A. Condino-Neto, C. Prando, A. Bonradenko, A. N. Spaan, L. Gilardin, J. Fellay, S. Lyonnet, K. Bilguvar, R. P. Lifton, S. Mane, M. S. Anderson, B. Boisson, V. Béziat, S. Y. Zhang, E. Vandreakos, O. Hermine, A. Pujol, P. Peterson, T. H. Mogensen, L. Rowen, J. Mond, S. Debette, X. de Lamballerie, X. Duval, F. Mentré, M. Zins, P. Soler-Palacin, R. Colobran, G. Gorochov, X. Solanich, S. Susen, J. Martinez-Picado, D. Raoult, M. Vasse, P. K. Gregersen, L. Piemonti, C. Rodríguez-Gallego, L. D. Notarangelo, H. C. Su, K. Kisand, S. Okada, A. Puel, E. Jouanguy, C. M. Rice, P. Tiberghien, Q. Zhang, A. Cobat, L. Abel, and J. L. Casanova. 2021. 'Autoantibodies neutralizing type I IFNs are present in ~4% of uninfected individuals over 70 years old and account for ~20% of COVID-19 deaths', *Sci Immunol*, 6.

Bbosa, N., P. Kaleebu, and D. Ssemwanga. 2019. 'HIV subtype diversity worldwide', *Curr Opin HIV AIDS*, 14: 153-60.

Behrens, A. J., S. Vasiljevic, L. K. Pritchard, D. J. Harvey, R. S. Andev, S. A. Krumm, W. B. Struwe, A. Cupo, A. Kumar, N. Zitzmann, G. E. Seabright, H. B. Kramer, D. I. Spencer, L. Royle, J. H. Lee, P. J. Klasse, D. R. Burton, I. A. Wilson, A. B. Ward, R. W. Sanders, J. P. Moore, K. J. Doores, and M. Crispin. 2016. 'Composition and Antigenic Effects of Individual Glycan Sites of a Trimeric HIV-1 Envelope Glycoprotein', *Cell Rep*, 14: 2695-706.

Beignon, A. S., K. McKenna, M. Skoberne, O. Manches, I. DaSilva, D. G. Kavanagh, M. Larsson, R. J. Gorelick, J. D. Lifson, and N. Bhardwaj. 2005. 'Endocytosis of HIV-1 activates plasmacytoid dendritic cells via Toll-like receptor-viral RNA interactions', *J Clin Invest*, 115: 3265-75.

Berger, E. A., R. W. Doms, E. M. Fenyö, B. T. M. Korber, D. R. Littman, J. P. Moore, Q. J. Sattentau, H. Schuitemaker, J. Sodroski, and R. A. Weiss. 1998. 'A new classification for HIV-1', *Nature*, 391: 240-40.

Berkowska, M. A., G. J. Driessen, V. Bikos, C. Grosserichter-Wagener, K. Stamatopoulos, A. Cerutti, B. He, K. Biermann, J. F. Lange, M. van der Burg, J. J. van Dongen, and M. C. van Zelm. 2011. 'Human memory B cells originate from three distinct germinal center-dependent and -independent maturation pathways', *Blood*, 118: 2150-8.

Berndsen, Zachary T., Srirupa Chakraborty, Xiaoning Wang, Christopher A. Cottrell, Jonathan L. Torres, Jolene K. Diedrich, Cesar A. López, John R. Yates, Marit J. van Gils, James C. Paulson, Sandrasegaram Gnanakaran, and Andrew B. Ward. 2020. 'Visualization of the HIV-1 Env glycan shield across scales', *Proceedings of the National Academy of Sciences*, 117: 28014-25.

Bhiman, J. N., C. Anthony, N. A. Doria-Rose, O. Karimanzira, C. A. Schramm, T. Khoza, D. Kitchin, G. Botha, J. Gorman, N. J. Garrett, S. S. Abdool Karim, L. Shapiro, C. Williamson, P. D. Kwong, J. R. Mascola, L. Morris, and P. L. Moore. 2015. 'Viral variants that initiate and drive maturation of V1V2-directed HIV-1 broadly neutralizing antibodies', *Nat Med*, 21: 1332-6.

Bianchi, M., H. L. Turner, B. Nogal, C. A. Cottrell, D. Oyen, M. Pauthner, R. Bastidas, R. Nedellec, L. E. McCoy, I. A. Wilson, D. R. Burton, A. B. Ward, and L. Hangartner. 2018. 'Electron-Microscopy-Based Epitope Mapping Defines Specificities of Polyclonal Antibodies Elicited during HIV-1 BG505 Envelope Trimer Immunization', *Immunity*, 49: 288-300.e8.

Binley, J. M., E. A. Lybarger, E. T. Crooks, M. S. Seaman, E. Gray, K. L. Davis, J. M. Decker, D. Wycuff, L. Harris, N. Hawkins, B. Wood, C. Nathe, D. Richman, G. D. Tomaras, F. Bibollet-Ruche, J. E. Robinson, L. Morris, G. M. Shaw, D. C. Montefiori, and J. R. Mascola. 2008. 'Profiling the specificity of neutralizing antibodies in a large panel of plasmas from patients chronically infected with human immunodeficiency virus type 1 subtypes B and C', *J Virol*, 82: 11651-68.

Biram, A., J. Liu, H. Hezroni, N. Davidzohn, D. Schmiedel, E. Khatib-Massalha, M. Haddad, A. Grenov, S. Lebon, T. M. Salame, N. Dezorella, D. Hoffman, P. Abou Karam, M. Biton, T. Lapidot, M. Bemark, R. Avraham, S. Jung, and Z. Shulman. 2022. 'Bacterial infection disrupts established germinal center reactions through monocyte recruitment and impaired metabolic adaptation', *Immunity*, 55: 442-58.e8.

Blattner, C., J. H. Lee, K. Sliepen, R. Derking, E. Falkowska, A. T. de la Peña, A. Cupo, J. P. Julien, M. van Gils, P. S. Lee, W. Peng, J. C. Paulson, P. Poignard, D. R. Burton, J. P. Moore, R. W. Sanders, I. A. Wilson, and A. B. Ward. 2014. 'Structural delineation of a quaternary, cleavage-dependent epitope at the gp41-gp120 interface on intact HIV-1 Env trimers', *Immunity*, 40: 669-80.

Blissenbach, M., B. Grewe, B. Hoffmann, S. Brandt, and K. Uberla. 2010. 'Nuclear RNA export and packaging functions of HIV-1 Rev revisited', *J Virol*, 84: 6598-604.

Bonsignori, M., E. F. Kreider, D. Fera, R. R. Meyerhoff, T. Bradley, K. Wiehe, S. M. Alam, B. Aussedat, W. E. Walkowicz, K. K. Hwang, K. O. Saunders, R. Zhang, M. A. Gladden, A. Monroe, A. Kumar, S. M. Xia, M. Cooper, M. K. Louder, K. McKee, R. T. Bailer, B. W. Pier, C. A. Jette, G. Kelsoe, W. B. Williams, L. Morris, J. Kappes, K. Wagh, G. Kamanga, M. S. Cohen, P. T. Hraber, D. C. Montefiori, A. Trama, H. X. Liao, T. B. Kepler, M. A. Moody, F. Gao, S. J. Danishefsky, J. R. Mascola, G. M. Shaw, B. H. Hahn, S. C. Harrison, B. T. Korber, and B. F. Haynes. 2017. 'Staged induction of HIV-1 glycan-dependent broadly neutralizing antibodies', *Sci Transl Med*, 9.

Bonsignori, M., H. X. Liao, F. Gao, W. B. Williams, S. M. Alam, D. C. Montefiori, and B. F. Haynes. 2017. 'Antibody-virus co-evolution in HIV infection: paths for HIV vaccine development', *Immunol Rev*, 275: 145-60.

Bonsignori, M., K. Wiehe, S. K. Grimm, R. Lynch, G. Yang, D. M. Kozink, F. Perrin, A. J. Cooper, K. K. Hwang, X. Chen, M. Liu, K. McKee, R. J.

Parks, J. Eudailey, M. Wang, M. Clowse, L. G. Criscione-Schreiber, M. A. Moody, M. E. Ackerman, S. D. Boyd, F. Gao, G. Kelsoe, L. Verkoczy, G. D. Tomaras, H. X. Liao, T. B. Kepler, D. C. Montefiori, J. R. Mascola, and B. F. Haynes. 2014. 'An autoreactive antibody from an SLE/HIV-1 individual broadly neutralizes HIV-1', *J Clin Invest*, 124: 1835-43.

Bonsignori, M., T. Zhou, Z. Sheng, L. Chen, F. Gao, M. G. Joyce, G. Ozorowski, G. Y. Chuang, C. A. Schramm, K. Wiehe, S. M. Alam, T. Bradley, M. A. Gladden, K. K. Hwang, S. Iyengar, A. Kumar, X. Lu, K. Luo, M. C. Mangiapani, R. J. Parks, H. Song, P. Acharya, R. T. Bailer, A. Cao, A. Druz, I. S. Georgiev, Y. D. Kwon, M. K. Louder, B. Zhang, A. Zheng, B. J. Hill, R. Kong, C. Soto, J. C. Mullikin, D. C. Douek, D. C. Montefiori, M. A. Moody, G. M. Shaw, B. H. Hahn, G. Kelsoe, P. T. Hraber, B. T. Korber, S. D. Boyd, A. Z. Fire, T. B. Kepler, L. Shapiro, A. B. Ward, J. R. Mascola, H. X. Liao, P. D. Kwong, and B. F. Haynes. 2016. 'Maturation Pathway from Germline to Broad HIV-1 Neutralizer of a CD4-Mimic Antibody', *Cell*, 165: 449-63.

Borrell, M., I. Fernández, F. Etcheverrry, A. Ugarte, M. Plana, L. Leal, and F. García. 2021. 'High rates of long-term progression in HIV-1-positive elite controllers', *J Int AIDS Soc*, 24: e25675.

Bournazos, S., and J. V. Ravetch. 2017. 'Diversification of IgG effector functions', *Int Immunol*, 29: 303-10.

Bradford, H. F., L. Haljasmägi, M. Menon, T. C. R. McDonnell, K. Särekannu, M. Vanker, P. Peterson, C. Wincup, R. Abida, R. F. Gonzalez, V. Bondet, D. Duffy, D. A. Isenberg, K. Kisand, and C. Mauri. 2023. 'Inactive disease in patients with lupus is linked to autoantibodies to type I interferons that normalize blood IFNα and B cell subsets', *Cell Rep Med*, 4: 100894.

Bradley, T., D. Peppa, I. Pedroza-Pacheco, D. Li, D. W. Cain, R. Henao, V. Venkat, B. Hora, Y. Chen, N. A. Vandergrift, R. G. Overman, R. W. Edwards, C. W. Woods, G. D. Tomaras, G. Ferrari, G. S. Ginsburg, M. Connors, M. S. Cohen, M. A. Moody, P. Borrow, and B. F. Haynes. 2018. 'RAB11FIP5 Expression and Altered Natural Killer Cell Function Are Associated with Induction of HIV Broadly Neutralizing Antibody Responses', *Cell*, 175: 387-99.e17.

Bradley, Todd, Masayuki Kuraoka, Chen-Hao Yeh, Ming Tian, Huan Chen, Derek W. Cain, Xuejun Chen, Cheng Cheng, Ali H. Ellebedy, Robert Parks, Maggie Barr, Laura L. Sutherland, Richard M. Scearce, Cindy M. Bowman, Hilary Bouton-Verville, Sampa Santra, Kevin Wiehe, Mark G. Lewis, Ane Ogbe, Persephone Borrow, David Montefiori, Mattia Bonsignori, M. Anthony Moody, Laurent Verkoczy, Kevin O. Saunders, Rafi Ahmed, John R. Mascola, Garnett Kelsoe, Frederick W. Alt, and Barton F. Haynes. 2020. 'Immune checkpoint modulation enhances HIV-1 antibody induction', *Nature Communications*, 11: 948.

Brenchley, J. M., T. W. Schacker, L. E. Ruff, D. A. Price, J. H. Taylor, G. J. Beilman, P. L. Nguyen, A. Khoruts, M. Larson, A. T. Haase, and D. C. Douek. 2004. 'CD4+ T cell depletion during all stages of HIV disease occurs predominantly in the gastrointestinal tract', *J Exp Med*, 200: 749-59.

Brenchley, Jason M., David A. Price, Timothy W. Schacker, Tedi E. Asher, Guido Silvestri, Srinivas Rao, Zachary Kazzaz, Ethan Bornstein, Olivier Lambotte, Daniel Altmann, Bruce R. Blazar, Benigno Rodriguez, Leia Teixeira-Johnson, Alan Landay, Jeffrey N. Martin, Frederick M. Hecht, Louis J. Picker, Michael M. Lederman, Steven G. Deeks, and Daniel C. Douek. 2006. 'Microbial translocation is a cause of systemic immune activation in chronic HIV infection', *Nature Medicine*, 12: 1365-71.

Briney, B. S., J. R. Willis, and J. E. Crowe, Jr. 2012. 'Human peripheral blood antibodies with long HCDR3s are established primarily at original recombination using a limited subset of germline genes', *PLoS One*, 7: e36750.

Brochet, X., M. P. Lefranc, and V. Giudicelli. 2008. 'IMGT/V-QUEST: the highly customized and integrated system for IG and TR standardized V-J and V-D-J sequence analysis', *Nucleic Acids Res*, 36: W503-8.

Buchacher, A., R. Predl, K. Strutzenberger, W. Steinfellner, A. Trkola, M. Purtscher, G. Gruber, C. Tauer, F. Steindl, A. Jungbauer, and et al. 1994. 'Generation of human monoclonal antibodies against HIV-1 proteins; electrofusion and Epstein-Barr virus transformation for peripheral blood lymphocyte immortalization', *AIDS Res Hum Retroviruses*, 10: 359-69.

Buchbinder, S. P., D. V. Mehrotra, A. Duerr, D. W. Fitzgerald, R. Mogg, D. Li, P. B. Gilbert, J. R. Lama, M. Marmor, C. Del Rio, M. J. McElrath, D. R. Casimiro, K. M. Gottesdiener, J. A. Chodakewitz, L. Corey, and M. N. Robertson. 2008. 'Efficacy assessment of a cell-mediated immunity HIV-1 vaccine (the Step Study): a double-blind, randomised, placebo-controlled, test-of-concept trial', *Lancet*, 372: 1881-93.

Buonaguro, L., M. L. Tornesello, and F. M. Buonaguro. 2007. 'Human immunodeficiency virus type 1 subtype distribution in the worldwide epidemic: pathogenetic and therapeutic implications', *J Virol*, 81: 10209-19.

Burnett, John C., Kathryn Miller-Jensen, Priya S. Shah, Adam P. Arkin, and David V. Schaffer. 2009. 'Control of Stochastic Gene Expression by Host Factors at the HIV Promoter', *PLOS Pathogens*, 5: e1000260.

Burton, A. R., S. M. Guillaume, W. S. Foster, A. K. Wheatley, D. L. Hill, E. J. Carr, and M. A. Linterman. 2022. 'The memory B cell response to influenza vaccination is impaired in older persons', *Cell Rep*, 41: 111613.

Burton, Alice R., Laura J. Pallett, Laura E. McCoy, Kornelija Suveizdyte, Oliver E. Amin, Leo Swadling, Elena Alberts, Brian R. Davidson, Patrick T. F. Kennedy, Upkar S. Gill, Claudia Mauri, Paul A. Blair, Nadege Pelletier, and Mala K. Maini. 2018. 'Circulating and intrahepatic antiviral B cells are defective in hepatitis B', *The Journal of Clinical Investigation*, 128: 4588-603.

Burton, D. R., C. F. Barbas, 3rd, M. A. Persson, S. Koenig, R. M. Chanock, and R. A. Lerner. 1991. 'A large array of human monoclonal antibodies to type 1 human immunodeficiency virus from combinatorial libraries of asymptomatic seropositive individuals', *Proc Natl Acad Sci U S A*, 88: 10134-7.

Burton, D. R., and L. Hangartner. 2016. 'Broadly Neutralizing Antibodies to HIV and Their Role in Vaccine Design', *Annu Rev Immunol*, 34: 635-59.
Cai, H., J. Orwenyo, J. P. Giddens, Q. Yang, R. Zhang, C. C. LaBranche, D. C. Montefiori, and L. X. Wang. 2017. 'Synthetic Three-Component HIV-1 V3 Glycopeptide Immunogens Induce Glycan-Dependent Antibody Responses', *Cell Chem Biol*, 24: 1513-22.e4.
Cardoso, R. M., M. B. Zwick, R. L. Stanfield, R. Kunert, J. M. Binley, H. Katinger, D. R. Burton, and I. A. Wilson. 2005. 'Broadly neutralizing anti-HIV antibody 4E10 recognizes a helical conformation of a highly conserved fusion-associated motif in gp41', *Immunity*, 22: 163-73.
Carrington, M., and G. Alter. 2012. 'Innate immune control of HIV', *Cold Spring Harb Perspect Med*, 2: a007070.
Carsetti, R., G. Köhler, and M. C. Lamers. 1995. 'Transitional B cells are the target of negative selection in the B cell compartment', *J Exp Med*, 181: 2129-40.
Caskey, M., F. Klein, and M. C. Nussenzweig. 2019. 'Broadly neutralizing anti-HIV-1 monoclonal antibodies in the clinic', *Nat Med*, 25: 547-53.
Catalán, Diego, Miguel Andrés Mansilla, Ashley Ferrier, Lilian Soto, Kristine Oleinika, Juan Carlos Aguillón, and Octavio Aravena. 2021. 'Immunosuppressive Mechanisms of Regulatory B Cells', *Frontiers in Immunology*, 12.
CDC, Centers for Disease Control. 1981. 'Kaposi's sarcoma and Pneumocystis pneumonia among homosexual men--New York City and California'.
Chan, T. D., D. Gatto, K. Wood, T. Camidge, A. Basten, and R. Brink. 2009. 'Antigen affinity controls rapid T-dependent antibody production by driving the expansion rather than the differentiation or extrafollicular migration of early plasmablasts', *J Immunol*, 183: 3139-49.
Checkley, M. A., B. G. Luttge, and E. O. Freed. 2011. 'HIV-1 envelope glycoprotein biosynthesis, trafficking, and incorporation', *J Mol Biol*, 410: 582-608.
Chen, Lieping, and Dallas B. Flies. 2013. 'Molecular mechanisms of T cell co-stimulation and co-inhibition', *Nature Reviews Immunology*, 13: 227-42.
Chen, P., W. Hübner, M. A. Spinelli, and B. K. Chen. 2007. 'Predominant mode of human immunodeficiency virus transfer between T cells is mediated by sustained Env-dependent neutralization-resistant virological synapses', *J Virol*, 81: 12582-95.
Chen, Y., J. Zhang, K. K. Hwang, H. Bouton-Verville, S. M. Xia, A. Newman, Y. B. Ouyang, B. F. Haynes, and L. Verkoczy. 2013. 'Common tolerance mechanisms, but distinct cross-reactivities associated with gp41 and lipids, limit production of HIV-1 broad neutralizing antibodies 2F5 and 4E10', *J Immunol*, 191: 1260-75.
Chen, Z., and J. H. Wang. 2019. 'Signaling control of antibody isotype switching', *Adv Immunol*, 141: 105-64.
Chun, Tae-Wook, Richard T. Davey, Delphine Engel, H. Clifford Lane, and Anthony S. Fauci. 1999. 'Re-emergence of HIV after stopping therapy', *Nature*, 401: 874-75.

Cizmeci, D., G. Lofano, E. Rossignol, A. S. Dugast, D. Kim, G. Cavet, N. Nguyen, Y. C. Tan, M. S. Seaman, G. Alter, and B. Julg. 2021. 'Distinct clonal evolution of B-cells in HIV controllers with neutralizing antibody breadth', *Elife*, 10.

Cohen, K., M. Altfeld, G. Alter, and L. Stamatatos. 2014. 'Early preservation of CXCR5+ PD-1+ helper T cells and B cell activation predict the breadth of neutralizing antibody responses in chronic HIV-1 infection', *J Virol*, 88: 13310-21.

Collins, Andrew M., and Corey T. Watson. 2018. 'Immunoglobulin Light Chain Gene Rearrangements, Receptor Editing and the Development of a Self-Tolerant Antibody Repertoire', *Frontiers in Immunology*, 9.

Collis, A. V., A. P. Brouwer, and A. C. Martin. 2003. 'Analysis of the antigen combining site: correlations between length and sequence composition of the hypervariable loops and the nature of the antigen', *J Mol Biol*, 325: 337-54.

Cortez, Valerie, Bingjie Wang, Adam Dingens, Mitchell M. Chen, Keshet Ronen, Ivelin S. Georgiev, R. Scott McClelland, and Julie Overbaugh. 2015. 'The Broad Neutralizing Antibody Responses after HIV-1 Superinfection Are Not Dominated by Antibodies Directed to Epitopes Common in Single Infection', *PLOS Pathogens*, 11: e1004973.

Corti, D., J. P. Langedijk, A. Hinz, M. S. Seaman, F. Vanzetta, B. M. Fernandez-Rodriguez, C. Silacci, D. Pinna, D. Jarrossay, S. Balla-Jhagjhoorsingh, B. Willems, M. J. Zekveld, H. Dreja, E. O'Sullivan, C. Pade, C. Orkin, S. A. Jeffs, D. C. Montefiori, D. Davis, W. Weissenhorn, A. McKnight, J. L. Heeney, F. Sallusto, Q. J. Sattentau, R. A. Weiss, and A. Lanzavecchia. 2010. 'Analysis of memory B cell responses and isolation of novel monoclonal antibodies with neutralizing breadth from HIV-1-infected individuals', *PLoS One*, 5: e8805.

Cottrell, Christopher A., Jelle van Schooten, Charles A. Bowman, Meng Yuan, David Oyen, Mia Shin, Robert Morpurgo, Patricia van der Woude, Mariëlle van Breemen, Jonathan L. Torres, Raj Patel, Justin Gross, Leigh M. Sewall, Jeffrey Copps, Gabriel Ozorowski, Bartek Nogal, Devin Sok, Eva G. Rakasz, Celia Labranche, Vladimir Vigdorovich, Scott Christley, Diane G. Carnathan, D. Noah Sather, David Montefiori, Guido Silvestri, Dennis R. Burton, John P. Moore, Ian A. Wilson, Rogier W. Sanders, Andrew B. Ward, and Marit J. van Gils. 2020. 'Mapping the immunogenic landscape of near-native HIV-1 envelope trimers in non-human primates', *PLOS Pathogens*, 16: e1008753.

Croote, D., S. Darmanis, K. C. Nadeau, and S. R. Quake. 2018. 'High-affinity allergen-specific human antibodies cloned from single IgE B cell transcriptomes', *Science*, 362: 1306-09.

Czajkowsky, D. M., and Z. Shao. 2009. 'The human IgM pentamer is a mushroom-shaped molecule with a flexural bias', *Proc Natl Acad Sci U S A*, 106: 14960-5.

D’arc, Mirela, Ahidjo Ayouba, Amandine Esteban, Gerald H. Learn, Vanina Boué, Florian Liegeois, Lucie Etienne, Nikki Tagg, Fabian H. Leendertz, Christophe Boesch, Nadège F. Madinda, Martha M. Robbins, Maryke Gray, Amandine Cournil, Marcel Ooms, Michael Letko, Viviana A. Simon, Paul M. Sharp, Beatrice H. Hahn, Eric Delaporte, Eitel Mpoudi

Ngole, and Martine Peeters. 2015. 'Origin of the HIV-1 group O epidemic in western lowland gorillas', *Proceedings of the National Academy of Sciences*, 112: E1343-E52.

Dalgleish, A. G., P. C. Beverley, P. R. Clapham, D. H. Crawford, M. F. Greaves, and R. A. Weiss. 1984. 'The CD4 (T4) antigen is an essential component of the receptor for the AIDS retrovirus', *Nature*, 312: 763-7.

Day, C. L., D. E. Kaufmann, P. Kiepiela, J. A. Brown, E. S. Moodley, S. Reddy, E. W. Mackey, J. D. Miller, A. J. Leslie, C. DePierres, Z. Mncube, J. Duraiswamy, B. Zhu, Q. Eichbaum, M. Altfeld, E. J. Wherry, H. M. Coovadia, P. J. Goulder, P. Klenerman, R. Ahmed, G. J. Freeman, and B. D. Walker. 2006. 'PD-1 expression on HIV-specific T cells is associated with T-cell exhaustion and disease progression', *Nature*, 443: 350-4.

De Milito, A., A. Nilsson, K. Titanji, R. Thorstensson, E. Reizenstein, M. Narita, S. Grutzmeier, A. Sönnerborg, and F. Chiodi. 2004. 'Mechanisms of hypergammaglobulinemia and impaired antigen-specific humoral immunity in HIV-1 infection', *Blood*, 103: 2180-6.

deCamp, A., P. Hraber, R. T. Bailer, M. S. Seaman, C. Ochsenbauer, J. Kappes, R. Gottardo, P. Edlefsen, S. Self, H. Tang, K. Greene, H. Gao, X. Daniell, M. Sarzotti-Kelsoe, M. K. Gorny, S. Zolla-Pazner, C. C. LaBranche, J. R. Mascola, B. T. Korber, and D. C. Montefiori. 2014. 'Global panel of HIV-1 Env reference strains for standardized assessments of vaccine-elicited neutralizing antibodies', *J Virol*, 88: 2489-507.

Deeks, S. G., and B. D. Walker. 2007. 'Human immunodeficiency virus controllers: mechanisms of durable virus control in the absence of antiretroviral therapy', *Immunity*, 27: 406-16.

DeKosky, B. J., O. I. Lungu, D. Park, E. L. Johnson, W. Charab, C. Chrysostomou, D. Kuroda, A. D. Ellington, G. C. Ippolito, J. J. Gray, and G. Georgiou. 2016. 'Large-scale sequence and structural comparisons of human naive and antigen-experienced antibody repertoires', *Proc Natl Acad Sci U S A*, 113: E2636-45.

Dharan, A., N. Bachmann, S. Talley, V. Zwikelmaier, and E. M. Campbell. 2020. 'Nuclear pore blockade reveals that HIV-1 completes reverse transcription and uncoating in the nucleus', *Nat Microbiol*, 5: 1088-95.

Dietzen, Dennis J. 2018. '13 - Amino Acids, Peptides, and Proteins.' in Nader Rifai, Andrea Rita Horvath and Carl T. Wittwer (eds.), *Principles and Applications of Molecular Diagnostics* (Elsevier).

Domínguez Conde, C., C. Xu, L. B. Jarvis, D. B. Rainbow, S. B. Wells, T. Gomes, S. K. Howlett, O. Suchanek, K. Polanski, H. W. King, L. Mamanova, N. Huang, P. A. Szabo, L. Richardson, L. Bolt, E. S. Fasouli, K. T. Mahbubani, M. Prete, L. Tuck, N. Richoz, Z. K. Tuong, L. Campos, H. S. Mousa, E. J. Needham, S. Pritchard, T. Li, R. Elmentaite, J. Park, E. Rahmani, D. Chen, D. K. Menon, O. A. Bayraktar, L. K. James, K. B. Meyer, N. Yosef, M. R. Clatworthy, P. A. Sims, D. L. Farber, K. Saeb-Parsy, J. L. Jones, and S. A. Teichmann. 2022. 'Cross-tissue immune cell analysis reveals tissue-specific features in humans', *Science*, 376: eabl5197.

Doores, K. J., C. Bonomelli, D. J. Harvey, S. Vasiljevic, R. A. Dwek, D. R. Burton, M. Crispin, and C. N. Scanlan. 2010. 'Envelope glycans of immunodeficiency virions are almost entirely oligomannose antigens', *Proc Natl Acad Sci U S A*, 107: 13800-5.

Doria-Rose, N. A., H. R. Altae-Tran, R. S. Roark, S. D. Schmidt, M. S. Sutton, M. K. Louder, G. Y. Chuang, R. T. Bailer, V. Cortez, R. Kong, K. McKee, S. O'Dell, F. Wang, S. S. Abdool Karim, J. M. Binley, M. Connors, B. F. Haynes, M. A. Martin, D. C. Montefiori, L. Morris, J. Overbaugh, P. D. Kwong, J. R. Mascola, and I. S. Georgiev. 2017. 'Mapping Polyclonal HIV-1 Antibody Responses via Next-Generation Neutralization Fingerprinting', *PLoS Pathog*, 13: e1006148.

Doria-Rose, N. A., J. N. Bhiman, R. S. Roark, C. A. Schramm, J. Gorman, G. Y. Chuang, M. Pancera, E. M. Cale, M. J. Ernandes, M. K. Louder, M. Asokan, R. T. Bailer, A. Druz, I. R. Fraschilla, N. J. Garrett, M. Jarosinski, R. M. Lynch, K. McKee, S. O'Dell, A. Pegu, S. D. Schmidt, R. P. Staupe, M. S. Sutton, K. Wang, C. K. Wibmer, B. F. Haynes, S. Abdool-Karim, L. Shapiro, P. D. Kwong, P. L. Moore, L. Morris, and J. R. Mascola. 2016. 'New Member of the V1V2-Directed CAP256-VRC26 Lineage That Shows Increased Breadth and Exceptional Potency', *J Virol*, 90: 76-91.

Doria-Rose, N. A., R. M. Klein, M. G. Daniels, S. O'Dell, M. Nason, A. Lapedes, T. Bhattacharya, S. A. Migueles, R. T. Wyatt, B. T. Korber, J. R. Mascola, and M. Connors. 2010. 'Breadth of human immunodeficiency virus-specific neutralizing activity in sera: clustering analysis and association with clinical variables', *J Virol*, 84: 1631-6.

Doria-Rose, N. A., C. A. Schramm, J. Gorman, P. L. Moore, J. N. Bhiman, B. J. DeKosky, M. J. Ernandes, I. S. Georgiev, H. J. Kim, M. Pancera, R. P. Staupe, H. R. Altae-Tran, R. T. Bailer, E. T. Crooks, A. Cupo, A. Druz, N. J. Garrett, K. H. Hoi, R. Kong, M. K. Louder, N. S. Longo, K. McKee, M. Nonyane, S. O'Dell, R. S. Roark, R. S. Rudicell, S. D. Schmidt, D. J. Sheward, C. Soto, C. K. Wibmer, Y. Yang, Z. Zhang, J. C. Mullikin, J. M. Binley, R. W. Sanders, I. A. Wilson, J. P. Moore, A. B. Ward, G. Georgiou, C. Williamson, S. S. Abdool Karim, L. Morris, P. D. Kwong, L. Shapiro, and J. R. Mascola. 2014. 'Developmental pathway for potent V1V2-directed HIV-neutralizing antibodies', *Nature*, 509: 55-62.

Dosenovic, P., L. von Boehmer, A. Escolano, J. Jardine, N. T. Freund, A. D. Gitlin, A. T. McGuire, D. W. Kulp, T. Oliveira, L. Scharf, J. Pietzsch, M. D. Gray, A. Cupo, M. J. van Gils, K. H. Yao, C. Liu, A. Gazumyan, M. S. Seaman, P. J. Björkman, R. W. Sanders, J. P. Moore, L. Stamatatos, W. R. Schief, and M. C. Nussenzweig. 2015. 'Immunization for HIV-1 Broadly Neutralizing Antibodies in Human Ig Knockin Mice', *Cell*, 161: 1505-15.

Dreja, H., E. O'Sullivan, C. Pade, K. M. Greene, H. Gao, K. Aubin, J. Hand, A. Isaksen, C. D'Souza, W. Leber, D. Montefiori, M. S. Seaman, J. Anderson, C. Orkin, and A. McKnight. 2010. 'Neutralization activity in a geographically diverse East London cohort of human immunodeficiency virus type 1-infected patients: clade C infection results in a stronger and

broader humoral immune response than clade B infection', *J Gen Virol*, 91: 2794-803.

Duan, H., X. Chen, J. C. Boyington, C. Cheng, Y. Zhang, A. J. Jafari, T. Stephens, Y. Tsybovsky, O. Kalyuzhniy, P. Zhao, S. Menis, M. C. Nason, E. Normandin, M. Mukhamedova, B. J. DeKosky, L. Wells, W. R. Schief, M. Tian, F. W. Alt, P. D. Kwong, and J. R. Mascola. 2018. 'Glycan Masking Focuses Immune Responses to the HIV-1 CD4-Binding Site and Enhances Elicitation of VRC01-Class Precursor Antibodies', *Immunity*, 49: 301-11.e5.

Dubay, J. W., S. R. Dubay, H. J. Shin, and E. Hunter. 1995. 'Analysis of the cleavage site of the human immunodeficiency virus type 1 glycoprotein: requirement of precursor cleavage for glycoprotein incorporation', *J Virol*, 69: 4675-82.

Dugast, A. S., K. Arnold, G. Lofano, S. Moore, M. Hoffner, M. Simek, P. Poignard, M. Seaman, T. J. Suscovich, F. Pereyra, B. D. Walker, D. Lauffenburger, D. S. Kwon, B. F. Keele, and G. Alter. 2017. 'Virus-driven Inflammation Is Associated With the Development of bNAbs in Spontaneous Controllers of HIV', *Clin Infect Dis*, 64: 1098-104.

Earl, P. L., R. W. Doms, and B. Moss. 1990. 'Oligomeric structure of the human immunodeficiency virus type 1 envelope glycoprotein', *Proc Natl Acad Sci U S A*, 87: 648-52.

Ehrhardt, G. R., J. T. Hsu, L. Gartland, C. M. Leu, S. Zhang, R. S. Davis, and M. D. Cooper. 2005. 'Expression of the immunoregulatory molecule FcRH4 defines a distinctive tissue-based population of memory B cells', *J Exp Med*, 202: 783-91.

Esbjörnsson, Joakim, Fredrik Månsson, Wilma Martínez-Arias, Elzbieta Vincic, Antonio J. Biague, Zacarias J. da Silva, Eva Maria Fenyö, Hans Norrgren, and Patrik Medstrand. 2010. 'Frequent CXCR4 tropism of HIV-1 subtype A and CRF02_AG during late-stage disease - indication of an evolving epidemic in West Africa', *Retrovirology*, 7: 23.

Escolano, Amelia, Harry B. Gristick, Morgan E. Abernathy, Julia Merkenschlager, Rajeev Gautam, Thiago Y. Oliveira, Joy Pai, Anthony P. West, Christopher O. Barnes, Alexander A. Cohen, Haoqing Wang, Jovana Golijanin, Daniel Yost, Jennifer R. Keeffe, Zijun Wang, Peng Zhao, Kai-Hui Yao, Jens Bauer, Lilian Nogueira, Han Gao, Alisa V. Voll, David C. Montefiori, Michael S. Seaman, Anna Gazumyan, Murillo Silva, Andrew T. McGuire, Leonidas Stamatatos, Darrell J. Irvine, Lance Wells, Malcolm A. Martin, Pamela J. Bjorkman, and Michel C. Nussenzweig. 2019. 'Immunization expands B cells specific to HIV-1 V3 glycan in mice and macaques', *Nature*, 570: 468-73.

Euler, Z., Van Den Kerkhof TL, R. D. Kouyos, D. C. Tully, T. M. Allen, A. Trkola, R. W. Sanders, H. Schuitemaker, and V. A. N. Gils MJ. 2019. 'Lower Broadly Neutralizing Antibody Responses in Female Versus Male HIV-1 Infected Injecting Drug Users', *Viruses*, 11.

Euler, Z., M. J. van Gils, E. M. Bunnik, P. Phung, B. Schweighardt, T. Wrin, and H. Schuitemaker. 2010. 'Cross-reactive neutralizing humoral immunity does not protect from HIV type 1 disease progression', *J Infect Dis*, 201: 1045-53.

Fagarasan, S., and T. Honjo. 2003. 'Intestinal IgA synthesis: regulation of front-line body defences', *Nat Rev Immunol*, 3: 63-72.

Falkowska, E., K. M. Le, A. Ramos, K. J. Doores, J. H. Lee, C. Blattner, A. Ramirez, R. Derking, M. J. van Gils, C. H. Liang, R. McBride, B. von Bredow, S. S. Shivatare, C. Y. Wu, P. Y. Chan-Hui, Y. Liu, T. Feizi, M. B. Zwick, W. C. Koff, M. S. Seaman, K. Swiderek, J. P. Moore, D. Evans, J. C. Paulson, C. H. Wong, A. B. Ward, I. A. Wilson, R. W. Sanders, P. Poignard, and D. R. Burton. 2014. 'Broadly neutralizing HIV antibodies define a glycan-dependent epitope on the prefusion conformation of gp41 on cleaved envelope trimers', *Immunity*, 40: 657-68.

Falkowska, E., A. Ramos, Y. Feng, T. Zhou, S. Moquin, L. M. Walker, X. Wu, M. S. Seaman, T. Wrin, P. D. Kwong, R. T. Wyatt, J. R. Mascola, P. Poignard, and D. R. Burton. 2012. 'PGV04, an HIV-1 gp120 CD4 binding site antibody, is broad and potent in neutralization but does not induce conformational changes characteristic of CD4', *J Virol*, 86: 4394-403.

Feng, Y., C. C. Broder, P. E. Kennedy, and E. A. Berger. 1996. 'HIV-1 entry cofactor: functional cDNA cloning of a seven-transmembrane, G protein-coupled receptor', *Science*, 272: 872-7.

Ferrante, A., L. J. Beard, and R. G. Feldman. 1990. 'IgG subclass distribution of antibodies to bacterial and viral antigens', *Pediatr Infect Dis J*, 9: S16-24.

Fiebig, E. W., D. J. Wright, B. D. Rawal, P. E. Garrett, R. T. Schumacher, L. Peddada, C. Heldebrant, R. Smith, A. Conrad, S. H. Kleinman, and M. P. Busch. 2003. 'Dynamics of HIV viremia and antibody seroconversion in plasma donors: implications for diagnosis and staging of primary HIV infection', *Aids*, 17: 1871-9.

Flynn, N. M., D. N. Forthal, C. D. Harro, F. N. Judson, K. H. Mayer, and M. F. Para. 2005. 'Placebo-controlled phase 3 trial of a recombinant glycoprotein 120 vaccine to prevent HIV-1 infection', *J Infect Dis*, 191: 654-65.

Francis, A. C., and G. B. Melikyan. 2018. 'Single HIV-1 Imaging Reveals Progression of Infection through CA-Dependent Steps of Docking at the Nuclear Pore, Uncoating, and Nuclear Transport', *Cell Host Microbe*, 23: 536-48.e6.

Freed, Eric O. 2015. 'HIV-1 assembly, release and maturation', *Nature Reviews Microbiology*, 13: 484-96.

Freund, N. T., J. A. Horwitz, L. Nogueira, S. A. Sievers, L. Scharf, J. F. Scheid, A. Gazumyan, C. Liu, K. Velinzon, A. Goldenthal, R. W. Sanders, J. P. Moore, P. J. Bjorkman, M. S. Seaman, B. D. Walker, F. Klein, and M. C. Nussenzweig. 2015. 'A New Glycan-Dependent CD4-Binding Site Neutralizing Antibody Exerts Pressure on HIV-1 In Vivo', *PLoS Pathog*, 11: e1005238.

Freund, N. T., H. Wang, L. Scharf, L. Nogueira, J. A. Horwitz, Y. Bar-On, J. Golijanin, S. A. Sievers, D. Sok, H. Cai, J. C. Cesar Lorenzi, A. Halper-Stromberg, I. Toth, A. Piechocka-Trocha, H. B. Gristick, M. J. van Gils, R. W. Sanders, L. X. Wang, M. S. Seaman, D. R. Burton, A. Gazumyan, B. D. Walker, A. P. West, Jr., P. J. Bjorkman, and M. C. Nussenzweig.

2017. 'Coexistence of potent HIV-1 broadly neutralizing antibodies and antibody-sensitive viruses in a viremic controller', *Sci Transl Med*, 9.

Frey, Gary, Hanqin Peng, Sophia Rits-Volloch, Marco Morelli, Yifan Cheng, and Bing Chen. 2008. 'A fusion-intermediate state of HIV-1 gp41 targeted by broadly neutralizing antibodies', *Proceedings of the National Academy of Sciences*, 105: 3739-44.

Fuller, M. J., and A. J. Zajac. 2003. 'Ablation of CD8 and CD4 T cell responses by high viral loads', *J Immunol*, 170: 477-86.

Furman, P. A., J. A. Fyfe, M. H. St Clair, K. Weinhold, J. L. Rideout, G. A. Freeman, S. N. Lehrman, D. P. Bolognesi, S. Broder, and H. Mitsuya. 1986. 'Phosphorylation of 3'-azido-3'-deoxythymidine and selective interaction of the 5'-triphosphate with human immunodeficiency virus reverse transcriptase', *Proceedings of the National Academy of Sciences*, 83: 8333-37.

Gallo, Robert C., Syed Z. Salahuddin, Mikulas Popovic, Gene M. Shearer, Mark Kaplan, Barton F. Haynes, Thomas J. Palker, Robert Redfield, James Oleske, Bijan Safai, Gilbert White, Paul Foster, and Phillip D. Markham. 1984. 'Frequent Detection and Isolation of Cytopathic Retroviruses (HTLV-III) from Patients with AIDS and at Risk for AIDS', *Science*, 224: 500-03.

Gao, F., M. Bonsignori, H. X. Liao, A. Kumar, S. M. Xia, X. Lu, F. Cai, K. K. Hwang, H. Song, T. Zhou, R. M. Lynch, S. M. Alam, M. A. Moody, G. Ferrari, M. Berrong, G. Kelsoe, G. M. Shaw, B. H. Hahn, D. C. Montefiori, G. Kamanga, M. S. Cohen, P. Hraber, P. D. Kwong, B. T. Korber, J. R. Mascola, T. B. Kepler, and B. F. Haynes. 2014. 'Cooperation of B cell lineages in induction of HIV-1-broadly neutralizing antibodies', *Cell*, 158: 481-91.

Garber, D. A., D. R. Adams, P. Guenthner, J. Mitchell, K. Kelley, T. Schoofs, A. Gazumyan, M. Nason, M. S. Seaman, J. McNicholl, M. C. Nussenzweig, and W. Heneine. 2020. 'Durable protection against repeated penile exposures to simian-human immunodeficiency virus by broadly neutralizing antibodies', *Nat Commun*, 11: 3195.

Gautam, Rajeev, Yoshiaki Nishimura, Amarendra Pegu, Martha C. Nason, Florian Klein, Anna Gazumyan, Jovana Golijanin, Alicia Buckler-White, Reza Sadjadpour, Keyun Wang, Zachary Mankoff, Stephen D. Schmidt, Jeffrey D. Lifson, John R. Mascola, Michel C. Nussenzweig, and Malcolm A. Martin. 2016. 'A single injection of anti-HIV-1 antibodies protects against repeated SHIV challenges', *Nature*, 533: 105-09.

Gazzard, BG, and on behalf of the BHIVA Treatment Guidelines Writing Group. 2008. 'British HIV Association guidelines for the treatment of HIV-1-infected adults with antiretroviral therapy 2008', *HIV Medicine*, 9: 563-608.

Gentile, M., T. Adrian, A. Scheidler, M. Ewald, F. Dianzani, G. Pauli, and H. R. Gelderblom. 1994. 'Determination of the size of HIV using adenovirus type 2 as an internal length marker', *J Virol Methods*, 48: 43-52.

Georgiev, I. S., N. A. Doria-Rose, T. Zhou, Y. D. Kwon, R. P. Staupe, S. Moquin, G. Y. Chuang, M. K. Louder, S. D. Schmidt, H. R. Altae-Tran, R. T. Bailer, K. McKee, M. Nason, S. O'Dell, G. Ofek, M. Pancera, S. Srivatsan, L. Shapiro, M. Connors, S. A. Migueles, L. Morris, Y.

Nishimura, M. A. Martin, J. R. Mascola, and P. D. Kwong. 2013. 'Delineating antibody recognition in polyclonal sera from patterns of HIV-1 isolate neutralization', *Science*, 340: 751-6.

Geretti, Anna Maria. 2006. 'HIV-1 subtypes: epidemiology and significance for HIV management', *Current opinion in infectious diseases*, 19: 1-7.

Goo, L., V. Chohan, R. Nduati, and J. Overbaugh. 2014. 'Early development of broadly neutralizing antibodies in HIV-1-infected infants', *Nat Med*, 20: 655-8.

Goodnow, C. C., J. Crosbie, S. Adelstein, T. B. Lavoie, S. J. Smith-Gill, R. A. Brink, H. Pritchard-Briscoe, J. S. Wotherspoon, R. H. Loblay, K. Raphael, and et al. 1988. 'Altered immunoglobulin expression and functional silencing of self-reactive B lymphocytes in transgenic mice', *Nature*, 334: 676-82.

Goonetilleke, N., M. K. Liu, J. F. Salazar-Gonzalez, G. Ferrari, E. Giorgi, V. V. Ganusov, B. F. Keele, G. H. Learn, E. L. Turnbull, M. G. Salazar, K. J. Weinhold, S. Moore, N. Letvin, B. F. Haynes, M. S. Cohen, P. Hraber, T. Bhattacharya, P. Borrow, A. S. Perelson, B. H. Hahn, G. M. Shaw, B. T. Korber, and A. J. McMichael. 2009. 'The first T cell response to transmitted/founder virus contributes to the control of acute viremia in HIV-1 infection', *J Exp Med*, 206: 1253-72.

Gorman, J., G. Y. Chuang, Y. T. Lai, C. H. Shen, J. C. Boyington, A. Druz, H. Geng, M. K. Louder, K. McKee, R. Rawi, R. Verardi, Y. Yang, B. Zhang, N. A. Doria-Rose, B. Lin, P. L. Moore, L. Morris, L. Shapiro, J. R. Mascola, and P. D. Kwong. 2020. 'Structure of Super-Potent Antibody CAP256-VRC26.25 in Complex with HIV-1 Envelope Reveals a Combined Mode of Trimer-Apex Recognition', *Cell Rep*, 31: 107488.

Gorny, M. K., R. Pan, C. Williams, X. H. Wang, B. Volsky, T. O'Neal, B. Spurrier, J. M. Sampson, L. Li, M. S. Seaman, X. P. Kong, and S. Zolla-Pazner. 2012. 'Functional and immunochemical cross-reactivity of V2-specific monoclonal antibodies from HIV-1-infected individuals', *Virology*, 427: 198-207.

Gorny, M. K., X. H. Wang, C. Williams, B. Volsky, K. Revesz, B. Witover, S. Burda, M. Urbanski, P. Nyambi, C. Krachmarov, A. Pinter, S. Zolla-Pazner, and A. Nadas. 2009. 'Preferential use of the VH5-51 gene segment by the human immune response to code for antibodies against the V3 domain of HIV-1', *Mol Immunol*, 46: 917-26.

Gorny, Miroslaw K., Jared Sampson, Huiguang Li, Xunqing Jiang, Maxim Totrov, Xiao-Hong Wang, Constance Williams, Timothy O'Neal, Barbara Volsky, Liuzhe Li, Timothy Cardozo, Phillipe Nyambi, Susan Zolla-Pazner, and Xiang-Peng Kong. 2011. 'Human Anti-V3 HIV-1 Monoclonal Antibodies Encoded by the VH5-51/VL Lambda Genes Define a Conserved Antigenic Structure', *PLoS One*, 6: e27780.

Gray, E. S., M. C. Madiga, T. Hermanus, P. L. Moore, C. K. Wibmer, N. L. Tumba, L. Werner, K. Mlisana, S. Sibeko, C. Williamson, S. S. Abdool Karim, and L. Morris. 2011. 'The neutralization breadth of HIV-1 develops incrementally over four years and is associated with CD4+ T cell decline and high viral load during acute infection', *J Virol*, 85: 4828-40.

Gray, E. S., P. L. Moore, I. A. Choge, J. M. Decker, F. Bibollet-Ruche, H. Li, N. Leseka, F. Treurnicht, K. Mlisana, G. M. Shaw, S. S. Karim, C. Williamson, and L. Morris. 2007. 'Neutralizing antibody responses in acute human immunodeficiency virus type 1 subtype C infection', *J Virol*, 81: 6187-96.

Gray, E. S., N. Taylor, D. Wycuff, P. L. Moore, G. D. Tomaras, C. K. Wibmer, A. Puren, A. DeCamp, P. B. Gilbert, B. Wood, D. C. Montefiori, J. M. Binley, G. M. Shaw, B. F. Haynes, J. R. Mascola, and L. Morris. 2009. 'Antibody specificities associated with neutralization breadth in plasma from human immunodeficiency virus type 1 subtype C-infected blood donors', *J Virol*, 83: 8925-37.

Gray, G. E., L. G. Bekker, F. Laher, M. Malahleha, M. Allen, Z. Moodie, N. Grunenberg, Y. Huang, D. Grove, B. Prigmore, J. J. Kee, D. Benkeser, J. Hural, C. Innes, E. Lazarus, G. Meintjes, N. Naicker, D. Kalonji, M. Nchabeleng, M. Sebe, N. Singh, P. Kotze, S. Kassim, T. Dubula, V. Naicker, W. Brumskine, C. N. Ncayiya, A. M. Ward, N. Garrett, G. Kistnasami, Z. Gaffoor, P. Selepe, P. B. Makhoba, M. P. Mathebula, P. Mda, T. Adonis, K. S. Mapetla, B. Modibedi, T. Philip, G. Kobane, C. Bentley, S. Ramirez, S. Takuva, M. Jones, M. Sikhosana, M. Atujuna, M. Andrasik, N. S. Hejazi, A. Puren, L. Wiesner, S. Phogat, C. Diaz Granados, M. Koutsoukos, O. Van Der Meeren, S. W. Barnett, N. Kanesa-Thasan, J. G. Kublin, M. J. McElrath, P. B. Gilbert, H. Janes, and L. Corey. 2021. 'Vaccine Efficacy of ALVAC-HIV and Bivalent Subtype C gp120-MF59 in Adults', *N Engl J Med*, 384: 1089-100.

Griffith, Sarah A., and Laura E. McCoy. 2021. 'To bnAb or Not to bnAb: Defining Broadly Neutralising Antibodies Against HIV-1', *Frontiers in Immunology*, 12.

Guadalupe, M., E. Reay, S. Sankaran, T. Prindiville, J. Flamm, A. McNeil, and S. Dandekar. 2003. 'Severe CD4+ T-cell depletion in gut lymphoid tissue during primary human immunodeficiency virus type 1 infection and substantial delay in restoration following highly active antiretroviral therapy', *J Virol*, 77: 11708-17.

Gupta, Ravindra K., Sultan Abdul-Jawad, Laura E. McCoy, Hoi Ping Mok, Dimitra Peppa, Maria Salgado, Javier Martinez-Picado, Monique Nijhuis, Annemarie M. J. Wensing, Helen Lee, Paul Grant, Eleni Nastouli, Jonathan Lambert, Matthew Pace, Fanny Salasc, Christopher Monit, Andrew J. Innes, Luke Muir, Laura Waters, John Frater, Andrew M. L. Lever, Simon G. Edwards, Ian H. Gabriel, and Eduardo Olavarria. 2019. 'HIV-1 remission following CCR5Δ32/Δ32 haematopoietic stem-cell transplantation', *Nature*, 568: 244-48.

Gupta, Ravindra Kumar, Dimitra Peppa, Alison L. Hill, Cristina Gálvez, Maria Salgado, Matthew Pace, Laura E. McCoy, Sarah A. Griffith, John Thornhill, Aljawharah Alrubayyi, Laura E. P. Huyveneers, Eleni Nastouli, Paul Grant, Simon G. Edwards, Andrew J. Innes, John Frater, Monique Nijhuis, Anne Marie J. Wensing, Javier Martinez-Picado, and Eduardo Olavarria. 2020. 'Evidence for HIV-1 cure after CCR5Δ32/Δ32 allogeneic haemopoietic stem-cell transplantation 30 months post analytical treatment interruption: a case report', *The Lancet HIV*, 7: e340-e47.

Haffar, O. K., D. J. Dowbenko, and P. W. Berman. 1988. 'Topogenic analysis of the human immunodeficiency virus type 1 envelope glycoprotein, gp160, in microsomal membranes', *J Cell Biol*, 107: 1677-87.

Haim, Hillel, Ignacio Salas, and Joseph Sodroski. 2013. 'Proteolytic Processing of the Human Immunodeficiency Virus Envelope Glycoprotein Precursor Decreases Conformational Flexibility', *Journal of Virology*, 87: 1884-89.

Halverson, R., R. M. Torres, and R. Pelanda. 2004. 'Receptor editing is the main mechanism of B cell tolerance toward membrane antigens', *Nat Immunol*, 5: 645-50.

Hammer, S. M., M. E. Sobieszczyk, H. Janes, S. T. Karuna, M. J. Mulligan, D. Grove, B. A. Koblin, S. P. Buchbinder, M. C. Keefer, G. D. Tomaras, N. Frahm, J. Hural, C. Anude, B. S. Graham, M. E. Enama, E. Adams, E. DeJesus, R. M. Novak, I. Frank, C. Bentley, S. Ramirez, R. Fu, R. A. Koup, J. R. Mascola, G. J. Nabel, D. C. Montefiori, J. Kublin, M. J. McElrath, L. Corey, and P. B. Gilbert. 2013. 'Efficacy trial of a DNA/rAd5 HIV-1 preventive vaccine', *N Engl J Med*, 369: 2083-92.

Han, Q., J. A. Jones, N. I. Nicely, R. K. Reed, X. Shen, K. Mansouri, M. Louder, A. M. Trama, S. M. Alam, R. J. Edwards, M. Bonsignori, G. D. Tomaras, B. Korber, D. C. Montefiori, J. R. Mascola, M. S. Seaman, B. F. Haynes, and K. O. Saunders. 2019. 'Difficult-to-neutralize global HIV-1 isolates are neutralized by antibodies targeting open envelope conformations', *Nat Commun*, 10: 2898.

Havenar-Daughton, C., D. G. Carnathan, A. Torrents de la Peña, M. Pauthner, B. Briney, S. M. Reiss, J. S. Wood, K. Kaushik, M. J. van Gils, S. L. Rosales, P. van der Woude, M. Locci, K. M. Le, S. W. de Taeye, D. Sok, A. U. R. Mohammed, J. Huang, S. Gumber, A. Garcia, S. P. Kasturi, B. Pulendran, J. P. Moore, R. Ahmed, G. Seumois, D. R. Burton, R. W. Sanders, G. Silvestri, and S. Crotty. 2016. 'Direct Probing of Germinal Center Responses Reveals Immunological Features and Bottlenecks for Neutralizing Antibody Responses to HIV Env Trimer', *Cell Rep*, 17: 2195-209.

Havenar-Daughton, C., M. Lindqvist, A. Heit, J. E. Wu, S. M. Reiss, K. Kendric, S. Bélanger, S. P. Kasturi, E. Landais, R. S. Akondy, H. M. McGuire, M. Bothwell, P. A. Vagefi, E. Scully, G. D. Tomaras, M. M. Davis, P. Poignard, R. Ahmed, B. D. Walker, B. Pulendran, M. J. McElrath, D. E. Kaufmann, and S. Crotty. 2016. 'CXCL13 is a plasma biomarker of germinal center activity', *Proc Natl Acad Sci U S A*, 113: 2702-7.

Haynes, B. F., J. Fleming, E. W. St Clair, H. Katinger, G. Stiegler, R. Kunert, J. Robinson, R. M. Scearce, K. Plonk, H. F. Staats, T. L. Ortel, H. X. Liao, and S. M. Alam. 2005. 'Cardiolipin polyspecific autoreactivity in two broadly neutralizing HIV-1 antibodies', *Science*, 308: 1906-8.

Haynes, B. F., P. B. Gilbert, M. J. McElrath, S. Zolla-Pazner, G. D. Tomaras, S. M. Alam, D. T. Evans, D. C. Montefiori, C. Karnasuta, R. Sutthent, H. X. Liao, A. L. DeVico, G. K. Lewis, C. Williams, A. Pinter, Y. Fong, H. Janes, A. DeCamp, Y. Huang, M. Rao, E. Billings, N. Karasavvas, M. L. Robb, V. Ngauy, M. S. de Souza, R. Paris, G. Ferrari, R. T. Bailer, K. A. Soderberg, C. Andrews, P. W. Berman, N. Frahm, S. C. De Rosa, M. D. Alpert, N. L. Yates, X. Shen, R. A. Koup, P. Pitisuttithum, J.

Kaewkungwal, S. Nitayaphan, S. Rerks-Ngarm, N. L. Michael, and J. H. Kim. 2012. 'Immune-correlates analysis of an HIV-1 vaccine efficacy trial', *N Engl J Med*, 366: 1275-86.

He, B., X. Qiao, P. J. Klasse, A. Chiu, A. Chadburn, D. M. Knowles, J. P. Moore, and A. Cerutti. 2006. 'HIV-1 envelope triggers polyclonal Ig class switch recombination through a CD40-independent mechanism involving BAFF and C-type lectin receptors', *J Immunol*, 176: 3931-41.

Hemelaar, J. 2012. 'The origin and diversity of the HIV-1 pandemic', *Trends Mol Med*, 18: 182-92.

Hemelaar, J., R. Elangovan, J. Yun, L. Dickson-Tetteh, I. Fleminger, S. Kirtley, B. Williams, E. Gouws-Williams, and P. D. Ghys. 2019. 'Global and regional molecular epidemiology of HIV-1, 1990-2015: a systematic review, global survey, and trend analysis', *Lancet Infect Dis*, 19: 143-55.

Hemelaar, J., E. Gouws, P. D. Ghys, and S. Osmanov. 2011. 'Global trends in molecular epidemiology of HIV-1 during 2000-2007', *Aids*, 25: 679-89.

Henrich, Timothy J., Hiroyu Hatano, Oliver Bacon, Louise E. Hogan, Rachel Rutishauser, Alison Hill, Mary F. Kearney, Elizabeth M. Anderson, Susan P. Buchbinder, Stephanie E. Cohen, Mohamed Abdel-Mohsen, Christopher W. Pohlmeyer, Remi Fromentin, Rebecca Hoh, Albert Y. Liu, Joseph M. McCune, Jonathan Spindler, Kelly Metcalf-Pate, Kristen S. Hobbs, Cassandra Thanh, Erica A. Gibson, Daniel R. Kuritzkes, Robert F. Siliciano, Richard W. Price, Douglas D. Richman, Nicolas Chomont, Janet D. Siliciano, John W. Mellors, Steven A. Yukl, Joel N. Blankson, Teri Liegler, and Steven G. Deeks. 2017. 'HIV-1 persistence following extremely early initiation of antiretroviral therapy (ART) during acute HIV-1 infection: An observational study', *PLOS Medicine*, 14: e1002417.

Hermansen, Johanne U., Geir E. Tjønnfjord, Ludvig A. Munthe, Kjetil Taskén, and Sigrid S. Skånland. 2018. 'Cryopreservation of primary B cells minimally influences their signaling responses', *Scientific Reports*, 8: 17651.

Hess, J., A. Werner, T. Wirth, F. Melchers, H. M. Jäck, and T. H. Winkler. 2001. 'Induction of pre-B cell proliferation after de novo synthesis of the pre-B cell receptor', *Proc Natl Acad Sci U S A*, 98: 1745-50.

Hieter, P. A., J. V. Maizel, and P. Leder. 1982. 'Evolution of human immunoglobulin kappa J region genes', *Journal of Biological Chemistry*, 257: 1516-22.

Hioe, C. E., T. Wrin, M. S. Seaman, X. Yu, B. Wood, S. Self, C. Williams, M. K. Gorny, and S. Zolla-Pazner. 2010. 'Anti-V3 monoclonal antibodies display broad neutralizing activities against multiple HIV-1 subtypes', *PLoS One*, 5: e10254.

Hogarth, P. Mark. 2015. 'Fc Receptors: Introduction', *Immunological Reviews*, 268: 1-5.

Holla, Prasida, Brian Dizon, Abhijit A. Ambegaonkar, Noga Rogel, Ella Goldschmidt, Arun K. Boddapati, Haewon Sohn, Dan Sturdevant, James W. Austin, Lela Kardava, Li Yuesheng, Poching Liu, Susan Moir, Susan K. Pierce, and Asaf Madi. 2021. 'Shared transcriptional profiles

of atypical B cells suggest common drivers of expansion and function in malaria, HIV, and autoimmunity', *Science Advances*, 7: eabg8384.
Hoogenboom, Hennie R. 2005. 'Selecting and screening recombinant antibody libraries', *Nature Biotechnology*, 23: 1105-16.
Hoot, S., A. T. McGuire, K. W. Cohen, R. K. Strong, L. Hangartner, F. Klein, R. Diskin, J. F. Scheid, D. N. Sather, D. R. Burton, and L. Stamatatos. 2013. 'Recombinant HIV envelope proteins fail to engage germline versions of anti-CD4bs bNAbs', *PLoS Pathog*, 9: e1003106.
Hraber, P., B. T. Korber, A. S. Lapedes, R. T. Bailer, M. S. Seaman, H. Gao, K. M. Greene, F. McCutchan, C. Williamson, J. H. Kim, S. Tovanabutra, B. H. Hahn, R. Swanstrom, M. M. Thomson, F. Gao, L. Harris, E. Giorgi, N. Hengartner, T. Bhattacharya, J. R. Mascola, and D. C. Montefiori. 2014. 'Impact of clade, geography, and age of the epidemic on HIV-1 neutralization by antibodies', *J Virol*, 88: 12623-43.
Hu, Q., T. Xu, W. Zhang, and C. Huang. 2022. 'Bach2 regulates B cell survival to maintain germinal centers and promote B cell memory', *Biochem Biophys Res Commun*, 618: 86-92.
Huang, C. C., M. Tang, M. Y. Zhang, S. Majeed, E. Montabana, R. L. Stanfield, D. S. Dimitrov, B. Korber, J. Sodroski, I. A. Wilson, R. Wyatt, and P. D. Kwong. 2005. 'Structure of a V3-containing HIV-1 gp120 core', *Science*, 310: 1025-8.
Huang, J., B. H. Kang, E. Ishida, T. Zhou, T. Griesman, Z. Sheng, F. Wu, N. A. Doria-Rose, B. Zhang, K. McKee, S. O'Dell, G. Y. Chuang, A. Druz, I. S. Georgiev, C. A. Schramm, A. Zheng, M. G. Joyce, M. Asokan, A. Ransier, S. Darko, S. A. Migueles, R. T. Bailer, M. K. Louder, S. M. Alam, R. Parks, G. Kelsoe, T. Von Holle, B. F. Haynes, D. C. Douek, V. Hirsch, M. S. Seaman, L. Shapiro, J. R. Mascola, P. D. Kwong, and M. Connors. 2016. 'Identification of a CD4-Binding-Site Antibody to HIV that Evolved Near-Pan Neutralization Breadth', *Immunity*, 45: 1108-21.
Huang, J., B. H. Kang, M. Pancera, J. H. Lee, T. Tong, Y. Feng, H. Imamichi, I. S. Georgiev, G. Y. Chuang, A. Druz, N. A. Doria-Rose, L. Laub, K. Sliepen, M. J. van Gils, A. T. de la Peña, R. Derking, P. J. Klasse, S. A. Migueles, R. T. Bailer, M. Alam, P. Pugach, B. F. Haynes, R. T. Wyatt, R. W. Sanders, J. M. Binley, A. B. Ward, J. R. Mascola, P. D. Kwong, and M. Connors. 2014. 'Broad and potent HIV-1 neutralization by a human antibody that binds the gp41-gp120 interface', *Nature*, 515: 138-42.
Huang, Jinghe, Nicole A. Doria-Rose, Nancy S. Longo, Leo Laub, Chien-Li Lin, Ellen Turk, Byong H. Kang, Stephen A. Migueles, Robert T. Bailer, John R. Mascola, and Mark Connors. 2013. 'Isolation of human monoclonal antibodies from peripheral blood B cells', *Nature Protocols*, 8: 1907-15.
Huang, W., S. H. Eshleman, J. Toma, S. Fransen, E. Stawiski, E. E. Paxinos, J. M. Whitcomb, A. M. Young, D. Donnell, F. Mmiro, P. Musoke, L. A. Guay, J. B. Jackson, N. T. Parkin, and C. J. Petropoulos. 2007. 'Coreceptor tropism in human immunodeficiency virus type 1 subtype D: high prevalence of CXCR4 tropism and heterogeneous composition of viral populations', *J Virol*, 81: 7885-93.

Ignatovich, Olga, Ian M. Tomlinson, Peter T. Jones, and Greg Winter. 1997. 'The creation of diversity in the human immunoglobulin Vλ repertoire11Edited by J. Karn', *Journal of Molecular Biology*, 268: 69-77.

IJspeert, H, P. A. van Schouwenburg, D. van Zessen, I. Pico-Knijnenburg, G. J. Driessen, A. P. Stubbs, and M. van der Burg. 2016. 'Evaluation of the Antigen-Experienced B-Cell Receptor Repertoire in Healthy Children and Adults', *Front Immunol*, 7: 410.

Islam, Saiful, Amit Zeisel, Simon Joost, Gioele La Manno, Pawel Zajac, Maria Kasper, Peter Lönnerberg, and Sten Linnarsson. 2014. 'Quantitative single-cell RNA-seq with unique molecular identifiers', *Nature Methods*, 11: 163-66.

Ivan, B., Z. Sun, H. Subbaraman, N. Friedrich, and A. Trkola. 2019. 'CD4 occupancy triggers sequential pre-fusion conformational states of the HIV-1 envelope trimer with relevance for broadly neutralizing antibody activity', *PLoS Biol*, 17: e3000114.

Jaitin, D. A., E. Kenigsberg, H. Keren-Shaul, N. Elefant, F. Paul, I. Zaretsky, A. Mildner, N. Cohen, S. Jung, A. Tanay, and I. Amit. 2014. 'Massively parallel single-cell RNA-seq for marker-free decomposition of tissues into cell types', *Science*, 343: 776-9.

Jaitin, Diego Adhemar, Hadas Keren-Shaul, Naama Elefant, and Ido Amit. 2015. 'Each cell counts: Hematopoiesis and immunity research in the era of single cell genomics', *Seminars in Immunology*, 27: 67-71.

Jardine, J. G., D. W. Kulp, C. Havenar-Daughton, A. Sarkar, B. Briney, D. Sok, F. Sesterhenn, J. Ereño-Orbea, O. Kalyuzhniy, I. Deresa, X. Hu, S. Spencer, M. Jones, E. Georgeson, Y. Adachi, M. Kubitz, A. C. deCamp, J. P. Julien, I. A. Wilson, D. R. Burton, S. Crotty, and W. R. Schief. 2016. 'HIV-1 broadly neutralizing antibody precursor B cells revealed by germline-targeting immunogen', *Science*, 351: 1458-63.

Jardine, J. G., T. Ota, D. Sok, M. Pauthner, D. W. Kulp, O. Kalyuzhniy, P. D. Skog, T. C. Thinnes, D. Bhullar, B. Briney, S. Menis, M. Jones, M. Kubitz, S. Spencer, Y. Adachi, D. R. Burton, W. R. Schief, and D. Nemazee. 2015. 'HIV-1 VACCINES. Priming a broadly neutralizing antibody response to HIV-1 using a germline-targeting immunogen', *Science*, 349: 156-61.

Jardine, J., J. P. Julien, S. Menis, T. Ota, O. Kalyuzhniy, A. McGuire, D. Sok, P. S. Huang, S. MacPherson, M. Jones, T. Nieusma, J. Mathison, D. Baker, A. B. Ward, D. R. Burton, L. Stamatatos, D. Nemazee, I. A. Wilson, and W. R. Schief. 2013. 'Rational HIV immunogen design to target specific germline B cell receptors', *Science*, 340: 711-6.

Jeong, Seong-In, Jung-Wook Kim, Kyung-Phil Ko, Byung-Kyu Ryu, Min-Goo Lee, Hyo-Jong Kim, and Sung-Gil Chi. 2018. 'XAF1 forms a positive feedback loop with IRF-1 to drive apoptotic stress response and suppress tumorigenesis', *Cell Death & Disease*, 9: 806.

Johnson, G., and T. T. Wu. 1998. 'Preferred CDRH3 lengths for antibodies with defined specificities', *Int Immunol*, 10: 1801-5.

Jolly, C., K. Kashefi, M. Hollinshead, and Q. J. Sattentau. 2004. 'HIV-1 cell to cell transfer across an Env-induced, actin-dependent synapse', *J Exp Med*, 199: 283-93.

Jolly, C., and Q. J. Sattentau. 2004. 'Retroviral spread by induction of virological synapses', *Traffic*, 5: 643-50.

Jones, P. L., T. Korte, and R. Blumenthal. 1998. 'Conformational changes in cell surface HIV-1 envelope glycoproteins are triggered by cooperation between cell surface CD4 and co-receptors', *J Biol Chem*, 273: 404-9.

Julg, B., and D. H. Barouch. 2019. 'Neutralizing antibodies for HIV-1 prevention', *Curr Opin HIV AIDS*, 14: 318-24.

Julg, B., P. T. Liu, K. Wagh, W. M. Fischer, P. Abbink, N. B. Mercado, J. B. Whitney, J. P. Nkolola, K. McMahan, L. J. Tartaglia, E. N. Borducchi, S. Khatiwada, M. Kamath, J. A. LeSuer, M. S. Seaman, S. D. Schmidt, J. R. Mascola, D. R. Burton, B. T. Korber, and D. H. Barouch. 2017. 'Protection against a mixed SHIV challenge by a broadly neutralizing antibody cocktail', *Sci Transl Med*, 9.

Julg, Boris, Kathryn E. Stephenson, Kshitij Wagh, Sabrina C. Tan, Rebecca Zash, Stephen Walsh, Jessica Ansel, Diane Kanjilal, Joseph Nkolola, Victoria E. K. Walker-Sperling, Jasper Ophel, Katherine Yanosick, Erica N. Borducchi, Lori Maxfield, Peter Abbink, Lauren Peter, Nicole L. Yates, Martina S. Wesley, Tom Hassell, Huub C. Gelderblom, Allen deCamp, Bryan T. Mayer, Alicia Sato, Monica W. Gerber, Elena E. Giorgi, Lucio Gama, Richard A. Koup, John R. Mascola, Ana Monczor, Sofia Lupo, Charlotte-Paige Rolle, Roberto Arduino, Edwin DeJesus, Georgia D. Tomaras, Michael S. Seaman, Bette Korber, and Dan H. Barouch. 2022. 'Safety and antiviral activity of triple combination broadly neutralizing monoclonal antibody therapy against HIV-1: a phase 1 clinical trial', *Nature Medicine*, 28: 1288-96.

Julien, J. P., A. Cupo, D. Sok, R. L. Stanfield, D. Lyumkis, M. C. Deller, P. J. Klasse, D. R. Burton, R. W. Sanders, J. P. Moore, A. B. Ward, and I. A. Wilson. 2013. 'Crystal structure of a soluble cleaved HIV-1 envelope trimer', *Science*, 342: 1477-83.

Julien, J. P., D. Sok, R. Khayat, J. H. Lee, K. J. Doores, L. M. Walker, A. Ramos, D. C. Diwanji, R. Pejchal, A. Cupo, U. Katpally, R. S. Depetris, R. L. Stanfield, R. McBride, A. J. Marozsan, J. C. Paulson, R. W. Sanders, J. P. Moore, D. R. Burton, P. Poignard, A. B. Ward, and I. A. Wilson. 2013. 'Broadly neutralizing antibody PGT121 allosterically modulates CD4 binding via recognition of the HIV-1 gp120 V3 base and multiple surrounding glycans', *PLoS Pathog*, 9: e1003342.

Kapembwa, M. S., S. C. Fleming, N. Sewankambo, D. Serwadda, S. Lucas, A. Moody, and G. E. Griffin. 1991. 'Altered small-intestinal permeability associated with diarrhoea in human-immunodeficiency-virus-infected Caucasian and African subjects', *Clin Sci (Lond)*, 81: 327-34.

Kardava, Lela, Susan Moir, Naisha Shah, Wei Wang, Richard Wilson, Clarisa M. Buckner, Brian H. Santich, Leo J. Y. Kim, Emily E. Spurlin, Amy K. Nelson, Adam K. Wheatley, Christopher J. Harvey, Adrian B. McDermott, Kai W. Wucherpfennig, Tae-Wook Chun, John S. Tsang, Yuxing Li, and Anthony S. Fauci. 2014. 'Abnormal B cell memory subsets dominate HIV-specific responses in infected individuals', *The Journal of Clinical Investigation*, 124: 3252-62.

Kepler, T. B., H. X. Liao, S. M. Alam, R. Bhaskarabhatla, R. Zhang, C. Yandava, S. Stewart, K. Anasti, G. Kelsoe, R. Parks, K. E. Lloyd, C.

Stolarchuk, J. Pritchett, E. Solomon, E. Friberg, L. Morris, S. S. Karim, M. S. Cohen, E. Walter, M. A. Moody, X. Wu, H. R. Altae-Tran, I. S. Georgiev, P. D. Kwong, S. D. Boyd, A. Z. Fire, J. R. Mascola, and B. F. Haynes. 2014. 'Immunoglobulin gene insertions and deletions in the affinity maturation of HIV-1 broadly reactive neutralizing antibodies', *Cell Host Microbe*, 16: 304-13.

Kiepiela, P., K. Ngumbela, C. Thobakgale, D. Ramduth, I. Honeyborne, E. Moodley, S. Reddy, C. de Pierres, Z. Mncube, N. Mkhwanazi, K. Bishop, M. van der Stok, K. Nair, N. Khan, H. Crawford, R. Payne, A. Leslie, J. Prado, A. Prendergast, J. Frater, N. McCarthy, C. Brander, G. H. Learn, D. Nickle, C. Rousseau, H. Coovadia, J. I. Mullins, D. Heckerman, B. D. Walker, and P. Goulder. 2007. 'CD8+ T-cell responses to different HIV proteins have discordant associations with viral load', *Nat Med*, 13: 46-53.

Kikuchi, Kazu, Anne Y. Lai, Chia-Lin Hsu, and Motonari Kondo. 2005. 'IL-7 receptor signaling is necessary for stage transition in adult B cell development through up-regulation of EBF', *Journal of Experimental Medicine*, 201: 1197-203.

Kim, A. S., D. P. Leaman, and M. B. Zwick. 2014. 'Antibody to gp41 MPER alters functional properties of HIV-1 Env without complete neutralization', *PLoS Pathog*, 10: e1004271.

King, H. W., N. Orban, J. C. Riches, A. J. Clear, G. Warnes, S. A. Teichmann, and L. K. James. 2021. 'Single-cell analysis of human B cell maturation predicts how antibody class switching shapes selection dynamics', *Sci Immunol*, 6.

Klein, F., R. Diskin, J. F. Scheid, C. Gaebler, H. Mouquet, I. S. Georgiev, M. Pancera, T. Zhou, R. B. Incesu, B. Z. Fu, P. N. Gnanapragasam, T. Y. Oliveira, M. S. Seaman, P. D. Kwong, P. J. Bjorkman, and M. C. Nussenzweig. 2013. 'Somatic mutations of the immunoglobulin framework are generally required for broad and potent HIV-1 neutralization', *Cell*, 153: 126-38.

Klein, F., C. Gaebler, H. Mouquet, D. N. Sather, C. Lehmann, J. F. Scheid, Z. Kraft, Y. Liu, J. Pietzsch, A. Hurley, P. Poignard, T. Feizi, L. Morris, B. D. Walker, G. Fätkenheuer, M. S. Seaman, L. Stamatatos, and M. C. Nussenzweig. 2012. 'Broad neutralization by a combination of antibodies recognizing the CD4 binding site and a new conformational epitope on the HIV-1 envelope protein', *J Exp Med*, 209: 1469-79.

Knox, James J., Marcus Buggert, Lela Kardava, Kelly E. Seaton, Michael A. Eller, David H. Canaday, Merlin L. Robb, Mario A. Ostrowski, Steven G. Deeks, Mark K. Slifka, Georgia D. Tomaras, Susan Moir, M. Anthony Moody, and Michael R. Betts. 2017. 'T-bet+ B cells are induced by human viral infections and dominate the HIV gp140 response', *JCI Insight*, 2.

KÖhler, G., and C. Milstein. 1975. 'Continuous cultures of fused cells secreting antibody of predefined specificity', *Nature*, 256: 495-97.

Kong, R., M. K. Louder, K. Wagh, R. T. Bailer, A. deCamp, K. Greene, H. Gao, J. D. Taft, A. Gazumyan, C. Liu, M. C. Nussenzweig, B. Korber, D. C. Montefiori, and J. R. Mascola. 2015. 'Improving neutralization potency

and breadth by combining broadly reactive HIV-1 antibodies targeting major neutralization epitopes', *J Virol*, 89: 2659-71.

Kong, R., K. Xu, T. Zhou, P. Acharya, T. Lemmin, K. Liu, G. Ozorowski, C. Soto, J. D. Taft, R. T. Bailer, E. M. Cale, L. Chen, C. W. Choi, G. Y. Chuang, N. A. Doria-Rose, A. Druz, I. S. Georgiev, J. Gorman, J. Huang, M. G. Joyce, M. K. Louder, X. Ma, K. McKee, S. O'Dell, M. Pancera, Y. Yang, S. C. Blanchard, W. Mothes, D. R. Burton, W. C. Koff, M. Connors, A. B. Ward, P. D. Kwong, and J. R. Mascola. 2016. 'Fusion peptide of HIV-1 as a site of vulnerability to neutralizing antibody', *Science*, 352: 828-33.

Kouyos, R. D., P. Rusert, C. Kadelka, M. Huber, A. Marzel, H. Ebner, M. Schanz, T. Liechti, N. Friedrich, D. L. Braun, A. U. Scherrer, J. Weber, T. Uhr, N. S. Baumann, C. Leemann, H. Kuster, J. P. Chave, M. Cavassini, E. Bernasconi, M. Hoffmann, A. Calmy, M. Battegay, A. Rauch, S. Yerly, V. Aubert, T. Klimkait, J. Böni, K. J. Metzner, H. F. Günthard, and A. Trkola. 2018. 'Tracing HIV-1 strains that imprint broadly neutralizing antibody responses', *Nature*, 561: 406-10.

Krachmarov, C. P., W. J. Honnen, S. C. Kayman, M. K. Gorny, S. Zolla-Pazner, and A. Pinter. 2006. 'Factors determining the breadth and potency of neutralization by V3-specific human monoclonal antibodies derived from subjects infected with clade A or clade B strains of human immunodeficiency virus type 1', *J Virol*, 80: 7127-35.

Kräutler, N. J., D. Suan, D. Butt, K. Bourne, J. R. Hermes, T. D. Chan, C. Sundling, W. Kaplan, P. Schofield, J. Jackson, A. Basten, D. Christ, and R. Brink. 2017. 'Differentiation of germinal center B cells into plasma cells is initiated by high-affinity antigen and completed by Tfh cells', *J Exp Med*, 214: 1259-67.

Krebs, S. J., Y. D. Kwon, C. A. Schramm, W. H. Law, G. Donofrio, K. H. Zhou, S. Gift, V. Dussupt, I. S. Georgiev, S. Schätzle, J. R. McDaniel, Y. T. Lai, M. Sastry, B. Zhang, M. C. Jarosinski, A. Ransier, A. L. Chenine, M. Asokan, R. T. Bailer, M. Bose, A. Cagigi, E. M. Cale, G. Y. Chuang, S. Darko, J. I. Driscoll, A. Druz, J. Gorman, F. Laboune, M. K. Louder, K. McKee, L. Mendez, M. A. Moody, A. M. O'Sullivan, C. Owen, D. Peng, R. Rawi, E. Sanders-Buell, C. H. Shen, A. R. Shiakolas, T. Stephens, Y. Tsybovsky, C. Tucker, R. Verardi, K. Wang, J. Zhou, T. Zhou, G. Georgiou, S. M. Alam, B. F. Haynes, M. Rolland, G. R. Matyas, V. R. Polonis, A. B. McDermott, D. C. Douek, L. Shapiro, S. Tovanabutra, N. L. Michael, J. R. Mascola, M. L. Robb, P. D. Kwong, and N. A. Doria-Rose. 2019. 'Longitudinal Analysis Reveals Early Development of Three MPER-Directed Neutralizing Antibody Lineages from an HIV-1-Infected Individual', *Immunity*, 50: 677-91.e13.

Kurimoto, K., Y. Yabuta, Y. Ohinata, Y. Ono, K. D. Uno, R. G. Yamada, H. R. Ueda, and M. Saitou. 2006. 'An improved single-cell cDNA amplification method for efficient high-density oligonucleotide microarray analysis', *Nucleic Acids Res*, 34: e42.

Kwong, Peter D., Richard Wyatt, James Robinson, Raymond W. Sweet, Joseph Sodroski, and Wayne A. Hendrickson. 1998. 'Structure of an HIV gp120 envelope glycoprotein in complex with the CD4 receptor and a neutralizing human antibody', *Nature*, 393: 648-59.

Laidlaw, B. J., J. E. Craft, and S. M. Kaech. 2016. 'The multifaceted role of CD4(+) T cells in CD8(+) T cell memory', *Nat Rev Immunol*, 16: 102-11.

Laidlaw, B. J., T. H. Schmidt, J. A. Green, C. D. Allen, T. Okada, and J. G. Cyster. 2017. 'The Eph-related tyrosine kinase ligand Ephrin-B1 marks germinal center and memory precursor B cells', *J Exp Med*, 214: 639-49.

Lambotte, O., F. Boufassa, Y. Madec, A. Nguyen, C. Goujard, L. Meyer, C. Rouzioux, A. Venet, and J. F. Delfraissy. 2005. 'HIV controllers: a homogeneous group of HIV-1-infected patients with spontaneous control of viral replication', *Clin Infect Dis*, 41: 1053-6.

Landais, E., X. Huang, C. Havenar-Daughton, B. Murrell, M. A. Price, L. Wickramasinghe, A. Ramos, C. B. Bian, M. Simek, S. Allen, E. Karita, W. Kilembe, S. Lakhi, M. Inambao, A. Kamali, E. J. Sanders, O. Anzala, V. Edward, L. G. Bekker, J. Tang, J. Gilmour, S. L. Kosakovsky-Pond, P. Phung, T. Wrin, S. Crotty, A. Godzik, and P. Poignard. 2016. 'Broadly Neutralizing Antibody Responses in a Large Longitudinal Sub-Saharan HIV Primary Infection Cohort', *PLoS Pathog*, 12: e1005369.

Lane, H. C., H. Masur, L. C. Edgar, G. Whalen, A. H. Rook, and A. S. Fauci. 1983. 'Abnormalities of B-cell activation and immunoregulation in patients with the acquired immunodeficiency syndrome', *N Engl J Med*, 309: 453-8.

'LANL Sequence Database'.

Larimore, K., M. W. McCormick, H. S. Robins, and P. D. Greenberg. 2012. 'Shaping of human germline IgH repertoires revealed by deep sequencing', *J Immunol*, 189: 3221-30.

Lee, J. H., D. P. Leaman, A. S. Kim, A. Torrents de la Peña, K. Sliepen, A. Yasmeen, R. Derking, A. Ramos, S. W. de Taeye, G. Ozorowski, F. Klein, D. R. Burton, M. C. Nussenzweig, P. Poignard, J. P. Moore, P. J. Klasse, R. W. Sanders, M. B. Zwick, I. A. Wilson, and A. B. Ward. 2015. 'Antibodies to a conformational epitope on gp41 neutralize HIV-1 by destabilizing the Env spike', *Nat Commun*, 6: 8167.

Lee, J. H., H. J. Sutton, C. A. Cottrell, I. Phung, G. Ozorowski, L. M. Sewall, R. Nedellec, C. Nakao, M. Silva, S. T. Richey, J. L. Torres, W. H. Lee, E. Georgeson, M. Kubitz, S. Hodges, T. M. Mullen, Y. Adachi, K. M. Cirelli, A. Kaur, C. Allers, M. Fahlberg, B. F. Grasperge, J. P. Dufour, F. Schiro, P. P. Aye, O. Kalyuzhniy, A. Liguori, D. G. Carnathan, G. Silvestri, X. Shen, D. C. Montefiori, R. S. Veazey, A. B. Ward, L. Hangartner, D. R. Burton, D. J. Irvine, W. R. Schief, and S. Crotty. 2022. 'Long-primed germinal centres with enduring affinity maturation and clonal migration', *Nature*, 609: 998-1004.

Lee, Jaewoong, Mark E. Robinson, Ning Ma, Dewan Artadji, Mohamed A. Ahmed, Gang Xiao, Teresa Sadras, Gauri Deb, Janet Winchester, Kadriye Nehir Cosgun, Huimin Geng, Lai N. Chan, Kohei Kume, Teemu P. Miettinen, Ye Zhang, Matthew A. Nix, Lars Klemm, Chun Wei Chen, Jianjun Chen, Vishal Khairnar, Arun P. Wiita, Andrei Thomas-Tikhonenko, Michael Farzan, Jae U. Jung, David M. Weinstock, Scott R. Manalis, Michael S. Diamond, Nagarajan Vaidehi, and Markus

Müschen. 2020. 'IFITM3 functions as a PIP3 scaffold to amplify PI3K signalling in B cells', *Nature*, 588: 491-97.

Lefranc, Marie-Paule, Véronique Giudicelli, Patrice Duroux, Joumana Jabado-Michaloud, Géraldine Folch, Safa Aouinti, Emilie Carillon, Hugo Duvergey, Amélie Houles, Typhaine Paysan-Lafosse, Saida Hadi-Saljoqi, Souphatta Sasorith, Gérard Lefranc, and Sofia Kossida. 2015. 'IMGT®, the international ImMunoGeneTics information system® 25 years on', *Nucleic Acids Research*, 43: D413-D22.

Li, Bo, and Colin N. Dewey. 2011. 'RSEM: accurate transcript quantification from RNA-Seq data with or without a reference genome', *BMC Bioinformatics*, 12: 323.

Liao, H. X., M. Bonsignori, S. M. Alam, J. S. McLellan, G. D. Tomaras, M. A. Moody, D. M. Kozink, K. K. Hwang, X. Chen, C. Y. Tsao, P. Liu, X. Lu, R. J. Parks, D. C. Montefiori, G. Ferrari, J. Pollara, M. Rao, K. K. Peachman, S. Santra, N. L. Letvin, N. Karasavvas, Z. Y. Yang, K. Dai, M. Pancera, J. Gorman, K. Wiehe, N. I. Nicely, S. Rerks-Ngarm, S. Nitayaphan, J. Kaewkungwal, P. Pitisuttithum, J. Tartaglia, F. Sinangil, J. H. Kim, N. L. Michael, T. B. Kepler, P. D. Kwong, J. R. Mascola, G. J. Nabel, A. Pinter, S. Zolla-Pazner, and B. F. Haynes. 2013. 'Vaccine induction of antibodies against a structurally heterogeneous site of immune pressure within HIV-1 envelope protein variable regions 1 and 2', *Immunity*, 38: 176-86.

Liao, H. X., R. Lynch, T. Zhou, F. Gao, S. M. Alam, S. D. Boyd, A. Z. Fire, K. M. Roskin, C. A. Schramm, Z. Zhang, J. Zhu, L. Shapiro, J. C. Mullikin, S. Gnanakaran, P. Hraber, K. Wiehe, G. Kelsoe, G. Yang, S. M. Xia, D. C. Montefiori, R. Parks, K. E. Lloyd, R. M. Scearce, K. A. Soderberg, M. Cohen, G. Kamanga, M. K. Louder, L. M. Tran, Y. Chen, F. Cai, S. Chen, S. Moquin, X. Du, M. G. Joyce, S. Srivatsan, B. Zhang, A. Zheng, G. M. Shaw, B. H. Hahn, T. B. Kepler, B. T. Korber, P. D. Kwong, J. R. Mascola, and B. F. Haynes. 2013. 'Co-evolution of a broadly neutralizing HIV-1 antibody and founder virus', *Nature*, 496: 469-76.

Liberzon, A., C. Birger, H. Thorvaldsdóttir, M. Ghandi, J. P. Mesirov, and P. Tamayo. 2015. 'The Molecular Signatures Database (MSigDB) hallmark gene set collection', *Cell Syst*, 1: 417-25.

Lin, Y. R., K. R. Parks, C. Weidle, A. S. Naidu, A. Khechaduri, A. O. Riker, B. Takushi, J. H. Chun, A. J. Borst, D. Veesler, A. Stuart, P. Agrawal, M. Gray, M. Pancera, P. S. Huang, and L. Stamatatos. 2020. 'HIV-1 VRC01 Germline-Targeting Immunogens Select Distinct Epitope-Specific B Cell Receptors', *Immunity*, 53: 840-51.e6.

Lindeman, Ida, Guy Emerton, Lira Mamanova, Omri Snir, Krzysztof Polanski, Shuo-Wang Qiao, Ludvig M. Sollid, Sarah A. Teichmann, and Michael J. T. Stubbington. 2018. 'BraCeR: B-cell-receptor reconstruction and clonality inference from single-cell RNA-seq', *Nature Methods*, 15: 563-65.

Liu, M., G. Yang, K. Wiehe, N. I. Nicely, N. A. Vandergrift, W. Rountree, M. Bonsignori, S. M. Alam, J. Gao, B. F. Haynes, and G. Kelsoe. 2015. 'Polyreactivity and autoreactivity among HIV-1 antibodies', *J Virol*, 89: 784-98.

Liu, Y., W. Cao, M. Sun, and T. Li. 2020. 'Broadly neutralizing antibodies for HIV-1: efficacies, challenges and opportunities', *Emerg Microbes Infect*, 9: 194-206.

Locci, M., C. Havenar-Daughton, E. Landais, J. Wu, M. A. Kroenke, C. L. Arlehamn, L. F. Su, R. Cubas, M. M. Davis, A. Sette, E. K. Haddad, P. Poignard, and S. Crotty. 2013. 'Human circulating PD-1+CXCR3-CXCR5+ memory Tfh cells are highly functional and correlate with broadly neutralizing HIV antibody responses', *Immunity*, 39: 758-69.

Lundgren J, Babiker A, Gordin F, Emery S, Grund B, Sharma S, . 2015. 'Initiation of Antiretroviral Therapy in Early Asymptomatic HIV Infection', *New England Journal of Medicine*, 373: 795-807.

Lyles, R. H., A. Muñoz, T. E. Yamashita, H. Bazmi, R. Detels, C. R. Rinaldo, J. B. Margolick, J. P. Phair, and J. W. Mellors. 2000. 'Natural history of human immunodeficiency virus type 1 viremia after seroconversion and proximal to AIDS in a large cohort of homosexual men. Multicenter AIDS Cohort Study', *J Infect Dis*, 181: 872-80.

Lyumkis, Dmitry, Jean-Philippe Julien, Natalia de Val, Albert Cupo, Clinton S. Potter, Per-Johan Klasse, Dennis R. Burton, Rogier W. Sanders, John P. Moore, Bridget Carragher, Ian A. Wilson, and Andrew B. Ward. 2013. 'Cryo-EM Structure of a Fully Glycosylated Soluble Cleaved HIV-1 Envelope Trimer', *Science*, 342: 1484-90.

Mabuka, J. M., A. S. Dugast, D. M. Muema, T. Reddy, Y. Ramlakhan, Z. Euler, N. Ismail, A. Moodley, K. L. Dong, L. Morris, B. D. Walker, G. Alter, and T. Ndung'u. 2017. 'Plasma CXCL13 but Not B Cell Frequencies in Acute HIV Infection Predicts Emergence of Cross-Neutralizing Antibodies', *Front Immunol*, 8: 1104.

MacLeod, D. T., N. M. Choi, B. Briney, F. Garces, L. S. Ver, E. Landais, B. Murrell, T. Wrin, W. Kilembe, C. H. Liang, A. Ramos, C. B. Bian, L. Wickramasinghe, L. Kong, K. Eren, C. Y. Wu, C. H. Wong, S. L. Kosakovsky Pond, I. A. Wilson, D. R. Burton, and P. Poignard. 2016. 'Early Antibody Lineage Diversification and Independent Limb Maturation Lead to Broad HIV-1 Neutralization Targeting the Env High-Mannose Patch', *Immunity*, 44: 1215-26.

Macosko, E. Z., A. Basu, R. Satija, J. Nemesh, K. Shekhar, M. Goldman, I. Tirosh, A. R. Bialas, N. Kamitaki, E. M. Martersteck, J. J. Trombetta, D. A. Weitz, J. R. Sanes, A. K. Shalek, A. Regev, and S. A. McCarroll. 2015. 'Highly Parallel Genome-wide Expression Profiling of Individual Cells Using Nanoliter Droplets', *Cell*, 161: 1202-14.

Makhdoomi, M. A., L. Khan, S. Kumar, H. Aggarwal, R. Singh, R. Lodha, M. Singla, B. K. Das, S. K. Kabra, and K. Luthra. 2017. 'Evolution of cross-neutralizing antibodies and mapping epitope specificity in plasma of chronic HIV-1-infected antiretroviral therapy-naïve children from India', *J Gen Virol*, 98: 1879-91.

Makita, Sohei, Hiroaki Takatori, and Hiroshi Nakajima. 2021. 'Post-Transcriptional Regulation of Immune Responses and Inflammatory Diseases by RNA-Binding ZFP36 Family Proteins', *Frontiers in Immunology*, 12.

Mamede, João I., Gianguido C. Cianci, Meegan R. Anderson, and Thomas J. Hope. 2017. 'Early cytoplasmic uncoating is associated with infectivity

of HIV-1', *Proceedings of the National Academy of Sciences*, 114: E7169-E78.
Mansky, L. M., and H. M. Temin. 1995. 'Lower in vivo mutation rate of human immunodeficiency virus type 1 than that predicted from the fidelity of purified reverse transcriptase', *J Virol*, 69: 5087-94.
Matsuda, F., K. Ishii, P. Bourvagnet, Ki Kuma, H. Hayashida, T. Miyata, and T. Honjo. 1998. 'The complete nucleotide sequence of the human immunoglobulin heavy chain variable region locus', *J Exp Med*, 188: 2151-62.
Mayer, C. T., A. Gazumyan, E. E. Kara, A. D. Gitlin, J. Golijanin, C. Viant, J. Pai, T. Y. Oliveira, Q. Wang, A. Escolano, M. Medina-Ramirez, R. W. Sanders, and M. C. Nussenzweig. 2017. 'The microanatomic segregation of selection by apoptosis in the germinal center', *Science*, 358.
Mbah, H. A., S. Burda, M. K. Gorny, C. Williams, K. Revesz, S. Zolla-Pazner, and P. N. Nyambi. 2001. 'Effect of soluble CD4 on exposure of epitopes on primary, intact, native human immunodeficiency virus type 1 virions of different genetic clades', *J Virol*, 75: 7785-8.
McCoy, L. E., and Á McKnight. 2017. 'Lessons learned from humoral responses of HIV patients', *Curr Opin HIV AIDS*, 12: 195-202.
McCoy, L. E., M. J. van Gils, G. Ozorowski, T. Messmer, B. Briney, J. E. Voss, D. W. Kulp, M. S. Macauley, D. Sok, M. Pauthner, S. Menis, C. A. Cottrell, J. L. Torres, J. Hsueh, W. R. Schief, I. A. Wilson, A. B. Ward, R. W. Sanders, and D. R. Burton. 2016. 'Holes in the Glycan Shield of the Native HIV Envelope Are a Target of Trimer-Elicited Neutralizing Antibodies', *Cell Rep*, 16: 2327-38.
McCoy, Laura E. 2018. 'The expanding array of HIV broadly neutralizing antibodies', *Retrovirology*, 15: 70.
McCoy, Laura E., and Dennis R. Burton. 2017. 'Identification and specificity of broadly neutralizing antibodies against HIV', *Immunological Reviews*, 275: 11-20.
McCoy, Laura E., Emilia Falkowska, Katie J. Doores, Khoa Le, Devin Sok, Marit J. van Gils, Zelda Euler, Judith A. Burger, Michael S. Seaman, Rogier W. Sanders, Hanneke Schuitemaker, Pascal Poignard, Terri Wrin, and Dennis R. Burton. 2015. 'Incomplete Neutralization and Deviation from Sigmoidal Neutralization Curves for HIV Broadly Neutralizing Monoclonal Antibodies', *PLOS Pathogens*, 11: e1005110.
McCoy, Laura E., Elisabetta Groppelli, Christophe Blanchetot, Hans de Haard, Theo Verrips, Lucy Rutten, Robin A. Weiss, and Clare Jolly. 2014. 'Neutralisation of HIV-1 cell-cell spread by human and llama antibodies', *Retrovirology*, 11: 83.
McDougal, J. S., M. S. Kennedy, J. M. Sligh, S. P. Cort, A. Mawle, and J. K. Nicholson. 1986. 'Binding of HTLV-III/LAV to T4+ T cells by a complex of the 110K viral protein and the T4 molecule', *Science*, 231: 382-5.
McGuire, A. T., S. Hoot, A. M. Dreyer, A. Lippy, A. Stuart, K. W. Cohen, J. Jardine, S. Menis, J. F. Scheid, A. P. West, W. R. Schief, and L. Stamatatos. 2013. 'Engineering HIV envelope protein to activate germline B cell receptors of broadly neutralizing anti-CD4 binding site antibodies', *J Exp Med*, 210: 655-63.

McInnes, L., Healy, J., Melville, J. 2018. 'Umap: Uniform manifold approximation and projection for dimension reduction', *arXiv preprint arXiv:1802.03426.*

McLellan, Jason S., Marie Pancera, Chris Carrico, Jason Gorman, Jean-Philippe Julien, Reza Khayat, Robert Louder, Robert Pejchal, Mallika Sastry, Kaifan Dai, Sijy O'Dell, Nikita Patel, Syed Shahzad-ul-Hussan, Yongping Yang, Baoshan Zhang, Tongqing Zhou, Jiang Zhu, Jeffrey C. Boyington, Gwo-Yu Chuang, Devan Diwanji, Ivelin Georgiev, Young Do Kwon, Doyung Lee, Mark K. Louder, Stephanie Moquin, Stephen D. Schmidt, Zhi-Yong Yang, Mattia Bonsignori, John A. Crump, Saidi H. Kapiga, Noel E. Sam, Barton F. Haynes, Dennis R. Burton, Wayne C. Koff, Laura M. Walker, Sanjay Phogat, Richard Wyatt, Jared Orwenyo, Lai-Xi Wang, James Arthos, Carole A. Bewley, John R. Mascola, Gary J. Nabel, William R. Schief, Andrew B. Ward, Ian A. Wilson, and Peter D. Kwong. 2011. 'Structure of HIV-1 gp120 V1/V2 domain with broadly neutralizing antibody PG9', *Nature*, 480: 336-43.

Meffre, E., A. Louie, J. Bannock, L. J. Kim, J. Ho, C. C. Frear, L. Kardava, W. Wang, C. M. Buckner, Y. Wang, O. R. Fankuchen, K. R. Gittens, T. W. Chun, Y. Li, A. S. Fauci, and S. Moir. 2016. 'Maturational characteristics of HIV-specific antibodies in viremic individuals', *JCI Insight*, 1.

Melchers, F. 2015. 'Checkpoints that control B cell development', *J Clin Invest*, 125: 2203-10.

Melikyan, G. B., R. M. Markosyan, H. Hemmati, M. K. Delmedico, D. M. Lambert, and F. S. Cohen. 2000. 'Evidence that the transition of HIV-1 gp41 into a six-helix bundle, not the bundle configuration, induces membrane fusion', *J Cell Biol*, 151: 413-23.

Mellors, J. W., C. R. Rinaldo, Jr., P. Gupta, R. M. White, J. A. Todd, and L. A. Kingsley. 1996. 'Prognosis in HIV-1 infection predicted by the quantity of virus in plasma', *Science*, 272: 1167-70.

Mendoza, P., H. Gruell, L. Nogueira, J. A. Pai, A. L. Butler, K. Millard, C. Lehmann, I. Suárez, T. Y. Oliveira, J. C. C. Lorenzi, Y. Z. Cohen, C. Wyen, T. Kümmerle, T. Karagounis, C. L. Lu, L. Handl, C. Unson-O'Brien, R. Patel, C. Ruping, M. Schlotz, M. Witmer-Pack, I. Shimeliovich, G. Kremer, E. Thomas, K. E. Seaton, J. Horowitz, A. P. West, Jr., P. J. Bjorkman, G. D. Tomaras, R. M. Gulick, N. Pfeifer, G. Fätkenheuer, M. S. Seaman, F. Klein, M. Caskey, and M. C. Nussenzweig. 2018. 'Combination therapy with anti-HIV-1 antibodies maintains viral suppression', *Nature*, 561: 479-84.

Merindol, N., A. Riquet, V. Szablewski, J. F. Eliaou, A. Puisieux, and N. Bonnefoy. 2014. 'The emerging role of Twist proteins in hematopoietic cells and hematological malignancies', *Blood Cancer J*, 4: e206.

Merk, A., and S. Subramaniam. 2013. 'HIV-1 envelope glycoprotein structure', *Curr Opin Struct Biol*, 23: 268-76.

Migueles, S. A., M. S. Sabbaghian, W. L. Shupert, M. P. Bettinotti, F. M. Marincola, L. Martino, C. W. Hallahan, S. M. Selig, D. Schwartz, J. Sullivan, and M. Connors. 2000. 'HLA B*5701 is highly associated with restriction of virus replication in a subgroup of HIV-infected long term nonprogressors', *Proc Natl Acad Sci U S A*, 97: 2709-14.

Moir, S., C. M. Buckner, J. Ho, W. Wang, J. Chen, A. J. Waldner, J. G. Posada, L. Kardava, M. A. O'Shea, S. Kottilil, T. W. Chun, M. A. Proschan, and A. S. Fauci. 2010. 'B cells in early and chronic HIV infection: evidence for preservation of immune function associated with early initiation of antiretroviral therapy', *Blood*, 116: 5571-9.

Moir, S., and A. S. Fauci. 2009. 'B cells in HIV infection and disease', *Nat Rev Immunol*, 9: 235-45.

Moir, S., J. Ho, A. Malaspina, W. Wang, A. C. DiPoto, M. A. O'Shea, G. Roby, S. Kottilil, J. Arthos, M. A. Proschan, T. W. Chun, and A. S. Fauci. 2008. 'Evidence for HIV-associated B cell exhaustion in a dysfunctional memory B cell compartment in HIV-infected viremic individuals', *J Exp Med*, 205: 1797-805.

Moir, Susan, Angela Malaspina, Oxana K. Pickeral, Eileen T. Donoghue, Joshua Vasquez, Natalie J. Miller, Surekha R. Krishnan, Marie A. Planta, John F. Turney, J. Shawn Justement, Shyamasundaran Kottilil, Mark Dybul, JoAnn M. Mican, Colin Kovacs, Tae-Wook Chun, Charles E. Birse, and Anthony S. Fauci. 2004. 'Decreased Survival of B Cells of HIV-viremic Patients Mediated by Altered Expression of Receptors of the TNF Superfamily', *Journal of Experimental Medicine*, 200: 587-600.

Montefiori, D. C., C. Karnasuta, Y. Huang, H. Ahmed, P. Gilbert, M. S. de Souza, R. McLinden, S. Tovanabutra, A. Laurence-Chenine, E. Sanders-Buell, M. A. Moody, M. Bonsignori, C. Ochsenbauer, J. Kappes, H. Tang, K. Greene, H. Gao, C. C. LaBranche, C. Andrews, V. R. Polonis, S. Rerks-Ngarm, P. Pitisuttithum, S. Nitayaphan, J. Kaewkungwal, S. G. Self, P. W. Berman, D. Francis, F. Sinangil, C. Lee, J. Tartaglia, M. L. Robb, B. F. Haynes, N. L. Michael, and J. H. Kim. 2012. 'Magnitude and breadth of the neutralizing antibody response in the RV144 and Vax003 HIV-1 vaccine efficacy trials', *J Infect Dis*, 206: 431-41.

Montefiori, D. C., M. Roederer, L. Morris, and M. S. Seaman. 2018. 'Neutralization tiers of HIV-1', *Curr Opin HIV AIDS*, 13: 128-36.

Montezuma-Rusca, J. M., S. Moir, L. Kardava, C. M. Buckner, A. Louie, L. J. Kim, B. H. Santich, W. Wang, O. R. Fankuchen, G. Diaz, J. R. Daub, S. D. Rosenzweig, T. W. Chun, Y. Li, R. C. Braylan, K. R. Calvo, and A. S. Fauci. 2015. 'Bone marrow plasma cells are a primary source of serum HIV-1-specific antibodies in chronically infected individuals', *J Immunol*, 194: 2561-8.

Moody, M. A., F. Gao, T. C. Gurley, J. D. Amos, A. Kumar, B. Hora, D. J. Marshall, J. F. Whitesides, S. M. Xia, R. Parks, K. E. Lloyd, K. K. Hwang, X. Lu, M. Bonsignori, A. Finzi, N. A. Vandergrift, S. M. Alam, G. Ferrari, X. Shen, G. D. Tomaras, G. Kamanga, M. S. Cohen, N. E. Sam, S. Kapiga, E. S. Gray, N. L. Tumba, L. Morris, S. Zolla-Pazner, M. K. Gorny, J. R. Mascola, B. H. Hahn, G. M. Shaw, J. G. Sodroski, H. X. Liao, D. C. Montefiori, P. T. Hraber, B. T. Korber, and B. F. Haynes. 2015. 'Strain-Specific V3 and CD4 Binding Site Autologous HIV-1 Neutralizing Antibodies Select Neutralization-Resistant Viruses', *Cell Host Microbe*, 18: 354-62.

Moody, M. A., I. Pedroza-Pacheco, N. A. Vandergrift, C. Chui, K. E. Lloyd, R. Parks, K. A. Soderberg, A. T. Ogbe, M. S. Cohen, H. X. Liao, F. Gao,

A. J. McMichael, D. C. Montefiori, L. Verkoczy, G. Kelsoe, J. Huang, P. R. Shea, M. Connors, P. Borrow, and B. F. Haynes. 2016. 'Immune perturbations in HIV-1-infected individuals who make broadly neutralizing antibodies', *Sci Immunol*, 1: aag0851.

Moore, P. L., E. T. Crooks, L. Porter, P. Zhu, C. S. Cayanan, H. Grise, P. Corcoran, M. B. Zwick, M. Franti, L. Morris, K. H. Roux, D. R. Burton, and J. M. Binley. 2006. 'Nature of nonfunctional envelope proteins on the surface of human immunodeficiency virus type 1', *J Virol*, 80: 2515-28.

Morgan, Dhakshayini, and Vinay Tergaonkar. 2022. 'Unraveling B cell trajectories at single cell resolution', *Trends in Immunology*, 43: 210-29.

Mouat, I. C., and M. S. Horwitz. 2022. 'Age-associated B cells in viral infection', *PLoS Pathog*, 18: e1010297.

Mouquet, H., L. Scharf, Z. Euler, Y. Liu, C. Eden, J. F. Scheid, A. Halper-Stromberg, P. N. Gnanapragasam, D. I. Spencer, M. S. Seaman, H. Schuitemaker, T. Feizi, M. C. Nussenzweig, and P. J. Bjorkman. 2012. 'Complex-type N-glycan recognition by potent broadly neutralizing HIV antibodies', *Proc Natl Acad Sci U S A*, 109: E3268-77.

Munro, J. B., J. Gorman, X. Ma, Z. Zhou, J. Arthos, D. R. Burton, W. C. Koff, J. R. Courter, A. B. Smith, 3rd, P. D. Kwong, S. C. Blanchard, and W. Mothes. 2014. 'Conformational dynamics of single HIV-1 envelope trimers on the surface of native virions', *Science*, 346: 759-63.

Murin, C. D., J. P. Julien, D. Sok, R. L. Stanfield, R. Khayat, A. Cupo, J. P. Moore, D. R. Burton, I. A. Wilson, and A. B. Ward. 2014. 'Structure of 2G12 Fab2 in complex with soluble and fully glycosylated HIV-1 Env by negative-stain single-particle electron microscopy', *J Virol*, 88: 10177-88.

Ndhlovu, Z. M., P. Kamya, N. Mewalal, H. N. Kløverpris, T. Nkosi, K. Pretorius, F. Laher, F. Ogunshola, D. Chopera, K. Shekhar, M. Ghebremichael, N. Ismail, A. Moodley, A. Malik, A. Leslie, P. J. Goulder, S. Buus, A. Chakraborty, K. Dong, T. Ndung'u, and B. D. Walker. 2015. 'Magnitude and Kinetics of CD8+ T Cell Activation during Hyperacute HIV Infection Impact Viral Set Point', *Immunity*, 43: 591-604.

Ne Enrico, Robert-Jan Palstra, and Tokameh Mahmoudi. 2018. 'Chapter Six - Transcription: Insights From the HIV-1 Promoter.' in Friedemann Loos (ed.), *International Review of Cell and Molecular Biology* (Academic Press).

Nicholas, K. J., E. K. Zern, L. Barnett, R. M. Smith, S. L. Lorey, C. A. Copeland, S. Sadagopal, and S. A. Kalams. 2013. 'B cell responses to HIV antigen are a potent correlate of viremia in HIV-1 infection and improve with PD-1 blockade', *PLoS One*, 8: e84185.

Nicholson, J. K., G. D. Cross, C. S. Callaway, and J. S. McDougal. 1986. 'In vitro infection of human monocytes with human T lymphotropic virus type III/lymphadenopathy-associated virus (HTLV-III/LAV)', *J Immunol*, 137: 323-9.

Nogal, B., L. E. McCoy, M. J. van Gils, C. A. Cottrell, J. E. Voss, R. Andrabi, M. Pauthner, C. H. Liang, T. Messmer, R. Nedellec, M. Shin, H. L. Turner, G. Ozorowski, R. W. Sanders, D. R. Burton, and A. B. Ward. 2020. 'HIV envelope trimer-elicited autologous neutralizing antibodies

bind a region overlapping the N332 glycan supersite', *Sci Adv*, 6: eaba0512.

Nyamweya, Samuel, Andrea Hegedus, Assan Jaye, Sarah Rowland-Jones, Katie L. Flanagan, and Derek C. Macallan. 2013. 'Comparing HIV-1 and HIV-2 infection: Lessons for viral immunopathogenesis', *Reviews in Medical Virology*, 23: 221-40.

Obeng-Adjei, Nyamekye, Silvia Portugal, Prasida Holla, Shanping Li, Haewon Sohn, Abhijit Ambegaonkar, Jeff Skinner, Georgina Bowyer, Ogobara K. Doumbo, Boubacar Traore, Susan K. Pierce, and Peter D. Crompton. 2017. 'Malaria-induced interferon-γ drives the expansion of Tbethi atypical memory B cells', *PLOS Pathogens*, 13: e1006576.

Oettinger, M. A., D. G. Schatz, C. Gorka, and D. Baltimore. 1990. 'RAG-1 and RAG-2, adjacent genes that synergistically activate V(D)J recombination', *Science*, 248: 1517-23.

Okulicz, J. F., and O. Lambotte. 2011. 'Epidemiology and clinical characteristics of elite controllers', *Curr Opin HIV AIDS*, 6: 163-8.

Ozorowski, G., J. Pallesen, N. de Val, D. Lyumkis, C. A. Cottrell, J. L. Torres, J. Copps, R. L. Stanfield, A. Cupo, P. Pugach, J. P. Moore, I. A. Wilson, and A. B. Ward. 2017. 'Open and closed structures reveal allostery and pliability in the HIV-1 envelope spike', *Nature*, 547: 360-63.

Pallarès, N., J. P. Frippiat, V. Giudicelli, and M. P. Lefranc. 1998. 'The human immunoglobulin lambda variable (IGLV) genes and joining (IGLJ) segments', *Exp Clin Immunogenet*, 15: 8-18.

Pan, R., M. K. Gorny, S. Zolla-Pazner, and X. P. Kong. 2015. 'The V1V2 Region of HIV-1 gp120 Forms a Five-Stranded Beta Barrel', *J Virol*, 89: 8003-10.

Pancera, M., T. Zhou, A. Druz, I. S. Georgiev, C. Soto, J. Gorman, J. Huang, P. Acharya, G. Y. Chuang, G. Ofek, G. B. Stewart-Jones, J. Stuckey, R. T. Bailer, M. G. Joyce, M. K. Louder, N. Tumba, Y. Yang, B. Zhang, M. S. Cohen, B. F. Haynes, J. R. Mascola, L. Morris, J. B. Munro, S. C. Blanchard, W. Mothes, M. Connors, and P. D. Kwong. 2014. 'Structure and immune recognition of trimeric pre-fusion HIV-1 Env', *Nature*, 514: 455-61.

Park, S. R., H. Zan, Z. Pal, J. Zhang, A. Al-Qahtani, E. J. Pone, Z. Xu, T. Mai, and P. Casali. 2009. 'HoxC4 binds to the promoter of the cytidine deaminase AID gene to induce AID expression, class-switch DNA recombination and somatic hypermutation', *Nat Immunol*, 10: 540-50.

Parker Miller, E., M. T. Finkelstein, M. C. Erdman, P. C. Seth, and D. Fera. 2021. 'A Structural Update of Neutralizing Epitopes on the HIV Envelope, a Moving Target', *Viruses*, 13.

Pauthner, M., C. Havenar-Daughton, D. Sok, J. P. Nkolola, R. Bastidas, A. V. Boopathy, D. G. Carnathan, A. Chandrashekar, K. M. Cirelli, C. A. Cottrell, A. M. Eroshkin, J. Guenaga, K. Kaushik, D. W. Kulp, J. Liu, L. E. McCoy, A. L. Oom, G. Ozorowski, K. W. Post, S. K. Sharma, J. M. Steichen, S. W. de Taeye, T. Tokatlian, A. Torrents de la Peña, S. T. Butera, C. C. LaBranche, D. C. Montefiori, G. Silvestri, I. A. Wilson, D. J. Irvine, R. W. Sanders, W. R. Schief, A. B. Ward, R. T. Wyatt, D. H. Barouch, S. Crotty, and D. R. Burton. 2017. 'Elicitation of Robust Tier 2 Neutralizing Antibody Responses in Nonhuman Primates by HIV

Envelope Trimer Immunization Using Optimized Approaches', *Immunity*, 46: 1073-88.e6.

Pereyra, Florencia, Marylyn M. Addo, Daniel E. Kaufmann, Yang Liu, Toshiyuki Miura, Almas Rathod, Brett Baker, Alicja Trocha, Rachel Rosenberg, Elizabeth Mackey, Peggy Ueda, Zhigang Lu, Daniel Cohen, Terri Wrin, Christos J. Petropoulos, Eric S. Rosenberg, and Bruce D. Walker. 2008. 'Genetic and Immunologic Heterogeneity among Persons Who Control HIV Infection in the Absence of Therapy', *The Journal of Infectious Diseases*, 197: 563-71.

Phad, Ganesh E., Dora Pinto, Mathilde Foglierini, Murodzhon Akhmedov, Riccardo L. Rossi, Emilia Malvicini, Antonino Cassotta, Chiara Silacci Fregni, Ludovica Bruno, Federica Sallusto, and Antonio Lanzavecchia. 2022. 'Clonal structure, stability and dynamics of human memory B cells and circulating plasmablasts', *Nature Immunology*, 23: 1-10.

Picelli, S., O. R. Faridani, A. K. Björklund, G. Winberg, S. Sagasser, and R. Sandberg. 2014. 'Full-length RNA-seq from single cells using Smart-seq2', *Nat Protoc*, 9: 171-81.

Picelli, Simone, Åsa K. Björklund, Omid R. Faridani, Sven Sagasser, Gösta Winberg, and Rickard Sandberg. 2013. 'Smart-seq2 for sensitive full-length transcriptome profiling in single cells', *Nature Methods*, 10: 1096-98.

Picker, Louis J., Jeffrey D. Lifson, Michael Gale, Jr., Scott G. Hansen, and Klaus Früh. 2023. 'Programming cytomegalovirus as an HIV vaccine', *Trends in Immunology*, 44: 287-304.

Pinter, A., W. J. Honnen, P. D'Agostino, M. K. Gorny, S. Zolla-Pazner, and S. C. Kayman. 2005. 'The C108g epitope in the V2 domain of gp120 functions as a potent neutralization target when introduced into envelope proteins derived from human immunodeficiency virus type 1 primary isolates', *J Virol*, 79: 6909-17.

Pinto, D., C. Fenwick, C. Caillat, C. Silacci, S. Guseva, F. Dehez, C. Chipot, S. Barbieri, A. Minola, D. Jarrossay, G. D. Tomaras, X. Shen, A. Riva, M. Tarkowski, O. Schwartz, T. Bruel, J. Dufloo, M. S. Seaman, D. C. Montefiori, A. Lanzavecchia, D. Corti, G. Pantaleo, and W. Weissenhorn. 2019. 'Structural Basis for Broad HIV-1 Neutralization by the MPER-Specific Human Broadly Neutralizing Antibody LN01', *Cell Host Microbe*, 26: 623-37.e8.

Pitisuttithum, P., P. Gilbert, M. Gurwith, W. Heyward, M. Martin, F. van Griensven, D. Hu, J. W. Tappero, and K. Choopanya. 2006. 'Randomized, double-blind, placebo-controlled efficacy trial of a bivalent recombinant glycoprotein 120 HIV-1 vaccine among injection drug users in Bangkok, Thailand', *J Infect Dis*, 194: 1661-71.

Platt, E. J., M. M. Gomes, and D. Kabat. 2012. 'Kinetic mechanism for HIV-1 neutralization by antibody 2G12 entails reversible glycan binding that slows cell entry', *Proc Natl Acad Sci U S A*, 109: 7829-34.

Platt, E. J., K. Wehrly, S. E. Kuhmann, B. Chesebro, and D. Kabat. 1998. 'Effects of CCR5 and CD4 cell surface concentrations on infections by macrophagetropic isolates of human immunodeficiency virus type 1', *J Virol*, 72: 2855-64.

Plotkin, S. A. 2010. 'Correlates of protection induced by vaccination', *Clin Vaccine Immunol*, 17: 1055-65.

Polański, Krzysztof, Matthew D. Young, Zhichao Miao, Kerstin B. Meyer, Sarah A. Teichmann, and Jong-Eun Park. 2020. 'BBKNN: fast batch alignment of single cell transcriptomes', *Bioinformatics*, 36: 964-65.

Pollara, J., D. Easterhoff, and G. G. Fouda. 2017. 'Lessons learned from human HIV vaccine trials', *Curr Opin HIV AIDS*, 12: 216-21.

Pollara, Justin, Santosh Khanal, R. Whitney Edwards, Bhavna Hora, Guido Ferrari, Barton F. Haynes, and Todd Bradley. 2022. 'Single-cell analysis of immune cell transcriptome during HIV-1 infection and therapy', *BMC Immunology*, 23: 48.

Pone, E. J., H. Zan, J. Zhang, A. Al-Qahtani, Z. Xu, and P. Casali. 2010. 'Toll-like receptors and B-cell receptors synergize to induce immunoglobulin class-switch DNA recombination: relevance to microbial antibody responses', *Crit Rev Immunol*, 30: 1-29.

Popovic, Mikulas, M. G. Sarngadharan, Elizabeth Read, and Robert C. Gallo. 1984. 'Detection, Isolation, and Continuous Production of Cytopathic Retroviruses (HTLV-III) from Patients with AIDS and Pre-AIDS', *Science*, 224: 497-500.

Portugal, S., N. Obeng-Adjei, S. Moir, P. D. Crompton, and S. K. Pierce. 2017. 'Atypical memory B cells in human chronic infectious diseases: An interim report', *Cell Immunol*, 321: 18-25.

Portugal, Silvia, Christopher M. Tipton, Haewon Sohn, Younoussou Kone, Jing Wang, Shanping Li, Jeff Skinner, Kimmo Virtaneva, Daniel E. Sturdevant, Stephen F. Porcella, Ogobara K. Doumbo, Safiatou Doumbo, Kassoum Kayentao, Aissata Ongoiba, Boubacar Traore, Inaki Sanz, Susan K. Pierce, and Peter D. Crompton. 2015. 'Malaria-associated atypical memory B cells exhibit markedly reduced B cell receptor signaling and effector function', *Elife*, 4: e07218.

Prigent, J., A. Jarossay, C. Planchais, C. Eden, J. Dufloo, A. Kök, V. Lorin, O. Vratskikh, T. Couderc, T. Bruel, O. Schwartz, M. S. Seaman, O. Ohlenschläger, J. D. Dimitrov, and H. Mouquet. 2018. 'Conformational Plasticity in Broadly Neutralizing HIV-1 Antibodies Triggers Polyreactivity', *Cell Rep*, 23: 2568-81.

Pugach, P., G. Ozorowski, A. Cupo, R. Ringe, A. Yasmeen, N. de Val, R. Derking, H. J. Kim, J. Korzun, M. Golabek, K. de Los Reyes, T. J. Ketas, J. P. Julien, D. R. Burton, I. A. Wilson, R. W. Sanders, P. J. Klasse, A. B. Ward, and J. P. Moore. 2015. 'A native-like SOSIP.664 trimer based on an HIV-1 subtype B env gene', *J Virol*, 89: 3380-95.

Ramsköld, Daniel, Shujun Luo, Yu-Chieh Wang, Robin Li, Qiaolin Deng, Omid R. Faridani, Gregory A. Daniels, Irina Khrebtukova, Jeanne F. Loring, Louise C. Laurent, Gary P. Schroth, and Rickard Sandberg. 2012. 'Full-length mRNA-Seq from single-cell levels of RNA and individual circulating tumor cells', *Nature Biotechnology*, 30: 777-82.

Randolph, G. J. 2001. 'Dendritic cell migration to lymph nodes: cytokines, chemokines, and lipid mediators', *Semin Immunol*, 13: 267-74.

Rankovic, S., J. Varadarajan, R. Ramalho, C. Aiken, and I. Rousso. 2017. 'Reverse Transcription Mechanically Initiates HIV-1 Capsid Disassembly', *J Virol*, 91.

REED, L.J., and H. MUENCH. 1938. 'A SIMPLE METHOD OF ESTIMATING FIFTY PER CENT ENDPOINTS12', *American Journal of Epidemiology*, 27: 493-97.

Rees-Spear, Chloe, and Laura E. McCoy. 2021. 'Vaccine responses in ageing and chronic viral infection', *Oxford Open Immunology*, 2: iqab007.

Reeves, D. B., E. R. Duke, T. A. Wagner, S. E. Palmer, A. M. Spivak, and J. T. Schiffer. 2018. 'A majority of HIV persistence during antiretroviral therapy is due to infected cell proliferation', *Nat Commun*, 9: 4811.

Reif, Karin, Eric H. Ekland, Lars Ohl, Hideki Nakano, Martin Lipp, Reinhold Förster, and Jason G. Cyster. 2002. 'Balanced responsiveness to chemoattractants from adjacent zones determines B-cell position', *Nature*, 416: 94-99.

Rerks-Ngarm, S., P. Pitisuttithum, J. L. Excler, S. Nitayaphan, J. Kaewkungwal, N. Premsri, P. Kunasol, N. Karasavvas, A. Schuetz, V. Ngauy, F. Sinangil, P. Dawson, A. C. deCamp, S. Phogat, S. Garunathan, J. Tartaglia, C. DiazGranados, S. Ratto-Kim, P. Pegu, M. Eller, C. Karnasuta, D. C. Montefiori, S. Sawant, N. Vandergrift, S. Wills, G. D. Tomaras, M. L. Robb, N. L. Michael, J. H. Kim, S. Vasan, and R. J. O'Connell. 2017. 'Randomized, Double-Blind Evaluation of Late Boost Strategies for HIV-Uninfected Vaccine Recipients in the RV144 HIV Vaccine Efficacy Trial', *J Infect Dis*, 215: 1255-63.

Rerks-Ngarm, S., P. Pitisuttithum, S. Nitayaphan, J. Kaewkungwal, J. Chiu, R. Paris, N. Premsri, C. Namwat, M. de Souza, E. Adams, M. Benenson, S. Gurunathan, J. Tartaglia, J. G. McNeil, D. P. Francis, D. Stablein, D. L. Birx, S. Chunsuttiwat, C. Khamboonruang, P. Thongcharoen, M. L. Robb, N. L. Michael, P. Kunasol, and J. H. Kim. 2009. 'Vaccination with ALVAC and AIDSVAX to prevent HIV-1 infection in Thailand', *N Engl J Med*, 361: 2209-20.

Richardson, S. I., F. Ayres, N. P. Manamela, B. Oosthuysen, Z. Makhado, B. E. Lambson, L. Morris, and P. L. Moore. 2021. 'HIV Broadly Neutralizing Antibodies Expressed as IgG3 Preserve Neutralization Potency and Show Improved Fc Effector Function', *Front Immunol*, 12: 733958.

Richardson, S. I., B. E. Lambson, A. R. Crowley, A. Bashirova, C. Scheepers, N. Garrett, S. Abdool Karim, N. N. Mkhize, M. Carrington, M. E. Ackerman, P. L. Moore, and L. Morris. 2019. 'IgG3 enhances neutralization potency and Fc effector function of an HIV V2-specific broadly neutralizing antibody', *PLoS Pathog*, 15: e1008064.

Richman, D. D., T. Wrin, S. J. Little, and C. J. Petropoulos. 2003. 'Rapid evolution of the neutralizing antibody response to HIV type 1 infection', *Proc Natl Acad Sci U S A*, 100: 4144-9.

Ringe, R. P., R. W. Sanders, A. Yasmeen, H. J. Kim, J. H. Lee, A. Cupo, J. Korzun, R. Derking, T. van Montfort, J. P. Julien, I. A. Wilson, P. J. Klasse, A. B. Ward, and J. P. Moore. 2013. 'Cleavage strongly influences whether soluble HIV-1 envelope glycoprotein trimers adopt a native-like conformation', *Proc Natl Acad Sci U S A*, 110: 18256-61.

Ringe Rajesh, P., Gabriel Ozorowski, Kimmo Rantalainen, B. Struwe Weston, Katie Matthews, L. Torres Jonathan, Anila Yasmeen, A. Cottrell Christopher, J. Ketas Thomas, C. LaBranche Celia, C. Montefiori David, Albert Cupo, Max Crispin, A. Wilson Ian, B. Ward Andrew, W.

Sanders Rogier, P. J. Klasse, and P. Moore John. 2017. 'Reducing V3 Antigenicity and Immunogenicity on Soluble, Native-Like HIV-1 Env SOSIP Trimers', *Journal of Virology*, 91: e00677-17.

Robbiani, Davide F., Christian Gaebler, Frauke Muecksch, Julio C. C. Lorenzi, Zijun Wang, Alice Cho, Marianna Agudelo, Christopher O. Barnes, Anna Gazumyan, Shlomo Finkin, Thomas Hägglöf, Thiago Y. Oliveira, Charlotte Viant, Arlene Hurley, Hans-Heinrich Hoffmann, Katrina G. Millard, Rhonda G. Kost, Melissa Cipolla, Kristie Gordon, Filippo Bianchini, Spencer T. Chen, Victor Ramos, Roshni Patel, Juan Dizon, Irina Shimeliovich, Pilar Mendoza, Harald Hartweger, Lilian Nogueira, Maggi Pack, Jill Horowitz, Fabian Schmidt, Yiska Weisblum, Eleftherios Michailidis, Alison W. Ashbrook, Eric Waltari, John E. Pak, Kathryn E. Huey-Tubman, Nicholas Koranda, Pauline R. Hoffman, Anthony P. West, Charles M. Rice, Theodora Hatziioannou, Pamela J. Bjorkman, Paul D. Bieniasz, Marina Caskey, and Michel C. Nussenzweig. 2020. 'Convergent antibody responses to SARS-CoV-2 in convalescent individuals', *Nature*, 584: 437-42.

Robertson, D. L., J. P. Anderson, J. A. Bradac, J. K. Carr, B. Foley, R. K. Funkhouser, F. Gao, B. H. Hahn, M. L. Kalish, C. Kuiken, G. H. Learn, T. Leitner, F. McCutchan, S. Osmanov, M. Peeters, D. Pieniazek, M. Salminen, P. M. Sharp, S. Wolinsky, and B. Korber. 2000. 'HIV-1 nomenclature proposal', *Science*, 288: 55-6.

Robertson, D. L., B. H. Hahn, and P. M. Sharp. 1995. 'Recombination in AIDS viruses', *J Mol Evol*, 40: 249-59.

Roco, J. A., L. Mesin, S. C. Binder, C. Nefzger, P. Gonzalez-Figueroa, P. F. Canete, J. Ellyard, Q. Shen, P. A. Robert, J. Cappello, H. Vohra, Y. Zhang, C. R. Nowosad, A. Schiepers, L. M. Corcoran, K. M. Toellner, J. M. Polo, M. Meyer-Hermann, G. D. Victora, and C. G. Vinuesa. 2019. 'Class-Switch Recombination Occurs Infrequently in Germinal Centers', *Immunity*, 51: 337-50.e7.

Roff, S. R., E. N. Noon-Song, and J. K. Yamamoto. 2014. 'The Significance of Interferon-γ in HIV-1 Pathogenesis, Therapy, and Prophylaxis', *Front Immunol*, 4: 498.

Rogozin, I. B., and M. Diaz. 2004. 'Cutting edge: DGYW/WRCH is a better predictor of mutability at G:C bases in Ig hypermutation than the widely accepted RGYW/WRCY motif and probably reflects a two-step activation-induced cytidine deaminase-triggered process', *J Immunol*, 172: 3382-4.

Rosás-Umbert, Miriam, Anuska Llano, Rocío Bellido, Alex Olvera, Marta Ruiz-Riol, Muntsa Rocafort, A. Fernández Marco, Patricia Cobarsi, Manel Crespo, Lucy Dorrell, Jorge del Romero, José Alcami, Roger Paredes, Christian Brander, and Beatriz Mothe. 2019. 'Mechanisms of Abrupt Loss of Virus Control in a Cohort of Previous HIV Controllers', *Journal of Virology*, 93: e01436-18.

Roskin, K. M., K. J. L. Jackson, J. Y. Lee, R. A. Hoh, S. A. Joshi, K. K. Hwang, M. Bonsignori, I. Pedroza-Pacheco, H. X. Liao, M. A. Moody, A. Z. Fire, P. Borrow, B. F. Haynes, and S. D. Boyd. 2020. 'Aberrant B cell repertoire selection associated with HIV neutralizing antibody breadth', *Nat Immunol*, 21: 199-209.

Ross, J. M., R. Ying, C. L. Celum, J. M. Baeten, K. K. Thomas, P. M. Murnane, H. van Rooyen, J. P. Hughes, and R. V. Barnabas. 2018. 'Modeling HIV disease progression and transmission at population-level: The potential impact of modifying disease progression in HIV treatment programs', *Epidemics*, 23: 34-41.

Rouers, A., J. Klingler, B. Su, A. Samri, G. Laumond, S. Even, V. Avettand-Fenoel, C. Richetta, N. Paul, F. Boufassa, L. Hocqueloux, H. Mouquet, C. Rouzioux, O. Lambotte, B. Autran, S. Graff-Dubois, C. Moog, and A. Moris. 2017. 'HIV-Specific B Cell Frequency Correlates with Neutralization Breadth in Patients Naturally Controlling HIV-Infection', *eBioMedicine*, 21: 158-69.

Ruprecht, C. R., A. Krarup, L. Reynell, A. M. Mann, O. F. Brandenberg, L. Berlinger, I. A. Abela, R. R. Regoes, H. F. Günthard, P. Rusert, and A. Trkola. 2011. 'MPER-specific antibodies induce gp120 shedding and irreversibly neutralize HIV-1', *J Exp Med*, 208: 439-54.

Rusert, P., R. D. Kouyos, C. Kadelka, H. Ebner, M. Schanz, M. Huber, D. L. Braun, N. Hozé, A. Scherrer, C. Magnus, J. Weber, T. Uhr, V. Cippa, C. W. Thorball, H. Kuster, M. Cavassini, E. Bernasconi, M. Hoffmann, A. Calmy, M. Battegay, A. Rauch, S. Yerly, V. Aubert, T. Klimkait, J. Böni, J. Fellay, R. R. Regoes, H. F. Günthard, and A. Trkola. 2016. 'Determinants of HIV-1 broadly neutralizing antibody induction', *Nat Med*, 22: 1260-67.

Rutherford, G. W., A. R. Lifson, N. A. Hessol, W. W. Darrow, P. M. O'Malley, S. P. Buchbinder, J. L. Barnhart, T. W. Bodecker, L. Cannon, L. S. Doll, and et al. 1990. 'Course of HIV-I infection in a cohort of homosexual and bisexual men: an 11 year follow up study', *Bmj*, 301: 1183-8.

Sagar, M., X. Wu, S. Lee, and J. Overbaugh. 2006. 'Human immunodeficiency virus type 1 V1-V2 envelope loop sequences expand and add glycosylation sites over the course of infection, and these modifications affect antibody neutralization sensitivity', *J Virol*, 80: 9586-98.

Sajadi, M. M., A. Dashti, Z. Rikhtegaran Tehrani, W. D. Tolbert, M. S. Seaman, X. Ouyang, N. Gohain, M. Pazgier, D. Kim, G. Cavet, J. Yared, R. R. Redfield, G. K. Lewis, and A. L. DeVico. 2018. 'Identification of Near-Pan-neutralizing Antibodies against HIV-1 by Deconvolution of Plasma Humoral Responses', *Cell*, 173: 1783-95.e14.

Samson, M., F. Libert, B. J. Doranz, J. Rucker, C. Liesnard, C. M. Farber, S. Saragosti, C. Lapoumeroulie, J. Cognaux, C. Forceille, G. Muyldermans, C. Verhofstede, G. Burtonboy, M. Georges, T. Imai, S. Rana, Y. Yi, R. J. Smyth, R. G. Collman, R. W. Doms, G. Vassart, and M. Parmentier. 1996. 'Resistance to HIV-1 infection in caucasian individuals bearing mutant alleles of the CCR-5 chemokine receptor gene', *Nature*, 382: 722-5.

Sanders, R. W., R. Derking, A. Cupo, J. P. Julien, A. Yasmeen, N. de Val, H. J. Kim, C. Blattner, A. T. de la Peña, J. Korzun, M. Golabek, K. de Los Reyes, T. J. Ketas, M. J. van Gils, C. R. King, I. A. Wilson, A. B. Ward, P. J. Klasse, and J. P. Moore. 2013. 'A next-generation cleaved, soluble HIV-1 Env trimer, BG505 SOSIP.664 gp140, expresses multiple epitopes for broadly neutralizing but not non-neutralizing antibodies', *PLoS Pathog*, 9: e1003618.

Sanders, R. W., M. J. van Gils, R. Derking, D. Sok, T. J. Ketas, J. A. Burger, G. Ozorowski, A. Cupo, C. Simonich, L. Goo, H. Arendt, H. J. Kim, J. H. Lee, P. Pugach, M. Williams, G. Debnath, B. Moldt, M. J. van Breemen, G. Isik, M. Medina-Ramírez, J. W. Back, W. C. Koff, J. P. Julien, E. G. Rakasz, M. S. Seaman, M. Guttman, K. K. Lee, P. J. Klasse, C. LaBranche, W. R. Schief, I. A. Wilson, J. Overbaugh, D. R. Burton, A. B. Ward, D. C. Montefiori, H. Dean, and J. P. Moore. 2015. 'HIV-1 VACCINES. HIV-1 neutralizing antibodies induced by native-like envelope trimers', *Science*, 349: aac4223.

Sanders, R. W., M. Venturi, L. Schiffner, R. Kalyanaraman, H. Katinger, K. O. Lloyd, P. D. Kwong, and J. P. Moore. 2002. 'The mannose-dependent epitope for neutralizing antibody 2G12 on human immunodeficiency virus type 1 glycoprotein gp120', *J Virol*, 76: 7293-305.

Sandler, N. G., and D. C. Douek. 2012. 'Microbial translocation in HIV infection: causes, consequences and treatment opportunities', *Nat Rev Microbiol*, 10: 655-66.

Sarzotti-Kelsoe, M., R. T. Bailer, E. Turk, C. L. Lin, M. Bilska, K. M. Greene, H. Gao, C. A. Todd, D. A. Ozaki, M. S. Seaman, J. R. Mascola, and D. C. Montefiori. 2014. 'Optimization and validation of the TZM-bl assay for standardized assessments of neutralizing antibodies against HIV-1', *J Immunol Methods*, 409: 131-46.

Sather, D. N., J. Armann, L. K. Ching, A. Mavrantoni, G. Sellhorn, Z. Caldwell, X. Yu, B. Wood, S. Self, S. Kalams, and L. Stamatatos. 2009. 'Factors associated with the development of cross-reactive neutralizing antibodies during human immunodeficiency virus type 1 infection', *J Virol*, 83: 757-69.

Sattentau, Q. J., and J. P. Moore. 1991. 'Conformational changes induced in the human immunodeficiency virus envelope glycoprotein by soluble CD4 binding', *J Exp Med*, 174: 407-15.

Saunders, K. O., L. K. Verkoczy, C. Jiang, J. Zhang, R. Parks, H. Chen, M. Housman, H. Bouton-Verville, X. Shen, A. M. Trama, R. Scearce, L. Sutherland, S. Santra, A. Newman, A. Eaton, K. Xu, I. S. Georgiev, M. G. Joyce, G. D. Tomaras, M. Bonsignori, S. G. Reed, A. Salazar, J. R. Mascola, M. A. Moody, D. W. Cain, M. Centlivre, S. Zurawski, G. Zurawski, H. P. Erickson, P. D. Kwong, S. M. Alam, Y. Levy, D. C. Montefiori, and B. F. Haynes. 2017. 'Vaccine Induction of Heterologous Tier 2 HIV-1 Neutralizing Antibodies in Animal Models', *Cell Rep*, 21: 3681-90.

Schacker, T., A. C. Collier, J. Hughes, T. Shea, and L. Corey. 1996. 'Clinical and epidemiologic features of primary HIV infection', *Ann Intern Med*, 125: 257-64.

Scharf, L., J. F. Scheid, J. H. Lee, A. P. West, Jr., C. Chen, H. Gao, P. N. Gnanapragasam, R. Mares, M. S. Seaman, A. B. Ward, M. C. Nussenzweig, and P. J. Bjorkman. 2014. 'Antibody 8ANC195 reveals a site of broad vulnerability on the HIV-1 envelope spike', *Cell Rep*, 7: 785-95.

Scharf, L., H. Wang, H. Gao, S. Chen, A. W. McDowall, and P. J. Bjorkman. 2015. 'Broadly Neutralizing Antibody 8ANC195 Recognizes Closed and Open States of HIV-1 Env', *Cell*, 162: 1379-90.

Scheepers, C., V. Bekker, C. Anthony, S. I. Richardson, B. Oosthuysen, T. Moyo, P. Kgagudi, D. Kitchin, M. Nonyane, T. York, D. Mielke, B. M. Mabvakure, Z. Sheng, B. E. Lambson, A. Ismail, N. J. Garrett, S. S. Abdool Karim, L. Shapiro, C. Williamson, L. Morris, and P. L. Moore. 2020. 'Antibody Isotype Switching as a Mechanism to Counter HIV Neutralization Escape', *Cell Rep*, 33: 108430.

Scheid, J. F., J. A. Horwitz, Y. Bar-On, E. F. Kreider, C. L. Lu, J. C. Lorenzi, A. Feldmann, M. Braunschweig, L. Nogueira, T. Oliveira, I. Shimeliovich, R. Patel, L. Burke, Y. Z. Cohen, S. Hadrigan, A. Settler, M. Witmer-Pack, A. P. West, Jr., B. Juelg, T. Keler, T. Hawthorne, B. Zingman, R. M. Gulick, N. Pfeifer, G. H. Learn, M. S. Seaman, P. J. Bjorkman, F. Klein, S. J. Schlesinger, B. D. Walker, B. H. Hahn, M. C. Nussenzweig, and M. Caskey. 2016. 'HIV-1 antibody 3BNC117 suppresses viral rebound in humans during treatment interruption', *Nature*, 535: 556-60.

Scheid, J. F., H. Mouquet, N. Feldhahn, M. S. Seaman, K. Velinzon, J. Pietzsch, R. G. Ott, R. M. Anthony, H. Zebroski, A. Hurley, A. Phogat, B. Chakrabarti, Y. Li, M. Connors, F. Pereyra, B. D. Walker, H. Wardemann, D. Ho, R. T. Wyatt, J. R. Mascola, J. V. Ravetch, and M. C. Nussenzweig. 2009. 'Broad diversity of neutralizing antibodies isolated from memory B cells in HIV-infected individuals', *Nature*, 458: 636-40.

Scheid, J. F., H. Mouquet, B. Ueberheide, R. Diskin, F. Klein, T. Y. Oliveira, J. Pietzsch, D. Fenyo, A. Abadir, K. Velinzon, A. Hurley, S. Myung, F. Boulad, P. Poignard, D. R. Burton, F. Pereyra, D. D. Ho, B. D. Walker, M. S. Seaman, P. J. Bjorkman, B. T. Chait, and M. C. Nussenzweig. 2011. 'Sequence and structural convergence of broad and potent HIV antibodies that mimic CD4 binding', *Science*, 333: 1633-7.

Schommers, P., H. Gruell, M. E. Abernathy, M. K. Tran, A. S. Dingens, H. B. Gristick, C. O. Barnes, T. Schoofs, M. Schlotz, K. Vanshylla, C. Kreer, D. Weiland, U. Holtick, C. Scheid, M. M. Valter, M. J. van Gils, R. W. Sanders, J. J. Vehreschild, O. A. Cornely, C. Lehmann, G. Fätkenheuer, M. S. Seaman, J. D. Bloom, P. J. Bjorkman, and F. Klein. 2020. 'Restriction of HIV-1 Escape by a Highly Broad and Potent Neutralizing Antibody', *Cell*, 180: 471-89.e22.

Schoofs, T., C. O. Barnes, N. Suh-Toma, J. Golijanin, P. Schommers, H. Gruell, A. P. West, Jr., F. Bach, Y. E. Lee, L. Nogueira, I. S. Georgiev, R. T. Bailer, J. Czartoski, J. R. Mascola, M. S. Seaman, M. J. McElrath, N. A. Doria-Rose, F. Klein, M. C. Nussenzweig, and P. J. Bjorkman. 2019. 'Broad and Potent Neutralizing Antibodies Recognize the Silent Face of the HIV Envelope', *Immunity*, 50: 1513-29.e9.

Schoofs, T., F. Klein, M. Braunschweig, E. F. Kreider, A. Feldmann, L. Nogueira, T. Oliveira, J. C. Lorenzi, E. H. Parrish, G. H. Learn, A. P. West, Jr., P. J. Bjorkman, S. J. Schlesinger, M. S. Seaman, J. Czartoski, M. J. McElrath, N. Pfeifer, B. H. Hahn, M. Caskey, and M. C. Nussenzweig. 2016. 'HIV-1 therapy with monoclonal antibody 3BNC117 elicits host immune responses against HIV-1', *Science*, 352: 997-1001.

Schröder, A. R., P. Shinn, H. Chen, C. Berry, J. R. Ecker, and F. Bushman. 2002. 'HIV-1 integration in the human genome favors active genes and local hotspots', *Cell*, 110: 521-9.

Schroeder, H. W., Jr., and L. Cavacini. 2010. 'Structure and function of immunoglobulins', *J Allergy Clin Immunol*, 125: S41-52.

Schwickert, T. A., G. D. Victora, D. R. Fooksman, A. O. Kamphorst, M. R. Mugnier, A. D. Gitlin, M. L. Dustin, and M. C. Nussenzweig. 2011. 'A dynamic T cell-limited checkpoint regulates affinity-dependent B cell entry into the germinal center', *J Exp Med*, 208: 1243-52.

Seaman, M. S., H. Janes, N. Hawkins, L. E. Grandpre, C. Devoy, A. Giri, R. T. Coffey, L. Harris, B. Wood, M. G. Daniels, T. Bhattacharya, A. Lapedes, V. R. Polonis, F. E. McCutchan, P. B. Gilbert, S. G. Self, B. T. Korber, D. C. Montefiori, and J. R. Mascola. 2010. 'Tiered categorization of a diverse panel of HIV-1 Env pseudoviruses for assessment of neutralizing antibodies', *J Virol*, 84: 1439-52.

Sela-Culang, Inbal, Vered Kunik, and Yanay Ofran. 2013. 'The Structural Basis of Antibody-Antigen Recognition', *Frontiers in Immunology*, 4.

Setliff, I., A. R. Shiakolas, K. A. Pilewski, A. A. Murji, R. E. Mapengo, K. Janowska, S. Richardson, C. Oosthuysen, N. Raju, L. Ronsard, M. Kanekiyo, J. S. Qin, K. J. Kramer, A. R. Greenplate, W. J. McDonnell, B. S. Graham, M. Connors, D. Lingwood, P. Acharya, L. Morris, and I. S. Georgiev. 2019. 'High-Throughput Mapping of B Cell Receptor Sequences to Antigen Specificity', *Cell*, 179: 1636-46.e15.

Shaik, M. M., H. Peng, J. Lu, S. Rits-Volloch, C. Xu, M. Liao, and B. Chen. 2019. 'Structural basis of coreceptor recognition by HIV-1 envelope spike', *Nature*, 565: 318-23.

Shao, Y., S. Y. Kim, D. Shin, M. S. Kim, H. W. Suh, Z. H. Piao, M. Jeong, S. H. Lee, S. R. Yoon, B. H. Lim, W. H. Kim, J. K. Ahn, and I. Choi. 2010. 'TXNIP regulates germinal center generation by suppressing BCL-6 expression', *Immunol Lett*, 129: 78-84.

Sharp, P. M., and B. H. Hahn. 2011. 'Origins of HIV and the AIDS pandemic', *Cold Spring Harbor perspectives in medicine, 1(1), a006841.*

Shaw, G. M., and E. Hunter. 2012. 'HIV transmission', *Cold Spring Harb Perspect Med*, 2.

Shen, R., H. E. Richter, R. H. Clements, L. Novak, K. Huff, D. Bimczok, S. Sankaran-Walters, S. Dandekar, P. R. Clapham, L. E. Smythies, and P. D. Smith. 2009. 'Macrophages in vaginal but not intestinal mucosa are monocyte-like and permissive to human immunodeficiency virus type 1 infection', *J Virol*, 83: 3258-67.

Shi, B., L. Ma, X. He, X. Wang, P. Wang, L. Zhou, and X. Yao. 2014. 'Comparative analysis of human and mouse immunoglobulin variable heavy regions from IMGT/LIGM-DB with IMGT/HighV-QUEST', *Theor Biol Med Model*, 11: 30.

Siliciano, J. D., J. Kajdas, D. Finzi, T. C. Quinn, K. Chadwick, J. B. Margolick, C. Kovacs, S. J. Gange, and R. F. Siliciano. 2003. 'Long-term follow-up studies confirm the stability of the latent reservoir for HIV-1 in resting CD4+ T cells', *Nat Med*, 9: 727-8.

Simek, M. D., W. Rida, F. H. Priddy, P. Pung, E. Carrow, D. S. Laufer, J. K. Lehrman, M. Boaz, T. Tarragona-Fiol, G. Miiro, J. Birungi, A. Pozniak,

D. A. McPhee, O. Manigart, E. Karita, A. Inwoley, W. Jaoko, J. Dehovitz, L. G. Bekker, P. Pitisuttithum, R. Paris, L. M. Walker, P. Poignard, T. Wrin, P. E. Fast, D. R. Burton, and W. C. Koff. 2009. 'Human immunodeficiency virus type 1 elite neutralizers: individuals with broad and potent neutralizing activity identified by using a high-throughput neutralization assay together with an analytical selection algorithm', *J Virol*, 83: 7337-48.

Simonich, C. A., K. L. Williams, H. P. Verkerke, J. A. Williams, R. Nduati, K. K. Lee, and J. Overbaugh. 2016. 'HIV-1 Neutralizing Antibodies with Limited Hypermutation from an Infant', *Cell*, 166: 77-87.

Sims, G. P., R. Ettinger, Y. Shirota, C. H. Yarboro, G. G. Illei, and P. E. Lipsky. 2005. 'Identification and characterization of circulating human transitional B cells', *Blood*, 105: 4390-8.

Slavin, Daniela A., Nicolás P. Koritschoner, Claudio C. Prieto, Fernando J. López-Díaz, Bruno Chatton, and José Luis Bocco. 2004. 'A new role for the Krüppel-like transcription factor KLF6 as an inhibitor of c-Jun proto-oncoprotein function', *Oncogene*, 23: 8196-205.

Smith, G. P. 1985. 'Filamentous fusion phage: novel expression vectors that display cloned antigens on the virion surface', *Science*, 228: 1315-7.

Sok, D., K. J. Doores, B. Briney, K. M. Le, K. L. Saye-Francisco, A. Ramos, D. W. Kulp, J. P. Julien, S. Menis, L. Wickramasinghe, M. S. Seaman, W. R. Schief, I. A. Wilson, P. Poignard, and D. R. Burton. 2014. 'Promiscuous glycan site recognition by antibodies to the high-mannose patch of gp120 broadens neutralization of HIV', *Sci Transl Med*, 6: 236ra63.

Sok, D., M. Pauthner, B. Briney, J. H. Lee, K. L. Saye-Francisco, J. Hsueh, A. Ramos, K. M. Le, M. Jones, J. G. Jardine, R. Bastidas, A. Sarkar, C. H. Liang, S. S. Shivatare, C. Y. Wu, W. R. Schief, C. H. Wong, I. A. Wilson, A. B. Ward, J. Zhu, P. Poignard, and D. R. Burton. 2016. 'A Prominent Site of Antibody Vulnerability on HIV Envelope Incorporates a Motif Associated with CCR5 Binding and Its Camouflaging Glycans', *Immunity*, 45: 31-45.

Sok, D., M. J. van Gils, M. Pauthner, J. P. Julien, K. L. Saye-Francisco, J. Hsueh, B. Briney, J. H. Lee, K. M. Le, P. S. Lee, Y. Hua, M. S. Seaman, J. P. Moore, A. B. Ward, I. A. Wilson, R. W. Sanders, and D. R. Burton. 2014. 'Recombinant HIV envelope trimer selects for quaternary-dependent antibodies targeting the trimer apex', *Proc Natl Acad Sci U S A*, 111: 17624-9.

Stacey, A. R., P. J. Norris, L. Qin, E. A. Haygreen, E. Taylor, J. Heitman, M. Lebedeva, A. DeCamp, D. Li, D. Grove, S. G. Self, and P. Borrow. 2009. 'Induction of a striking systemic cytokine cascade prior to peak viremia in acute human immunodeficiency virus type 1 infection, in contrast to more modest and delayed responses in acute hepatitis B and C virus infections', *J Virol*, 83: 3719-33.

Stavnezer, J., J. E. Guikema, and C. E. Schrader. 2008. 'Mechanism and regulation of class switch recombination', *Annu Rev Immunol*, 26: 261-92.

Stebegg, Marisa, Saumya D. Kumar, Alyssa Silva-Cayetano, Valter R. Fonseca, Michelle A. Linterman, and Luis Graca. 2018. 'Regulation of the Germinal Center Response', *Frontiers in Immunology*, 9.

Stephenson, Emily, Gary Reynolds, Rachel A. Botting, Fernando J. Calero-Nieto, Michael D. Morgan, Zewen Kelvin Tuong, Karsten Bach, Waradon Sungnak, Kaylee B. Worlock, Masahiro Yoshida, Natsuhiko Kumasaka, Katarzyna Kania, Justin Engelbert, Bayanne Olabi, Jarmila Stremenova Spegarova, Nicola K. Wilson, Nicole Mende, Laura Jardine, Louis C. S. Gardner, Issac Goh, Dave Horsfall, Jim McGrath, Simone Webb, Michael W. Mather, Rik G. H. Lindeboom, Emma Dann, Ni Huang, Krzysztof Polanski, Elena Prigmore, Florian Gothe, Jonathan Scott, Rebecca P. Payne, Kenneth F. Baker, Aidan T. Hanrath, Ina C. D. Schim van der Loeff, Andrew S. Barr, Amada Sanchez-Gonzalez, Laura Bergamaschi, Federica Mescia, Josephine L. Barnes, Eliz Kilich, Angus de Wilton, Anita Saigal, Aarash Saleh, Sam M. Janes, Claire M. Smith, Nusayhah Gopee, Caroline Wilson, Paul Coupland, Jonathan M. Coxhead, Vladimir Yu Kiselev, Stijn van Dongen, Jaume Bacardit, Hamish W. King, Stephen Baker, John R. Bradley, Gordon Dougan, Ian G. Goodfellow, Ravindra K. Gupta, Christoph Hess, Nathalie Kingston, Paul J. Lehner, Nicholas J. Matheson, Willem H. Owehand, Caroline Saunders, Kenneth G. C. Smith, Charlotte Summers, James E. D. Thaventhiran, Mark Toshner, Michael P. Weekes, Ashlea Bucke, Jo Calder, Laura Canna, Jason Domingo, Anne Elmer, Stewart Fuller, Julie Harris, Sarah Hewitt, Jane Kennet, Sherly Jose, Jenny Kourampa, Anne Meadows, Criona O'Brien, Jane Price, Cherry Publico, Rebecca Rastall, Carla Ribeiro, Jane Rowlands, Valentina Ruffolo, Hugo Tordesillas, Ben Bullman, Benjamin J. Dunmore, Stuart Fawke, Stefan Gräf, Josh Hodgson, Christopher Huang, Kelvin Hunter, Emma Jones, Ekaterina Legchenko, Cecilia Matara, Jennifer Martin, Ciara O'Donnell, Linda Pointon, Nicole Pond, Joy Shih, Rachel Sutcliffe, Tobias Tilly, Carmen Treacy, Zhen Tong, Jennifer Wood, Marta Wylot, Ariana Betancourt, Georgie Bower, Aloka De Sa, Madeline Epping, Oisin Huhn, Sarah Jackson, Isobel Jarvis, Jimmy Marsden, Francesca Nice, Georgina Okecha, Ommar Omarjee, Marianne Perera, Nathan Richoz, Rahul Sharma, Lori Turner, Eckart M. D. D. De Bie, Katherine Bunclark, Masa Josipovic, Michael Mackay, Alice Michael, Sabrina Rossi, Mayurun Selvan, Sarah Spencer, Cissy Yong, Ali Ansaripour, Lucy Mwaura, Caroline Patterson, Gary Polwarth, Petra Polgarova, Giovanni di Stefano, John Allison, Helen Butcher, Daniela Caputo, Debbie Clapham-Riley, Eleanor Dewhurst, Anita Furlong, Barbara Graves, Jennifer Gray, Tasmin Ivers, Mary Kasanicki, Emma Le Gresley, Rachel Linger, Sarah Meloy, Francesca Muldoon, Nigel Ovington, Sofia Papadia, Isabel Phelan, Hannah Stark, Kathleen E. Stirrups, Paul Townsend, Neil Walker, Jennifer Webster, Anthony J. Rostron, A. John Simpson, Sophie Hambleton, Elisa Laurenti, Paul A. Lyons, Kerstin B. Meyer, Marko Z. Nikolić, Christopher J. A. Duncan, Kenneth G. C. Smith, Sarah A. Teichmann, Menna R. Clatworthy, John C. Marioni, Berthold Göttgens, Muzlifah Haniffa, Immunology Cambridge Institute of Therapeutic, and Covid-BioResource Collaboration Infectious

Disease-National Institute of Health Research. 2021. 'Single-cell multi-omics analysis of the immune response in COVID-19', *Nature Medicine*, 27: 904-16.

Stephenson, K. E., K. Wagh, B. Korber, and D. H. Barouch. 2020. 'Vaccines and Broadly Neutralizing Antibodies for HIV-1 Prevention', *Annu Rev Immunol*, 38: 673-703.

Stewart, Alexander, Joseph Chi-Fung Ng, Gillian Wallis, Vasiliki Tsioligka, Franca Fraternali, and Deborah K. Dunn-Walters. 2021. 'Single-Cell Transcriptomic Analyses Define Distinct Peripheral B Cell Subsets and Discrete Development Pathways', *Frontiers in Immunology*, 12.

Stoeckius, Marlon, Christoph Hafemeister, William Stephenson, Brian Houck-Loomis, Pratip K. Chattopadhyay, Harold Swerdlow, Rahul Satija, and Peter Smibert. 2017. 'Simultaneous epitope and transcriptome measurement in single cells', *Nature Methods*, 14: 865-68.

Sun, Z. Y., K. J. Oh, M. Kim, J. Yu, V. Brusic, L. Song, Z. Qiao, J. H. Wang, G. Wagner, and E. L. Reinherz. 2008. 'HIV-1 broadly neutralizing antibody extracts its epitope from a kinked gp41 ectodomain region on the viral membrane', *Immunity*, 28: 52-63.

Sutton, Henry J., Racheal Aye, Azza H. Idris, Rachel Vistein, Eunice Nduati, Oscar Kai, Jedida Mwacharo, Xi Li, Xin Gao, T. Daniel Andrews, Marios Koutsakos, Thi H. O. Nguyen, Maxim Nekrasov, Peter Milburn, Auda Eltahla, Andrea A. Berry, Natasha Kc, Sumana Chakravarty, B. Kim Lee Sim, Adam K. Wheatley, Stephen J. Kent, Stephen L. Hoffman, Kirsten E. Lyke, Philip Bejon, Fabio Luciani, Katherine Kedzierska, Robert A. Seder, Francis M. Ndungu, and Ian A. Cockburn. 2021. 'Atypical B cells are part of an alternative lineage of B cells that participates in responses to vaccination and infection in humans', *Cell Reports*, 34.

Tang, C., D. Bagnara, N. Chiorazzi, M. D. Scharff, and T. MacCarthy. 2020. 'AID Overlapping and Polη Hotspots Are Key Features of Evolutionary Variation Within the Human Antibody Heavy Chain (IGHV) Genes', *Front Immunol*, 11: 788.

Tang, Fuchou, Catalin Barbacioru, Yangzhou Wang, Ellen Nordman, Clarence Lee, Nanlan Xu, Xiaohui Wang, John Bodeau, Brian B. Tuch, Asim Siddiqui, Kaiqin Lao, and M. Azim Surani. 2009. 'mRNA-Seq whole-transcriptome analysis of a single cell', *Nature Methods*, 6: 377-82.

Tanko, R. F., A. P. Soares, T. L. Müller, N. J. Garrett, N. Samsunder, Q. Abdool Karim, S. S. Abdool Karim, C. Riou, and W. A. Burgers. 2017. 'Effect of Antiretroviral Therapy on the Memory and Activation Profiles of B Cells in HIV-Infected African Women', *J Immunol*, 198: 1220-28.

Tay, J. Kenneth, Balasubramanian Narasimhan, and Trevor Hastie. 2023. 'Elastic Net Regularization Paths for All Generalized Linear Models', *Journal of Statistical Software*, 106: 1 - 31.

Taylor, J. J., K. A. Pape, and M. K. Jenkins. 2012. 'A germinal center-independent pathway generates unswitched memory B cells early in the primary response', *J Exp Med*, 209: 597-606.

Tchasovnikarova, I. A., R. T. Timms, N. J. Matheson, K. Wals, R. Antrobus, B. Göttgens, G. Dougan, M. A. Dawson, and P. J. Lehner. 2015. 'GENE SILENCING. Epigenetic silencing by the HUSH complex mediates position-effect variegation in human cells', *Science*, 348: 1481-85.

Tiller, T. 2011. 'Single B cell antibody technologies', *N Biotechnol*, 28: 453-7.
Tiller, T., E. Meffre, S. Yurasov, M. Tsuiji, M. C. Nussenzweig, and H. Wardemann. 2008. 'Efficient generation of monoclonal antibodies from single human B cells by single cell RT-PCR and expression vector cloning', *J Immunol Methods*, 329: 112-24.
Tonegawa, S. 1983. 'Somatic generation of antibody diversity', *Nature*, 302: 575-81.
Tongo, M., J. R. Dorfman, and D. P. Martin. 2015. 'High Degree of HIV-1 Group M (HIV-1M) Genetic Diversity within Circulating Recombinant Forms: Insight into the Early Events of HIV-1M Evolution', *J Virol*, 90: 2221-9.
Touizer, E., A. Alrubbayi, R. Ford, N. Hussain, P. P. Gerber, H. L. Shum, C. Rees-Spear, L. Muir, E. Gea-Mallorquí, J. Kopycinski, D. Jankovic, C. Pinder, T. A. Fox, I. Williams, C. Mullender, I. Maan, L. Waters, M. Johnson, S. Madge, M. Youle, T. Barber, F. Burns, S. Kinloch, S. Rowland-Jones, R. Gilson, N. J. Matheson, E. Morris, D. Peppa, and L. E. McCoy. 2022. 'Attenuated humoral responses in HIV infection after SARS-CoV-2 vaccination are linked to global B cell defects and cellular immune profiles', *bioRxiv*.
Trkola, Alexandra, Tatjana Dragic, James Arthos, James M. Binley, William C. Olson, Graham P. Allaway, Cecilia Cheng-Mayer, James Robinson, Paul J. Maddon, and John P. Moore. 1996. 'CD4-dependent, antibody-sensitive interactions between HIV-1 and its co-receptor CCR-5', *Nature*, 384: 184-87.
Tumanov, A., D. Kuprash, M. Lagarkova, S. Grivennikov, K. Abe, A. Shakhov, L. Drutskaya, C. Stewart, A. Chervonsky, and S. Nedospasov. 2002. 'Distinct role of surface lymphotoxin expressed by B cells in the organization of secondary lymphoid tissues', *Immunity*, 17: 239-50.
Ugolini, S., I. Mondor, P. W. Parren, D. R. Burton, S. A. Tilley, P. J. Klasse, and Q. J. Sattentau. 1997. 'Inhibition of virus attachment to CD4+ target cells is a major mechanism of T cell line-adapted HIV-1 neutralization', *J Exp Med*, 186: 1287-98.
UNAIDS. 2022. 'Global HIV & AIDS statistics — Fact sheet'.
van den Brink, E. N., J. Ter Meulen, F. Cox, M. A. Jongeneelen, A. Thijsse, M. Throsby, W. E. Marissen, P. M. Rood, A. B. Bakker, H. R. Gelderblom, B. E. Martina, A. D. Osterhaus, W. Preiser, H. W. Doerr, J. de Kruif, and J. Goudsmit. 2005. 'Molecular and biological characterization of human monoclonal antibodies binding to the spike and nucleocapsid proteins of severe acute respiratory syndrome coronavirus', *J Virol*, 79: 1635-44.
van Eeden, C., C. K. Wibmer, C. Scheepers, S. I. Richardson, M. Nonyane, B. Lambson, N. N. Mkhize, B. Vijayakumar, Z. Sheng, S. Stanfield-Oakley, J. N. Bhiman, V. Bekker, T. Hermanus, B. Mabvakure, A. Ismail, M. A. Moody, K. Wiehe, N. Garrett, S. A. Karim, H. Dirr, M. A. Fernandes, Y. Sayed, L. Shapiro, G. Ferrari, B. F. Haynes, P. L. Moore, and L. Morris. 2018. 'V2-Directed Vaccine-like Antibodies from HIV-1 Infection Identify an Additional K169-Binding Light Chain Motif with Broad ADCC Activity', *Cell Rep*, 25: 3123-35.e6.

van Gils, M. J., Z. Euler, B. Schweighardt, T. Wrin, and H. Schuitemaker. 2009. 'Prevalence of cross-reactive HIV-1-neutralizing activity in HIV-1-infected patients with rapid or slow disease progression', *Aids*, 23: 2405-14.

van Gils, M. J., T. L. van den Kerkhof, G. Ozorowski, C. A. Cottrell, D. Sok, M. Pauthner, J. Pallesen, N. de Val, A. Yasmeen, S. W. de Taeye, A. Schorcht, S. Gumbs, I. Johanna, K. Saye-Francisco, C. H. Liang, E. Landais, X. Nie, L. K. Pritchard, M. Crispin, G. Kelsoe, I. A. Wilson, H. Schuitemaker, P. J. Klasse, J. P. Moore, D. R. Burton, A. B. Ward, and R. W. Sanders. 2016. 'An HIV-1 antibody from an elite neutralizer implicates the fusion peptide as a site of vulnerability', *Nat Microbiol*, 2: 16199.

van Schooten, J., and M. J. van Gils. 2018. 'HIV-1 immunogens and strategies to drive antibody responses towards neutralization breadth', *Retrovirology*, 15: 74.

Venturi, Guglielmo M., LiLi Tu, Takafumi Kadono, Adil I. Khan, Yoko Fujimoto, Philip Oshel, Cheryl B. Bock, Ann S. Miller, Ralph M. Albrecht, Paul Kubes, Douglas A. Steeber, and Thomas F. Tedder. 2003. 'Leukocyte migration is regulated by L-selectin endoproteolytic release', *Immunity*, 19: 713-24.

Verkoczy, L., M. Diaz, T. M. Holl, Y. B. Ouyang, H. Bouton-Verville, S. M. Alam, H. X. Liao, G. Kelsoe, and B. F. Haynes. 2010. 'Autoreactivity in an HIV-1 broadly reactive neutralizing antibody variable region heavy chain induces immunologic tolerance', *Proc Natl Acad Sci U S A*, 107: 181-6.

Victora, G. D., T. A. Schwickert, D. R. Fooksman, A. O. Kamphorst, M. Meyer-Hermann, M. L. Dustin, and M. C. Nussenzweig. 2010. 'Germinal center dynamics revealed by multiphoton microscopy with a photoactivatable fluorescent reporter', *Cell*, 143: 592-605.

Vidarsson, Gestur, Gillian Dekkers, and Theo Rispens. 2014. 'IgG Subclasses and Allotypes: From Structure to Effector Functions', *Frontiers in Immunology*, 5.

Virshup, Isaac, Sergei Rybakov, Fabian J. Theis, Philipp Angerer, and F. Alexander Wolf. 2021. 'anndata: Annotated data', *bioRxiv*: 2021.12.16.473007.

Volpe, J. M., and T. B. Kepler. 2008. 'Large-scale analysis of human heavy chain V(D)J recombination patterns', *Immunome Res*, 4: 3.

Voss, J. E., R. Andrabi, L. E. McCoy, N. de Val, R. P. Fuller, T. Messmer, C. Y. Su, D. Sok, S. N. Khan, F. Garces, L. K. Pritchard, R. T. Wyatt, A. B. Ward, M. Crispin, I. A. Wilson, and D. R. Burton. 2017. 'Elicitation of Neutralizing Antibodies Targeting the V2 Apex of the HIV Envelope Trimer in a Wild-Type Animal Model', *Cell Rep*, 21: 222-35.

Wagh, K., E. F. Kreider, Y. Li, H. J. Barbian, G. H. Learn, E. Giorgi, P. T. Hraber, T. G. Decker, A. G. Smith, M. V. Gondim, L. Gillis, J. Wandzilak, G. Y. Chuang, R. Rawi, F. Cai, P. Pellegrino, I. Williams, J. Overbaugh, F. Gao, P. D. Kwong, B. F. Haynes, G. M. Shaw, P. Borrow, M. S. Seaman, B. H. Hahn, and B. Korber. 2018. 'Completeness of HIV-1 Envelope Glycan Shield at Transmission Determines Neutralization Breadth', *Cell Rep*, 25: 893-908.e7.

Wagh, Kshitij, Michael S. Seaman, Marshall Zingg, Tomas Fitzsimons, Dan H. Barouch, Dennis R. Burton, Mark Connors, David D. Ho, John R. Mascola, Michel C. Nussenzweig, Jeffrey Ravetch, Rajeev Gautam, Malcolm A. Martin, David C. Montefiori, and Bette Korber. 2018. 'Potential of conventional & bispecific broadly neutralizing antibodies for prevention of HIV-1 subtype A, C & D infections', *PLOS Pathogens*, 14: e1006860.

Walker, L. M., M. Huber, K. J. Doores, E. Falkowska, R. Pejchal, J. P. Julien, S. K. Wang, A. Ramos, P. Y. Chan-Hui, M. Moyle, J. L. Mitcham, P. W. Hammond, O. A. Olsen, P. Phung, S. Fling, C. H. Wong, S. Phogat, T. Wrin, M. D. Simek, W. C. Koff, I. A. Wilson, D. R. Burton, and P. Poignard. 2011. 'Broad neutralization coverage of HIV by multiple highly potent antibodies', *Nature*, 477: 466-70.

Walker, L. M., S. K. Phogat, P. Y. Chan-Hui, D. Wagner, P. Phung, J. L. Goss, T. Wrin, M. D. Simek, S. Fling, J. L. Mitcham, J. K. Lehrman, F. H. Priddy, O. A. Olsen, S. M. Frey, P. W. Hammond, S. Kaminsky, T. Zamb, M. Moyle, W. C. Koff, P. Poignard, and D. R. Burton. 2009. 'Broad and potent neutralizing antibodies from an African donor reveal a new HIV-1 vaccine target', *Science*, 326: 285-9.

Walker, L. M., M. D. Simek, F. Priddy, J. S. Gach, D. Wagner, M. B. Zwick, S. K. Phogat, P. Poignard, and D. R. Burton. 2010. 'A limited number of antibody specificities mediate broad and potent serum neutralization in selected HIV-1 infected individuals', *PLoS Pathog*, 6: e1001028.

Walter, Mark R. 2020. 'The Role of Structure in the Biology of Interferon Signaling', *Frontiers in Immunology*, 11.

Wang, H., C. O. Barnes, Z. Yang, M. C. Nussenzweig, and P. J. Bjorkman. 2018. 'Partially Open HIV-1 Envelope Structures Exhibit Conformational Changes Relevant for Coreceptor Binding and Fusion', *Cell Host Microbe*, 24: 579-92.e4.

Wang, H., H. B. Gristick, L. Scharf, A. P. West, R. P. Galimidi, M. S. Seaman, N. T. Freund, M. C. Nussenzweig, and P. J. Bjorkman. 2017. 'Asymmetric recognition of HIV-1 Envelope trimer by V1V2 loop-targeting antibodies', *Elife*, 6.

Wang, S., Q. Zhang, H. Hui, K. Agrawal, M. A. Y. Karris, and T. M. Rana. 2020. 'An atlas of immune cell exhaustion in HIV-infected individuals revealed by single-cell transcriptomics', *Emerg Microbes Infect*, 9: 2333-47.

Wang, X., Y. He, Q. Zhang, X. Ren, and Z. Zhang. 2021. 'Direct Comparative Analyses of 10X Genomics Chromium and Smart-seq2', *Genomics Proteomics Bioinformatics*, 19: 253-66.

Wardemann, H., S. Yurasov, A. Schaefer, J. W. Young, E. Meffre, and M. C. Nussenzweig. 2003. 'Predominant autoantibody production by early human B cell precursors', *Science*, 301: 1374-7.

Watanabe, A., K. Y. Su, M. Kuraoka, G. Yang, A. E. Reynolds, A. G. Schmidt, S. C. Harrison, B. F. Haynes, E. W. St Clair, and G. Kelsoe. 2019. 'Self-tolerance curtails the B cell repertoire to microbial epitopes', *JCI Insight*, 4.

Wei, X., J. M. Decker, H. Liu, Z. Zhang, R. B. Arani, J. M. Kilby, M. S. Saag, X. Wu, G. M. Shaw, and J. C. Kappes. 2002. 'Emergence of resistant human immunodeficiency virus type 1 in patients receiving fusion

inhibitor (T-20) monotherapy', *Antimicrob Agents Chemother*, 46: 1896-905.

Wei, X., J. M. Decker, S. Wang, H. Hui, J. C. Kappes, X. Wu, J. F. Salazar-Gonzalez, M. G. Salazar, J. M. Kilby, M. S. Saag, N. L. Komarova, M. A. Nowak, B. H. Hahn, P. D. Kwong, and G. M. Shaw. 2003. 'Antibody neutralization and escape by HIV-1', *Nature*, 422: 307-12.

Weinberg, J B, T J Matthews, B R Cullen, and M H Malim. 1991. 'Productive human immunodeficiency virus type 1 (HIV-1) infection of nonproliferating human monocytes', *Journal of Experimental Medicine*, 174: 1477-82.

Weiss, R. A. 2003. 'HIV and AIDS in relation to other pandemics. Among the viruses plaguing humans, HIV is a recent acquisition. Its outstanding success as an infection poses immense scientific challenges to human health and raises the question "What comes nest?"', *EMBO Rep*, 4 Spec No: S10-4.

West, A. P., Jr., L. Scharf, J. F. Scheid, F. Klein, P. J. Bjorkman, and M. C. Nussenzweig. 2014. 'Structural insights on the role of antibodies in HIV-1 vaccine and therapy', *Cell*, 156: 633-48.

Wherry, E. J., S. J. Ha, S. M. Kaech, W. N. Haining, S. Sarkar, V. Kalia, S. Subramaniam, J. N. Blattman, D. L. Barber, and R. Ahmed. 2007. 'Molecular signature of CD8+ T cell exhaustion during chronic viral infection', *Immunity*, 27: 670-84.

Whitney, J. B., A. L. Hill, S. Sanisetty, P. Penaloza-MacMaster, J. Liu, M. Shetty, L. Parenteau, C. Cabral, J. Shields, S. Blackmore, J. Y. Smith, A. L. Brinkman, L. E. Peter, S. I. Mathew, K. M. Smith, E. N. Borducchi, D. I. Rosenbloom, M. G. Lewis, J. Hattersley, B. Li, J. Hesselgesser, R. Geleziunas, M. L. Robb, J. H. Kim, N. L. Michael, and D. H. Barouch. 2014. 'Rapid seeding of the viral reservoir prior to SIV viraemia in rhesus monkeys', *Nature*, 512: 74-7.

Wibmer, C. K., J. Gorman, C. S. Anthony, N. N. Mkhize, A. Druz, T. York, S. D. Schmidt, P. Labuschagne, M. K. Louder, R. T. Bailer, S. S. Abdool Karim, J. R. Mascola, C. Williamson, P. L. Moore, P. D. Kwong, and L. Morris. 2016. 'Structure of an N276-Dependent HIV-1 Neutralizing Antibody Targeting a Rare V5 Glycan Hole Adjacent to the CD4 Binding Site', *J Virol*, 90: 10220-35.

Wibmer, C. K., S. I. Richardson, J. Yolitz, C. Cicala, J. Arthos, P. L. Moore, and L. Morris. 2018. 'Common helical V1V2 conformations of HIV-1 Envelope expose the α4β7 binding site on intact virions', *Nat Commun*, 9: 4489.

Wibmer, Constantinos Kurt, Jinal N. Bhiman, Elin S. Gray, Nancy Tumba, Salim S. Abdool Karim, Carolyn Williamson, Lynn Morris, and Penny L. Moore. 2013. 'Viral Escape from HIV-1 Neutralizing Antibodies Drives Increased Plasma Neutralization Breadth through Sequential Recognition of Multiple Epitopes and Immunotypes', *PLOS Pathogens*, 9: e1003738.

Williams, L. D., G. Ofek, S. Schätzle, J. R. McDaniel, X. Lu, N. I. Nicely, L. Wu, C. S. Lougheed, T. Bradley, M. K. Louder, K. McKee, R. T. Bailer, S. O'Dell, I. S. Georgiev, M. S. Seaman, R. J. Parks, D. J. Marshall, K. Anasti, G. Yang, X. Nie, N. L. Tumba, K. Wiehe, K. Wagh, B. Korber,

T. B. Kepler, S. Munir Alam, L. Morris, G. Kamanga, M. S. Cohen, M. Bonsignori, S. M. Xia, D. C. Montefiori, G. Kelsoe, F. Gao, J. R. Mascola, M. A. Moody, K. O. Saunders, H. X. Liao, G. D. Tomaras, G. Georgiou, and B. F. Haynes. 2017. 'Potent and broad HIV-neutralizing antibodies in memory B cells and plasma', *Sci Immunol*, 2.

Willis, J. R., J. A. Finn, B. Briney, G. Sapparapu, V. Singh, H. King, C. C. LaBranche, D. C. Montefiori, J. Meiler, and J. E. Crowe, Jr. 2016. 'Long antibody HCDR3s from HIV-naïve donors presented on a PG9 neutralizing antibody background mediate HIV neutralization', *Proc Natl Acad Sci U S A*, 113: 4446-51.

Wine, Y., A. P. Horton, G. C. Ippolito, and G. Georgiou. 2015. 'Serology in the 21st century: the molecular-level analysis of the serum antibody repertoire', *Curr Opin Immunol*, 35: 89-97.

Winter, G., A. D. Griffiths, R. E. Hawkins, and H. R. Hoogenboom. 1994. 'Making antibodies by phage display technology', *Annu Rev Immunol*, 12: 433-55.

Woldemeskel, Bezawit A., Abena K. Kwaa, and Joel N. Blankson. 2020. 'Viral reservoirs in elite controllers of HIV-1 infection: Implications for HIV cure strategies', *eBioMedicine*, 62.

Wu, D., J. Sun, T. Xu, S. Wang, G. Li, Y. Li, and Z. Cao. 2010. 'Stacking and energetic contribution of aromatic islands at the binding interface of antibody proteins', *Immunome Res*, 6 Suppl 1: S1.

Wu, X., Z. Y. Yang, Y. Li, C. M. Hogerkorp, W. R. Schief, M. S. Seaman, T. Zhou, S. D. Schmidt, L. Wu, L. Xu, N. S. Longo, K. McKee, S. O'Dell, M. K. Louder, D. L. Wycuff, Y. Feng, M. Nason, N. Doria-Rose, M. Connors, P. D. Kwong, M. Roederer, R. T. Wyatt, G. J. Nabel, and J. R. Mascola. 2010. 'Rational design of envelope identifies broadly neutralizing human monoclonal antibodies to HIV-1', *Science*, 329: 856-61.

Wyatt, R., P. D. Kwong, E. Desjardins, R. W. Sweet, J. Robinson, W. A. Hendrickson, and J. G. Sodroski. 1998. 'The antigenic structure of the HIV gp120 envelope glycoprotein', *Nature*, 393: 705-11.

Xu, H., X. Wang, and R. S. Veazey. 2013. 'Mucosal immunology of HIV infection', *Immunol Rev*, 254: 10-33.

Xu, J. L., and M. M. Davis. 2000. 'Diversity in the CDR3 region of V(H) is sufficient for most antibody specificities', *Immunity*, 13: 37-45.

Xu, Kai, Priyamvada Acharya, Rui Kong, Cheng Cheng, Gwo-Yu Chuang, Kevin Liu, Mark K. Louder, Sijy O'Dell, Reda Rawi, Mallika Sastry, Chen-Hsiang Shen, Baoshan Zhang, Tongqing Zhou, Mangaiarkarasi Asokan, Robert T. Bailer, Michael Chambers, Xuejun Chen, Chang W. Choi, Venkata P. Dandey, Nicole A. Doria-Rose, Aliaksandr Druz, Edward T. Eng, S. Katie Farney, Kathryn E. Foulds, Hui Geng, Ivelin S. Georgiev, Jason Gorman, Kurt R. Hill, Alexander J. Jafari, Young D. Kwon, Yen-Ting Lai, Thomas Lemmin, Krisha McKee, Tiffany Y. Ohr, Li Ou, Dongjun Peng, Ariana P. Rowshan, Zizhang Sheng, John-Paul Todd, Yaroslav Tsybovsky, Elise G. Viox, Yiran Wang, Hui Wei, Yongping Yang, Amy F. Zhou, Rui Chen, Lu Yang, Diana G. Scorpio, Adrian B. McDermott, Lawrence Shapiro, Bridget Carragher, Clinton S. Potter, John R. Mascola, and Peter D. Kwong. 2018. 'Epitope-based

vaccine design yields fusion peptide-directed antibodies that neutralize diverse strains of HIV-1', *Nature Medicine*, 24: 857-67.

Xu, Zhenming, Hong Zan, Egest J. Pone, Thach Mai, and Paolo Casali. 2012. 'Immunoglobulin class-switch DNA recombination: induction, targeting and beyond', *Nature Reviews Immunology*, 12: 517-31.

Yamamoto, T., R. M. Lynch, R. Gautam, R. Matus-Nicodemos, S. D. Schmidt, K. L. Boswell, S. Darko, P. Wong, Z. Sheng, C. Petrovas, A. B. McDermott, R. A. Seder, B. F. Keele, L. Shapiro, D. C. Douek, Y. Nishimura, J. R. Mascola, M. A. Martin, and R. A. Koup. 2015. 'Quality and quantity of TFH cells are critical for broad antibody development in SHIVAD8 infection', *Sci Transl Med*, 7: 298ra120.

Yamawaki, T. M., D. R. Lu, D. C. Ellwanger, D. Bhatt, P. Manzanillo, V. Arias, H. Zhou, O. K. Yoon, O. Homann, S. Wang, and C. M. Li. 2021. 'Systematic comparison of high-throughput single-cell RNA-seq methods for immune cell profiling', *BMC Genomics*, 22: 66.

Yang Shih, Tien-An, Eric Meffre, Mario Roederer, and Michel C. Nussenzweig. 2002. 'Role of BCR affinity in T cell–dependent antibody responses in vivo', *Nature Immunology*, 3: 570-75.

Yang, X., M. Wang, J. Wu, D. Shi, Y. Zhang, H. Zeng, Y. Zhu, C. Lan, Y. Deng, S. Guo, L. Xu, C. Ma, Y. Zhang, J. Ou, C. J. Liu, Y. Chen, Q. Wang, W. Xie, J. Guan, J. Ding, Z. Wang, C. Chang, W. Yang, H. Zhang, J. Chen, L. Qin, H. Zhou, J. X. Bei, L. Wei, G. Cao, X. Yu, and Z. Zhang. 2021. 'Large-scale analysis of 2,152 Ig-seq datasets reveals key features of B cell biology and the antibody repertoire', *Cell Rep*, 35: 109110.

Yoon, H., J. Macke, A. P. West, Jr., B. Foley, P. J. Bjorkman, B. Korber, and K. Yusim. 2015. 'CATNAP: a tool to compile, analyze and tally neutralizing antibody panels', *Nucleic Acids Res*, 43: W213-9.

Yu, L., and Y. Guan. 2014. 'Immunologic Basis for Long HCDR3s in Broadly Neutralizing Antibodies Against HIV-1', *Front Immunol*, 5: 250.

Yuan, M., C. A. Cottrell, G. Ozorowski, M. J. van Gils, S. Kumar, N. C. Wu, A. Sarkar, J. L. Torres, N. de Val, J. Copps, J. P. Moore, R. W. Sanders, A. B. Ward, and I. A. Wilson. 2019. 'Conformational Plasticity in the HIV-1 Fusion Peptide Facilitates Recognition by Broadly Neutralizing Antibodies', *Cell Host Microbe*, 25: 873-83.e5.

Yurkovetskiy, L., M. H. Guney, K. Kim, S. L. Goh, S. McCauley, A. Dauphin, W. E. Diehl, and J. Luban. 2018. 'Primate immunodeficiency virus proteins Vpx and Vpr counteract transcriptional repression of proviruses by the HUSH complex', *Nat Microbiol*, 3: 1354-61.

Zachau, H. G. 2000. 'The immunoglobulin kappa gene families of human and mouse: a cottage industry approach', *Biol Chem*, 381: 951-4.

Zhang, Lei, Adriana Irimia, Lingling He, Elise Landais, Kimmo Rantalainen, Daniel P. Leaman, Thomas Vollbrecht, Armando Stano, Daniel I. Sands, Arthur S. Kim, George Miiro, Jennifer Serwanga, Anton Pozniak, Dale McPhee, Oliver Manigart, Lawrence Mwananyanda, Etienne Karita, André Inwoley, Walter Jaoko, Jack DeHovitz, Linda-Gail Bekker, Punnee Pitisuttithum, Robert Paris, Susan Allen, Pascal Poignard, Dennis R. Burton, Ben Murrell, Andrew B. Ward, Jiang Zhu, Ian A. Wilson, Michael B. Zwick, and Iavi Protocol G Investigators.

2019. 'An MPER antibody neutralizes HIV-1 using germline features shared among donors', *Nature Communications*, 10: 5389.

Zhang, Linqi, Bharat Ramratnam, Klara Tenner-Racz, Yuxian He, Mika Vesanen, Sharon Lewin, Andrew Talal, Paul Racz, Alan S. Perelson, Bette T. Korber, Martin Markowitz, Yong Guo, Margarita Duran, Arlene Hurley, John Tsay, Yu-Ching Huang, Chia-Ching Wang, and David D. Ho. 1999. 'Quantifying Residual HIV-1 Replication in Patients Receiving Combination Antiretroviral Therapy', *New England Journal of Medicine*, 340: 1605-13.

Zheng, Grace X. Y., Jessica M. Terry, Phillip Belgrader, Paul Ryvkin, Zachary W. Bent, Ryan Wilson, Solongo B. Ziraldo, Tobias D. Wheeler, Geoff P. McDermott, Junjie Zhu, Mark T. Gregory, Joe Shuga, Luz Montesclaros, Jason G. Underwood, Donald A. Masquelier, Stefanie Y. Nishimura, Michael Schnall-Levin, Paul W. Wyatt, Christopher M. Hindson, Rajiv Bharadwaj, Alexander Wong, Kevin D. Ness, Lan W. Beppu, H. Joachim Deeg, Christopher McFarland, Keith R. Loeb, William J. Valente, Nolan G. Ericson, Emily A. Stevens, Jerald P. Radich, Tarjei S. Mikkelsen, Benjamin J. Hindson, and Jason H. Bielas. 2017. 'Massively parallel digital transcriptional profiling of single cells', *Nature Communications*, 8: 14049.

Zhou, T., I. Georgiev, X. Wu, Z. Y. Yang, K. Dai, A. Finzi, Y. D. Kwon, J. F. Scheid, W. Shi, L. Xu, Y. Yang, J. Zhu, M. C. Nussenzweig, J. Sodroski, L. Shapiro, G. J. Nabel, J. R. Mascola, and P. D. Kwong. 2010. 'Structural basis for broad and potent neutralization of HIV-1 by antibody VRC01', *Science*, 329: 811-7.

Zhou, T., R. M. Lynch, L. Chen, P. Acharya, X. Wu, N. A. Doria-Rose, M. G. Joyce, D. Lingwood, C. Soto, R. T. Bailer, M. J. Ernandes, R. Kong, N. S. Longo, M. K. Louder, K. McKee, S. O'Dell, S. D. Schmidt, L. Tran, Z. Yang, A. Druz, T. S. Luongo, S. Moquin, S. Srivatsan, Y. Yang, B. Zhang, A. Zheng, M. Pancera, T. Kirys, I. S. Georgiev, T. Gindin, H. P. Peng, A. S. Yang, J. C. Mullikin, M. D. Gray, L. Stamatatos, D. R. Burton, W. C. Koff, M. S. Cohen, B. F. Haynes, J. P. Casazza, M. Connors, D. Corti, A. Lanzavecchia, Q. J. Sattentau, R. A. Weiss, A. P. West, Jr., P. J. Bjorkman, J. F. Scheid, M. C. Nussenzweig, L. Shapiro, J. R. Mascola, and P. D. Kwong. 2015. 'Structural Repertoire of HIV-1-Neutralizing Antibodies Targeting the CD4 Supersite in 14 Donors', *Cell*, 161: 1280-92.

Zhou, T., J. Zhu, X. Wu, S. Moquin, B. Zhang, P. Acharya, I. S. Georgiev, H. R. Altae-Tran, G. Y. Chuang, M. G. Joyce, Y. D. Kwon, N. S. Longo, M. K. Louder, T. Luongo, K. McKee, C. A. Schramm, J. Skinner, Y. Yang, Z. Yang, Z. Zhang, A. Zheng, M. Bonsignori, B. F. Haynes, J. F. Scheid, M. C. Nussenzweig, M. Simek, D. R. Burton, W. C. Koff, J. C. Mullikin, M. Connors, L. Shapiro, G. J. Nabel, J. R. Mascola, and P. D. Kwong. 2013. 'Multidonor analysis reveals structural elements, genetic determinants, and maturation pathway for HIV-1 neutralization by VRC01-class antibodies', *Immunity*, 39: 245-58.

Zhu, P., E. Chertova, J. Bess, Jr., J. D. Lifson, L. O. Arthur, J. Liu, K. A. Taylor, and K. H. Roux. 2003. 'Electron tomography analysis of envelope

glycoprotein trimers on HIV and simian immunodeficiency virus virions', *Proc Natl Acad Sci U S A*, 100: 15812-7.

Ziegenhain, C., B. Vieth, S. Parekh, B. Reinius, A. Guillaumet-Adkins, M. Smets, H. Leonhardt, H. Heyn, I. Hellmann, and W. Enard. 2017. 'Comparative Analysis of Single-Cell RNA Sequencing Methods', *Mol Cell*, 65: 631-43.e4.